IMPERIAL COLLEGE OF SCIENCE, TECHNOLOGY AND MEDICINE

UNIVERSITY OF LONDON

ROYAL SCHOOL OF MINES

DEPARTMENT OF EARTH RESOURCES ENGINEERING

PETROLEUM ENGINEERING

A STUDY OF COLLOIDAL ASPHALTENE IN PETROLEUM RESERVOIRS

BY

SAAD FEHEID ALKAFEEF

A thesis submitted for the degree of Doctor of Philosophy of the University of London and for the Diploma of Imperial College

October, 1996

ABSTRACT

Asphaltene precipitation and deposition in petroleum reservoirs has been recognised to be a significant problem in the oil industry. The problems arising in petroleum reservoirs involve the interaction of asphaltenes with minerals which are exposed at the pore surfaces in reservoir rocks. This will cause permeability reduction as well as contributing to wettability reversal. Destabilising colloidal asphaltene during oil production will contribute to serious plugging problems in the well tubing and surface facilities.

This research covers colloidal asphaltene adsorption/deposition in petroleum reservoirs. The adsorption of colloidal asphaltene on reservoir rock surfaces has been investigated experimentally by determination of the surface potential of the rock cores under flow conditions. Surface potentials determined by streaming potential experiments can be in very considerable error as a result of surface conductivity, whereas streaming currents are free from this disadvantage. Streaming current measurements do however need a knowledge of the ratio A/L where A and L are the cross sectional area and length, respectively, of the effective capillaries. A novel method has been developed to estimate A/L by combining streaming potential and streaming current measurements so that the unambiguous streaming current method could be used. Negative surface potentials for rock cores became steadily more positive as asphaltene coated the pore surfaces. The reduction of permeability and flow efficiency agreed well with petrographic analysis.

Experiments were conducted to assess the impact of pore pressure on streaming potential and current measurements. It was observed that the behaviour of streaming potential and current as a function of pore pressure is direction dependent exhibiting a strong hysteresis. This phenomenon of hysteresis is important because of its direct link with the estimation of area to length ratio of pores and the related surface potential measurements. Separate experimental work was carried out to study the effects of pore size distribution in sandstone rocks on streaming potential and

current measurements. Based on the findings of this research, a theory has been developed to handle the double layer overlap in narrow pores. This theory has been validated with the experiment results carried out on sandstone formations.

The work also covered the determination of particle size distributions of asphaltene in hydrocarbon solvents, the adsorption of asphaltene on mineral particles, and the aggregation kinetics of asphaltene and model particles in such solvents. These experiments were carried out using laser back scattering technique. Hexadecyl napthalene has been designed, synthesised and used as an agent to adsorb on and sterically stabilise asphaltene particles in oils.

ACKNOWLEDGEMENTS

I would like to express my sincere thanks to my supervisor Dr. R. J. Gochin for his guidance and support throughout this work. I am also grateful to Dr. T.S. Daltaban for his initial discussions.

I am greatly indebted to Prof. A. L. Smith for his stimulating discussions, continuing encouragement, and advice during the execution of this research project.

I would like to thank the ERE staff for their friendly environment. In particular, I thank Dr. R. A. Dawe and Dr. X. D. Jing for their general discussion in petroleum engineering.

This research would not have been possible without the financial support of the Public Authority for Applied Education and Training of Kuwait. I must also thank my friends in the Kuwait Oil Company for their suggestion of this project.

I am also grateful to the administration of Core Laboratories for Advanced Technology of Calgary, Alberta, Canada represented by Mr. Brian J. Parsons, president, for their support and co-operation in this research project. Many thanks to Mr. Tony Ma, Mr. Mike McSwiney and Mr. Tom Martin and the rest of friends there for their useful technical discussions and advice.

I would like to thank Prof. G. A. Mansoori of University of Illinois at Chicago, USA, for his friendship, support and encouragement in tackling asphaltene problems.

My gratitude further extends to all my friends and colleagues in the Petroleum Engineering Group. Many thanks to my dearest friends, Dr. B. Elashahab, Mr. H. Naas and Mr. G. Badran.

Finally, I would like to thank my wife Cornelia and our daughter Selma for their loving support and believing that one day things would return to normality.

IN THE NAME OF GOD, THE MOST BENEFICENT AND THE MOST MERCIFUL

DEDICATION

To *my father for his love, support and encouragement to continue on the road of knowledge*

and

To *Prof. Alec L. Smith my mentor and friend who's travels around the world of Colloid Science and Surface Chemistry have been most enlightening*

TABLE OF CONTENTS

LIST OF FIGURES

Figure 8.30. Reversibility of wax crystallisation from Crude-B during reheated cycle.

LIST OF TABLES

NOMENCLATURE

A	Pore cross-sectional area (m^2)
A_i	Hamaker constant (J)
a	Radius of sphere (m)
D	Diffusion coefficient of a particle (m^2 sec^{-1})
e	Elementary charge (C)
E	Electric field (NC^{-1})
f	Pores A/L ratio
$G(\tau)$	Autocorrelation function
ΔG	Gibbs free energy change (J)
H	Surface-surface separation (m)
h	Pores half thickness (m)
ΔH	Enthalpy change (J)
I	Light intensity
$\overline{I^2}$	Mean square light intensity
$\left(\bar{I}\right)^2$	Square mean light intensity
I(t)	Light intensity at time t
I_s	Streaming current (A)
$\dot{I}_s$	$\frac{dI_s}{dP}$ $(AN^{-1}m^2)$
$I_{s(\infty)}$	Streaming current at a plane surface (A)
k	Boltzmann's constant (JK^{-1})
K	Specific conductivity of a solution ($ohm^{-1}m^{-1}$)
K'	Specific conductivity of a solution including surface conductivity (ohm^{-1} m^{-1})
K_{eff}	Effective conductivity of a liquid ($ohm^{-1}m^{-1}$)
K_L	Liquid Permeability, mD
K_{obs}	Observed value of K ($ohm^{-1}m^{-1}$)
k_{sv}	Light Scattering Vector

L	Length of Capillaries (m)
n_i^{∞}	Number of ions *i* per unit volume in the bulk of the solution (m^{-3})
P	Pressure (Pa)
ΔP	Differential Pressure (Pa)
q	Flow rate (m^3sec^{-1}) or density of atoms in colloidal particle ($1/m^{-3}$)
Q	Particle charge (C)
q_1	Flow rate after asphaltene adsorption (m^3sec^{-1})
q_o	Flow rate before asphaltene adsorption (m^3sec^{-1})
R	Solution resistance (ohm)
r	Centre-centre distance between spheres (m)
S	r/a
ΔS	Entropy change (JK^{-1})
T	Absolute temperature (K)
t	time (sec)
V_A	Attraction energy (J)
V_R	Repulsion energy (J)
V_s	Streaming potential (V)
$\dot{V}_s$	$\frac{dV_s}{dP}$ $(VN^{-1}m^2)$
V_T	The total potential energy of interaction (J)
W	Slow down factor of coagulation
x	Distance into the double layer (m); volume fraction of asphaltene in liquid (Chapter 6)
z	Valency of ion

Greek letters

β	Constant in London equation
ε	Permittivity of a material ($kg^{-1}m^{-3}s^4A^2$)
ε_o	Permittivity of a vaccum ($8.854*10^{-12}$ $kg^{-1}m^{-3}s^4A^2$)
ε_r	Relative permittivity (dielectric constant) equal to the ratio $\varepsilon/\varepsilon_o$
γ	Fractional thickness of adsorbed asphaltene layer

η	Medium viscosity (Pa.s)
κ	Debye-Hückel Reciprocal distance (m^{-1})
λ	Wavelength (m)
μ	Chemical potential ($Jmol^{-1}$)
$\overset{\Phi}{\mu}$	Standard chemical potential ($Jmol^{-1}$)
ν	Particle velocity ($m\ sec^{-1}$)
θ	Light scattering angle
θ_{SC}	Fraction of surface covered
ρ	Volume density of charge (cm^{-3})
τ	Adjustable time (sec)
ψ	Electrostatic potential (V)
$\psi_{(x)}$	Potential at a distance x from the surface (V)
ψ_o	Wall potential (V)
ζ	Zeta potential (V)
ζ_{Is}	Zeta potential by streaming current method (V)
ζ_{Vs}	Zeta potential by streaming potential method (V)

Unit Conversion Table

Field Units	SI Units
1 psi	6.895 kPa
1 cp	$1.0*10^{-3}$ Pa.s
1 mD	$9.869*10^{-16}\ m^2$

Units and Abbreviations

pA	10^{-12} A	Picoamperes
μA	10^{-6} A	Microamperes
mV	10^{-3} V	Millivolts
Å	10^{-10} m	Angstroms
nm	10^{-9} m	Nanometers
μm	10^{-6}	Micrometers

CHAPTER ONE

INTRODUCTION

1.1 DEFINITION OF THE PROBLEM

Asphaltene precipitation from petroleum reservoir fluids has proved to be a difficult problem to define and study. It is recognised to present serious problem in numerous oil systems worldwide. Asphaltene precipitation may occur deep in the reservoir formation and cause permeability reduction as well as contributing to serious plugging problems in oil well tubing and surface facilities. This phenomenon ranks as one of the highest-costing and most important safety problems in the production operation of the oil industry (Leontaritis *et al.* 1988)

There have been two approaches to dealing with asphaltene problems: one is associated with well maintenance by either improved technology in clean-up methods for unplugging lines or asphaltene dissolution; the second has been focused on anticipating the precipitation of asphaltene and keeping it dispersed.

The mechanism of formation of colloidal asphaltene in petroleum reservoirs has been a controversial issue for many years. Asphaltene flocculation and adsorption/deposition seems to have happened as a result of changes in physical parameters, such as: temperature, pressure, and composition. Destabilisation of colloidal asphaltene in a petroleum reservoir will cause formation plugging and wettability changes and can significantly affect the production efficiency of the reservoir during oil recovery. The damage caused by asphaltene in oil reservoirs is mainly a function of two mechanisms, the aggregation (i.e coagulation) of asphaltene particles and the adsorption of asphaltene to reservoir rock mineral surfaces.

The stability of a dispersion in colloid science terms refers to the resistance of the particles to flocculation (in this thesis the word flocculation, aggregation and coagulation are used interchangeably). The degree of this resistance is a measure of stability. Asphaltene colloidal dispersions in petroleum reservoirs are considered physically stable if free from any changes in physical properties. The behaviour of dispersions like asphaltene in oil reservoirs depends on the attractive and repulsive forces between adjacent particles. The interactions involved include van der Waals forces, steric effects and, in principle, electric double layer effects arising from charge at the interfaces. The combination of van der Waals and electric double layer forces was treated by Derjaguin, Landau, Verwey and Overbeek (the DLVO theory) originally applied to colloid particle stability.

The adsorption of asphaltene onto rock surfaces in oil reservoirs is clearly one of the factors that affect reservoir rock wettability, permeability and electrical properties. The contact between crude oil and rock is strongly dependent on the stability of an irreducible water film adsorbed on the rock surface not removed by vacuum/heat treatment. The existence of a stable water film, with the reservoir water-wet before the migration of oil, could affect the adhesion of the oil heavy end to rock surfaces. This could in principle be mediated by electrical double layer effects arising from the surface charges at the solid/water and water/oil interfaces.

In the case of crude oil, surface active polar and semi-polar compounds of O, N, and S contained in resins and asphaltenes are believed to play an important role in adsorption mechanisms with the rock mineral surfaces. The activation of crude oil surfactants by the aqueous phase at the oil/water/silica interface was studied by Brown and Neustadter, 1980. They showed that wettability, as indicated by contact angle, is strongly dependent on pH, interpreted as due to the activation of crude oil surfactant by the aqueous phase. The silica surface electric potential as shown by the electrokinetic zeta potential will clearly be a function of both pH and salinity, as will that of oil/water emulsion (Buckley *et al.* 1987).

Investigations into asphaltene precipitation have been impeded by a shortage of experimental data and information on precipitation mechanisms. Also, information on the properties of asphaltene colloidal particles in oil is not readily available. A detailed knowledge of asphaltene behaviour in oil reservoirs is required in order to understand any formation damage caused by it. An improved understanding of colloidal asphaltene behaviour is essential to predict its flocculation and adsorption/deposition in oil reservoirs. Research challenges in the colloidal asphaltene system for the last half a century have focused on how asphaltene is stabilised in petroleum reservoirs and relating this with the problems caused in reservoir formations and production facilities.

1.2 RESEARCH OBJECTIVES

The aims of the research project described in this thesis were first, to investigate experimentally, the adsorption mechanism of asphaltenes on reservoir rock surfaces under flow conditions, and second, to determine the particle size distributions during destabilisation of the asphaltene colloidal system. The general objective was to understand the asphaltene/rock adsorption characteristics and particle-particle aggregation kinetics in petroleum reservoirs. The particular objectives were :

- Critically examine the particle charge in non-aqueous dispersions,
- Determine the reservoir rock surface potential under flow conditions,
- Determine the influence of asphaltene adsorption on reservoir rock surface potential,
- Examine the formation damage caused by asphaltene adsorption,
- Effect of pores pressure and porosity on streaming potential and current measurements and related surface potentials.

- Effect of double layer overlap in non-aqueous system on rock surface potential measurements,
- Determine asphaltene particle size distributions in petroleum fluids.

1.3 APPROACH

The methodology designed to realise the objectives included two stages. The first stage is concerned with the formation damage caused by asphaltene adsorption on reservoir rock internal surfaces. To accomplish this, the initial step was to develop a new technique to determine the rock surface (zeta) potential under flow conditions without the surface conductivity error arising from a water film adsorbed on the rock surfaces.

The second stage involved the investigation of asphaltene particle size distributions in petroleum fluids. Wax cloud-point can also be investigated along with asphaltene particles by using the dynamic light back-scattering technique. The relative optical opacity of crude oil makes conventional light scattering measurements difficult. However, back scattering techniques, using dynamic laser light scattering (DLS) with optical fibre access can be used to give particle sizes and distributions. This can follow aggregation rates by introducing the laser beam (via fibre optics) if necessary through a thick window in a closed pressure cell.

1.4 ORGANISATION OF CHAPTERS

Chapter two introduces the current state of several aspects of asphaltene phenomena. The chapter emphasises various basic and applied aspects of research and investigation into asphaltene technology. The major topics discussed involve asphaltene chemistry, asphaltene-resin relationship, electrical properties of the

asphaltene/oil interface, asphaltene adsorption kinetics on mineral surfaces and theoretical aspects of asphaltene by molecular and thermodynamic approaches.

The definition and chemistry of colloidal asphaltene is discussed. The research technology used in defining the molecular structure of asphaltene has also been presented along with the history. Since resins play an important role in the colloidal stability of asphaltene in petroleum reservoirs it is necessary to review this relationship. The electrical charge of asphaltene has been suggested as important in its stability in petroleum fluids and has also been considered as a major factor in asphaltene deposition in reservoir formation and production facilities. The prediction of asphaltene flocculation onset in petroleum reservoirs has been widely investigated by using the equation of state approach and either molecular or colloidal thermodynamic models.

Chapter three reviews the theories of colloid science and the stability of particles in liquid dispersion. Also discussed in this chapter are the electrostatic forces that may be involved in colloid stability. This chapter explores the electrokinetic techniques used to measure the electrostatic potential of colloidal dispersions. This chapter also includes technique development used in determining rock surface potentials under petroleum fluids flow conditions

Chapter four discusses the basic principle of particle sizing by means of dynamic light scattering (DLS) technique. Due to the difficulty of making light scattering measurements in crude oil, this chapter introduces back scattering techniques using dynamic light scattering with fibre-optics to estimate particle size distributions in petroleum fluids.

Chapter five describes the details of all the apparatus and experimental procedure employed in this study. Firstly details the rock cores surface potential apparatus. Secondly it describes the electrode deposition of asphaltene under an electric field test. Thirdly a description of the particle size distribution apparatus. This

chapter also covers petrographic analysis, x-ray diffraction analysis and experimental error analysis.

Chapter six critically examines the particle charge in petroleum oil, the purpose here is to find out how important the particle charge is in a non-aqueous system. This will shed light on the mechanism of colloidal asphaltene stabilisation. Are asphaltene colloidal suspensions stabilised by electrical charge or not?. The chapter also, covers the investigation of the adsorption of asphaltene on reservoir rock surfaces by the streaming current method, this made possible by developing a novel method to estimate the rock cores pore area/length ratios by combining streaming potential and streaming current measurements as is described in Chapter 3 section 3.7. This is a necessary step before rock surface potentials can be calculated from observed streaming current measurements. Formation damage analysis caused by asphaltene adsorptions is also presented in this chapter.

Chapter seven investigates the effectiveness of pores pressure, hysteresis and rock pore sizes on streaming potential and current measurements and the related estimation of rock pores area/length and surface potentials. This chapter will present a theory for predicting the effect of double layer overlap in porous media. This theory will be supported by experimental data.

Chapter eight provides the investigation results of asphaltene particle size distributions in petroleum fluids under the influence of precipitant solvent and its adsorption on mineral particle surfaces by using the laser back scattering technique. Wax crystallisation (cloud-point) is also investigated.

Conclusions are given in Chapter nine. Several recommendations are made on aspects of colloidal asphaltene in petroleum reservoirs.

CHAPTER TWO

BACKGROUND TO ASPHALTENE PHENOMENA

2.1 INTRODUCTION

Asphaltene deposition has been a costly problem to oil producers around the world for many years. The nature of asphaltene has challenged many researchers, Nellensteyn (1924) and Katz and Beu (1945) were among the first to explore these substances. This phenomenon caused two kinds of problems to the petroleum engineers in general. For the reservoir engineers it means formation damage, but for the production engineers it means plugging in well bore, well tubing and surface equipment. Asphaltene deposition is a very serious problem to the oil companies because it causes a major economic and safety problems in production and processing.

Asphaltene deposition can occur deep in the reservoir, which constitutes formation damage. An example of this is the tarmat zone in the Minagish oil field in Kuwait (Osman, 1983), where asphaltene deposition is close to the oil water contact. This threatens the water drive mechanism advantage in oil production. Also asphaltene deposition has been found in some oil well tubing of deep reservoirs in Kuwait (Akbar *et al.*, 1989).

It is generally accepted (Leontaritis, 1988) that asphaltene coagulation and deposition happens as a result of changes in parameters such as reservoir pressure, reservoir fluid temperature and oil composition. It may also be influenced by the particle electrical charge (Preckshot *et al.*, 1943), (Lichaa, 1975,1977) and (Leontaritis 1989). Asphaltenes constitute the heavier and more polar (or, perhaps better, less non-polar) fractions of crude oil. The remaining fractions are resins and various aromatics.

The molecular weight of asphaltenes range from one thousand to several hundred thousand (Pfeiffer *et al.*, 1940) (Katz *et al.*, 1945).

This chapter provides a literature review on many aspects of the phenomena of asphaltene in petroleum reservoirs. The discussion is divided into three parts related to asphaltene chemistry. The first part covers asphaltene definition. The second part covers the asphaltene-resin relationship. The third part covers asphaltene electrical properties. The adsorption of asphaltene onto oil reservoir rock surfaces which could lead into reservoir formation damage and some of the asphaltene stability models in predicting flocculation (coagulation) will be also reviewed.

2.2 ASPHALTENE DEFINITION AND CHEMISTRY

Asphaltene fractions are defined operationally as that portion of a crude oil or bitumen which precipitates on addition of a low-molecular-weight paraffin (i.e. n-pentane, n-heptane) but which is soluble in toluene. Asphaltenes are brown to black amorphous solids with complex structures, involving carbon, hydrogen, nitrogen, oxygen and sulphur and are basically formed of condensed aromatic nuclei associated with alicyclic groups. The molecular weight of asphaltene ranges from one thousand to several hundred thousand with a particle density of approximately 1200 kg/m^3 and a spheroidal shape 30 to 65 Å in diameter (Witherspoon *et al.*, 1960).

For over a half century the composition, molecular structure and colloidal state of asphaltene in a crude oils and bitumens have been a matter of dispute among the scientific community with different descriptions of the state of asphaltene in crude oil including molecular entities dissolved in oil, as colloidal particles, or a combination of both. Nellensteyn (1924), described the nature of asphaltene as a colloid dispersion containing resins surrounding the asphaltene. By 1933, he suggested that the nuclei of what he calls asphaltene micelles contain microcrystalline graphite particles. Pfeiffer and Saal (1940) stated that asphaltenes consist of high molecular weight hydrocarbons of a predominantly aromatic character existing in a colloidal state.

In the 1950s, more work had been conducted on asphaltene complex structures using nuclear magnetic resonance (n.m.r.) and X-ray diffraction in which it was concluded that asphaltene consists of both aromatic and alkyl structures. Dickie and Yen in 1969 suggested that the asphaltene structural molecules are composed of n-alkyl moieties with islands of condensed aromatic disks. Varied information has been published concerning the association of metals with asphaltene. Ball *et al.* (1960), Dunning *et al.* (1960) and Eldib *et al.* (1960), all observed that asphaltenes contain trace of nickel and vanadium metals. They suggest that there is a relationship between the metal content and the nature of the asphaltene constituents in petroleum oil.

In the late 1970s Strausz and co-workers (Ignasiak *et al.,* 1977) investigated the degree of aromatic condensation in asphaltene colloidal structures, and concluded that the pericyclic aromatic condensation is lower than had been thought. By 1992 Strausz reported that petroleum asphaltenes were mainly derived from the catalytic cyclization, aromatization and condensation of n-alkanoates.

As indicated above, the nature of asphaltene fractions in crude oil has been a subject of numerous investigations. The actual physical constituents of the asphaltene fraction has proved to be difficult to define, because of the great complexity of the molecular structures. The chemical structure of asphaltene in crude oils has been investigated by a number of researchers. The common method used to investigate the structure of asphaltene are proton (^{1}H) and carbon (^{13}C) n.m.r. spectroscopy techniques to determine the average molecular composition of asphaltenes (Hasan *et al.,* 1985). ^{1}H n.m.r. spectroscopy has the limitation of a narrow range of chemical shift, resulting in difficulties in relating the results to the basic carbon skeleton. ^{13}C n.m.r. spectroscopy has become widely applied to characterise the average molecular structures of most petroleum heavy residues and coal derived liquids and can identify nitrogen, oxygen, and sulphur compounds. Figure 2.1 shows a hypothetical structure model of asphaltene. In this thesis no attempt will be made to elucidate further the molecular structure of asphaltene which will be seen as a dispersed soft solid. Rather the attempt will be made to investigate asphaltene adsorption on reservoir rock surfaces and its particle size distributions in petroleum fluids.

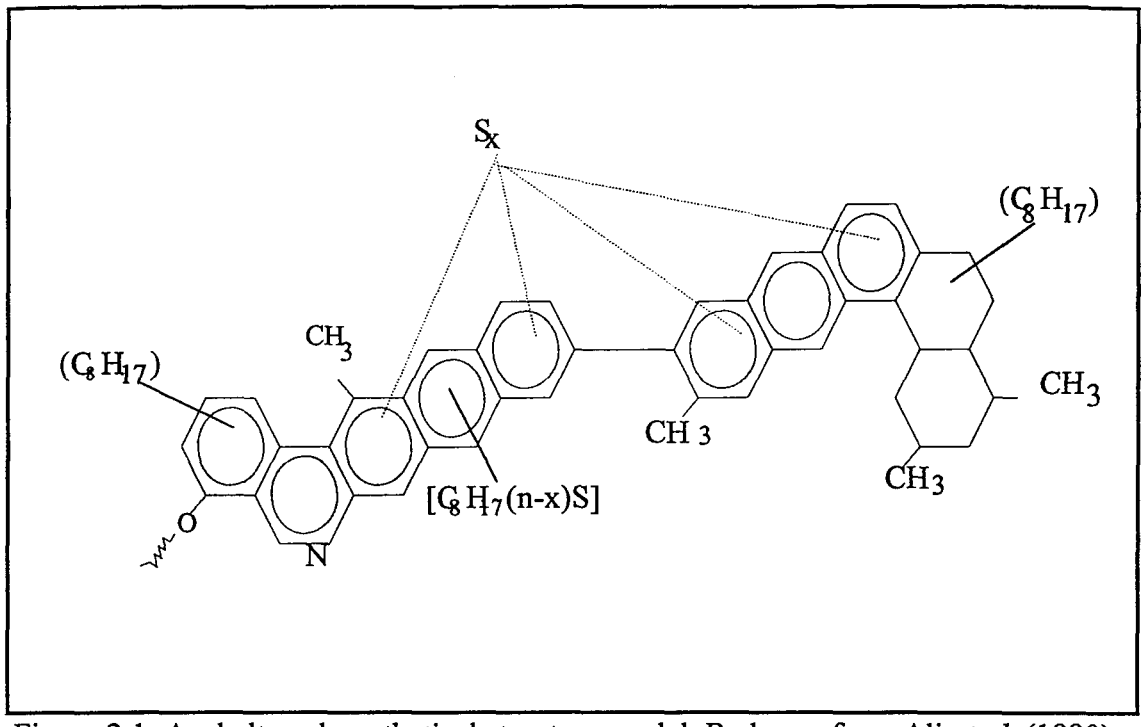

Figure 2.1. Asphaltene hypothetical structure model. Redrawn from Ali *et al.* (1990).

The aggregation of asphaltene particles has been studied by a number of researchers. Poindexter (1972) investigated aggregation and particulate motions in asphaltene colloidal suspensions using a dynamic nuclear polarisation (DNP) technique. This technique consists of examining the magnetic interaction between nuclei on diffusing solvent molecules and the free electrons present on a small portion of asphaltenes. He characterised asphaltene colloidal particle sizes in a variety of solvents. Poindexter concluded that asphaltene particle sizes are smaller in better solvents (for the asphaltene) and in such solvents expose more of the asphaltene proper.

Moschopedis *et al.* (1976) suggested in their work that intermolecular hydrogen bonding is involved in asphaltene association as reflected in the observed molecular weights. The intermolecular hydrogen bonds are present in the proton donor/acceptor asphaltene aggregates. If asphaltene needs to be dissolved (particle size reduced) in a solution phase a strong solvent is needed to break the intermolecular hydrogen bonds, as Poindexter reported in his work.

Other investigators studied the solubility of asphaltene in various solvents. Mitchell and Speight (1973) investigated the relationship between hydrocarbon solubility parameters and asphaltene solubility by comparing the weight of asphaltenes separated from Athabasca bitumen using different hydrocarbon solvents at 40 mole solvent to 1 mole bitumen ratios. Their results show that asphaltene precipitation can be correlated with physical properties as well as with the chemical structure of the solvents.

Nellensteyn (1933) found that the onset of asphaltene precipitation occurs on addition of a liquid having a surface tension below 24 mN/m (24 dynes/cm) at 25 °C, while the addition of a liquid having a surface tension exceeding 26 mN/m causes a total peptization. This implies that between 24 and 26 mN/m asphaltene flocculation or peptization may occur, though the whole concept is, to say the least, questionable.

2.3 ASPHALTENE-RESIN RELATIONSHIP

Petroleum resins have been defined as the fraction of oil not soluble in ethylacetate but soluble in n-heptane, toluene, and benzene at room temperature (Koots *et al.,* 1975). Resins have been investigated along with asphaltenes.

Sanchanen and Wassiliew (1927) reported that the molecular weight of resins depend upon the molecular weight of the crude oil and the nature of its formation. Mack (1932) considered that the resins are formed in the process of transformation of oils into asphaltenes either by air oxidation or by the direct influence of the elements oxygen and/or sulphur in the oil.

Witherspoon (1960) noted that resins are necessary to disperse the asphaltene in oil and thereby play an important role in the physical structure of petroleums and bitumens. Dickie and Yen (1967 & 1969) reported that resins play a crucial role in asphaltene aggregation and precipitation. Koots and Speight (1975) investigated the relationship of resins to asphaltene structures by separating asphaltenes and resins

from different Alberta crude oils and determining their elemental composition and molecular weights. They noted that asphaltene H/C ratios decrease relative to H/C ratio in resins indicating that aromatization is more advanced in asphaltene than resins. Also, that heteroatom elements in asphaltene structures are higher than in resins as shown in Table 2.1. Table 2.2 shows asphaltene elemental composition for different crude oils.

Table 2.1. Elemental analysis and atomic ratio of asphaltene and resin from Alberta crude oils.

Asphal&Resin Analysis			Elemental Analysis					Atomic Ratio			
API	Asph. w/w%	Asph. M.W.	C	H	O	N	S	H/C	O/C	N/C	S/C
16.5	12.9	6,669	81.91	8.11	1	1.18	7.8	1.19	0.009	0.012	0.036
34.8	0.9	4,251	88.49	8.21	1.38	1.61	0.31	1.11	0.012	0.016	0.001
22.8	11.7	3,782	82.79	7.52	1.58	2.14	5.97	1.09	0.011	0.014	0.025
27.4	6.4	3,602	85.71	7.81	1.3	1.36	5.82	1.09	0.011	0.014	0.025
40.1	2	2,669	86.5	7.74	3.05	1.3	1.41	1.07	0.026	0.013	0.006
API	Resin w/w%	Resin M.W.	C	H	O	N	S	H/C	O/C	N/C	S/C
16.5	38.4	863	81.94	11	1.45	0.51	5.1	1.61	0.013	0.005	0.023
34.8	12.2	786	86.06	11.9	1.06	0.48	0.5	1.66	0.009	0.005	0.002
22.8	16.5	802	84.37	10.82	1.12	0.43	3.26	1.54	0.01	0.004	0.14
27.4	14.3	821	85.15	11	0.54	0.28	3.03	1.55	0.005	0.003	0.013
40.1	9.9	851	86.91	11.46	0.96	0.21	0.46	1.58	0.008	0.002	0.002

This table reproduced from Koots and Speight (1975).

Table 2.2. Elemental analysis and atomic ratio of asphaltene from different crude oils.

Source	Elemental Analysis					Atomic Ratio			
	C	H	S	N	O	H/C	N/C	O/C	S/C
Saudia Arabia	81.1	8.6	6.9	0.5	2.9	1.27	0.0053	N/A	N/A
Kuwait	82.4	7.9	7.4	0.9	1.4	1.14	0.009	0.014	0.034
Iraq	78.9	8.1	12.2	0.7	0.2	1.2	N/A	N/A	N/A
Iran	83.8	7.5	5	1.4	2.3	1.07	0.014	0.021	0.022
Mexico	83	7.7	5.2	1.5	2	1.13	0.015	0.018	0.023
Venezuela	81.2	7.7	5.5	2.1	1.9	1.14	0.022	0.017	0.025

This table reproduced from Escobedo *et al.*, (1992) and Misbah-ul-Hasan *et al.*, (1988).

Ali *et al.* (1990) thought that the aromatic rings in asphaltene structures were a consequence of the condensation of resins with asphaltenes, taking this to be supported by an increase of aromatic carbons and aromatic non-bridge carbons as the temperature increased. All this seems unlikely.

2.4 ELECTRICAL PROPERTIES OF THE ASPHALTENE-OIL INTERFACE

As discussed earlier asphaltene flocculation may occur as a result of changes in thermodynamic parameters, such as reservoir pressure, reservoir fluid temperature and composition changes. However it is also commonly believed that it may affected by the particle charge, which is revealed by electrokinetic experiments.

Preckshot *et al.* (1943) were among the first to investigate the electrical charge of asphaltene particles. They proposed that asphaltene particles in crude oil possess a negative charge after observing their deposition onto the positive electrode when applying a field. They also thought that the streaming potential generated from crude oil flow actually precipitated asphaltene though this belief is not justified or supported by evidence.

Wright and Minesinger (1963) investigated the electrophoretic mobility of asphaltene in nitromethane. Nitromethane, selected in their study as the non-aqueous liquid, was based on van der Minne and Hermanie recommendations. Van der Minne and Hermanie (1952) had suggested that to measure the electrophoretic mobility of particles in non-aqueous solvents the suspending medium must have a minimum permittivity in the range of 10-15. The other advantages of the nitromethane are its low asphaltene solubility and availability of comparative electrophoretic mobility data. In their study asphaltene was obtained from 24 air-blown roofing asphalts and separated by n-pentane. All the 24 asphaltene samples were found to carry a positive electrical charge. Wright and Minesinger observed the following points to establish the validity of their conclusions:

* No particle migration was observed unless a potential was applied.
* The particles reversed direction upon reversal of electrical field.
* Asphaltene exhibited a positive electrophoretic velocity in a number of organic suspending liquids.
* There was no change in the electrophoretic mobility upon leaving the samples to stand for several weeks.

Lichaa (1975) investigated electrical effects on asphaltene deposition. His experiment involved mixing 200 ml crude oil containing asphaltenes with 200 ml diluent. The diluents chosen to reduce the sample viscosities were olive oil, Shell Donax T-6 transmission oil and refined oils derived from the Boscan crude oil and specified as oil 2 and oil 4. The mixed sample was placed in a 600 ml beaker. Stainless steel electrodes were placed in the sample at 2 mm spacing with 380 to 500 volts applied for a period of 3 to 5 days. The results showed asphaltene deposition to be found only on the negative electrode in the samples diluted with Shell transmission oil and olive oils, but no deposition were found in Boscan diluents oil 2 and oil 4. Lichaa proposed that because the Boscan crude oil contain 30% resins, they act as peptizing agents for asphaltene colloid particles and, as an adsorbed layer, mask what would otherwise be an electrokinetic effect.

In the present work a similar experiment was conducted using a Canadian crude oil and asphaltene deposition was also found on the negative electrode (Chapter 6, section 6.10).

Recently, Kokal *et al.* (1995) investigated the electrophoretic mobilities of asphaltene in an aqueous medium. They observed that asphaltene posses a negative charge at neutral pH. Rather unusually charge reversal was observed at high pH values for solutions. They explained the reversal in charge as due to the adsorption of positively charged multivalent ions to the negatively charged asphaltene surfaces. An increase in the ionic strength of the aqueous solution led to a decrease in asphaltene charge. This was no doubt due to the ionic strength effect on double layer

compression. The authors did not succeed in measuring the electrokinetic velocity of asphaltene in crude oil and low permittivity solvents.

Oil field experience has been held to suggest that the electric properties of asphaltene are relevant to the adsorption/deposition problems (Leontaritis *et al.*, 1988). Thus adsorption/deposition could be caused by asphaltene being electrically attracted to mineral or pipe surfaces that carry the opposite electrical charge. This has been investigated in the current thesis (Chapter 6).

2.5 ASPHALTENE ADSORPTION ON RESERVOIR ROCK MINERALS

Asphaltene adsorption/deposition on reservoir rock surfaces depends on the destabilisation of the asphaltene colloidal system, either by changing the chemical composition by diluting with solvent or changing the thermodynamic parameters (temperature and/or pressure). Any of them will affect the stability of the asphaltene colloidal system. The onset of asphaltene precipitation in petroleum fluid is the point at which asphaltene begins to separate and could result from, for example, reservoir acidation or the use of CO_2 injection for EOR (Enhanced Oil Recovery) projects. The suggested mechanism of asphaltene adsorption onto rock surface involves contact of the surface with crude oil, with the more polar parts of the asphaltene molecules oriented towards the surface and the non-polar portions oriented away from the rock surface (Kim *et al.*, 1990).

Asphaltene adsorption on petroleum reservoir rocks can have a strong role in wettability reversal and permeability reduction, described by reservoir engineers as formation damage (Crocker *et al.*, 1986), (Gonzalez *et al.*, 1991). Wettability is defined as "the tendency of one fluid to spread on or adhere to a solid surface in the presence of other immiscible fluids" (Craig, 1971). It can be interpreted as a measure of the affinity of the rock surface for the oil or water phase. Asphaltenes are considered to be lyophobic with respect to the low molecular weight paraffinic

hydrocarbons and lyophilic with respect to aromatics and resins (Newberry *et al.*, 1985).

Ramsden (1903) was among the first to observe the ability of solid particles or highly viscous matter to stabilise emulsions at the interface of two liquids. Menon and Wasan (1986) investigated the ability of a solid to stabilise emulsions through the adsorption of asphaltenes onto the surface. Their work investigated the influence of asphaltene adsorption onto the clay mineral sodium montmorillonite. It showed asphaltene adsorption to affect the contact angle at the water/oil/solid interface and the zeta potential of the solid particles. Menon and Wasan observed the isothermal adsorption density of asphaltenes in oil into sodium montmorillonite increased sharply at what they called the critical micelle concentration (CMC) point 0.55 g/l. A small amount of asphaltene adsorption changed the solid from hydrophilic to hydrophobic and the water contact angle was found to increase to 140°. The zeta potential at the clay/water interface showed no significant change with increasing asphaltene concentration.

Dubey and Waxman (1989) studied asphaltene adsorption on mineral surfaces. They concluded (not surprisingly) that the adsorption thickness of asphaltene decreased to some extent with increase in the solubility of asphaltene in the liquid phase used. Also, Dubey and Waxman claimed that the adsorption of asphaltene from nitrobenzene onto the clay surface was based on the electrical interaction between the clay as negatively charged and asphaltene as positively charged. The significant factors which control the adsorption of asphaltene on mineral surfaces were seen as:

* The presence, thickness, and stability of water films on the mineral surface.
* The chemical and structural nature of the mineral substrate.
* The contents of asphaltene and resin in the oil reservoir.
* The stability of asphaltene colloidal suspensions in the oil reservoir.

Gonzalez (1987) studied the adsorption of asphaltenes and resins from toluene solutions onto quartz and feldspar and the effect of this process on the electrical

properties of the minerals when interfaced with aqueous solutions. They observed that asphaltenes were adsorbed to a greater extent than resins and the adsorption of asphaltene and resins mixtures was found at least equivalent to the weight average of the adsorption of both components separately as shown in Figure 2.2. The electrophoretic mobility of both minerals in aqueous systems was not modified by the adsorption of both asphaltene and resins as shown in Figure 2.3, thus indicating that the adsorption layer on the mineral particles did not affect their surface charge, as Kokal *et al.* (1995) observed in their study.

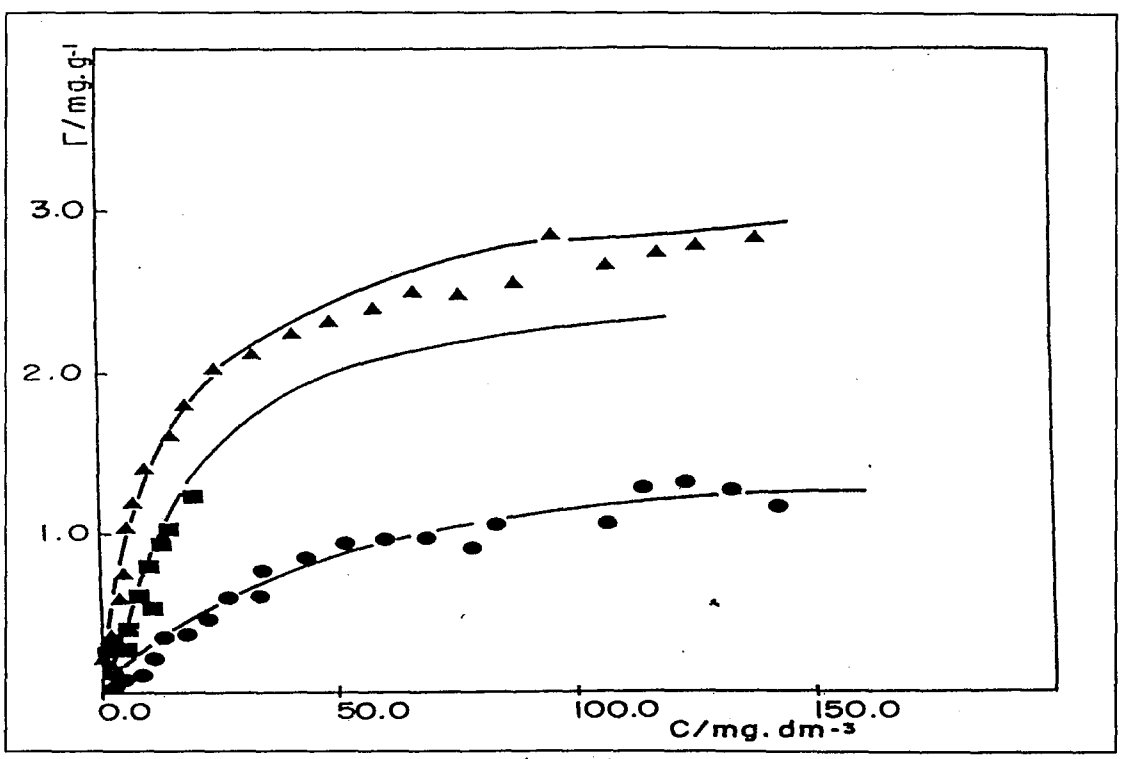

Figure 2.2. Adsorption of asphaltenes (▲), resins (■) and mixture of asphaltenes and resins on quartz (●) (After Gonzalez, 1987).

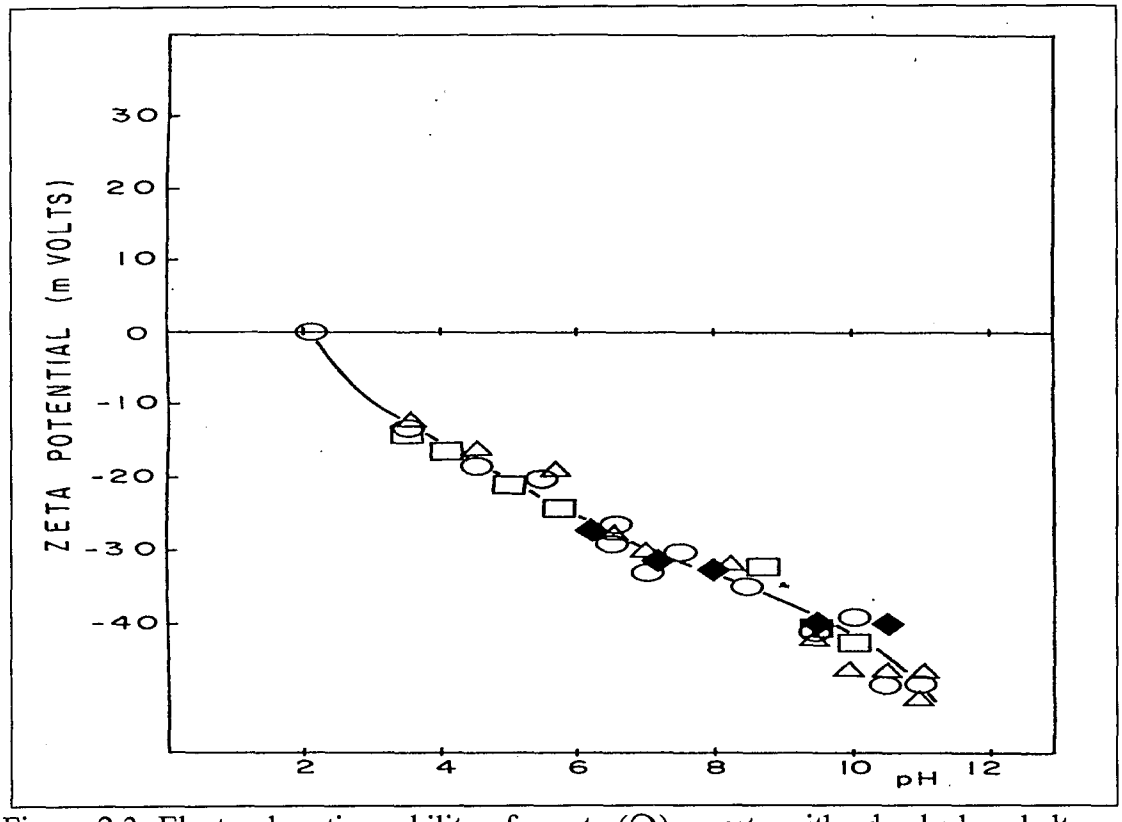

Figure 2.3. Electrophoretic mobility of quartz (○), quartz with adsorbed asphaltenes (◆) (Δ) and quartz with adsorbed resins (□) from two different Brazilian crude oils (After Gonzalez, 1987).

Alkafeef *et al.* (1995) investigated the adsorption of asphaltene on reservoir rock surfaces by a streaming current method under flow conditions. The surface potentials of reservoir rock cores in crude oil and hydrocarbon solvents were found to have small negative potentials. The negative surface potentials for the rock became steadily more positive as asphaltene coated the pore surfaces. The adsorption thickness of asphaltene on reservoir rock core surfaces was found to be a polylayer and not a monolayer as reported by Dubey and Waxman (1989) and Kokal *et al.* (1995). The rock formation damage agreed well with a petrographic analysis.

2.6 MODELS OF ASPHALTENE STABILITY

In 1940, Pfeiffer and Saal postulated that asphaltenes exist in bitumens as a colloidal dispersion. Later, in 1957, Witherspoon *et al.* agreed from their

ultracentrifuge study of Illinois crude oil that Pfeiffer and Saal's model for bitumens is also applicable to crude oil. Recently a new model has been developed by Leontaritis and Mansoori (1987) who revived and utilised a thermodynamic-colloidal model for predicting the phase behaviour of asphaltene. The differences between the Pfeiffer-Saal and Leontaritis-Mansoori models are in the natural state of asphaltene, i.e. of whether asphaltenes are monodisperse or polydisperse in oil. Recent researchers have generally agreed that asphaltenes in oil are polydisperse (Kawanaka *et al.*, 1988).

From the general information gathered by various researchers through the years, the following can be concluded:

* Asphaltene particles are surrounded by resins which act as colloid stabilising agents. The surround of resins is caused by the asphaltene kernel's attractive forces (van der Waals) forming a stabilising protective layer (shield). This stabilisation is due to the repulsive interaction between molecules adsorbed (resins) on the surface of neighbouring suspended particles (asphaltene); this phenomenon is an example of "steric stabilisation".
* Asphaltene particles carry a (very) small electrical charge in most crude oils and similar non-polar media. Any charge depends on the source of the oil.

2.6.1 Molecular-Thermodynamic Approach

Fussel (1979) studied the phase behaviour of asphaltic systems using a Redlich-Kwong model to calculate vapour-liquid and liquid-liquid equilibrium phase behaviour of asphaltic oil. Fussel concluded that asphaltene precipitation arises from separation into a heavy-liquid phase (asphaltene), a light-liquid phase and a vapour phase. Following that study, Hirschberg *et al.* (1984) proposed asphaltene entities as monodisperse polymeric molecules. A new approach was developed by Kawanaka-Mansoori (1988) to extend Hirschberg's work, in which they considered asphaltene to be in a polydisperse state. The difference between the Hirschberg *et al.* and

Kawanaka-Mansoori models is that the asphaltene separation in Hirschbergs' model is seen as a liquid-liquid phase equilibrium, whereas the Kawanaka-Mansoori's model it is seen as solid-liquid phase equilibrium. The question arising in the predicting of asphaltene flocculation in the molecular thermodynamic approach, taken into consideration the effect of resins on asphaltene phase behaviour, is the validity of the reversibility or irreversibility of asphaltene flocculation under the changing thermodynamic state.

2.6.2 Colloidal Approach

Leontaritis and Mansoori (1987) studied asphaltene flocculation by developing a thermodynamic colloidal model (T-C model) for predicting asphaltene phase behaviour. This model is based on their assumption that asphaltene exists in oil as solid particles in colloidal suspension, and that these particles are stabilised against further aggregation by resins adsorbed onto their surface which constitute a steric-entropic barrier. In addition there could in principle be other repulsive forces between asphaltene particles because of their similar electrical charge. These repulsive forces might be disturbed by pressure changes, Figure 2.4.

The T-C model used an equation of state approach to calculate where asphaltene might separate. They also studied resin concentration in the liquid phase by a calculation based on determining the split of peptizing agent (resins) between oil and asphaltene phases. They concluded that when the resin chemical potential in the liquid fell below a critical value, the colloidal asphaltene particles were at least partially uncovered so that flocculation could occur. This calculation was based on the Flory-Huggins statistical thermodynamic polymer theory.

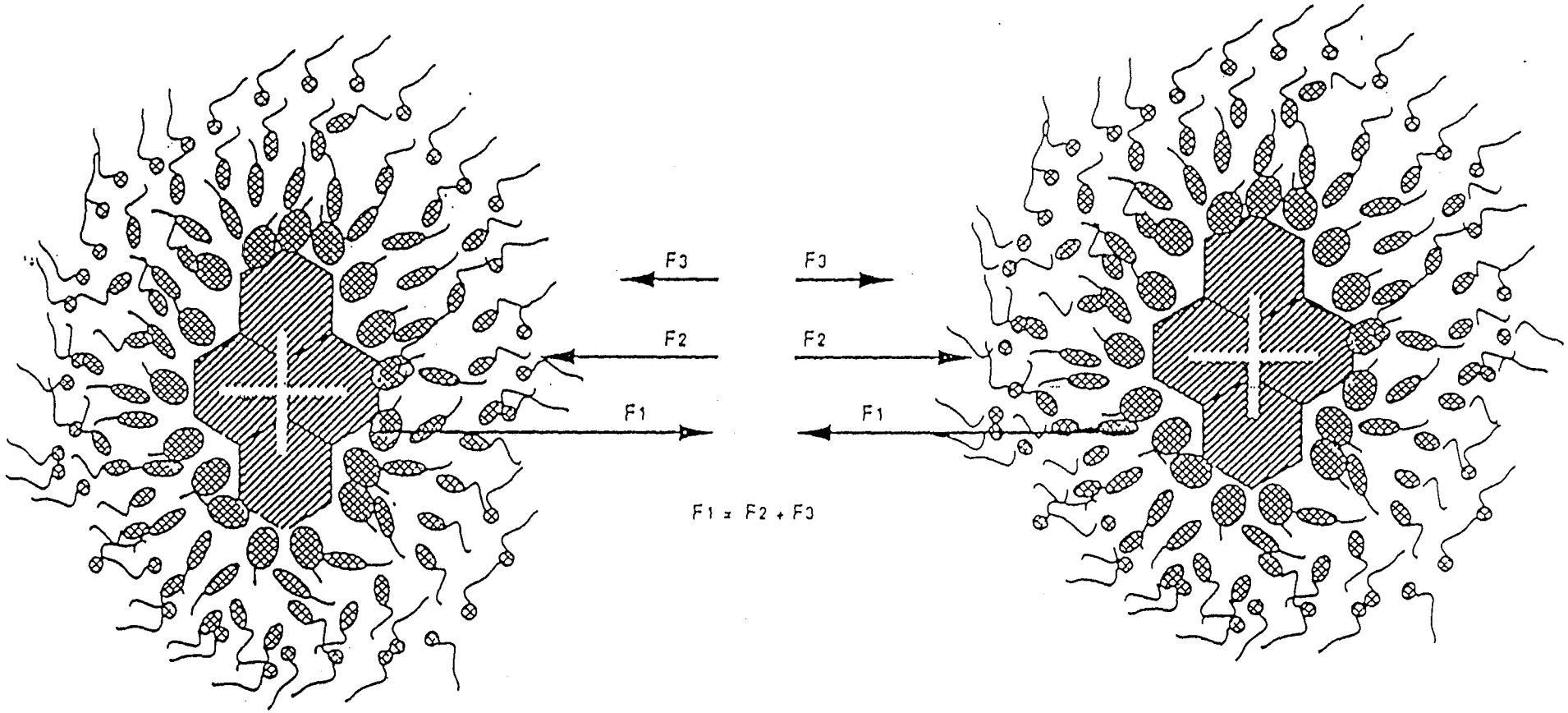

Figure 2.4. Force Balance on asphaltene micelles showing the effect of the electric charge (F1= attraction of asphaltene kernels, F2= steric repulsion of peptizing layers, F3=electrical repulsion due to the similar charges). After Leontaritis (1989).

2.7 SUMMARY

The major findings by past workers on asphaltene phenomena can be summarised as follows:

- Asphaltenes are a constituent of the heavier and less non-polar fraction of crude oils, which contain a variety of elements (C,H,N,O,S) and metals, particularly vanadium and nickel.
- Asphaltene are composed of alkyl moieties and condensed aromatics with molecular weights in the range of several hundred to several thousand.
- The asphaltene fraction is defined as being insoluble in n-alkanes, such as n-pentane and n-heptane, but soluble in toluene.
- Most workers agree that asphaltenes exist in crude oil as a colloidal dispersion though it is not clear whether it is a liquid/liquid (emulsion) or solid/liquid (colloidal suspension). [The present author prefers to think of asphaltenes as soft solids]
- Resins play a crucial role in asphaltene colloid stability.
- The H/C ratio in asphaltene is less than in resins and this indicates greater aromatization in asphaltene.
- Hetero-atoms proportions increase in asphaltenes relative to resins.
- Asphaltene possesses an electrical charge in oil, found to be positive though this depended on oil sources (in the present work the electrical potential is found to be very small in these circumstances and almost certainly negligible).
- Asphaltene electrical charge in water was found to be negative and the adsorption of asphaltene on mineral particles found not to effect the zeta potential of the particles in water.
- Asphaltene adsorption thickness was found to be multilayer.

CHAPTER THREE

THE COLLOID CHEMISTRY OF NON-AQUEOUS DISPERSIONS

3.1 INTRODUCTION

The particles in a colloidal dispersion are thermodynamically unstable owing to their excess surface free energy. However, this energy will be reduced by the aggregation which reduces the exposed surface area. Aggregation can lead to reversible loosely bound structures (flocs), or can produce irreversible structures (agglomerates). The latter may produce a thick deposit material giving irreversible separation of the two phases.

The stability of a colloid dispersion can be defined as its resistance to flocculation or coagulation. The degree of the "resistance" is used as a measure of the dispersion stability. Colloidal asphaltene can be considered physically stable in petroleum reservoirs as a result of the resins present when no deposition problems occur. A principal cause of aggregation is the van der Waals attractive forces between the particles. To promote stability a repulsive force must be present of sufficient range to overcome the van der Waals attraction. Such a force could in principle arise from electrical double layer overlap or from of steric repulsion.

So-called lyophobic sols are stabilised entirely by electric double layer interactions. The DLVO theory [Deryagin-Landau (1941) & Verwey-Overbeek (1948)] was developed to predict the behaviour of such dispersions from an understanding of the attractive and repulsive forces between adjacent particles. However, the applicability of the DLVO theory in understanding the behaviour of

colloidal asphaltene in petroleum reservoirs must be treated with caution, since the theory was not developed for the deposition of crude oil heavy ends, like asphaltene. Using the theory involves the measurement of the zeta potential of colloids, whereas in the crude oil case it is difficult to measure the zeta potential, due to the low permittivity and high viscosity of crude oil. Moreover, as will be shown in chapter six, electric charge is ineffective at producing a repulsive barrier in such crude oil or solvents.

3.2 THE NON-AQUEOUS DISPERSION

A non-aqueous dispersion is defined as one in which the liquid phase is other than water. The non-aqueous dispersions involved in this work are in non-polar liquids similar to hydrocarbons, with some exceptions to such as methanol. The polarity of a dispersion medium is usually measured by the relative permittivity of the liquid. Hydrocarbon solvents such as toluene, benzene and n-pentane have permittivity values at 2.4, 2.28 and 1.84 respectively, and this can be considered as non-polar whilst acetone, methanol and nitromethane have values of 21.4, 32.6 and 39.4 respectively and can said to be semi-polar (Inter. Critical Tables *edt.* Washburn, 1929). The relative permittivity for water has a value 78.3 and this is certainly polar.

The polarity of dispersions is important in understanding their stability and behaviour arising from the attractive and repulsive forces between the adjacent particles. For lyophobic sols inter-particle repulsion is assessed by zeta potential measurements and applying the DLVO theory. In the hydrocarbon case this is difficult. Several attempts, by a number of researchers, have been made to determine the zeta potential of particles in crude oil and/or hydrocarbon solvents (Kokal *et al.*, 1995), though with little success (Miller *et al.*, 1992).

It can be seen that the nature of colloidal asphaltene in crude oil differs considerably from a dispersion in an aqueous system. Asphaltene exists as a non-polar dispersion in petroleum crude oil, and measurements of its particle charge in

petroleum reservoirs are not readily available. Particle electric charge may or may not be significant, therefore a method is required to determine asphaltene zeta potential in crude oils. This method also, will help to understand asphaltene adsorption kinetics on reservoir rocks.

3.3 THE ELECTRIC DOUBLE LAYER

When a solid is immersed in an electrolyte, any possible charging mechanisms lead to what is called the electric double layer. The electric double layer consists of two regions: the compact region and the diffuse region. In the absence of adsorption the compact or stern region is empty of the centres of ions, whilst the outer diffuse region consists of similar charge (co-ions) repelled away from the surface and counter ions attracted in. The excess charge residing on the solid surface must be exactly balanced by an equal charge of opposite sign on the solution side. Ions from the solution phase may approach the surface only so far as their solvation shells will allow. This constitutes the compact part of the double layer. When there is specific adsorption of ions from solution these are seen as entering the compact layer and probably dehydrated, Figure 3.1.

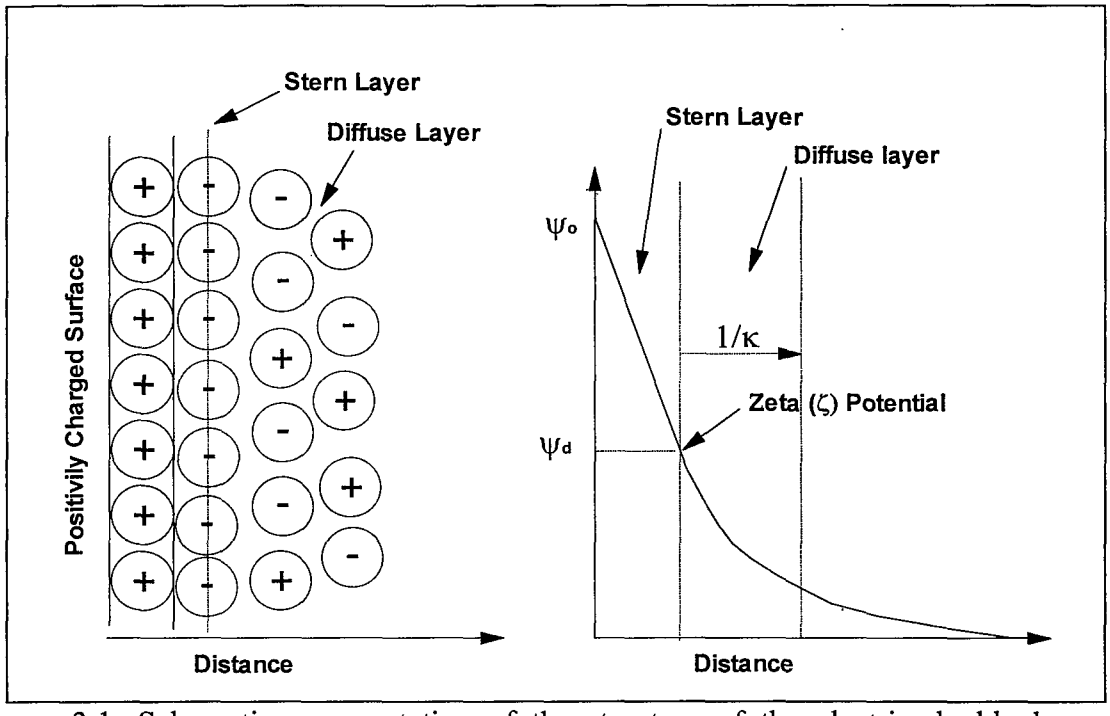

Figure 3.1. Schematic representation of the structure of the electric double layer according to stern's theory.

The theory of the diffuse part of double layer was developed independently by Gouy (1910) and Chapman (1913). They considered a plane charged surface to consist of a uniform charge, and the potential distribution outside this surface to be described by the Poisson equation.

$$\frac{d}{dx}\left(\varepsilon\frac{d\psi}{dx}\right) = -\rho \tag{3.1}$$

Where ψ is the electrostatic potential, ε is the permittivity and ρ is the volume density of charge. The distribution of ions (considered as point charges) about the charged surface is described by the Boltzmann relation.

$$n_i = n_i^{\infty} \exp\left[\frac{-z_i e\psi}{kT}\right] \tag{3.2}$$

The combination of Poisson and Boltzmann equations can be solved analytically for a flat double layer. If the assumption of Gouy and Chapman is used,

namely, that the surface can be treated as a mathematical plane of uniform "smeared out" charge with ε independent of distance x, then the distribution of potential from the surface is given by equation (3.3):

$$\varepsilon \frac{d^2\psi}{dx^2} = \sum_i z_i e_i n_i^{\infty} \exp(-z_i e\psi / kT) \tag{3.3}$$

Where:

$\psi(x)$ = The potential at a distance x from the surface.

z_i = The valency of ion i, (sign included).

e = The elementary charge.

n_i^{∞} = The number of ions i per cm^3 in the bulk of the solution.

k = Boltzmann's constant.

T = The absolute temperature.

For low potentials only:

$$\psi = \psi_o \exp(-\kappa x) \tag{3.4}$$

Where:

ψ_o = The wall potential.

ψ = The potential at distance x from the surface.

κ = The Debye-Hückel reciprocal distance.

$$\kappa^2 = \frac{e^2 \sum_i n_i z_i^2}{\varepsilon kT} \tag{3.5}$$

There are a several important assumptions in the Gouy-Chapman version of the Poisson-Boltzmann equation:

* The charged surface is assumed to be flat, of infinite extent and uniformly charged.
* The ions in the diffuse layer are point charges, distributed according to the Boltzmann equation.
* The liquid influences the diffuse layer only through its permittivity, which is constant throughout.

In a non-aqueous system like crude oil the diffuse layer thickness is much greater than in aqueous systems as a result of the much lower concentration of charge carriers, itself due to lower values of the liquid permittivity. Estimation of the diffuse layer thickness $\frac{1}{\kappa}$ in non-aqueous systems really requires a knowledge of the charge carriers present but, making the assumption that these are singly charged, an estimate can be made, based on the measured solvent electrical conductivity. This will be discussed in chapter seven in connection with applying a theory for the double layer in narrow capillaries.

The electrokinetic (zeta) potential (ζ) is considered to be the potential at the surface of shear sometimes inappropriately called the "slipping plane" parallel to the actual phase boundary but displaced somewhat into the liquid. In aqueous systems there is good evidence that $\zeta = \psi_d$, at least at low potentials. In aqueous systems it will be at least the diameter of a hydrated ions away from the particle surface. In non-aqueous systems the electric potential decay with distance is much smaller, therefore the zeta potential (and ψ_d) are close to the surface potential., Figure 3.2.

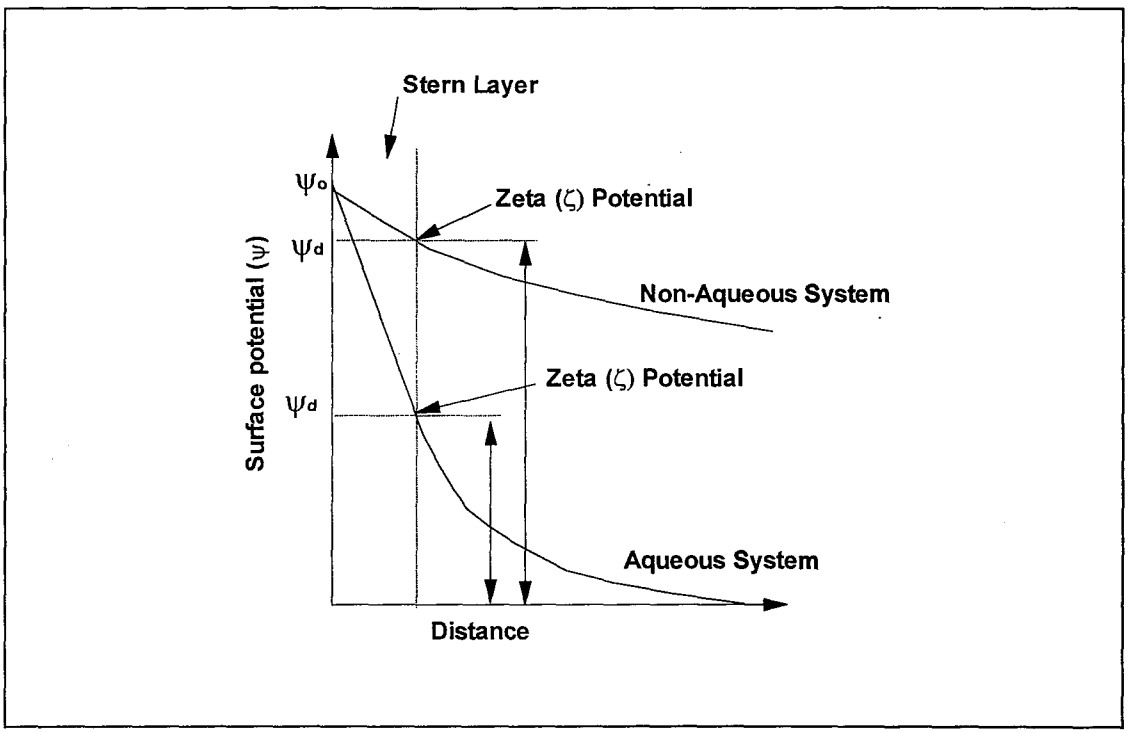

Figure 3.2. Double layer potentials in aqueous and non-aqueous systems.

3.4 THE ORIGIN OF SURFACE CHARGE

The electrical charge on a particle in suspension can play a role in it stability. The zeta potential and, from it, the electric charge can be obtained by electrokinetic techniques. There are several factors involved in charge production:

* Nature of the particle.
* Medium polarity.
* Surfactant content in the system.
* Water content in the system.

The surface charge of particles in non-polar media such as crude oil or hydrocarbon solvents is considered to be due to either proton or electron transfer/adsorption mechanisms. The general mechanism of charge generation in the absence of surfactant is through the dissociation of surface groups with either a proton being accepted or donated. In the colloidal asphaltene case, the presence of an

electrical charge on asphaltene as determined by microelectrophoresis (Wright *et al.*, 1963) and streaming current (Alkafeef *et al.*, 1995) provide little information as to the source of the charge. Winniford (1960) has postulated that asphaltene has many electronegative sites which are capable of strongly attracting a proton, e.g.,

$$-OH, = C = O, = N -$$

Wright and Minesinger (1963), speculate that the presence of asphaltene electrical charge as determined by microelectrophoresis in nitromethane may be due to one of the three sources:

* Interaction of asphaltenes with the nitromethane in such a way as to produce a charge through ion formation.
* Formation of charged molecular complex of asphaltene and aromatic molecules of the maltenes.
* The presence of trace metals in asphaltenes which may exhibit charge under the experimental conditions employed.

Wright and Minesinger speculated the positive charge of asphaltene in nitromethane was due to the dissociation of nitromethane as follows,

$$CH_3 - N\begin{matrix}//O\\ \backslash O\end{matrix} \xrightarrow{-H^+} \left[-CH_2 - N\begin{matrix}//O\\ \backslash O\end{matrix} \leftrightarrow CH_2 = N\begin{matrix}/O-\\ \backslash O\end{matrix} \right]$$

Kokal *et al.* (1995) observed that asphaltenes exhibit negative charge in aqueous NaCl solution. A charge reversal was observed at high pH in $CaCl_2$ and synthetic brine solutions. They speculated that the brine as well as the $CaCl_2$ contains other divalent cations, and in each case the charged reversal is brought about by the adsorption of oppositely charged multivalent ions (Ca^{2+}, Mg^{2+}) to the negatively charged asphaltene surface.

Eldib *et al.* (1960) showed that asphaltene contained vanadium and nickel metals ranging from 26.5 to 337 ppm. In another study by Eldib (1962) the migration velocity in electrophoresis increased with vanadium and nickel content in nitrobenzene. However, these results did not prove that the migration was due to the metal present.

The question of whether the surface accepts a proton and becomes positive or loses it to become negative will depend upon the relative acidity (in the Brönsted sense) of the surface relative to the liquid. The results of Labib and Williams (1984,1985) show that dry mica in nitromethane exhibits a positive charge. The addition of a small amount of water reversing its charge. Labib and Williams also indicate the importance of potential difference which could be developed when two metals brought into contact. They observed an enthalpy change when a solid was placed in contact with a liquid of lower "electron donicity" resulting in a positive surface charge.

In practice petroleum oils usually contain traces of water. Lyklema (1968) suggests that the presence of trace amounts of water in non-aqueous dispersions will adsorb tenaciously at the solid interface, where it influences the surface dissociation (and hence the surface potential), the surface conductance (and hence the electrokinetic properties) and competes with the adsorption of other molecules, thus indirectly affecting the stability, either favourably or unfavourably. This is supported by Labib and William (above) in the reversal of mica charge in the presence of water. Miller *et al.* (1992) observed that calcium carbonate particles can exhibit a significant zeta potential when dispersed in non-polar hydrocarbon media. In aromatic hydrocarbon media the surface potential of the particles was found to become more negative with time and, for toluene at least, an increase in the water concentration, Figure 3.3.

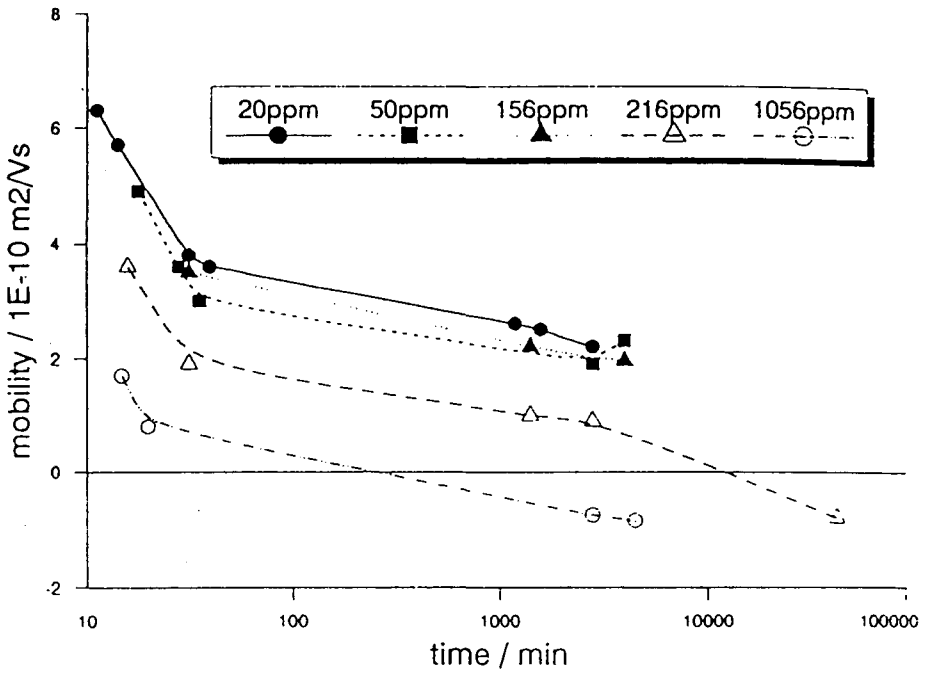

Figure 3.3. Temporal variation of electrophoretic mobility for calcium carbonate particles in toluene containing various concentrations of water. (After Miller *et al.* 1992)

In the present work asphaltene was found to have a small positive potential in pentane, toluene, isopar-h and crude oils as determined by streaming potential and current methods. The asphaltene particle charge in acetone was found to be negative (see Chapter six).

3.4.1 Electrostatic Repulsion

When two particles bearing a surface charge approach one another they are subject to a repulsion if the charges are of the same sign. This repulsion is due to the interaction of the double layers surrounding the particles and from the theory of the

double layer it is possible to evaluate the potential energy of interaction. There are two mechanistic model for this interaction.

* The constant surface potential model: When the surface potential is the result of the adsorption of potential-determining ions, the surface potential remains constant on approach and a reduction in surface charge density must therefore occur.
* The constant surface charge model: When the surface charge is the result of ionisation, the surface charge density may remain constant and the surface potential increased as the particles approache.

These differences only appear at short separations and are therefore less important in non aqueous situations than in aqueous ones.

3.4.2 The London-van der Waals Attractive Forces

The attraction between neutral atoms was introduced in 1873 by van der Waals. Later London (1930) considered the energy arising from the rapidly fluctuating dipole moment generated in a neutral atom. The fluctuating dipole in one atom momentarily polarises another one in the sense that the two atoms attract each other. The attractive potential energy found by London varies inversely as the sixth power of their distance of separation. The total interaction energy between two colloid particles (Hamaker, 1937) is large enough to compete with the double layer repulsion. This mechanism would be expected to play an important part in the stability of colloids. Hamaker (1937) considered the London forces to be pairwise additive, so the interaction energy between two collections of atoms is both significant and of long range. Hamaker relations all contain a constant, A, dependent on the nature of the two interacting materials and now widely known as the Hamaker constant. It is defined as;

$$A_{11} = \pi^2 q_1^2 \beta_{11} \qquad (3.6)$$

Where q_1 is the density of atoms in the colloidal particle and β_{11} is the constant in the London equation. When a particle of material 1 interacts with one of material 2 across a vacuum the effective Hamaker constant A_{12} is the geometric mean of the 1:1 and 2:2 interaction i.e;

$$A_{12} = A_{11}^{1/2} A_{22}^{1/2} \tag{3.7}$$

If there is a medium 3 between the particle then;

$$A_{132} = \left(A_{11}^{1/2} - A_{33}^{1/2}\right)\left(A_{22}^{1/2} - A_{33}^{1/2}\right) \tag{3.8}$$

This expression for A_{132} reveals the perhaps unexpected result that, if A_{33} lies between A_{11} and A_{22} then the product on the right hand side is negative which mean that the van der Waals interaction is in that case a repulsion !. If the effective Hamaker constant is written as A then for two semi infinite plates the interaction energy (V_A) becomes:

$$V_A = -\frac{A}{12\pi H^2} \tag{3.9}$$

Where H is the separation of the surfaces. For two sphere of equal radius;

$$V_A = -\frac{A}{6}\left[\frac{2}{S^2-4} + \frac{2}{S^2} + \ln\frac{S^2-4}{S^2}\right] \tag{3.10}$$

For two such spheres at short separation this latter reduces to,

$$V_A \cong -\frac{Aa}{12H} \tag{3.11}$$

Where:

S is the ratio r/a.

r is the separation of the spheres centers.

a is the sphere radius.

At large separation it reduces to,

$$V_A \propto -\frac{1}{r^6} \qquad \text{as for atoms} \qquad (3.12)$$

As London-van der Waals forces are essentially of electrical origin, a certain time is necessary for their propagation, and it is expected that if the time of travel of an electromagnetic wave from one atom to another is of the same order or larger than the time of the electronic fluctuations then the London-van der Waals forces will be smaller than that given by London. Casimir and Polder (1948) found that with increasing the distance the energy decreases from the inverse 6th power into an inverse 7th power. Schenkel and Kitchener (1960) derived an approximate expression to obtain an equation for the particle-particle interaction energy:

$$V_A = -\frac{A_{12}a}{\pi}\left[\frac{2.45\lambda_o}{120H^2} - \frac{\lambda_o^2}{1045H^3} + \frac{\lambda_o^3}{5.62x10^4 H^4}\right] \qquad (3.13)$$

where λ_o = London wavelength.

This is a good approximation for $H > \frac{1}{6}\lambda_o$. The difficulty in calculating the van der Waals interaction between particles is that of evaluating the Hamaker constant, A. There are two methods available to calculate Hamaker constant. The first is based on the assumption of pairwise additivity of intermolecular dispersion forces as described by Hamaker. The second makes use of the "macroscopic" approach by Lifshitz. In the latter method of Lifshitz, the interacting particles are treated "macroscopically" and characterised by frequency dependent complex permittivities. The attraction is seen as due to a fluctuating electromagnetic field in the gap, arising from spontaneous electric and magnetic polarisations within the media. The correlation between the fluctuation fields in the two bodies decreases the free energy of the system and thus constitutes attraction.

3.4.3 The Total Potential Energy Curves and The Stability of Colloids

The total potential (free) energy curves (V_T) are produced by the summation of the double layer repulsion energy and the van der Waals attraction energy.

$$V_T = V_R + V_A \tag{3.14}$$

The DLVO theory treats colloid stability as related to the total interaction energy, this being based on the existance of a potential energy barrier between colloid particles. The repulsive potential energy depends upon both the surface potential of the colloidal particles and the concentration of the electrolyte. This energy decreases exponentially with the distance between particles. At high surface potential and low electrolyte concentration this energy barrier is high and leading to dispersion stability. For the particles to come together the combined effects of Brownian motion and van der Waals attraction must overcome this repulsive barrier. The total potential energy curve can show a maximum (V_{max}) for two particle at a certain separation distance, Figure 3.4.

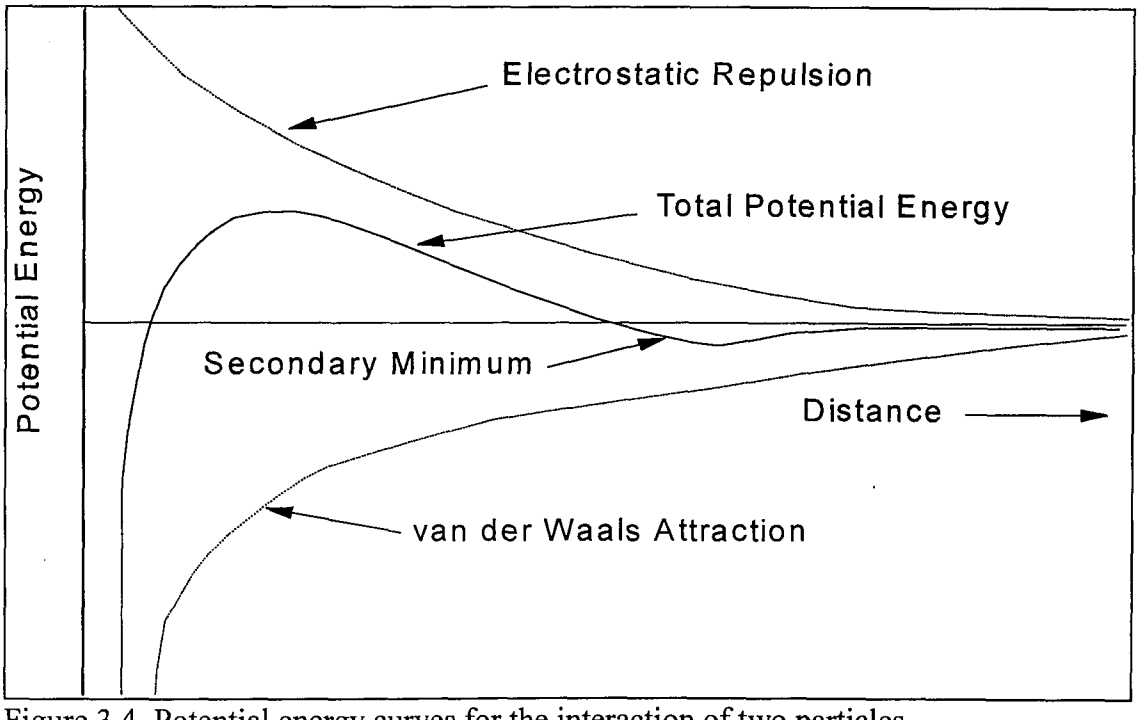

Figure 3.4. Potential energy curves for the interaction of two particles.

The dispersion will be stable so long as V_{max} is much larger than the thermal energy kT of the particles. Verwey and Overbeek estimate a value of 15kT to constitute a stability against coagulation. If there is no potential barrier then the resulting colloid will be unstable and rapid coagulation occurs. Verwey and Overbeek showed that a further potential energy minimum in aqueous systems, called the "secondary minimum", might develop for large particles, where these particles are weakly attracted. This arises from the fact that the double layer repulsion energy falls off exponentially and therefore more rapidly than the van der Waals attraction energy. Coagulation into this minimum is reversible. This effect is less important in non-aqueous systems, where the double layer repulsion (if it exists) is longer range.

3.5 STERIC STABILISATION IN NON-AQUEOUS DISPERSION

Macromolecules/polymers can have either a stabilising or flocculating effect in dispersions into which they are introduced. The flocculating effect occurs especially when the polymer adsorbs on the particle surfaces but is present in quantities which are insufficient to cover the surfaces completely. Then a given polymer molecule can adsorb on more than one particle thus "bridging" two or more small particles together resulting in flocculation.

Even a polymer which does not adsorb on the particles can cause (a weak) flocculation. This is most easily seen as due to an osmotic pressure tending to force the particles together and is called "depletion flocculation". However polymers are, under appropriate conditions, effective at producing repulsion between particles and hence dispersion stability. Where this occurs it has the advantage of being relatively resistant to electrolyte addition and in particularly suitable for non-aqueous dispersions where double layer repulsion does not occur because of the absence of a charging mechanism.

For this type of polymer stabilisation of dispersion to occur:

- The polymer has to adsorb on the particles.
- The dispersion medium has to be a "good solvent" for the polymer so that the chains are extended and freely moving.

These two conditions are to an extent contradictory. Thus polymers are chosen for dispersion stabilisation in which there is an adsorbing part and, separately, a dissolving part of the molecule e.g. a block co-polymer of the AB or ABA type, Figure 3.5. The freely dissolved chains then give a repulsion when similar particles approach, Figure 3.6.

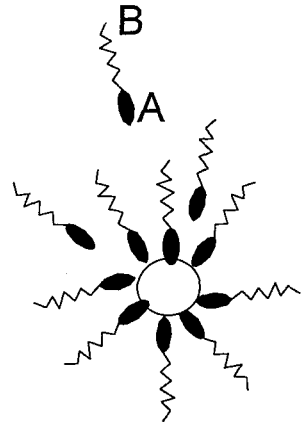

Figure 3.5.

The overlap region has a higher concentration of polymer and so produces an osmotic repulsion, Figure 3.6. The thermodynamic constituents of this positive free energy (repulsion) can be a positive enthalpy (ΔH) of overlap or a negative entropy (ΔS), such that:

$$\Delta G = \Delta H - T\Delta S \qquad (3.15)$$

The negative entropy of overlap can easily be seen since restriction of polymer chain freedom will occur which is therefore a decrease in entropy.

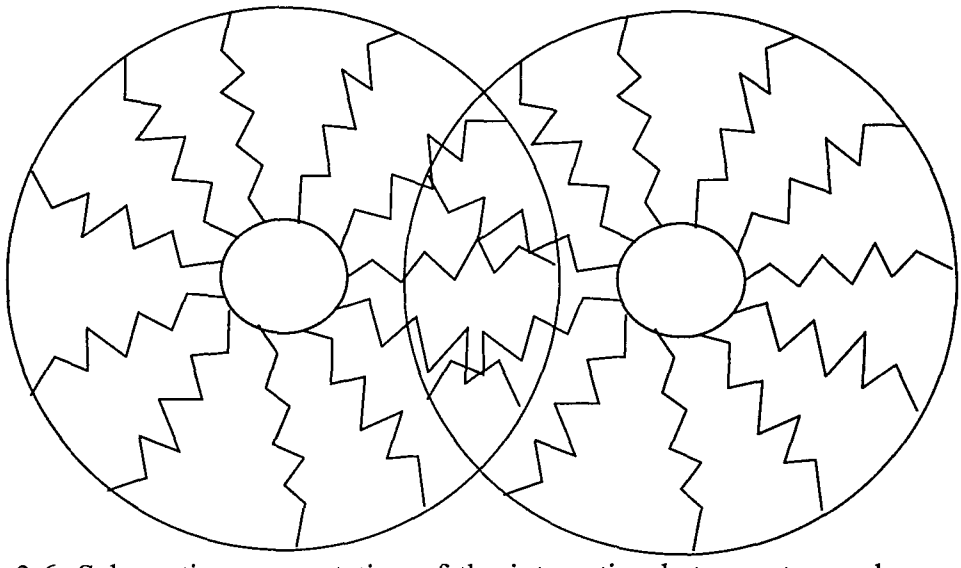

Figure 3.6. Schematic representation of the interaction between two polymer coated particles on approaching each other.

In this work the molecule choosen to give steric stabilisations in aliphatic/crude oil situations was 2-hexadecyl napthalene (HN):

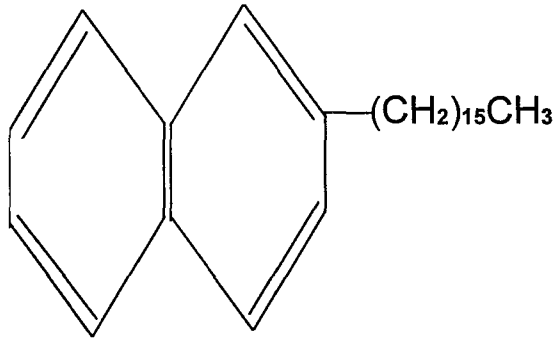

Figure 3.7. 2-hexadecyl napthalene

The hexadecyl chain will be in a good solvent in the alphatic oil and so will be in an extended state, most effective at promoting steric repulsion. The naphthalene group was chosen:

- because it is flat and hence, other things equal, it will have maximum adsorption on a surface.

- because the π electrons of the napthalene molecule will render it more polarisable with a high Hamaker coefficient and hence be more strongly adsorbed.

The preparation of 2-hexadecyl napthalene is outlined in Chapter 5 section (5.8.B).

3.6 ELECTROKINETIC PHENOMENA

Electrokinetics is the name given to study of phenomena resulting when a tangential electric field interacts with a charged surface immersed in electrolyte solution. There are four electrokinetic techniques all yielding, in principle, the same information. They can be classified as follows:

A- Applying a known electromotive force (e.m.f.):

1. ***Electrophoresis:*** Measure the movement of charged particles through stationary liquid (electrolyte medium).
2. ***Electro-osmosis:*** Measure the movement of liquid past a stationary solid.

B- Measuring the potential difference, produced by:

1. ***Streaming potential:*** Movement of liquid past a stationary solid.
2. ***Sedimentation potential:*** Movement of charged particles through a liquid (Dorn effect).

The electrokinetic behaviour depends on the potential at the surface of shear between the charged surface and the electrolyte solution. This potential is called the electrokinetic or zeta potential (ζ). The exact location of the shear plane is open to doubt but it is reasonable to place it at the inner plane of the diffuse layer so that $\zeta = \psi_d$. This is certainly the case at low potentials as has been shown by Smith (1969).

There are different experiments to determine the zeta potential of particles as classified earlier. In the case of ***electrophoresis*** a colloidal suspension is subjected to

an electric field and the speed of the particles is measured. The motion of the particle suspension can be followed using a suitable microscopic or a laser-Doppler technique. Recently a technique for assessing particle mobility has been developed referred to as the ***electroacoustic*** method. In this technique the particles undergo an oscillating motion at sonic or ultrasonic frequency and the resulting AC potential is measured.

Another electrokinetic process occurs when an electric field is applied to the end of a capillary filled with electrolyte liquid. This process called ***electro-osmosis***. When an electric field is applied, the counter ions carried near the capillary wall will move and carry liquid with them. The volume of liquid transported per unit time by known electric field can be used to determine the zeta potential of the capillary wall. But if instead of applying an electric field to a capillary we force the fluid through it, there will be a potential generated. This is called the ***streaming potential*** and again this method can be used to determine zeta potential.

When charged particles settle under either gravity or in a centrifugal field, the movement of the particles will cause an electric field to be setup and this can be measured. It is referred to as the ***sedimentation potential*** and the whole effect as the Dorn effect.

Electrophoresis is the most widely used of the electrokinetic procedures. However in low pemittivity and/or high viscosity liquids the method is difficult or impossible. Van der minne and Hermanie (1952) published criteria for the observation of valid electrophoretic mobilities in non-aqueous media:

1. The suspension medium should have a dielectric constant of at least 10-15 in order to measure the electrophoretic mobility easily.
2. The medium viscosity should be low.
3. The applied field should to be uniform to avoid turbulence in the liquid.
4. The motion of the particle should be rectilinear between electrodes and uniform.

5. The velocity should be independent of the position of the particle in the electric field.
6. The velocity should be proportional to the field strength and should reverse on reversal of the field.

It is clear that there is some difficulty in the observation of true electrophoresis in non-aqueous systems. The relationship between an observed electrophoretic or electrosmotic mobility and the ζ (zeta) potential causing it depends on the dimensionless product κa where κ is the Debye-Hückel reciprocal distance parameter and a is the particle radius (∞ for a flat surface). The best known expression refers to large κa (say > 200) and is the Smoluchowski (1921) expression;

$$v = \frac{E\varepsilon\zeta}{\eta} \tag{3.16}$$

Where v is the particle (or liquid) velocity, E is the electric field ($\frac{v}{E}$ is the mobility u), ε is the permittivity of the dispersion medium, η its viscosity and ζ the zeta potential required from the measurement.

At small κa (say <0.1) the Hückel expression can be used viz. (Henry equation);

$$v = \frac{2E\varepsilon\zeta}{3\eta} \tag{3.17}$$

At intermediate κa, although there are analytical experssion e.g. from Overbeek (1950) and from Booth (1950a) it is probably easiest to use the numerical solution of O'Brian and White (1978).

3.7 TECHNIQUE DEVELOPMENT

One of the considerations in this thesis is to study the electrokinetic potential of asphaltene in petroleum reservoirs oils. Therefore, it is required to establish a method to measure the electrical potential of a solid with two limitations in mind:

1. Suitability for measuring a potential in low permittiviy and high viscosity liquids.
2. Avoidance of surface conductivity errors which could be caused by any irreducible water film adsorbed on reservoir rock surfaces.

This can be achieved by using a ***streaming current*** method. That of ***streaming potential*** can be in considerable error as a result of surface conductivity, itself caused by the presence of an irreducible water film on rock surfaces.

When a fluid is forced to flow through a capillary or porous system possessing a surface charge, a streaming charge of ions of the double layer near the surface are carried towards one end, Figure 3.8. If we consider a single capillary with a walls negatively charged with respect to the solution, the net positive charge flows with the solution to the left hand end. If electrodes joined with a wire are placed at the ends then the positive charge flows back along it and can be measured with a low resistance ammeter. This current is called the ***streaming current*** (I_s). If no wire joins the electrodes then the current (charge) flows back through the solution in the capillary generating a potential difference between the end electrodes which is then termed the ***streaming potential*** (V_s).

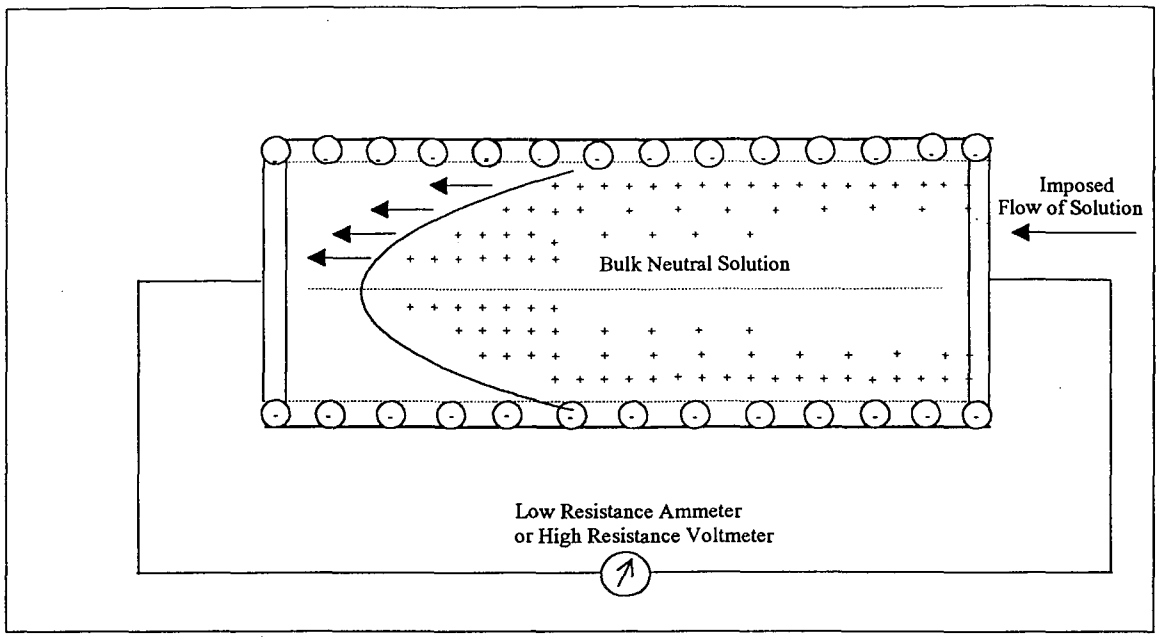

Figure 3.8 Solid-liquid streaming cell.

In a porous rock core containing capillaries radius a of the same length L, the streaming current is related to the zeta potential on the rock surface by:

$$I_s = \left(\frac{\sum \pi a^2}{L}\right)\left(\frac{\Delta P \varepsilon \zeta}{\eta}\right) \tag{3.18}$$

If the solution resistance is R then the streaming potential V_s which results is $I_s R$. However, R cannot be directly related to the conductivity of the liquid since a low resistance path caused by the irreducible water film adsorbed on the solid surface will often exist which is difficult or impossible to estimate. This is the origin of surface conductivity errors which can dominate and completely invalidate streaming potential measurements. The streaming potential is then given by:

$$V_s = I_s R \tag{3.19}$$

$$V_s = \left(\frac{\sum \pi a^2}{L}\right)\left(\frac{\Delta P \varepsilon \zeta}{\eta}\right)\left(\frac{L}{K' \sum \pi a^2}\right) \tag{3.20}$$

$$V_s = \left(\frac{\Delta P \varepsilon \zeta}{K' \eta} \right) \tag{3.21}$$

Where K' is the specific conductance of the solution including surface conductivity. In the case of oil flowing through rock pores the surface conductivity error can be very serious and dominate the measurements. In high conductivity liquids the error will be negligible but, apart from this case, the method of streaming current is much to be preferred as being both more fundamental and free from surface conductivity errors.

The difficulty with the streaming current method is to know the area/length (A/L) of the capillaries. This is of course, straightforward for a single uniform capillary. The estimation of pores A/L ratio of a model reservoir rock is critical and a special technique is required. A further operational difficulty arises from the necessity of measuring very small currents through the high impedance liquid. To do this a high quality picoammeter is required such as the Keithley Model 617.

This thesis will present a method new to petroleum engineering showing how area/length ratios for a porous systems can be obtained by combining streaming potential and current measurements on rock cores. This allows streaming current measurements, independent of surface conductivity errors, to be made on rock samples using crude oil and hydrocarbon solvents.

For a collection of capillaries all of length L and total area cross section A, the streaming current I_s given by equation (3.18) can be written as:

$$I_s = f\left(\frac{\Delta P \varepsilon \zeta}{\eta} \right) \tag{3.22}$$

Where, $$f = \left(\frac{\sum \pi a^2}{L} \right) \tag{3.23}$$

The streaming potential is given by equation (3.21), where $K^{/}$ is the conductivity of the current return path which includes a possible large contribution from surface conductivity caused by the water film adsorbed on the rock surfaces. Thus, for the same values of all parameters in equations (3.18) and (3.21),

$$\frac{I_s}{V_s} = fK^{/} \tag{3.24}$$

If K is the actual conductivity of the liquid independent of surface conductivity, which can be determined by a separate measurement, then dividing each side of equation (3.24) by the true conductivity K,

$$\left(\frac{1}{K}\right)\left(\frac{I_s}{V_s}\right) = f\left(\frac{K^{/}}{K}\right) \tag{3.25}$$

At high electrolyte concentrations the surface conductivity will be negligible and therefore $K^{/}$ = K(true) hence f can be determined by the value of $\frac{I_s}{KV_s}$ at the levelled off value as shown in Figure 3.9. The f value can in principle be estimated at one electrolyte solution concentration so long as it is high enough, but without a plot such as in Figure 3.9 it is difficult to be certain that the electrolyte concentration is indeed high enough (or unnecessary high)

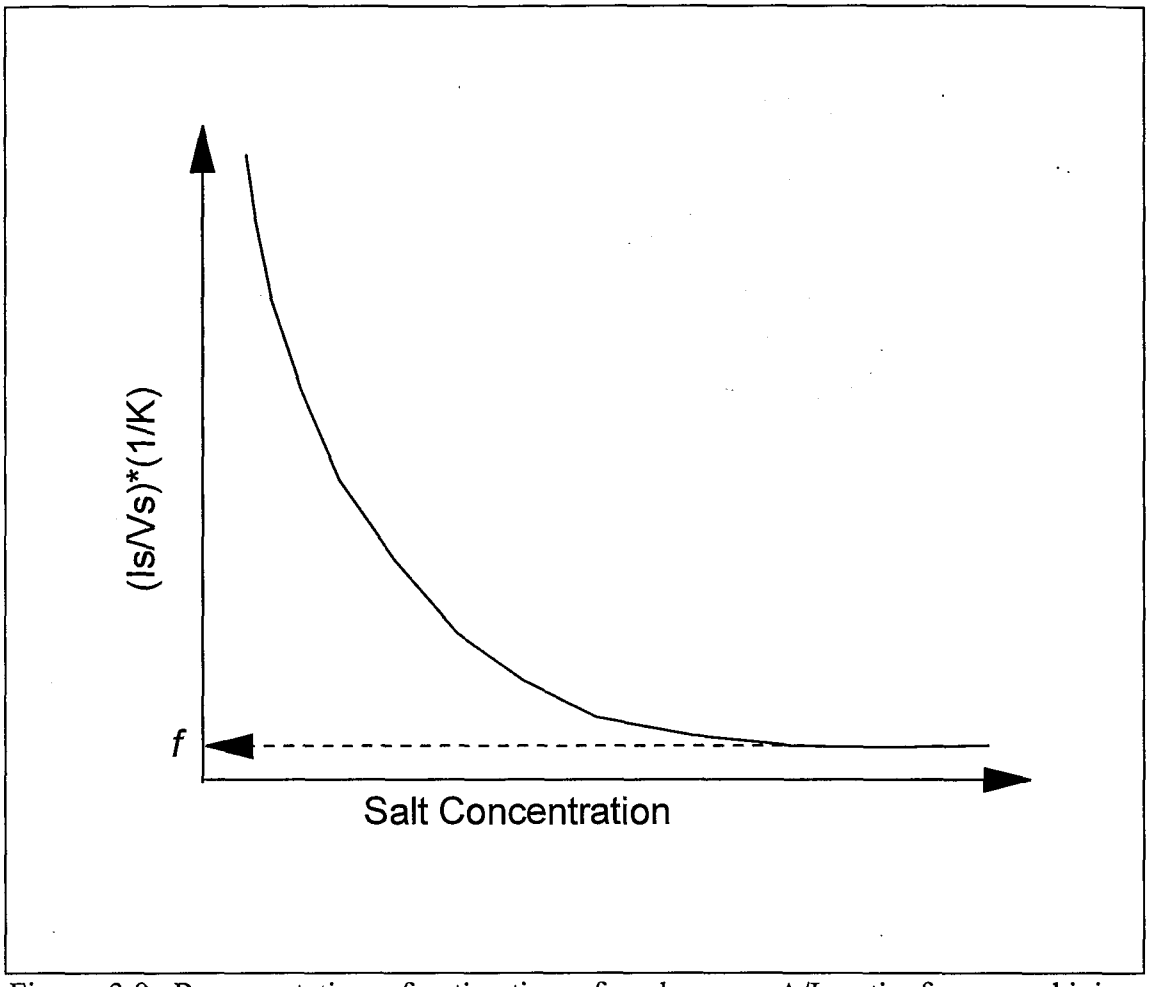

Figure 3.9. Representation of estimation of rock pores A/L ratio from combining streaming potential and current measurements.

This method was applied to reservoir rock cores so that the unambiguous streaming current method could be used. The adsorption of colloidal asphaltene on reservoir rock surfaces was investigated by this method (Chapter 6).

CHAPTER FOUR

LASER BACK SCATTERING TECHNIQUE

4.1 INTRODUCTION

Over the years, techniques have been devised whereby particle size distributions in fluids can be determined by detecting and analysing light scattered from an incident light signal of known intensity. However, with the methods and apparatus available, the utility of these techniques has been limited, particularly in cases where the fluid is coloured or opaque and strongly absorptive of the incident light. In such cases, the intensity of the scattered light may degraded below the limit at which it may be readily detected and analysed. Such is often the case with petroleum fluids. This chapter describes a laser back scattering technique combined with dynamic light scattering (DLS) using optical waveguides (fibre optics) to deliver the laser light to, and collect the scattered light from the petroleum fluid.

4.2 BROWNIAN MOTION

Particles suspended in a fluid are subject to random collisions with molecules of the suspending medium. When the particles are very small in diameter, such collisions give rise to a random particle movement which is called Brownian motion. The velocity and direction of the resulting motion are completely random. However, the velocity distribution of particles over time can be used to determine the particle size. The velocity distribution of a particle in Brownian motion is a function of the fluid temperature and viscosity. The particle velocity increases with increasing temperature and decreases with increase in viscosity as indicated by the Stokes-Einstein relation.

4.3 ELASTIC AND QUASI-ELASTIC SCATTERING

When light is incident on relatively stationary particles the scattered radiation is of the same wavelength as the incident light and the scattering process is said to be elastic. When the particles are moving rapidly, as in Brownian motion, there will be a small shift in the scattered frequency (a "Doppler" shift) leaving the process virtually (though not quite) elastic. Such scattering is said to be "quasi-elastic" and this is the basis of the sizing technique known by that name or as "Photon Correlation Spectroscopy" (PCS) or as "Dynamic Light Scattering" (DLS).

The small changes in frequency involved in this process require a source of very stable frequency and this property, combined with high intensity is found in the laser. The small changes in frequency require a "frequency beating" for their detection and measurement. The beating can either be with light from neighbouring particles (so called self-beating) or with a portion of non-scattered laser beam (local oscillator). See Figure 4.1.

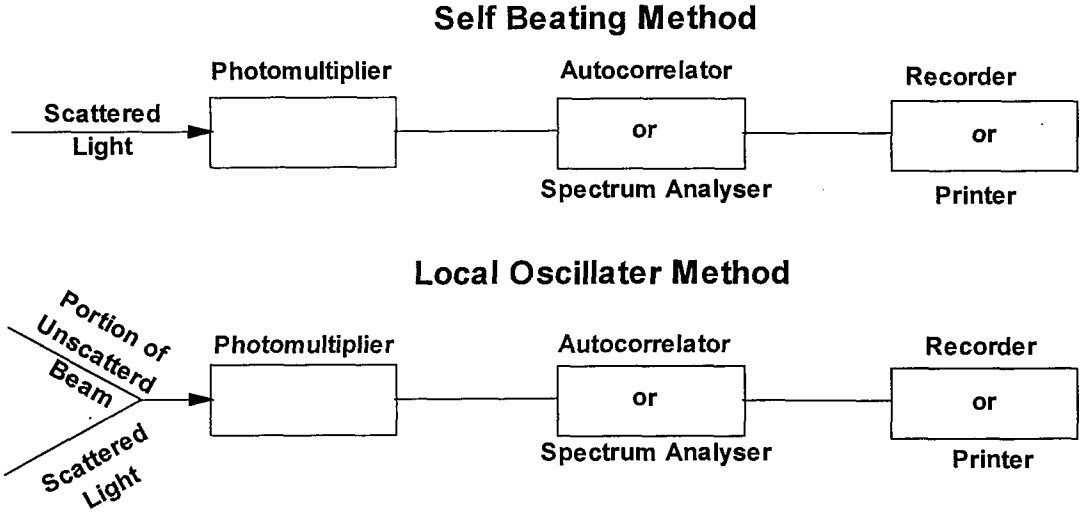

Figure 4.1. Schematic illustration of the various techniques used in light scattering experiments. (After Berne and Pecora, 1976)

4.4 PARTICLE SIZE DETERMINATION BY THE DLS TECHNIQUE

The determination of particle size distributions by means of dynamic light scattering (DLS) is now a well established technique. Until fairly recently light scattering studies to obtain particle size distributions of colloidal dispersions were conducted in the "time average" mode in which it was necessary to measure the intensity of light scattered at some angle θ from the straight through position and relate this to the incident intensity. Rather complex theory was required (Mie theory) to obtain size data and it was necessary to know the refractive index (and shape) of the particles (though not the viscosity of the dispersion medium).

The advent of the lasers immediately gave some advantage in that more powerful beams became available but the time average technique does not take advantage of the coherent, frequency stable characteristics of the laser. These are however exploited in the technique variously referred to as "intensity fluctuation spectroscopy" (IFS) or "quasi-elastic life scattering" (QLS) or, perhaps most frequently, "photon correlation spectroscopy" (PCS).

In this technique absolute intensities need not be measured. Instead the frequency shifts are detected which arise from the (quasi-elastic) scattering of the laser beam from moving particles (the Doppler effect). The movement may be systematic as in electrophoretic drift or random as in Brownian motion, the latter being exploited in size distribution analysis. The system can be twin beam (using a beam splitter), i.e. "local oscillator" for electrophoresis or single beam self beating, as usual in particle sizing. It is, if course, necessary to know in which mode the experiment operates which is not always the case, the local oscillator intensity must be less than ~5% for valid self beating measurements and greater than ~60% for true local oscillator mode.

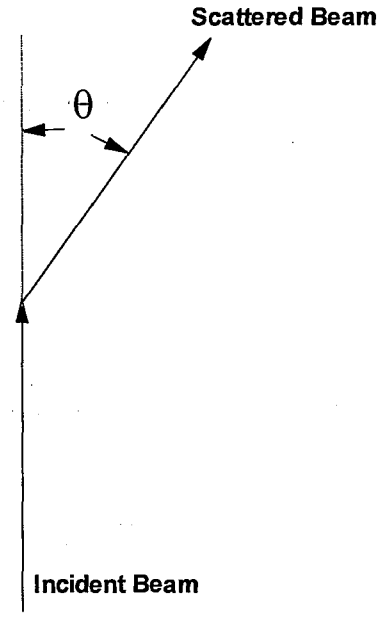

Figure 4.2.

In Figure 4.2 the scattering vector k is defined by:

$$k_{sv} = \frac{4\pi}{\lambda}\sin\frac{\theta}{2} = \frac{4\pi n}{\lambda_o}\sin\frac{\theta}{2} \qquad (4.1)$$

Where λ is the wavelength of the light in the medium and λ_o that in vacuum, n is the refractive index of the medium.

The "autocorrelation function" (ACF) (usually calculated internally in a commercial instrument) is defined as:

$$G(\tau) = \langle I(t) * I(t+\tau) \rangle \qquad (4.2)$$

Where I(t) refers to the intensity at time t and I(t+τ) at time τ later and $\langle\ \rangle$ indicates averaging. Clearly G(τ) falls from the mean square of the intensity $\overline{I^2}$ at short (zero) τ to the square mean $\left(\bar{I}\right)^2$ at very long intervals τ. Between these extremes ACF falls off more or less exponentially provided that there are enough scatterers in the sample

volume (Guassian statistics). The $G(\tau)$ is usually normalised by division by the long τ value $\left(\bar{I}\right)^2$ i.e. by $\langle I\rangle^2$ and $G(\tau)$ becomes $g(\tau)$ where;

$$g(\tau)=\frac{\langle I(t)*I(t+\tau)\rangle}{\langle I\rangle^2} \tag{4.3}$$

and clearly at large τ, $g(\tau)$ approaches unity.

For particles whose scattering is itself independent of time (e.g. spherical particles) and which can be assumed non-interacting (dilute) the ACF of the detected field. $g(\tau)$ is related to the translational diffusion coefficient (D) of the particle via:

$$g(\tau)=\exp\left(-Dk^2t\right) \tag{4.4}$$

Where k is the "scattering vector" defined by equation 4.1. The particle radius (a) can be obtained from the diffusion coefficient (D) via the Einstein-Stokes relation:

$$D=\frac{kT}{6\pi\eta a} \tag{4.5}$$

Where k here is the Boltzmann constant, T the absolute temperature and η the medium viscosity.

A polydisperse sample will have a correlation function which is the sum of a number of exponential decays. It is in general theoretically impossible to retrieve from such a complex correlation function the individual size contributions unless assumptions can be made. One such is that the correlation function arises from (say) just two exponential decays (a bimodal-distributions) but there are other algorithms e.g. one used by the Brookhaven instrument termed NNLS (Non-Negatively constrained Least Squares).

Alternatively the analysis (and display) can be in the frequency rather than the time domain as in the Leeds Northrup instrument. The time domain and frequency domain outputs are Fourier transforms of each other.

In strongly absorbing (coloured) dispersion media or very high particle number concentrations both time average and PCS experiments become difficult. Hence the development of back scatter techniques in which the incident beam is scattered back (and detected) from particles just inside a cell. Up to now this technique has suffered from the mixing of homodyne and heterodyne signals (the latter arising from light scattered back from the laser probe end face or cell wall). In the Brookhaven instrument such errors are avoided by separating the detecting pathways using fibre optics.

Figure 4.3 shows a schematic of the Brookhaven fibre-optic probe system. The scattering volume is defined by the intersection of the transmitting and receiving fibres fields. Since the system is designed to measure particle size in concentrates, it is very important to position the fibre probe such that the scattering volume is as close as possible to the inside of the cell wall without including any part of the wall itself. If the intersection point (scattered volume) is too deep inside the medium, the back scattered light will include multiple scattering and will be attenuated by absorption. If the cell wall is in the scattering volume reflections from it will constitute a local oscillator and mode will no longer be self beating. Thus positioning the fibre optic with respect to the cell wall is of primary importance in the Brookhaven instrument. Chapter 8 will present the results of asphaltene particle size distribution measurements and wax cloud-point in petroleum fluids using the laser back scattering technique via a fibre-optic probe.

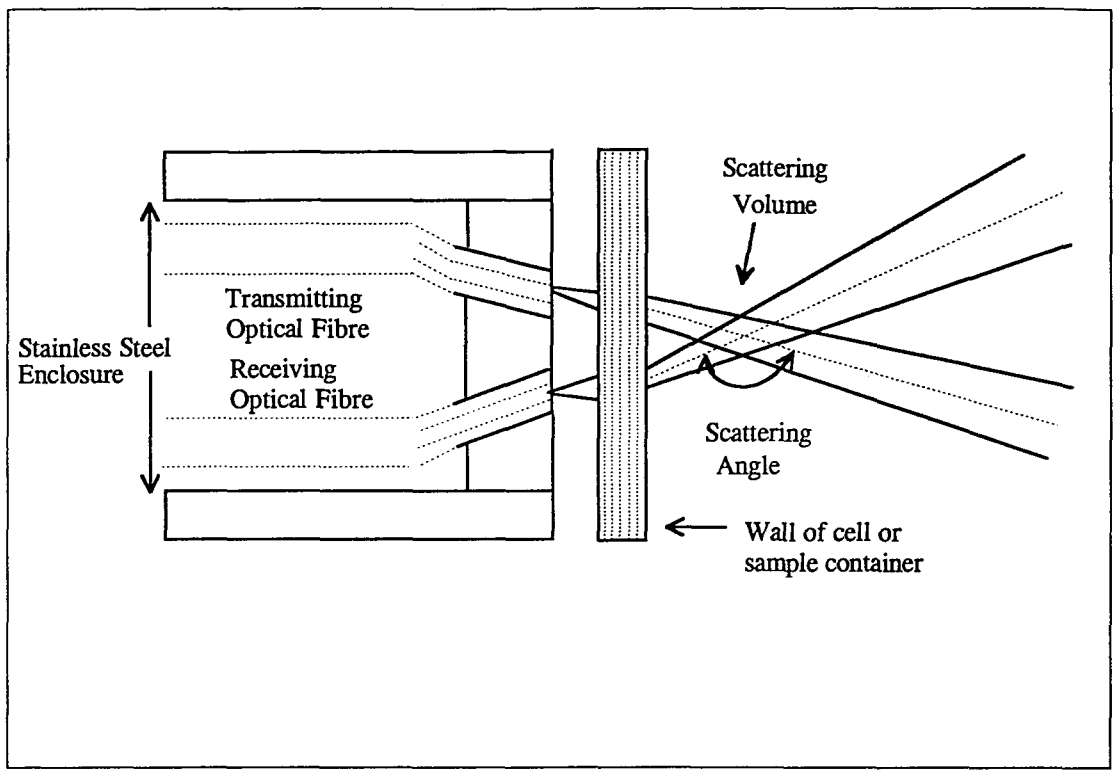

Figure 4.3. Schematic of non-invasive back scatter fibre-optic probe. (After Brookhaven Corp.)

CHAPTER FIVE

EXPERIMENTAL APPARATUS AND PROCEDURE

5.1 INTRODUCTION

It has been concluded in Chapter 3 that the determination of the electrokinetic potential of a solid in petroleum fluids is difficult due to the latter's low permittivity and/or high viscosity. However, any information on the electrokinetic properties of asphaltene in petroleum reservoirs will in principle be valuable in understanding its stability. To date there are only limited experimental data covering asphaltene's electrokinetic potential. Most of the results were based on electrophoretic mobilities of extracted asphaltene in semi-polar hydrocarbon solvents.

This chapter outlines all the experimental techniques and procedures used in investigating colloidal asphaltene, as follows:

A. Rock surface potential testing apparatus.
B. Electrode-deposition test under an electric field.
C. Laser back scattering technique for particle size distributions in petroleum fluid.

5.2 ELECTROKINETIC INITIAL TEST

In the initial stage of this research a preliminary test involved an investigation of the possible electric charge, and consequent electric potential, of asphaltene in petroleum crude oil was carried out. This involved streaming potential and current

measurements. A streaming cell manufactured for the project by Rank Brothers Scientific Instrument Division, Cambridge, UK was used in this test, Figure 5.1.

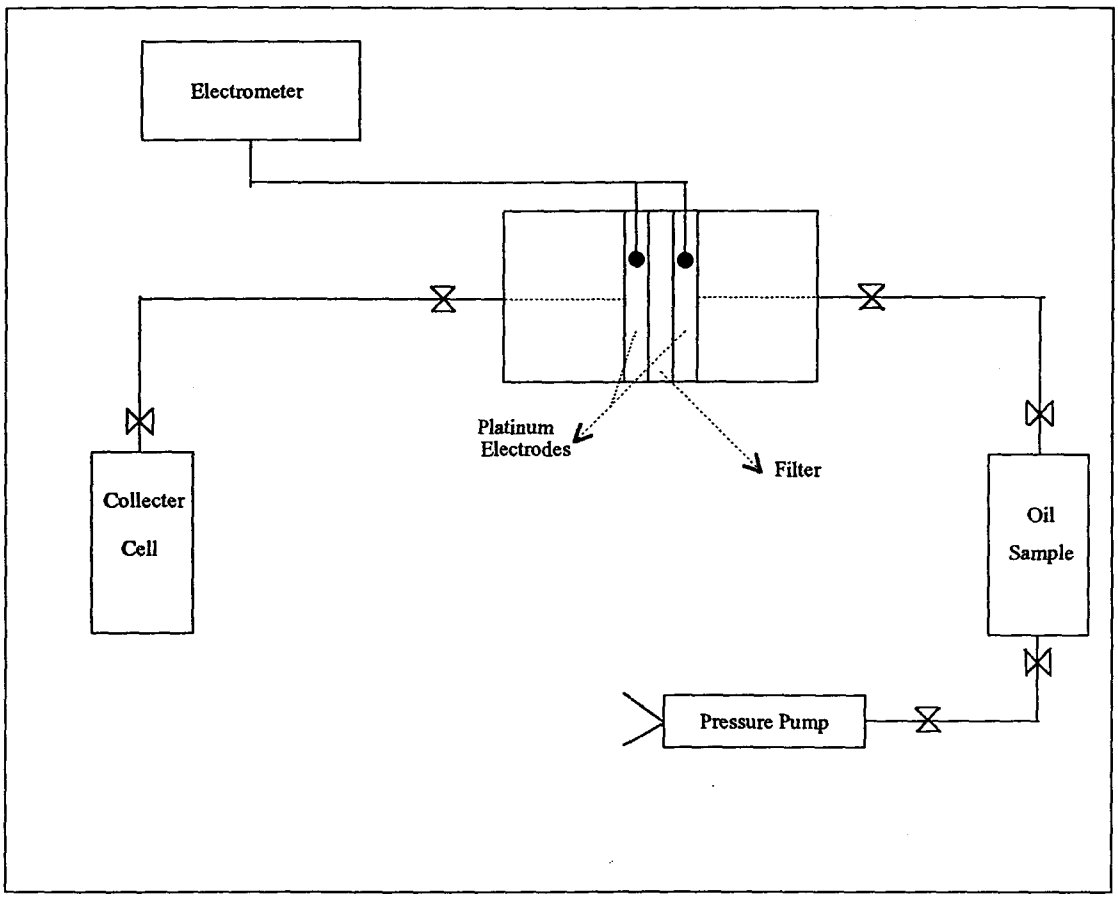

Figure 5.1. Streaming cell apparatus.

The streaming cell was made of high pressure PTFE/stainless steel and was similar to the one described by Jan *et al.*, (1994). The particle samples were trapped on a Millipore filter placed between two electrodes and liquid flowed through the "cake", with the potential being measured on a very high input resistance Keithley 617 model electrometer. Linearity between streaming potential V_s and the applied pressure difference, ΔP , was always observed and the results other than sign were independent of the flow direction, Figure 5.2. The initial test work confirmed several important points which can be summarised as follows:

1. With silica particles dispersed in water, potentials of order milivolts were obtained, validating the cell design and preparing its use with crude oil and hydrocarbon solvents.
2. Streaming potential measurements were observed in crude oil and hydrocarbon solvents and showed linearity with pressure gradient.
3. Silica particles in methanol and acetone were found to have small but significant negative potentials.
4. Asphaltene in crude oil appeared to have a definite positive potential similar to those found by Lichaa (1975), but of extremely small magnitude, about 0.0001 mV.

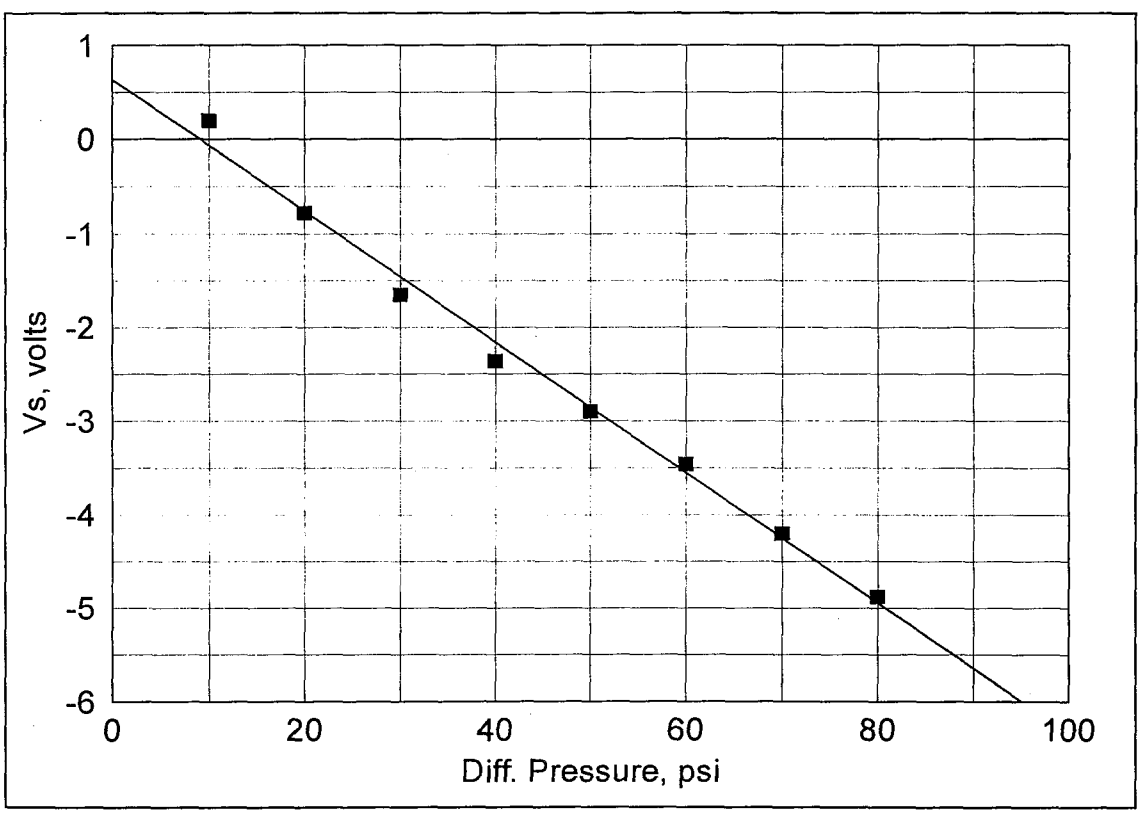

Figure 5.2. Streaming potential vs. differential pressure for north sea crude oil.

5.3 ROCK SURFACE POTENTIAL TESTING APPARATUS

Based on the streaming cell test results, an experimental apparatus was designed to measure the streaming potential and current of petroleum fluid flowing through reservoir rock cores and it is depicted schematically in Figure 5.3. Measurements were conducted at different flow rates. The measurements were carried out at room temperature. The experimental apparatus can be divided into four elements:

1. The pressure vessel.
2. Confining and pore pressure systems.
3. Liquid flow.
4. Electrical circuit.

5.3.1 The Pressure Vessel

The high pressure cylindrical vessel, also called the core holder, was fabricated from stainless steel and tested to withstand pressures up to 10,000 psi [69 MPa]. The vessel included top and bottom removable secured covers. The side of the vessel included an inlet port and inlet valve to permit confining (stress) pressure to be applied to the core sample. The flow tubing instems were connected direct to platinum faced stainless steel electrodes. The rock core sample was placed inside a Viton sleeve and was contained between the two instem electrodes. Two pieces of rubber were placed to cover the back face of the electrodes by inserted them through the tubing. This ensured that the electrodes made no electrical contact with the core holder. The two electrode instems are completely electrical isolated from the vessel body by Teflon "O" ring seal placed inside the vessel top and bottom covers. Extra measures were also taken in the design to avoid any other electrical conduction errors. This was accomplished by isolating the rest of the stainless steel electrode instem tubing from the apparatus elements by connecting the top and bottom parts of the instems with plastic tubing rated for working pressures up to 5000 psi [34.5 MPa], Figure 5.4.

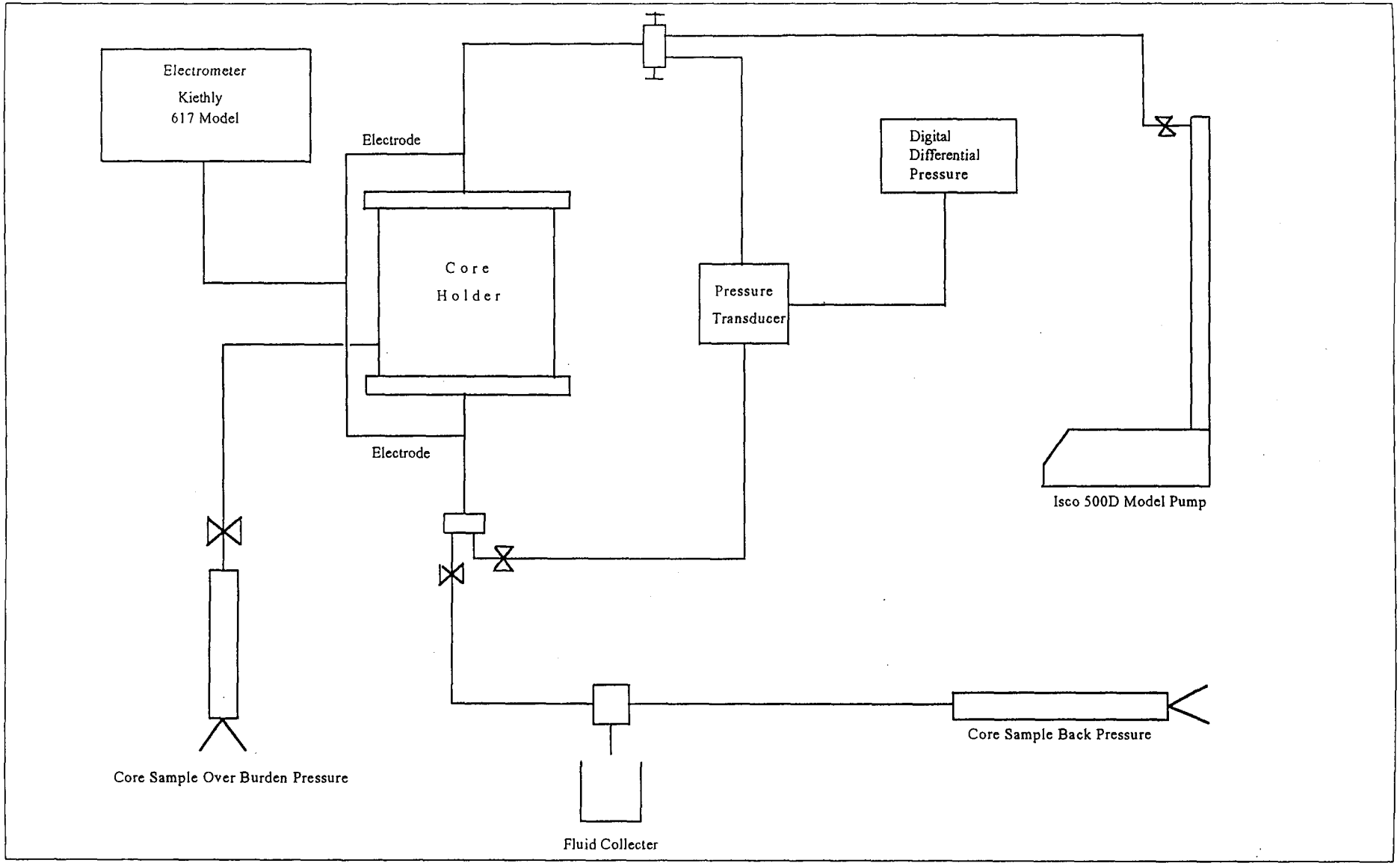

Figure 5.3. Schematic diagram for measuring the surface potential of reservoir rock samples.

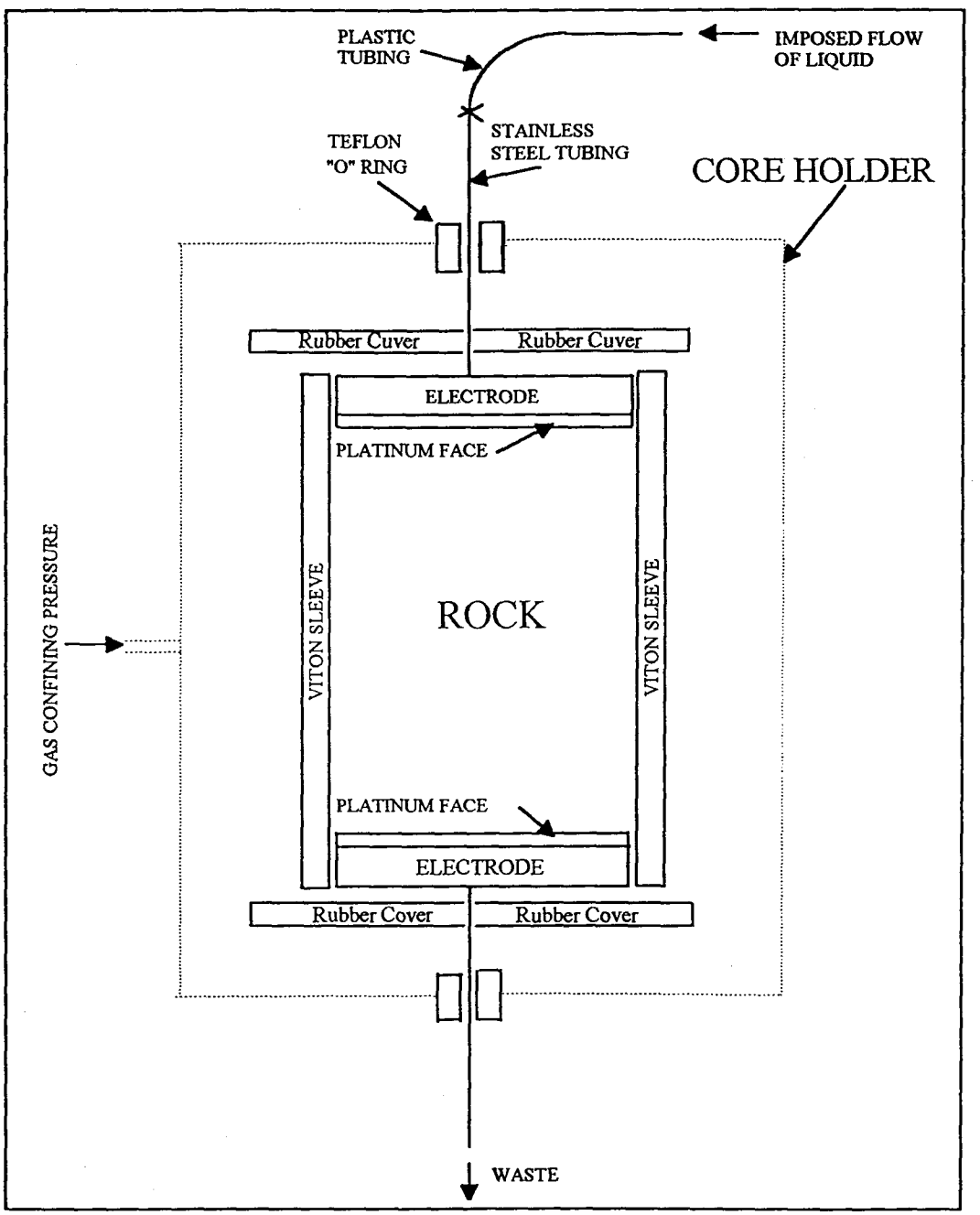

Figure 5.4. Schematic diagram of the Core Holder.

5.3.2 Confining and Pore Pressure Systems

The confining (stress) pressure system used in all experimental work was supplied from a nitrogen gas bottle into the core sample through the side inlet in the core holder. There are two advantages in using gas rather than mineral oil. Firstly, to isolate the core sample and electrodes from any electrical conduction which can affect streaming potential and current measurements. Secondly, to prevent the liquid flow from overriding the porous medium. The confining pressure applied on Berea sandstone samples was 1500 psi [10.35 MPa], whereas in Glauconitic sandstone (Alberta, Canada) samples it was 2300 psi [15.87 MPa].

The pore pressure, sometime called the fluid pressure is supplied through a back pressure regulator. The back pressure regulator unit was designed to control the pore pressure environment as required and was positioned at the bottom outlet of the core holder. To record the pore pressure a digital transducer manufacture by Validyne Engineering Corp. is positioned between the regulator and the top electrode instem. The digital transducers can be obtained with different ratings, in this work those of 100 psi [0.69 MPa] and 1000 psi [6.9 MPa] were used.

5.3.3 Liquid Flow

Two advance pumps "Isco 500D" and "D. P. Robinson" with different liquid capacities were used separately to pump the fluid through the core samples at different pressures and flow rates. Both pumps had programmable features to control the flow environment. The liquid flow through the core samples were introduced at different flow conditions with a constant time interval between. At each flow condition the core differential pressure and the desired streaming potential or current were recorded. A plot between differential pressure and streaming measurements (current or potential) always showed a linear correlation. To avoid core permeability damage during the measurements, liquid flowing through the core sample did not exceed the liquid

critical velocity. This could have disturb core grains structure stability and block the capillaries.

5.3.4 Electrical Circuit

The apparatus electrical connection is based on the principle of two-wire measurement as shown in Figure 5.3 using a Keithley Model 617 Programmable Electrometer. The Keithley 617 is a highly sensitive instrument designed to measure voltage, current, charge, and resistance. The voltage measurement range is between 10 μV and 200 V, whereas in current mode 0.1 fA and 20 mA. The advantage of using the Keithley 617 is the very high input impedance and extremely low input offset current. The Model 617 includes a standard IEEE-488 interface which allows full bus programmable operation. One of the features included in the Keithley Model 617 and used in this work is the data store mode using an internal buffer to log a series of readings.

5.4 DESIGN OF EXPERIMENTAL PROGRAMME

The aim of this experimental programme is to determine the surface potential of sandstone rock core samples under asphaltenic oil flow conditions by the streaming current method. The streaming current method does however need a knowledge of the rock pores cross sectional area to length ratio. This work introduces a novel method to show how the pores area/length ratio of a porous system can be obtained by combining streaming current and potential measurements. Two kinds of sandstone formations were used in this study, Berea sandstone (Cleveland Quarries, Amherst, Ohio, USA) and Glauconitic sandstone (Alberta, Canada) formations. Berea sandstone core samples were used to study the effect of asphaltene adsorption and pore pressure on the measured surface potential of the rocks. In order to quantify the effect of double layer overlap in narrow pores in hydrocarbon systems on the streaming current

selected Glauconitic sandstone formation samples with varying pore size distributions were tested.

5.5 EXPERIMENTAL PROCEDURE

The experimental procedure for determining the surface potentials of sandstone rocks at different flowing pressures at room temperatures is described in the following sections.

5.5.1 Preparation of Materials

(A) Preparation of Rock Samples

The rock samples were cut into cylindrical shapes with a diameter of 1.5 inches and length 3 inches using a diamond cutter available in the routine core analysis department at Core Lab of Calgary. Both end faces were sanded to make them parallel for good contact with the electrode faces. The rock core samples were cleaned using a flow through method, which involves a succession of solvents passed through the samples. All core samples were flushed first with toluene to remove oil residues if any, until the colour of the output fluid (toluene) remained the same, followed by a methanol flood to remove salts from the cores samples. The methanol output was tested with chloroform until the samples were salt free. The samples were then placed in a vacuum oven at 100 ^{o}C for over a week to remove bulk moisture from the samples. A core analysis was conducted to determine porosity and permeability by using advanced rock properties equipment. Details of core analysis descriptions for Berea and Glauconitic sandstone samples are included in Table 5.1 and Table 5.2 respectively.

(B) Preparation of *KCl* and Brine Solutions

Two aqueous electrolyte solutions were used in this study. The first solutions were eight different *KCl* concentrations ranging from 0 to 7.456 g/l. *KCl* solutions used in estimating rock core pores area/length ratio so that streaming current rather than streaming potential could be used. The second electrolyte solution was a synthetic reservoir brine made up from Atcor Provost Field, Lloydminster Pool, located in Alberta, Canada. A simulated formation brine mixture is shown in Table 5.3. Solutions were made in de-ionised water and stirred for at least 48 hours to make sure all the coarse particles were dissolved, after which they filtered through a 0.45 μm filter.

(C) Conductivity Measurements

The solution conductivities were measured with a commercial digital conductivity meter, the conductivity meter being calibrated with standard solutions. All conductivity measurements were corrected to 25 °C as a standard temperature. Table 5.4 lists the conductivity measurements for all the electrolyte solutions. The conductivity of *KCl* solutions was found to be in close agreement with the published conductivity of standard solutions at 25 °C.

(D) pH Measurements

pH measurements of the electrolyte solutions were made by a commercial pH meter. The meter was calibrated using standard buffers. All electrolyte solutions under test were similarly equilibrated at 25 °C. All *KCl* solutions and Atcor Provost brine found to have neutral pH (5 to 6).

(E) Petroleum Fluids

An underlying principle of this study was to investigate the possible electric charge of asphaltene in crude oil and hydrocarbon solvents. Asphaltene adsorption onto reservoir rock core surfaces was investigated by two different procedures. The first procedure used extracted asphaltene from Saskatchewan, Canada crude oil dispersed in hydrocarbon solutions. The extraction procedure involved the precipitation of asphaltenes from the crude oil by using an excess of n-pentane. This method followed the procedure described in ASTM D-3279. The hydrocarbon solutions consist of a mixture of n-pentane and toluene with 1:1 volume ratios and are referred as "pentol". The second procedure involved the use of a natural asphaltenic crude oil supplied by Atcor Ltd, Calgary, Alberta, Canada. Table 5.5 lists the petroleum fluids used in this study.

5.5.2 Streaming Potential and Current Measurements

The first step before the measurements is to place the dry core sample inside the Viton sleeve and then place it between electrodes, the two electrode instems passing smoothly through the top and bottom of the core holder covers. As indicated in section (5.3.1) the two electrodes were completely without electrical contact with the core holder or the rest of the apparatus elements during the measurements. After the core sample was placed inside the core holder vessel and both core holder covers installed, the confining pressure was applied carefully to the sample at a desired pressure supplied from a pressurised nitrogen bottle. The electrical insulation between the electrodes was checked by a Keithley electrometer type 617 before introducing the fluid into the core sample. The main test involved measuring the streaming current and the resulting streaming potential resulting from liquid flow through the core sample, at various pressures, both measurements being made by the Keithley 617.

The Keithley Model 617 can measure voltages in the range of 10 μV to 200V at input impedance of order 10^{14} Ω and can resolve currents as low as 0.1 fA. The

instrument was first allowed to warm up for a minimum two hours to reach rated accuracy. During voltage measurements the instrument was placed in the guarded mode. In current measurements at very low levels (crude oil and hydrocarbon solvents) the measurements can be affected by noise current generated in the cable or from other sources. To minimise this effect the cable was kept short and the core holder body used as a shield by connection to input low (the core holder vessel was isolated from the two electrode instems). In both measurements the instrument was always zeroed by the zero correct button and set for autorange readings. During measurements the instrument was set in data storage mode that allowed the logging of a series of readings at specific intervals of time. One minute time interval reading was chosen to store all measurement, this being enough time to allow the measurements to stabilise during changing conditions.

5.5.3 Surface Potential Measurements

Asphaltene and reservoir rock surface potentials in petroleum fluids are calculated from streaming current measurements using equation (3.22).

$$I_s = f\left(\frac{\Delta P \varepsilon \zeta}{\eta}\right)$$

The knowledge of pores area/length ratio was obtained by combining streaming current and potential measurements over a range of electrolyte concentrations as described in Chapter 3 section (3.7)

5.5.4 Petrographic Analysis

Asphaltene adsorption on reservoir rock core surfaces was examined by thin section analysis. The method consists of impregnating the sample under vacuum or vacuum and pressure (1000 psi [6.9 MPa] - nitrogen driven when necessary) with a

low viscosity epoxy resin. This epoxy resin is mixed with a pink fluorescent dye in order to discern porosity. The sample is then cut, mounted onto a glass slide and ground to 30 μm. Carbonate mineral staining techniques that include a mixture of Alizarin-Red-S and potassium ferricyanide were then applied before a cover glass was finally put on. In some cases, sodium cobaltinitrite was used to stain potassium bearing minerals. The completed thin section is examined using a polarising microscope and photographs of areas of interest were produced.

5.5.5 X-Ray Diffraction Analysis

X-ray diffraction is usually used to provide a semi-quantitative estimate of whole rock mineral contents. To obtain satisfactory results a representative sample has to be desegregated and then separated by floatation into greater than and less than 2 μm size fraction. Rock particle size reduction is usually performed by the use of a mechanical device such as the micronizing mill to avoid crystallite damage due to excessive strain which may lead to diffraction line broadening. The micronizing mill device is necessary to produce very reproducible particle size distributions without damaging the crystal lattice this being an important criterion in quantitative analysis. Each fraction is analysed separately, reported separately and mathematically recombined to provide a bulk composition. The less than two micron size fraction (clay fraction) is subjected to a four step analysis: at room humidity, after glycolation and where necessary, after heat treatment and acid digestion. The clay fraction is prepared by dispersion in sodium hexmetaphosphate solution and flocculation in magnesium chloride solution. This also stabilises the ionic state of some clays. The glycolation treatment is used to identify swelling clays such as smectites, vermiculite and mixed layer clays. The heat treatment aids the identification of chlorite types and swelling clays. Where further identification of clay type in a chlorite-kaolinite mix is necessary, the sample is digested in warm dilute hydrochloric acid, which decomposes iron-rich chlorites. The analysis was conducted in the geoscience department of Core Laboratories of Calgary, Alberta, Canada. Berea sandstone and Glauconitic sandstone core samples XRD analyses can be found in Appendix A.

5.5.6 Error Analysis

The electrical properties measurements of cores are subject to error if they are made before the rock and its saturating fluid reach equilibrium. The rock surface potential accuracy is influenced by errors in the streaming current, streaming potential and of course liquid conductivity measurements. If these measurements are biased or have high variance, this can lead to serious errors in the calculated rock surface potentials. Both streaming current and potential measurements are considered very sensitive phenomena. There are some unrecognised factors that may influences surface potential measurements such as electrode polarisations, temperature and core/electrodes face contact.

To obtain correct surface potentials for cores it is necessary to make a series of measurements to ensure equilibrium. The effect of salinity on rock surface potentials can also play a significant role in streaming current and potential measurements. This work well demonstrates how error caused by surface conduction will dominate streaming potential measurements (see next chapter).

Table 5.6. shows error analysis in the experimental measurements on Berea sandstone core plugs with 1" length and 1.5" diameter. The analysis is based on high electrolyte solution results to avoid surface conduction errors. The values were estimated by using statistical analysis derived by "TableCurve", a mathematical commercial software package developed by Jandel Scientific, San Rafael, California, USA. Streaming current measurement shows fewer errors than streaming potential this no doubt due to the surface conduction effect on streaming potential. The errors will be reduced with increasing solution conductivities and increased in non-aqueous systems, but these errors will minimise in the streaming current method. Since the measurements are a function of time interval, that based on one minute per changed flow condition was chosen. The errors involved here will not be significant. Moreover, each measurement consists of a number of readings to obtain the linearity correlation needed. However, most of the correlations shows smooth linearity readings. The time interval errors in experimental readings were found to be ± 1%.

The low error values found in the streaming current method correspond with the excellent agreement with Berea sandstone particle surface potentials determined by the electrophoresis method in high electrolyte solutions (Schramm *et al.*, 1991).

5.6 ELECTRODE-DEPOSITION UNDER ELECTRIC FIELD

Experiments involving electrical effects on asphaltene particles were conducted in order to relate these effects to the adsorption/deposition problems in petroleum reservoir rock formations. This test also serves to define the type of the charge (+ or -) that asphaltene particles may possess, to gave rough estimates of the asphaltene ζ potential and relate this to the results of adsorption on rock surfaces.

In this test a special conductivity cell was designed consisting of two stainless steel plate electrodes with an average area of 8.76 cm^2. The two plates are held in parallel position by Teflon holder with a 2 mm space separating them as shown in Figure 5.5. An Alberta crude oil was selected which contained a large amount of asphaltene as determined by ASTM D-3279 procedure method. The cell was then immersed in a beaker that contained the selected crude oil. A voltage of 170 V was applied to the electrodes, giving a field strength of 850 Vcm^{-1}. The experiment was carried out at two different time frames, one was for a month and the other for a week.

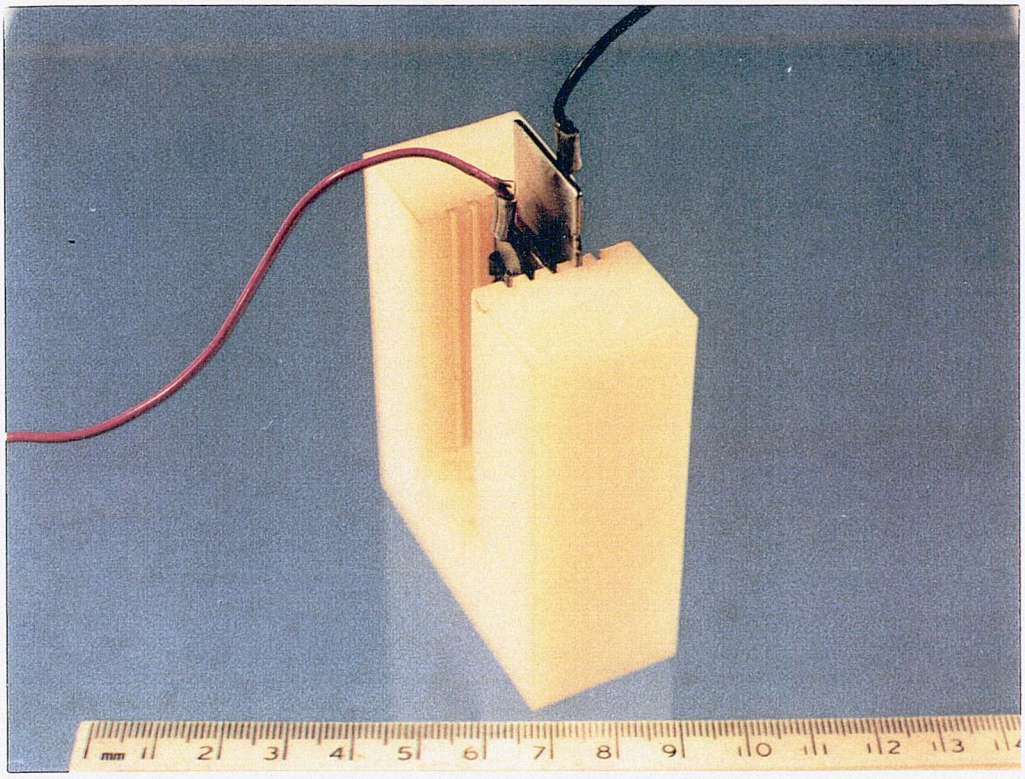

Figure 5.5. Picture of the conductivity cell

At the end of experiments, both electrodes were carefully removed from the Teflon holder. The electrodes were then inspected, noting at which electrode deposition had occurred. This deposited material was further checked for its asphaltene content by the previous procedure. These tests were repeated to verify the outcome results. The results are given in Chapter 6 section (6.10).

5.7 LASER BACK SCATTERING APPARATUS

The particle size distribution of a solid in crude oil cannot be easily determined by conventional techniques. A laser back scattering technique was therefore used to avoid the difficulty in strongly absorbing dispersion media such as crude oil.

5.7.1 Instrument Description

The technique uses photon correlation spectroscopy (PCS), also called quasi elastic light scattering (QELS), but in the back scatter mode (actually ~150° rather than 180°) rather than the more conventional forward or 90° scattering. This is particularly useful for concentrated dispersions or for strongly absorbing solutions as in this work. This technique was described in Chapter 4. The instrument used in this work was supplied by Brookhaven Instruments (U.S.A) and called "FOQEL". The particle detection range was from 2 nm up to 10 μm and the suspension concentrations up to 40%. The instrument was supplied with a fibre optic probe to allow measurements in remote locations and in hostile environment.

To use the Brookhaven instrument, the fluid sample is held in a transparent cell or one with a transparent window. A light signal generated by an internal diode laser is transmitted down on optical fibre and directed at the sample from an output at the tip of a transceiving probe. Laser light scattered back from a scattering volume in the sample on which the tip is focused is received by another fibre positioned at the same tip. This can be seen in Figure 4.3 in Chapter 4.

Despite the relative sophistication of such an instrument, the measurement of particle size distribution in the foregoing manner remains difficult if the fluid has strongly absorbing characteristics like crude oil. This is because a considerable amount of laser light is absorbed and the intensity of back scattered light can be very weak. In our version of the Brookhaven instrument, in order to go through a thick window in high pressure cells the optical probe has a focus point distance from the probe tip to the centre of the scattering volume of about 4 mm. If the fluid medium is a crude oil then this distance is too far if one is using a thin window. To overcome this problem two different cells was designed and manufactured by Rank Brothers Scientific Instrument division, Cambridge, UK. The first cell was designed in a rectangular shape from black (carbon filled) PTFE with a 3.8 mm thick push fit quartz window. The other cell consisted of a cylindrical housing made from thick plastic material, with a window (quartz) held in one end of the cylindrical housing with a

thickness of 3.8 mm. A Brookhaven optical probe is inserted inside the housing until its face contacts the window, Figure 5.6. Both cells can be used with almost any solvent (and certainly with toluene, Pentol and crude oil).

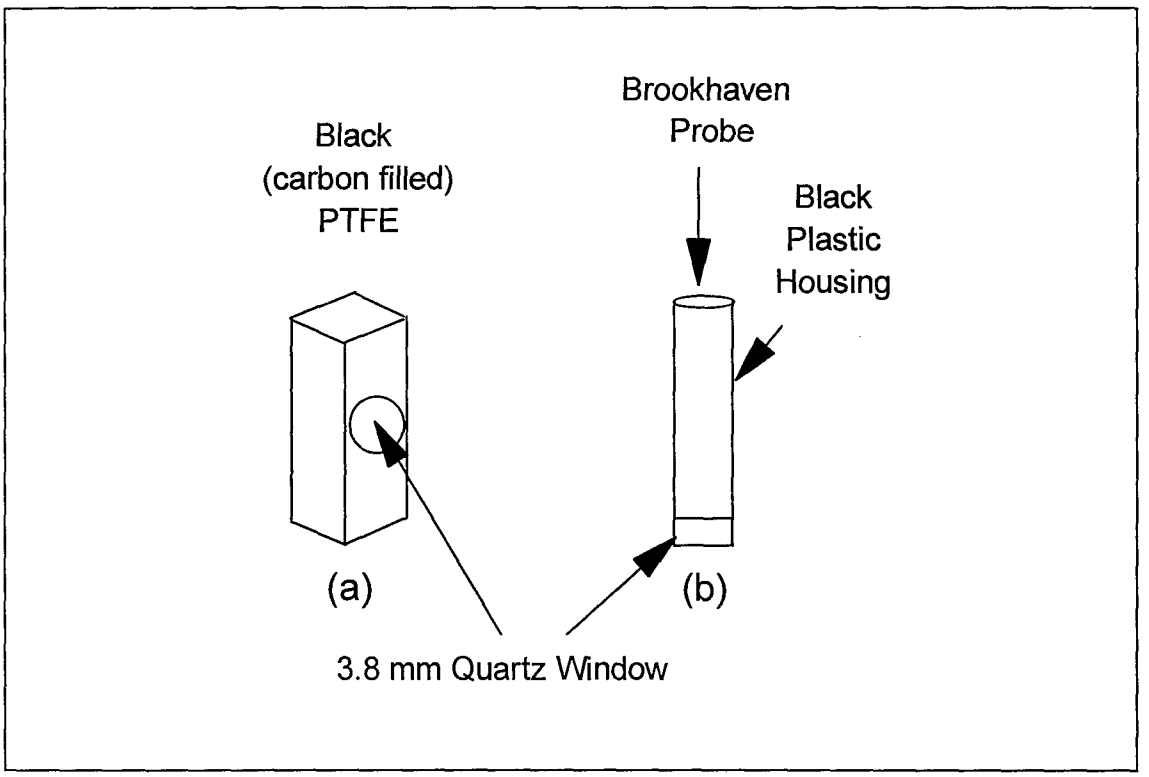

Figure 5.6. Schematic diagram of the cells used in the laser back scattering technique.

5.7.2 Instrument Calibration

The Brookhaven instrument was checked with a Duke Scientific Corporation certified particle size standards using the two cells designed for this work. The particle size standards were prepared by Duke's in response to the need for traceable methods of particle size analysis. The monodisperse polymer microsphere particles were calibrated by Duke's with methodology traceable to the National Institute of Standards and Technology (NIST). 50 nm, 0.5 μm, 1.0 μm and 3.0 μm Duke particle size standards were used in the calibrations. The calibration results with the Brookhaven instrument using both cells were found to be in good agreement with Duke's standards

particle size. At this point the Brookhaven instrument is ready to use in petroleum fluid with the two cells.

5.8 EXPERIMENTAL PROCEDURE

The experimental procedure for determining the particle size distributions in a petroleum fluid by laser back scattering technique at ambient conditions is described in the following sections.

(A) Preparation of Asphaltenic and Mineral Samples

As indicated earlier the objective of using the laser light back scattering technique was to monitor the change in asphaltene particle size in the presence of additives and to investigate asphaltene adsorption on mineral particles by monitoring the change in size of those particles.

Asphaltene solutions at different concentrations were made up in toluene. The asphaltene used in this study was extracted from Saskatchewan Canada crude oil. The extraction procedure followed the method described in ASTM D-3279. The solutions were stirred for a period of time to ensure that asphaltene particles had dissolved in the toluene. To confirm that the solutions no longer contained colloidal asphaltene particles the particle size was always checked. Asphaltene particle aggregate size was also determined on the addition of non-solvents to the toluene solutions.

Asphaltene adsorption on mineral particle surfaces were investigated by the addition of asphaltene solutions to mineral particles dispersed in toluene and hexadecane solutions. Two types of mineral particles were used in this study, hydrophobic silica and carbon.

(B) Preparation of 2-Hexadecyl Naphthalene

Crude oil resins play an important role in asphaltene stability in petroleum reservoirs. This research took a further step in understanding asphaltene stability and its adsorption on reservoir rock mineral surfaces by developing an analogue of the resins in crude oil. This was 2-hexadecyl naphthalene which is later referred to as HN, Figure 5.7 (page 76) shows the results of an ir spectroscopic investigation of the HN.

The reasoning behind the selection of this molecule as a possible stabilising agent for asphaltene and other particles in crude oil and aliphatic solvents is outlined in Chapter 3 section 3.5. Hexadecyl naphthalene (HN) is shown in Figure 3.7.

HN was prepared by the Wolff - Kishner reduction (Anderson, 1953) [Huaing - Minlon modification] of 2-hexadecanoyl naphthalene (compound II, Figure 5.8), itself prepared by the method of Buu - Hoi & Cagnint (1945) by the Fredel - Graft's reaction between 2-hexadecanoyl chloride (palmtoyl chloride) and naphthalene in the presence of anhydrous aluminium chloride and nitrobenzene. The presence of nitrobenzene seems to ensure the formation of the 2-isomer rather than a mixture of the 1- and 2-isomers. The compound II obtained was then vacuum distilled.

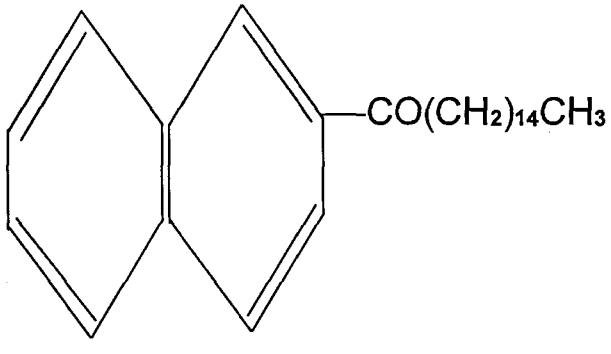

Figure 5.8. 2-hexadecanoyl naphthalene

The HN obtained, slightly yellow, was purified by column chromatography on an alumina column in 60-80 petroleum ether. Its purity was confirmed by melting point and ir spectroscopy. An alternative synthesis, which would be more appropriate

for commercial exploitation, if needed, would be to react naphthalene directly with hexadecanol in the presence of an appropriate catalyst. This would gave a mixture of isomers but this should not matter.

(C) Waxy Crude Oil

Since both asphaltene and wax particles exist alongside each other in petroleum oil, it was considered necessary to observe the two phenomena in crude oil using the laser back scattering technique. The purpose here was to identify and distinguish between the observed particles including formation solid particles that may also exist in oil. Two Canadian asphaltene free waxy crude oils were used. Particle size changes were observed as a function of temperature to determine the wax cloud point and investigate its reversibility.

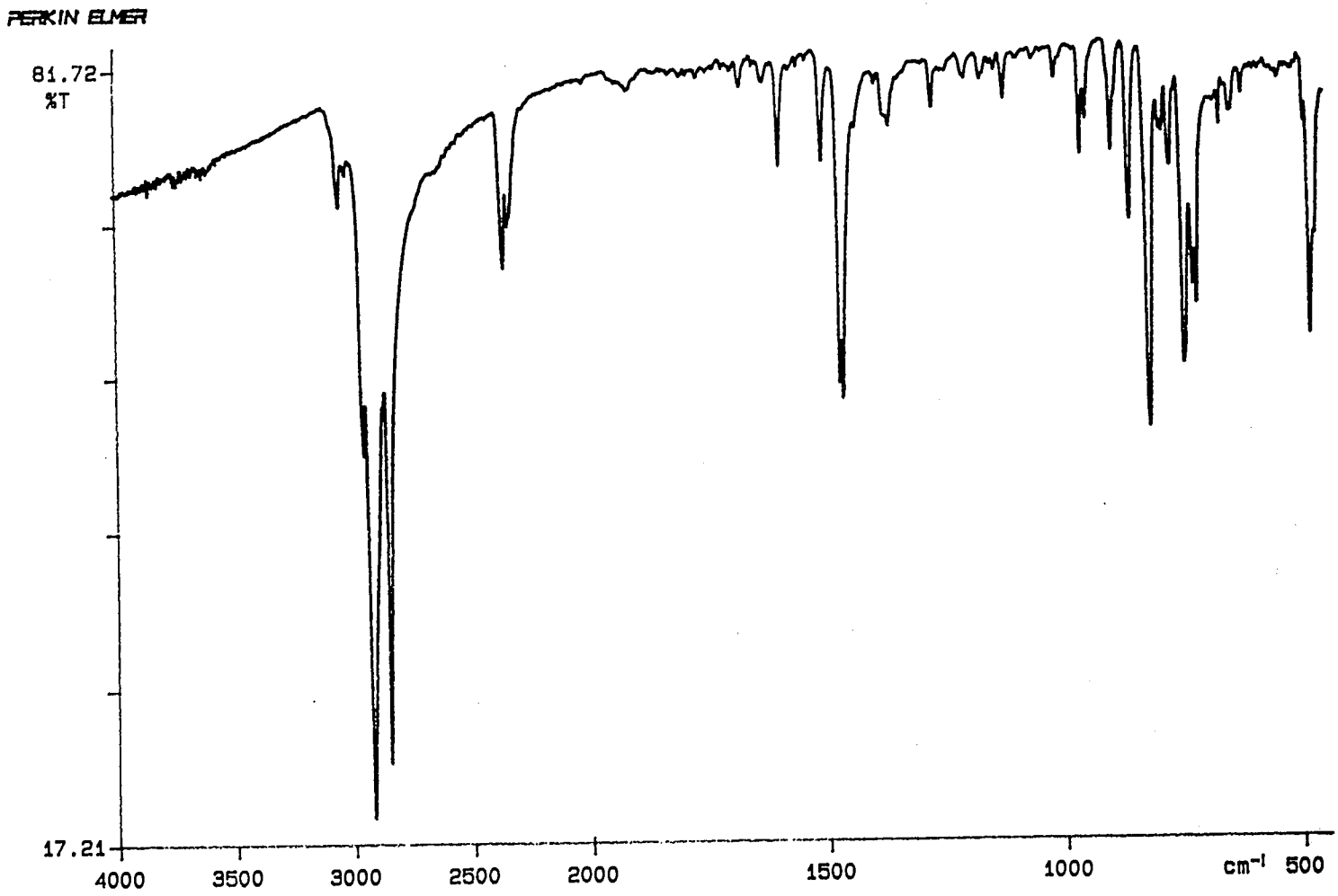

Figure 5.7. IR spectroscopy of 2-Hexadecyl Naphthalene.

Table 5.1. Berea Sandstone Cores Analysis.

Core No.	L (cm)	A (cm^2)	Air Perm. (mD)	Porosity (fraction)	Grain Den. (kg/m^3)
B-1	4.328	4.776	447	0.218	2,653
B-2	4.423	4.724	566	0.213	2,663
B-3	4.371	4.727	541	0.219	2,663
B-4	4.376	4.729	539	0.219	2,655
B-5	4.353	4.772	506	0.223	2,659
B-6	4.414	4.799	482	0.229	2,660
B-7	4.387	4.768	364	0.222	2,650
B-8	4.355	4.778	376	0.217	2,650

Table 5.2. Glauconitic Sandstone Cores Analysis.

Core No.	L (cm)	A (cm^2)	Air Perm. (mD)	Porosity (fraction)	Grain Den. (kg/m^3)
G-1	4.723	11.58	0.44	0.126	2,650
G-2	4.745	11.58	1.99	0.157	2,670
G-3	4.395	4.968	4.3	0.161	2,640
G-4	4.732	11.58	3.2	0.169	2,680
G-5	4.693	11.58	2.88	0.183	2,650
G-6	4.805	11.58	9.47	0.19	2,650
G-7	4.667	4.842	11.9	0.198	2,650
G-8	4.522	4.788	16.7	0.202	2,630
G-9	4.605	4.828	21.8	0.214	2,650
G-10	4.675	4.838	50.5	0.231	2,650
G-11	4.585	4.956	112	0.232	2,640
G-12	4.822	11.103	404	0.232	2,630
G-13	5.709	11.157	1,460	0.257	2,640

Table 5.3. Simulated Atcor Brine Mixture.

Composition	Typical Values (grams/litre)
$NaHCO_3$	2.95
$NaCl$	25.329
$CaCl_2$	1.44
KCl	0.61
$MgCl_2*6H_2O$	2.468
$Na2SO_4$	2.406

Table 5.4. Electrical Conductivity Measurements.

Solution	EC @ 25C° (mho/m)
DIW (0.0 g/l)	$1*10^{-4}$
KCl1 (0.07456 g/l)	0.01515
KCl2 (0.41008 g/l)	0.07858
KCl3 (0.7456 g/l)	0.1416
KCl4 (2.4232 g/l)	0.4453
KCl5 (3.2620 g/l)	0.585
KCl6 (4.1008 g/l)	0.696
KCl7 (5.7784 g/l)	0.928
KCl8 (7.456 g/l)	1.162
Atcor Provost Brine	4.43

Table 5.5. List of crude oils and hydrocarbon solvents used in surface potential calculations at 25 °C.

Medium	Viscosity, cp	Dielectric Constant,ε
Atcor Crude Oil	5	15
Forties Crude Oil	1.5	20*
Isopar-H	5	2
Methanol	0.623	32.6
Acetone	0.327	21
Toluene	0.59	2.4
n-Pentane	0.224	1.84

* Assumed.

CHAPTER SIX

RESERVOIR ROCK SURFACE POTENTIAL UNDER ASPHALTENIC OIL FLOW CONDITIONS

6.1 INTRODUCTION

Through the years the scientific community in the petroleum industry have suggested that the electric charge and consequent interparticle repulsion of colloidal asphaltene in petroleum reservoirs play an important role in its stability. This chapter first examines theoretically particles in crude oil to determine, if they are electrically charged, how important it is to their inter-particle repulsion. The theoretical results will be compared with the surface potential experimental results of asphaltene and/or solid in petroleum fluids.

6.2 THE EFFECT OF PARTICLE CHARGE IN PETROLEUM OIL

The effectiveness of particle electric potential at producing particle-particle or particle-surface forces when they are immersed in a low dielectric constant medium, can be compared to the effect of the same potential in water.

The repulsion force between two like charges, each Q, separated by distance r in a vacuum or solvent (dielectric constant ε_r) not supporting electrolytic dissociation is:

$$\frac{Q^2}{\varepsilon_r r^2} \qquad \text{(unrationalised)} \qquad (6.1)$$

with, under the same conditions,

$$Q = \psi \varepsilon a \tag{6.2}$$

where a is the particle radius and ψ is the particle potential. So the potential energy (free energy) of interaction V_R will be:

$$\int_{r=\infty}^{r=0} \text{Force}\, dr = \frac{\varepsilon a^2 \psi^2}{r} \tag{6.3}$$

This will slow down the diffusion controlled aggregation rate by a factor "W" where "W" is given by (Verwey and Overbeek, 1948):

$$W = 2a \int_{2a}^{\infty} \frac{1}{r^2} \exp\left(\frac{V_{(total)}}{kT}\right) dr \tag{6.4}$$

Where $V_{(total)}$ is the total potential energy of interaction produced by the summation of the double layer repulsion energy and the van der Waals attraction energy. If we give the electrostatic repulsion the best chance by taking the attraction as zero, then the kinetic slow down factor "W" will be:

$$W = 2a \int_{2a}^{\infty} \frac{1}{r^2} \exp\left(\frac{V_{(repulsion)}}{kT}\right) dr \tag{6.5}$$

With, $\frac{V_R}{kT}$ now:

$$\frac{\varepsilon \psi^2 a^2}{kT} \frac{1}{r} \left(= \frac{b}{r}\right) \tag{6.6}$$

Where $b = \frac{\varepsilon \psi^2 a^2}{kT}$, then equation (6.5) becomes:

$$W = \int_{2a}^{\infty} \frac{1}{r^2} \exp\left(\frac{b}{r}\right) dr \tag{6.7}$$

$$= \frac{2a}{b}\left[\exp\left(\frac{b}{2a}\right) - 1\right] \tag{6.8}$$

Now if we take an example to calculate the kinetic slow down factor "W" for the same charged particle in oil and (separately) water situations with:

$\psi = 50$ mV , particle radius a = 1000 Å , oil dielectric constant = 2, then parameter b = 1.352E-4, and $\frac{2a}{b} = 0.1479$ (in cgs units). The slow down factor in oil will be about 128. In an aqueous solution, the electrostatic repulsion (V_R) (Verwey & Overbeek, 1948) will be:

$$V_R = \frac{\varepsilon a \psi^2}{2} \ln\left(1 + e^{-\kappa H}\right) \qquad \text{(unrationalised)} \tag{6.9}$$

With the same parameters as before, and A = 1.0 kT, the total energy turns out to be ~ 100 kT. So that we are dealing in "W" with factors of exp(100) which in this case is huge.

Thus electrostatic repulsion, even if figures like 50 mV could be achieved for zeta potentials in low dielectric solvents (and they cannot), does not match the repulsion (and the "W" values) commonly reached in water, this despite the fact that the repulsion reaches out to greater distances in low dielectric solvents.

6.3 STREAMING POTENTIAL AND CURRENT MEASUREMENTS

Streaming potential and current measurements are associated with the presence of electrical charges on solid surfaces. In the petroleum industry streaming potential measurements have been used through the interpretation of electric logs to define reservoir formations. The investigations of Wyllie (1951) and Hill *et al.* (1959) recognised that a correction needs to be made to recorded spontaneous potential logs for streaming potential originating from the difference in pressures between the mud column and the formation. The parameters involved in the measurement of streaming potential and current during flow conditions are:

1. Pressure differential.
2. Liquid conductivity.
3. Pore pressure.
4. Pore size of the flow channel.
5. Double layer overlap, especially in non-aqueous system.

The first two points are discussed in this chapter, whereas the last three points will be deferred to the next chapter.

6.3.1 EFFECT OF PRESSURE DIFFERENTIAL

In order to measure streaming potential and current in a porous system the liquid must be forced to flow by an applied pressure difference. Figures 6.1 and 6.2 are the plots of streaming potential and current versus pressure differential for the flow generated from *KCl* solutions through Berea sandstone cores (Table 5.4). Each point on the plot represents the average of one minute values of streaming potential/current. These plots indicate that both measurements are proportional to pressure gradient. The direction of the slopes with respect to electrode electrical

connection indicate the sign of the electrokinetic potential, in this case indicating that Berea sandstone possesses a negative charge, relative to the flowing liquid.

These figures also indicate that the streaming potential and current measurements are of the order of hundreds of milivolts and tens of micro-amps respectively in low aqueous electrolyte concentrations and, especially for the streaming potential, decrease with increasing conductivity. Figure 6.3 shows that streaming potential values in Atcor Provost brine are scattered, whereas in dilute *KCl* aqueous solutions they are much smoother. This is due to the much higher conductivity in the Atcor Provost brine.

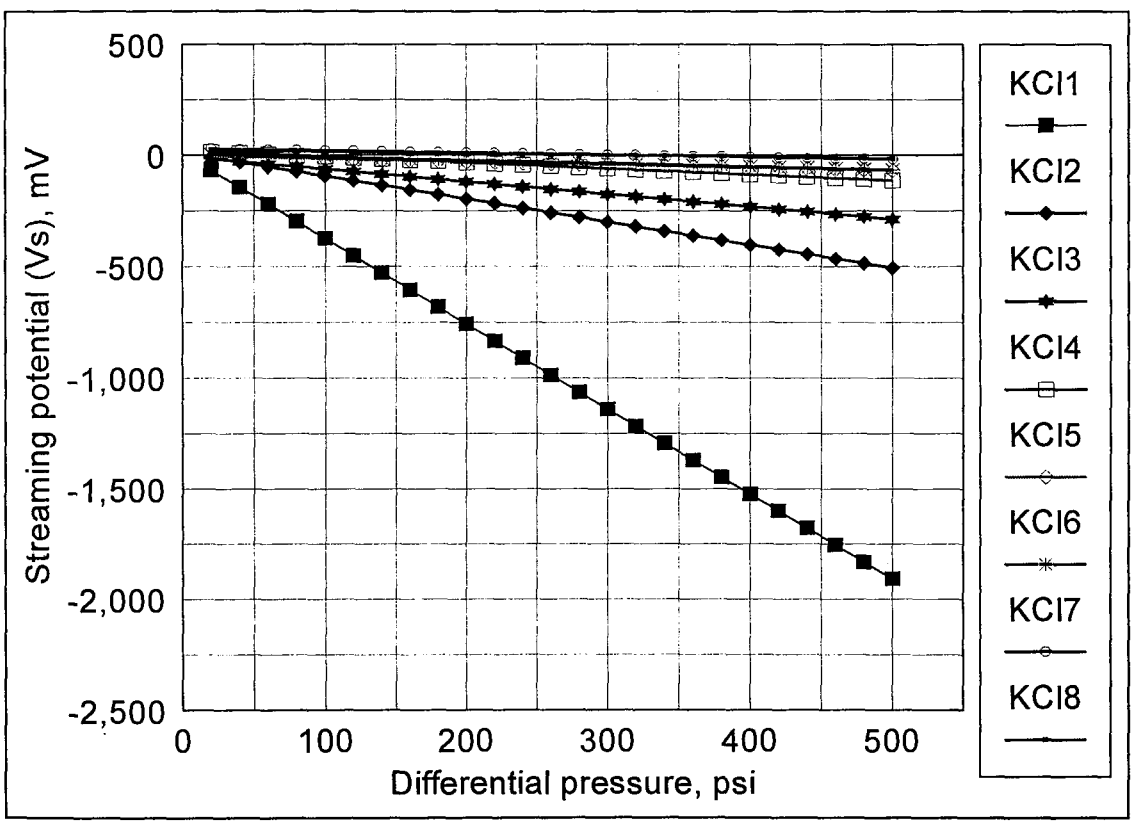

Figure 6.1. Streaming potential vs. differential pressure for various *KCl* solutions.

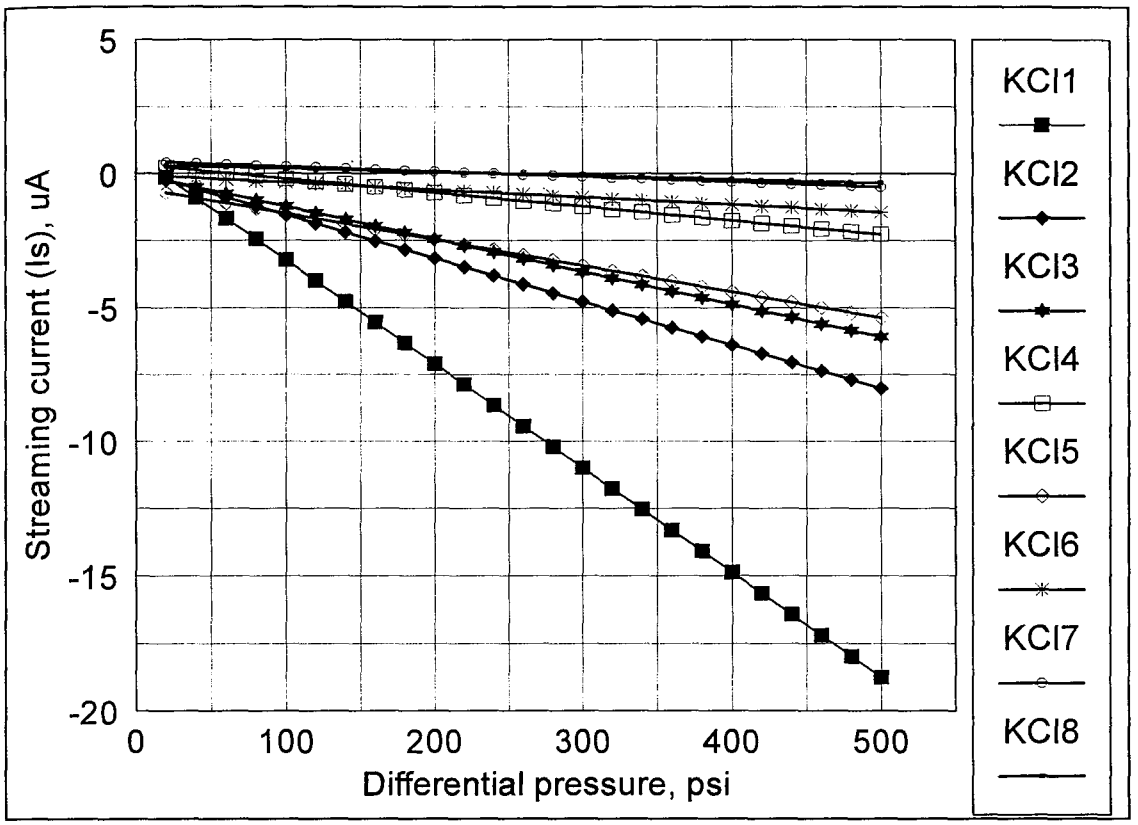

Figure 6.2. Streaming current vs. differential pressure for various *KCl* solutions.

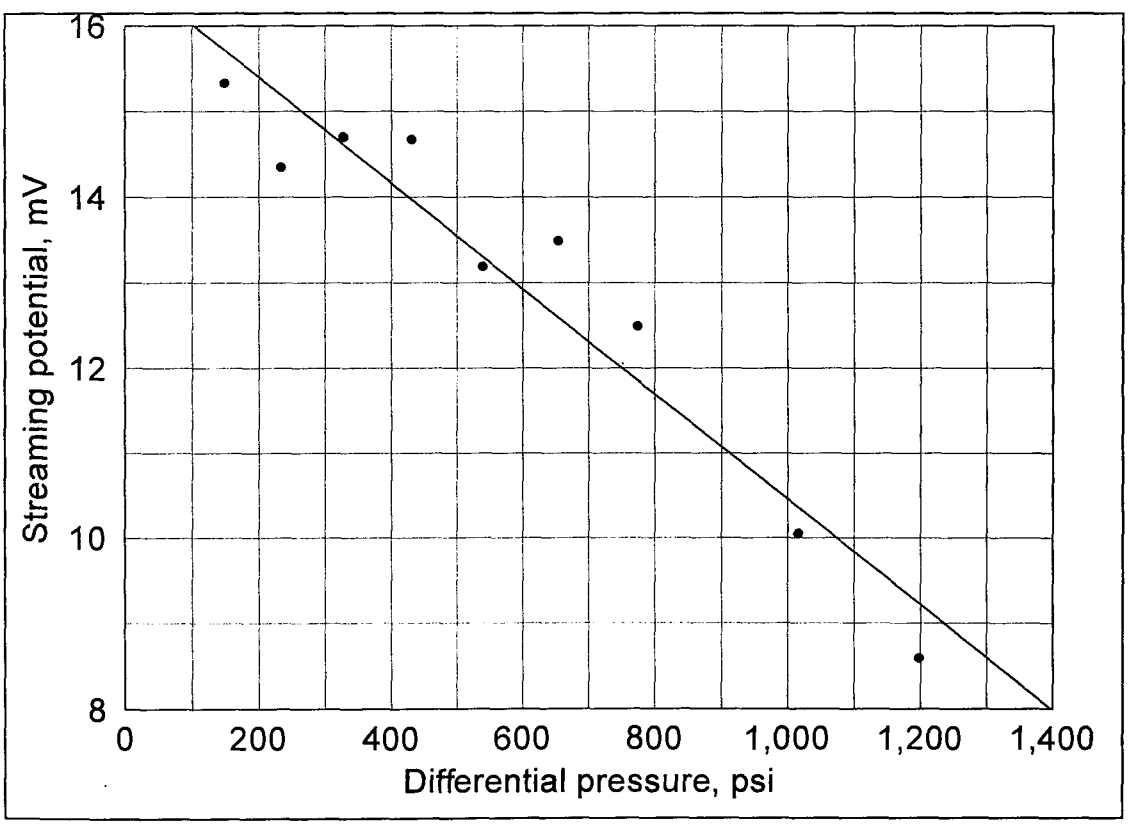

Figure 6.3. Streaming potential vs. differential pressure for Atcor Provost brine in Berea sandstone.

6.3.2 EFFECT OF LIQUID CONDUCTIVITY

The liquid conductivity is an important parameter in the study of the electrokinetic potential in porous system. Crude oil and hydrocarbon solvents are of low conductivity, mainly due to the low concentration of charge carriers, (though a little arises from the higher viscosity).

Figures 6.4 and 6.5 show typical plots of streaming potential and current versus liquid conductivity for various values of differential pressure ranging from 100 [0.69 MPa] to 1000 psi [6.9 MPa]. These plots indicate that for a constant differential pressure both measurements decrease with increasing conductivity. The decrease of streaming current is due to the decrease of electrokinetic potential (seen as the Stern potential ψ_d) even at constant wall potential ψ_o. That of the streaming potential is due to this same effect plus the decrease of the potential drop in high electrolyte (low resistance) when the streaming current flows back through the solution to constitute the streaming potential.

It is possible to measure the streaming current directly by drawing it off through a low impedance path which short-circuits the return path through the conducting liquid. The liquid path resistance involved in the streaming potential cannot be directly related to the conductivity of the liquid since a low resistance path at the solid surface (surface conductivity) always exists. In the case of aqueous solutions this arises from the double layer at the surface (unless by chance the surface potential is zero) which produce a net adsorption of electrolyte near the surface. In the case of crude oil in rock pores (as in much of this work) it arises from the presence of an irreducible (in practice) layer of adsorbed water at the rock surface. The streaming current method is much to be preferred as being both more fundamental and free from surface conductivity errors.

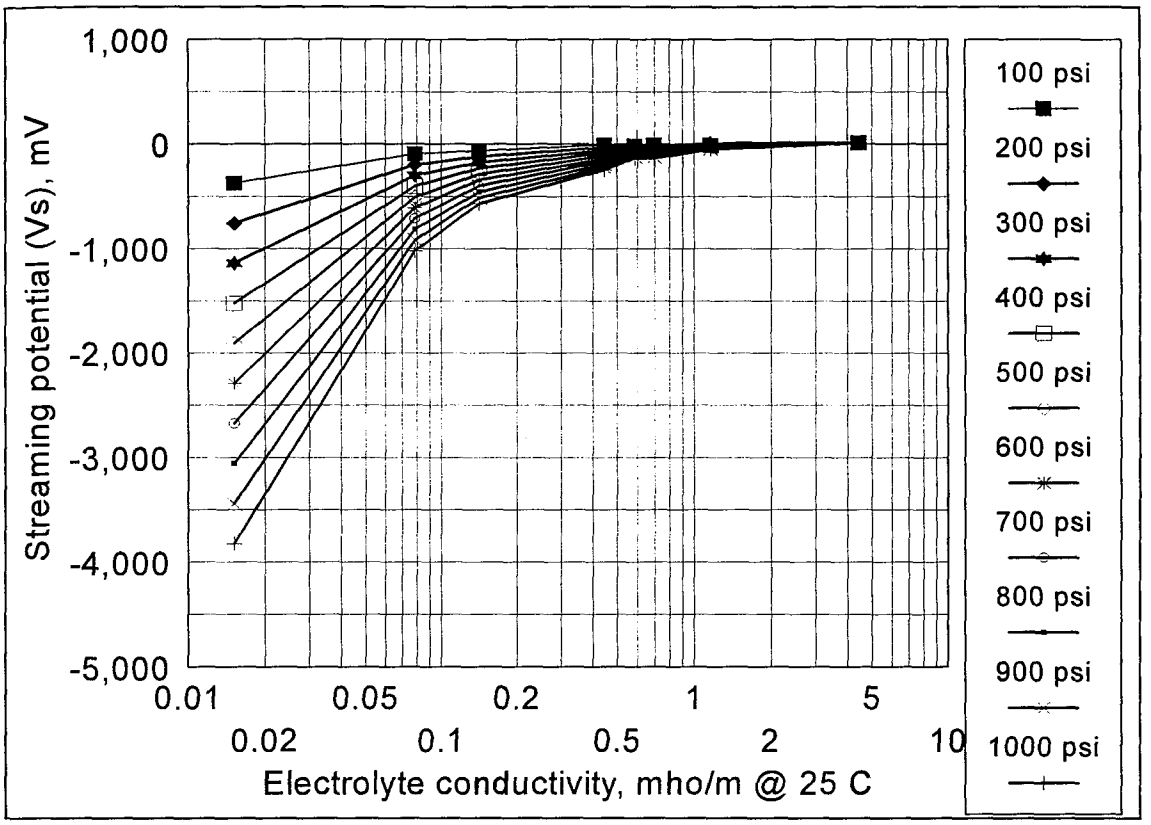

Figure 6.4. Streaming potential vs. conductivity for aqueous *KCl* solutions in Berea sandstone.

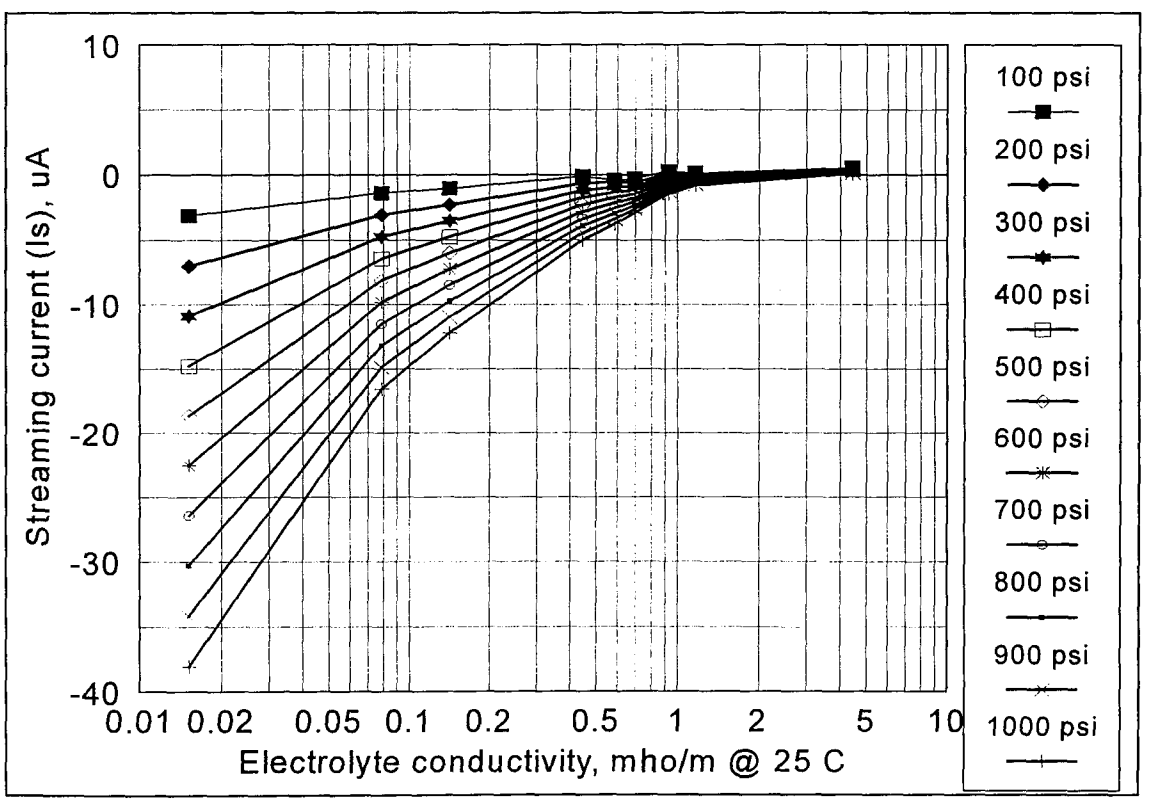

Figure 6.5. Streaming current measurements vs. conductivity for aqueous *KCl* solutions in Berea sandstone.

6.4 ESTIMATION OF ROCK PORES AREA/LENGTH RATIO

In low electrolyte concentrations, such as crude oil, the surface conductivity will dominate streaming potential measurements and therefore also any derived electrokinetic potentials. Surface conductivity is not involved in streaming current measurements though the pores area/length is now required. Chapter 3, section 3.7, introduced a novel method to show how area/length ratios for a porous systems can be obtained by combining streaming potential and streaming current measurements on rock cores and avoiding the arbitrary assumptions involved in the Briggs method (1928).

Figure 6.6 shows an example of the method in Berea sandstone (sample B-2) by plotting $\frac{I_s}{KV_s}$ against *KCl* (aqueous) concentrations. The plot shows clearly the influence of surface conductivity at low electrolyte concentration. With increasing electrolyte concentration the surface conductivity rapidly decreases to the point where $\frac{I_s}{KV_s}$ levelled off at a value of $2*10^{-5}$ m. As defined by equation (3.25) the value of $2*10^{-5}$ m from Figure 6.6 represents the ratio of pore area cross-section to length of the rock core.

Both the expression for streaming current and streaming potential make the assumption that the capillary (pore) diameter is a good deal larger than the double layer thickness. This is certainly valid for the *KCl* solution measurements used to obtain f (equation 3.25) but must in general be questioned for non-aqueous measurements. However, this assumption will be made for sandstone core samples used in this work, for which we have microscopic and mercury injection capillary pressure evidence indicates that the pores are large enough to validate the expressions given. The double layer overlap in narrow pores will be discussed in detail in the next chapter.

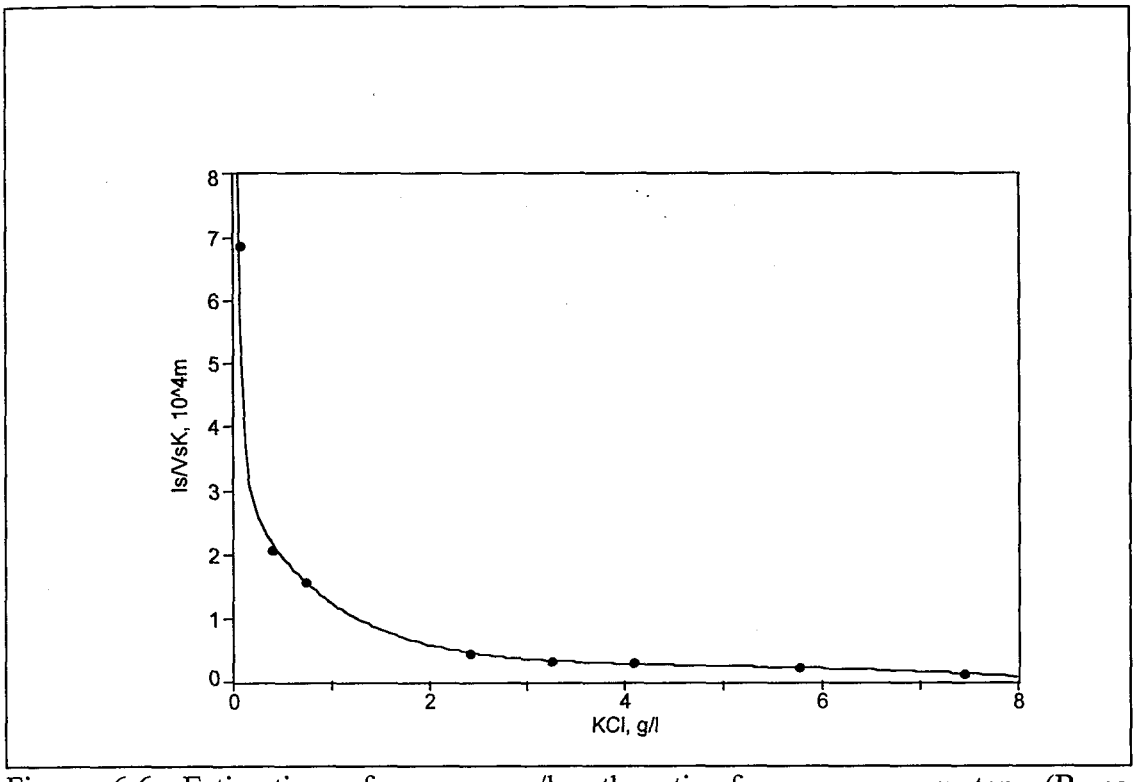

Figure 6.6. Estimating of pores area/length ratio for a porous system (Berea sandstone).

This method can be regarded as a significant improvement on that usually attributed to Briggs (1928) in which it is assumed that 0.1 mol dm^{-3} concentration of electrolyte is sufficient to make the effect of surface conductivity negligible. In the present method the concentration necessary to make a justified assumption is determined directly from experimental data as shown in Figure 6.6. A further important advantage of the present method is that it gives a value of $\Sigma A / L$ which can be used in other analysis.

6.5 AQUEOUS ELECTROKINETIC POTENTIALS

The electrokinetic (zeta) potential of reservoir sandstone rock cores in *KCl* solutions and Atcor Provost reservoir brine are calculated from streaming potential and current measurements. The results from streaming potential data did not, naturally, agree with the zeta potential values calculated from the data on streaming

current. This of course is due to the influence of surface conductivity on streaming potential data.

Table 6.1 and Figure 6.7 represent Berea sandstone zeta potentials from streaming potential (ζ_{Vs}) and current data (ζ_{Is}) in *KCl* solutions. The potentials by streaming current were calculated after obtaining the pores A/L ratio of Berea cores as above. An example of the calculation of zeta potential for a rock core is given in Appendix B. The plot gives a convenient opportunity for illustrating the influence of surface conductivity. As can be seen, at low electrolyte concentrations surface conductivity dominated and invalidated streaming potential measurements. A reduction of the influence of surface conductivity can be seen at higher conductivities.

Table 6.1. Berea Sandstone (Sample B-1) Surface Potential From Streaming Potential and Current Data.

Solution	$\dot{V}_s$ $(VN^{-1}m^2)$	$\dot{I}_s$ $(AN^{-1}m^2)$	ζ_{Vs}* (mV)	ζ_{Is}** (mV)
DIW	-1.728E-6	-3.705E-12	-0.25	-76.33
KCl1	-3.779E-7	-4.466E-12	-8.26	-92.02
KCl2	-1.643E-7	-2.281E-12	-18.62	-47.0
KCl3	-9.689E-8	-2.331E-12	-19.78	-48.02
KCl4	-2.353E-8	-9.871E-13	-15.11	-20.33
KCl5	-1.593E-8	-6.674E-13	-13.44	-13.75
KCl6	-1.558E-8	-7.281E-13	-15.64	-15.0
KCl7	-1.147E-8	-7.451E-13	-15.35	-15.35
KCl8	-7.314E-9	-5.946E-13	-12.25	-12.25
Atcor Brine	-8.919E-10	-2.770E-13	-5.7	-5.7

* See Table 5.4. for solution conductivities.

** B-1 pores A/L= $7*10^{-5}$ m.

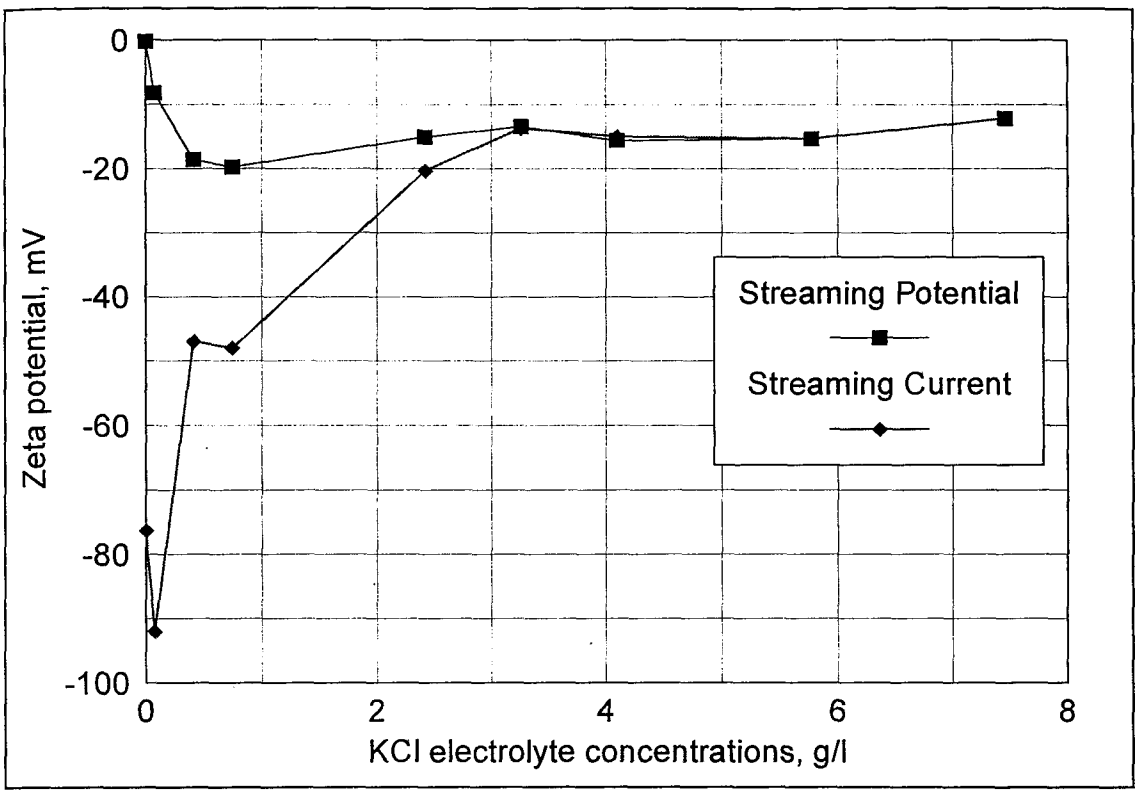

Figure 6.7. Berea sandstone surface potential from streaming current and (invalidly) from streaming potentials.

In the streaming current curve, which is the validly calculated surface potential, increasing ionic strength caused compression in electric double layer and therefore a reduced surface potential. The streaming current data at concentrated electrolyte solutions are in good agreement with the work of Schramm *et al.* (1991). This investigated the electrophoretic mobilities (and zeta potentials) of desegregated Berea sandstone (obtained from the same location, Cleveland Quarries,Ohio) in *NaCl* solutions.

6.6 HYDROCARBON ELECTROKINETIC POTENTIALS

In early experiments (Chapter 5 section 5.2) the streaming potential of asphaltene particles were measured by trapping them on a Millipore filter and flowing hydrocarbon solvents and crude oil through the "cake". Asphaltene zeta potentials were calculated using equation (3.21) (though later work showed streaming potentials

to be invalid relative to streaming currents, the sign of the potential will still be valid). It is shown in Table 6.2. that asphaltene particles are positively charged in isopar-H, n-pentane and crude oil, whereas in acetone they exhibit negative potentials. As shown in Table 6.2 apparent asphaltene particle potentials are very small and almost negligible due to the surface conductivity errors.

Table 6.2. Asphaltene Zeta Potential in Hydrocarbon Systems From Streaming Potential Data.

Solvent *	K_{trure} (mho/m)	Dielectric constant (ε_r)	$\dot{V}_s$ $(VN^{-1}m^2)$	ζ_{Vs} (mV) (apparent)
Acetone	1.2E-5	20.7	-2.523E-6	-0.054
n-Pentane	1.0E-12	1.84	1.179E-4	4.269E-6
Isopar-H	4.0E-13	2	8.585E-5	9.696E-6
Forties crude oil	1.0E-8	20	6.8E-6	5.76E-4

* See Table 5.5.

Figure 6.8 and Table 6.3 represent asphaltene precipitation from Forties crude oil (North Sea crude) on Millipore filters by the addition of n-pentane in the ratio 1:0.5. The zeta potential of a Millipore filter itself in Forties crude oil was derived from streaming potential measurements and calculated using equation (3.21). The Millipore filters (negative) zeta potential decreased numerically with increasing amount of precipitated asphaltene. However, those potentials are effected by surface conductivity errors.

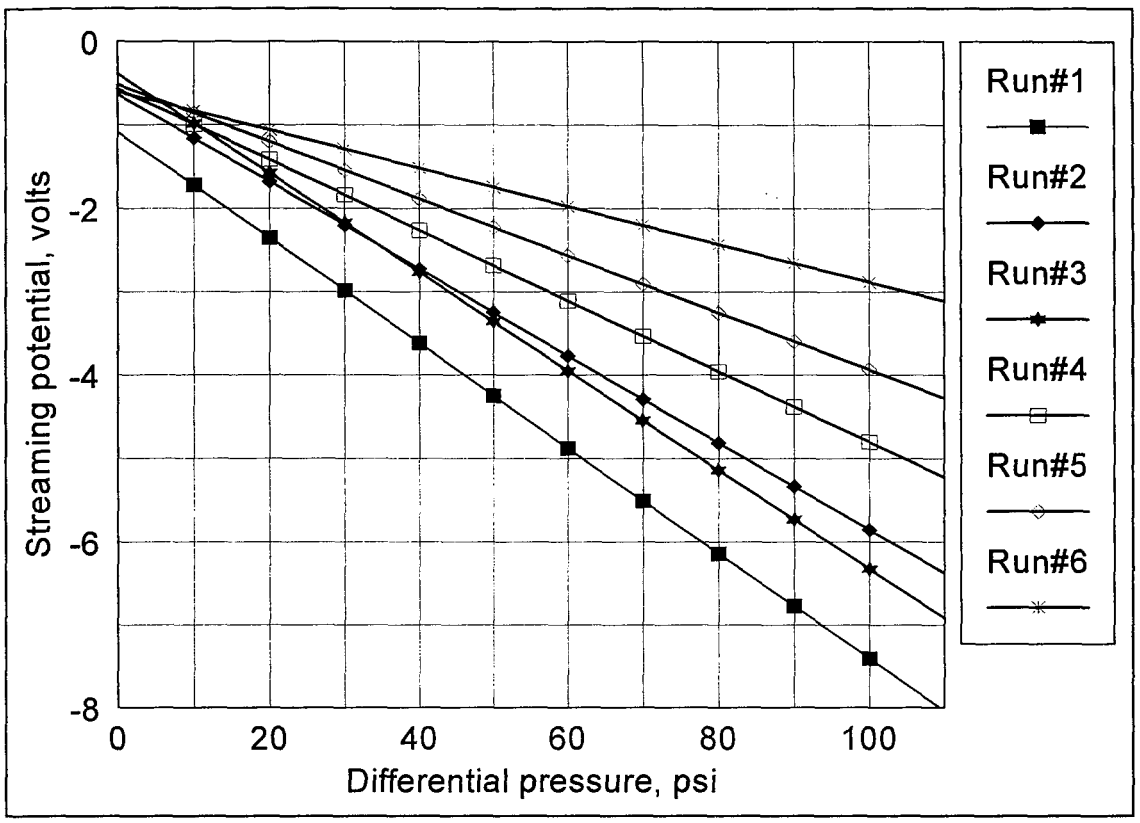

Figure 6.8. Streaming potential measurements during asphaltene precipitation from Forties crude oil by n-pentane.

Table 6.3. Millipore Experiment, Zeta Potential During Asphaltene Precipitation by n-Pentane.

Forties crude oil *	$\dot{V}_s$ $(VN^{-1}m^2)$	ζ_{vs} (mV)
W/O n-pentane	-1.011E-5	-8.564E-4
Run# 1	-9.166E-6	-7.764E-4
Run# 2	-7.571E-6	-6.413E-4
Run# 3	-8.61E-6	-7.293E-4
Run# 4	-6.142E-6	-5.203E-4
Run# 5	-4.956E-6	-4.198E-4
Run# 6	-3.311E-6	-2.805E-4

* η = 1.5cp and conductivity assumed $1*10^{-8}$ $ohm^{-1}m^{-1}$.

Table 6.4 presents dry sandstone cores surface potential interfacing with hydrocarbon solvents and crude oil from streaming potential and current measurements. The rock cores are found to have negative surface potentials in hydrocarbons. The experimental results indicate that surface conductivity, indeed, dominated and invalidated streaming potential measurements. The Keithley Model 617, made it possible to measure very low currents of order 10^{-10} A in a very low permittivity medium such as toluene. The rock cores surface potential in semi-polar solvents (acetone & methanol) are found to be negative and not dissimilar to those in water. In non-polar liquid such as toluene, pentol and crude oil small negative potentials were found.

Table 6.4. Sandstone Rock Cores Surface Potential in Hydrocarbon Systems.

Solvent	K_{true} (mho/m)	Dielectric constant (ε_r)	$\dot{V}_s$ $(VN^{-1}m^2)$	$\dot{I}_s$ $(AN^{-1}m^2)$	ζ_{Vs} (mV)	ζ_{Is} (mV)
Acetone	1.2E-5	20.7	-4.1E-6	-3.684E-12	-0.088	-94
Methanol	5.8E-4	32.6	-4.86E-6	-7.25E-13	-6.1	-22.4
Toluene	1.0E-12	2.4	-3.78E-7	-4.73E-17	-1.05E-8	-0.06
Pentol	1.0E-12**	1.84-2.4	N/M*	-5.888E-17	N/M*	-0.026
Atcor crude oil	3.74E-8	15	N/M	-2.01E-15	N/M	-3.03

* not measured. ** assumed.

6.7 ASPHALTENIC OIL ELECTROKINETIC POTENTIALS

The theoretical treatment above concluded that the charge of particles in crude oil will not lead to significant inter-particles electrostatic repulsion. To illustrate the theoretical results with experimental data, asphaltene particle potential and adsorption on rock cores surfaces have been investigated in hydrocarbon solvents and crude oil from streaming current data.

After the merits of streaming current rather than streaming potential measurements were appreciated, experiments were performed on dried sandstone rock cores with asphaltene dispersions in both pentol and in crude oil "Atcor Provost Field". Zeta potentials were calculated from streaming currents (equation 3.22) after A/L ratios were obtained by the method described above.

Figure 6.9 shows the results for Berea sandstone (sample B-1) in pentol solutions. In the absence of dispersed asphaltene the zeta potential of the rock surface was negative (0.05 mV) being less negative at increasing asphaltene concentrations, eventually becoming essentially zero at asphaltene concentrations above 1.5 *g/l.* Above this concentration the surface potential will be of asphaltene rather than Berea sandstone. Although described as "essentially zero" the potentials can be seen to be very slightly positive as in the earlier Millipore experiments. The results indicate the very much greater sensitivity of streaming current measurements over those of conventional electrophoresis (though see the rough 15 days electrophoresis measurements in section 6.10).

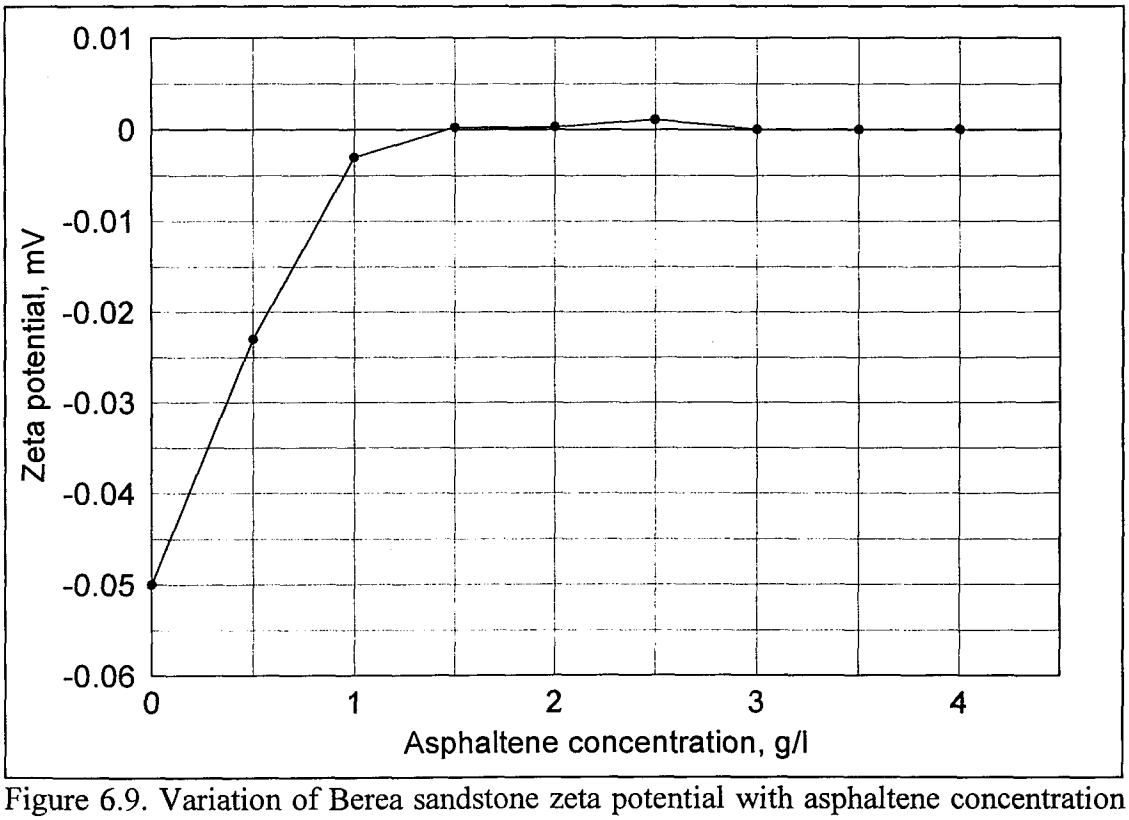

Figure 6.9. Variation of Berea sandstone zeta potential with asphaltene concentration in Pentol solutions.

Figure 6.10 shows dry Berea sandstone (sample B-6) surface potentials in Atcor Provost crude oil. The crude oil was introduced into the core sample at a constant flow rate of 0.15 ml/min. for a period of 25 days. The sample B-6 zeta potentials were calculated from the observed streaming currents with the knowledge of pores A/L ratio. As can be seen the sandstone zeta potential is initially negative but becomes gradually less negative with time, no doubt as asphaltene adsorbs onto the surface. The zeta potential this time does not quite reach zero or become slightly positive. This may be due to the presence of resins along with the asphaltene in crude oil. According to Gonzalez et al (1987), asphaltenes were adsorbed to a greater extent than resins, and the adsorption of the mixtures was at least equivalent to the weighted average of the adsorption of both components separately (see Figure 2.2). This study shows a significant effect of asphaltene adsorption on rock surface potentials.

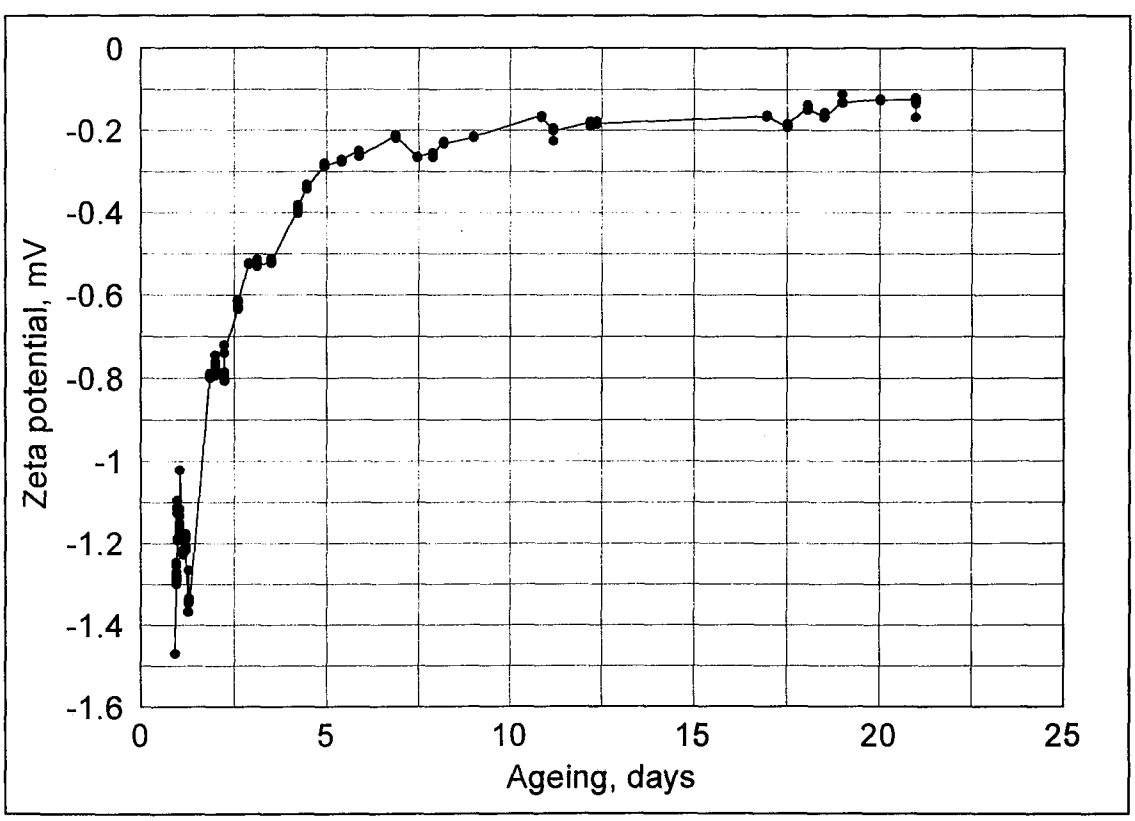

Figure 6.10. Variation of Berea sandstone zeta potential with ageing in Atcor Provost crude oil.

6.8 FORMATION DAMAGE ANALYSIS

It is concluded from the previous section that as asphaltene deposits/adsorbs on the rock pore surfaces, the reservoir rock negative surface potential became steadily more positive. Of course, as the pores become blocked the value of A/L will fall. This section aims to provide an insight into the effect of asphaltene adsorption on the absolute pores A/L, permeability and production efficiency.

6.8.1 Asphaltene Adsorption Thickness

This section deals quantitatively with the effect of asphaltene adsorption on rock pores radius. This can be estimated by assuming Poiseuille laminar flow conditions in the pores.

Suppose we have a core sample consisting of (n) capillaries each of radius (a) and length (l). Using Poiseuille law, the effect of a deposited layer of asphaltene (γ) thick can be estimated:

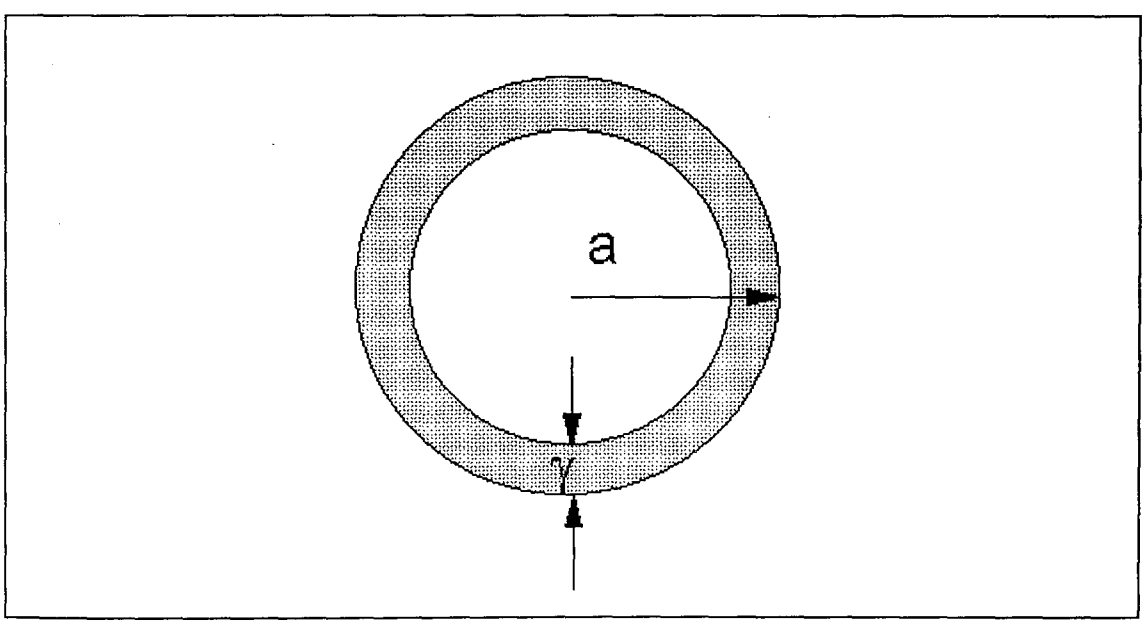

Figure 6.11. Schematic diagram representing the core capillary.

$$q_o = \frac{n\pi a_o^4 P}{8\eta l} \tag{6.10}$$

$$q_1 = \frac{n\pi a_1^4 P}{8\eta l} = \frac{n\pi P}{8\eta l}(a-\gamma)^4 \tag{6.11}$$

Where q is the rate of flow, q_o before constriction, q_1 after.

then,

$$q_1 = \frac{n\pi a^4 P}{8\eta l}\left(1-\frac{\gamma}{a}\right)^4 \tag{6.12}$$

hence,

$$q_1 = q_o\left(1-\frac{\gamma}{a}\right)^4 \tag{6.13}$$

$$\therefore \text{ Asphaltene adsorption thickness ratio}\left(\frac{\gamma}{a}\right) = 1-\left(\frac{q_1}{q_o}\right)^{1/4} \tag{6.14}$$

Figure 6.12 show relative asphaltene adsorption thickness as based on pores in a B-1 sample using asphaltenic Pentol solutions. The thickness of asphaltene is calculated from equation (6.14) and plotted against asphaltene concentrations in pentol. The flow rates indicated a plateau of asphaltene adsorption at around a relative pore blocking thickness of $\gamma / a = 0.3$ which was also the point at which the asphaltene streaming current reached a plateau.

Figure 6.13 shows asphaltene adsorption thicknesses in a B-6 sample from asphaltenic Atcor crude oil under a constant flow condition. The thickness calculated using equation (6.14) and plotted against the time of flooding. After 10 days the adsorption reached an asphaltene thickness (γ / a) at a plateau of 0.3.

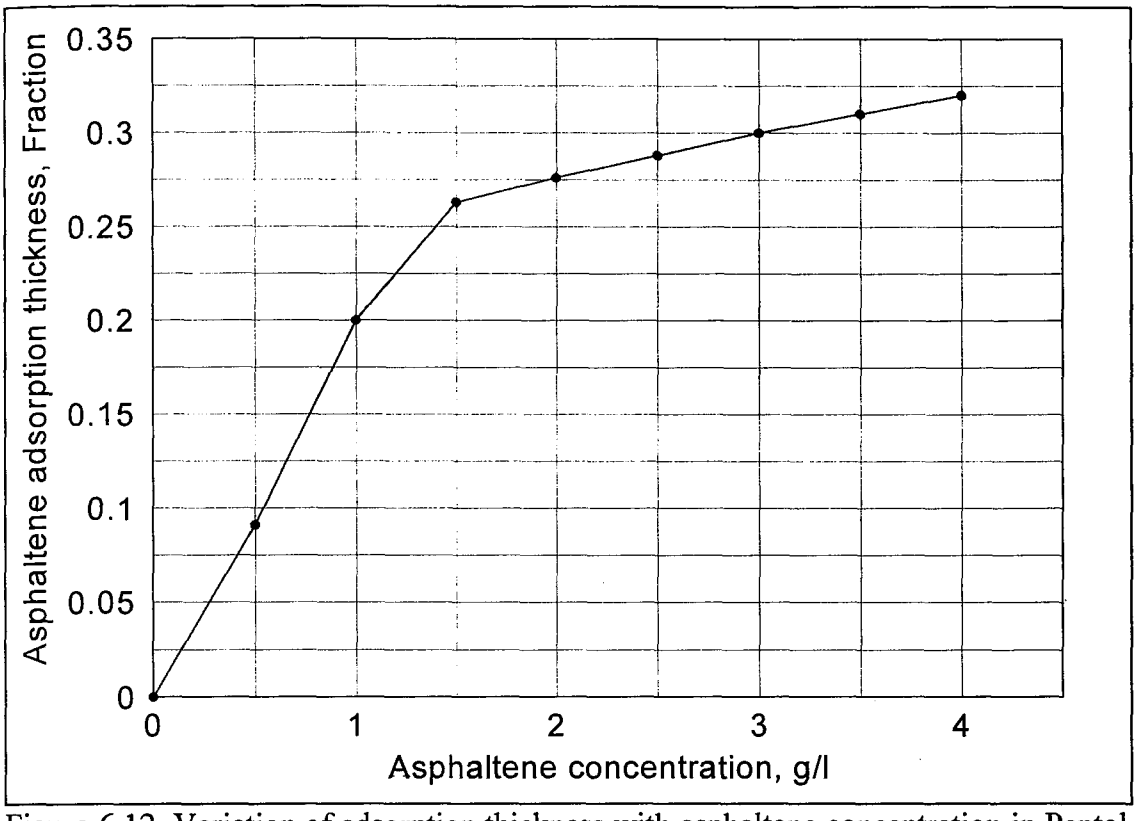

Figure 6.12. Variation of adsorption thickness with asphaltene concentration in Pentol solutions.

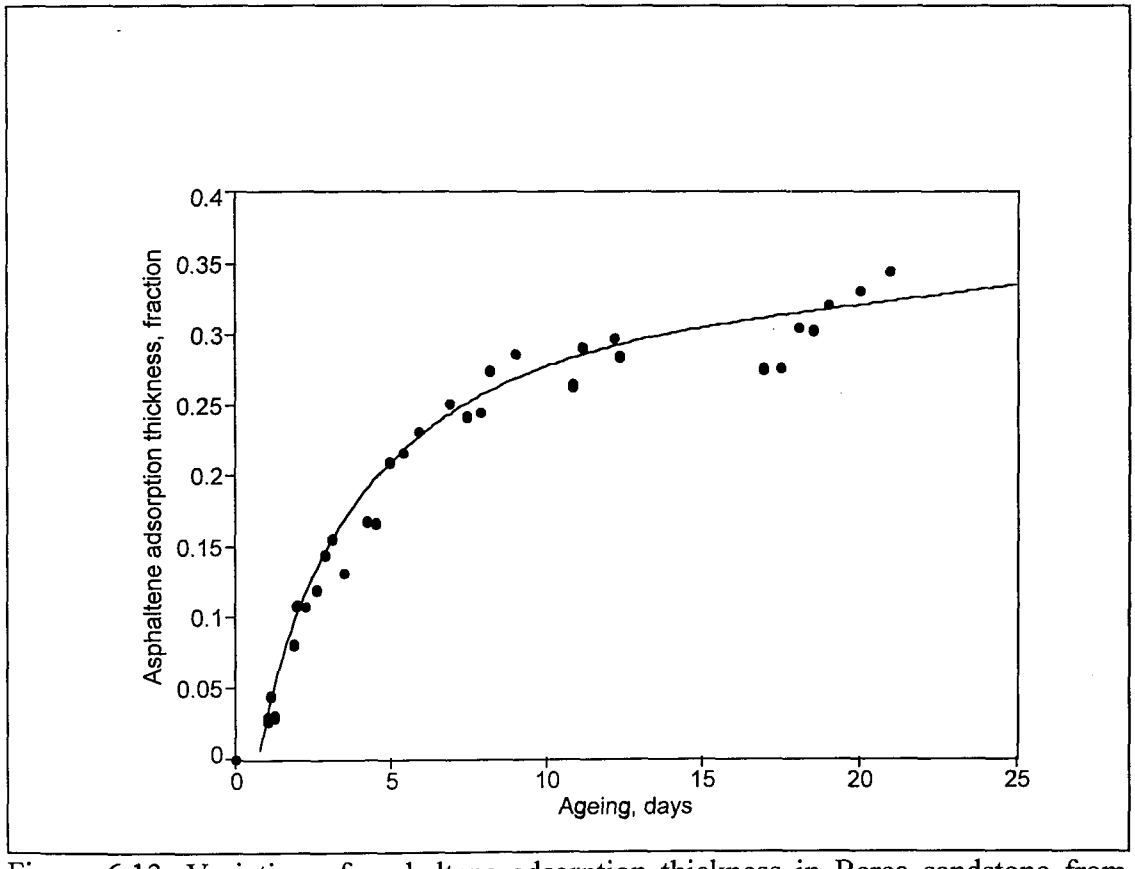

Figure 6.13. Variation of asphaltene adsorption thickness in Berea sandstone from Atcor crude oil.

6.8.2 ROCK PORES A/L RATIO

The reduction in rock core pores area caused by asphaltene adsorption on rock surfaces can be estimated in a similar quantitative way as radius reduction. But the fraction of radius blocked is not the same as the fraction of area (cross section) blocked and neither fraction is the fractional flow blocked. The damage on the cross-sectional of rock pores can be estimated as follow:

From Poiseuille law, equation (6.10), taking the length L to be unchanged:

$$q \alpha A^2 \tag{6.15}$$

So that:

$$\frac{(A/L)_I}{(A/L)_o} = \left(\frac{q_I}{q_o}\right)^{1/2} \tag{6.16}$$

This allows (A/L) values, necessary to calculate ζ from streaming currents, to be determined as blocking proceeds. Figures 6.14 and 6.15 show pores A/L ratio reduction in pentol solutions and Atcor crude oil respectively. In the pentol solution case, the pores A/L ($7*10^{-5}$m) of sample B-1 reduced rapidly with increasing asphaltene concentrations up to 1.5 g/*l*, then the reduction slowed down and reached a plateau of $3.4*10^{-5}$ m. In Atcor crude oil case, the B-6 sample pores A/L ($2.5*10^{-5}$m) decreases rapidly up to 6 days, after that the reduction rate slowe down and reached a plateau of $1.21*10^{-5}$ m.

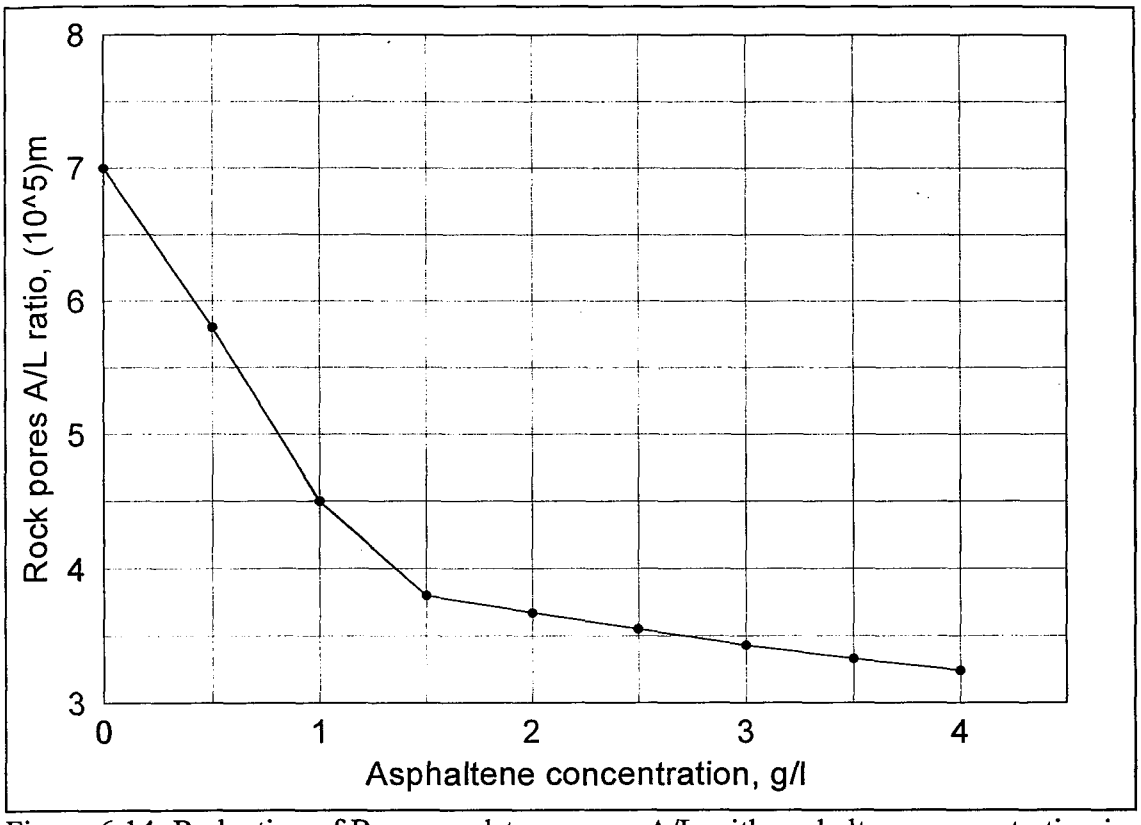

Figure 6.14. Reduction of Berea sandstone pores A/L with asphaltene concentration in Pentol solutions.

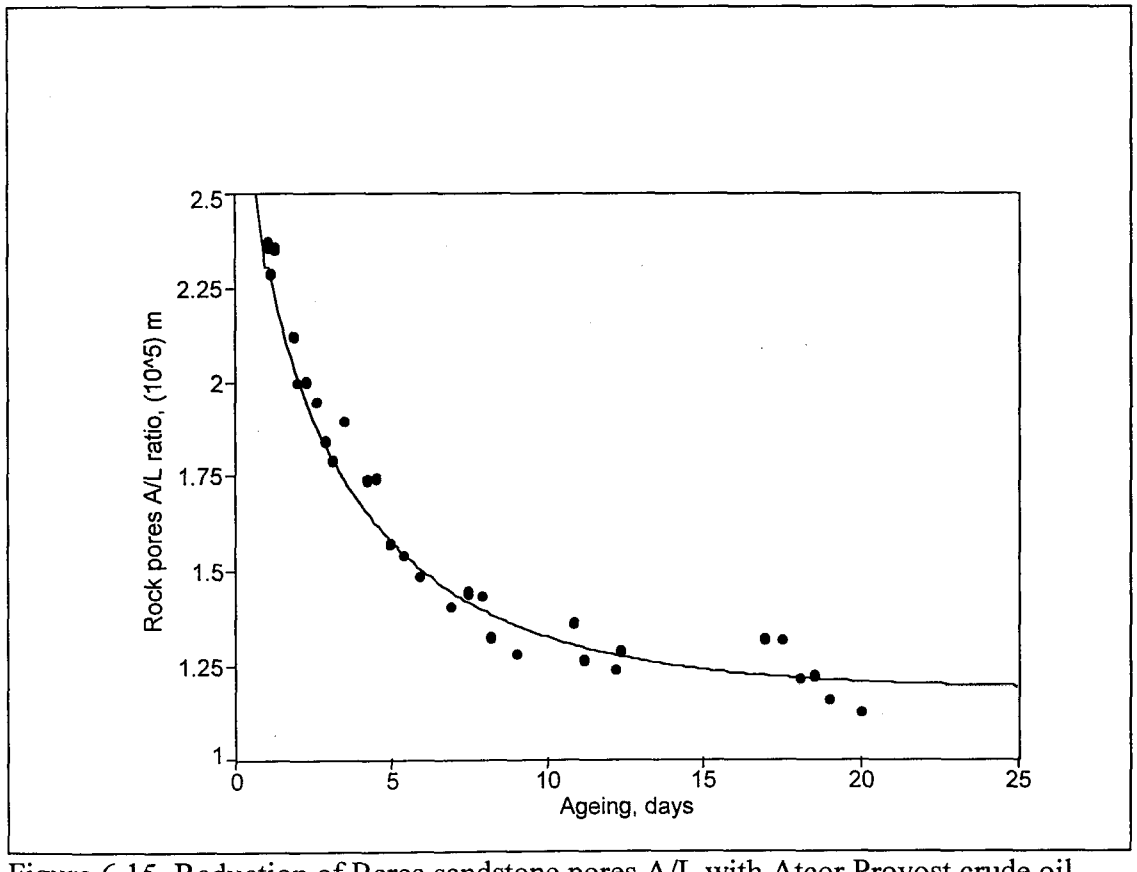

Figure 6.15. Reduction of Berea sandstone pores A/L with Atcor Provost crude oil.

Since the fraction of radius blocked γ / a can be estimated by equation (6.14), the fraction of cross-sectional area blocked follows as:

$$2\left(\frac{\gamma}{a}\right)-\left(\frac{\gamma}{a}\right)^2 \qquad (6.17)$$

We can asses the damage caused by asphaltene adsorption on rock pores area in sandstone cores from equation (6.17). Earlier Figure 6.12 shows that asphaltene adsorption thickness from Pentol solutions reached a plateau of ~0.33. This fraction of radius blocked corresponds to a 55% area blocked. A similar result from Figure 6.13 shows that asphaltene thickness reached to a plateau at 0.34 with Atcor crude oil. This similarly corresponds to a 56% blocking in rock pores cross-sectional area under Atcor crude oil.

6.8.3 PERMEABILITY AND FLOW EFFICIENCY

Obviously, any reduction in rock pores cross sectional area will affect other reservoir rock characteristics. Figure 6.16 shows the reduction in the effective permeability calculated from flow data, using the Darcy equation, plotted against asphaltene concentrations in pentol solutions. As asphaltene concentration increases the rock effective permeability dramatically decreases to a limit of 70% reduction when asphaltene concentrations in pentol reached above 1.5 g/*l*.

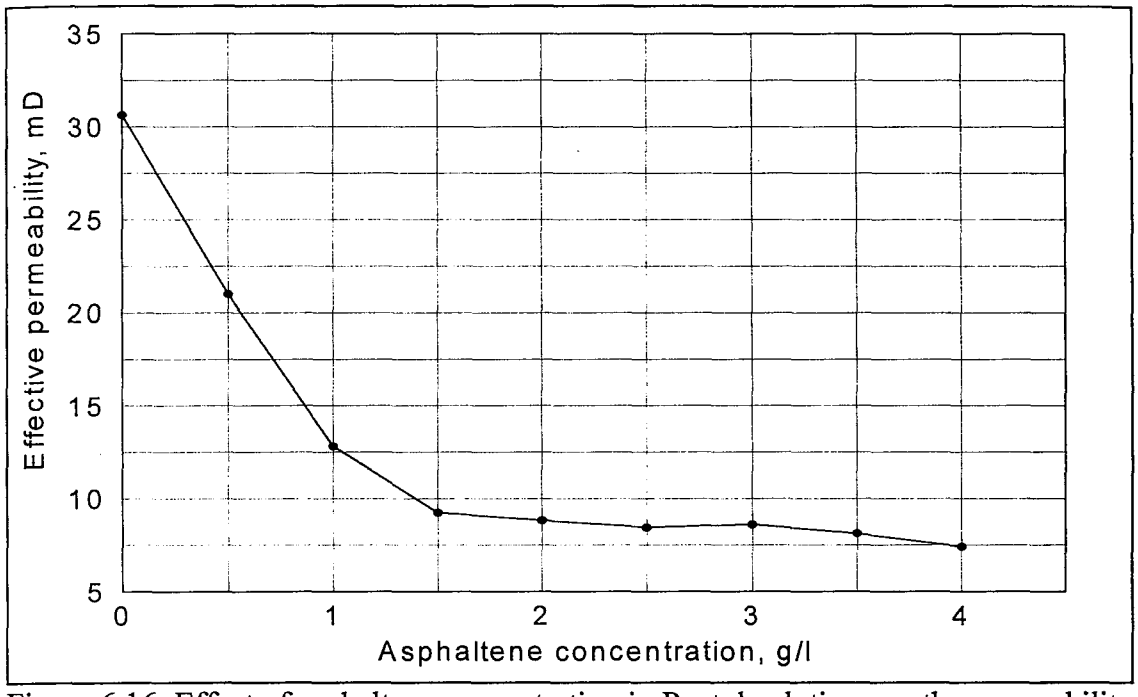

Figure 6.16. Effect of asphaltene concentration in Pentol solutions on the permeability of sample B-1.

Figure 6.17 presents the damage in the effective permeability of sample B-6 from Atcor crude oil flow (0.15 ml/min.). Sample B-6 permeability dropped steadily with time during Atcor oil flood from 4.8 mD and reached a plateau value of 0.3 mD. This indicates that the damage by asphaltene adsorption from Atcor oil is significant and reached 93% reduction.

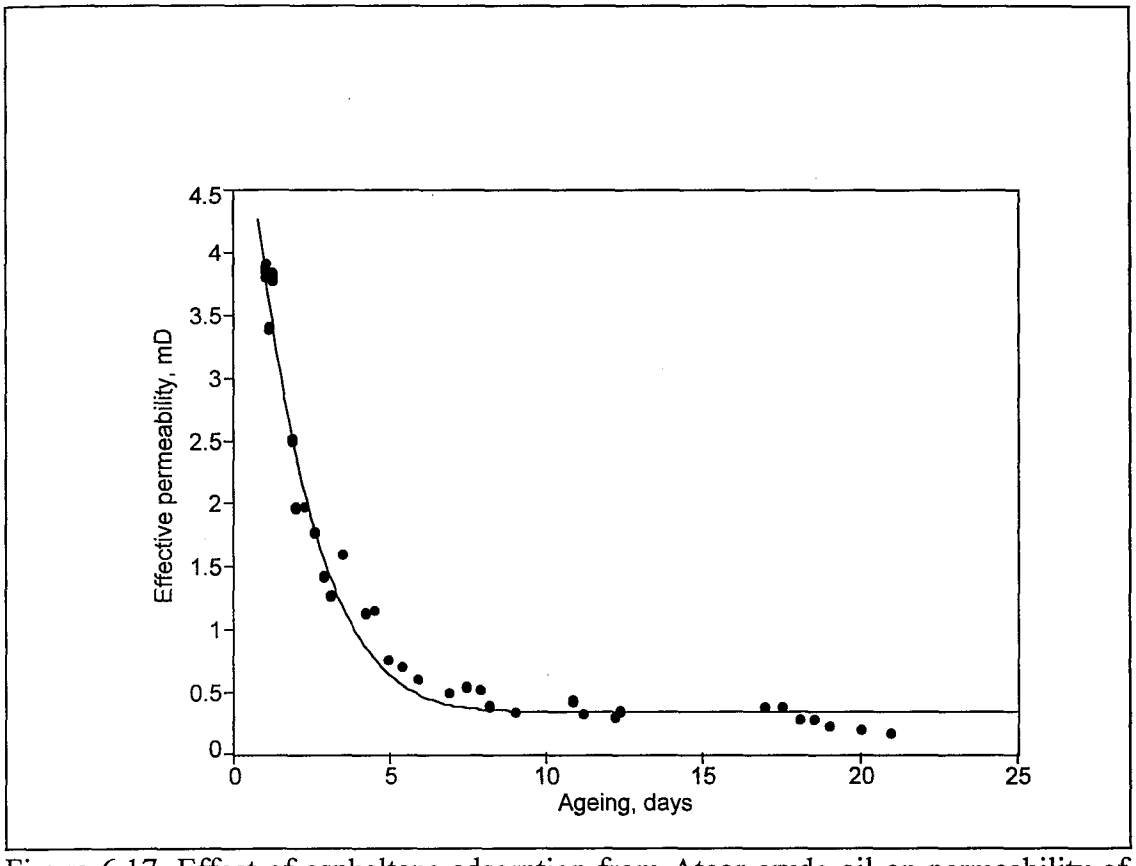

Figure 6.17. Effect of asphaltene adsorption from Atcor crude oil on permeability of sample B-6.

Figures 6.18 and 6.19 show the flow efficiency of pentol solutions and Atcor crude oil respectively. In Figure 6.18, the flow rate droped sharply as asphaltene concentrations increased up to 1.5 g/*l*. Above 1.5 g/*l* asphaltene concentration, the flow rate reduction slowed down and reached a plateau of 76%. In Figure 6.19 the pseudo-flow efficiency of Atcor crude oil (0.15 ml/min.) also droped sharply with time (up to 8 days) as asphaltene adsorbed onto the rock surfaces. The flow rate stabilised at 0.037 ml/min., which reflected a 75% damage in the flow rate. From the previous examples presented in this section it is concluded that asphaltene adsorption can play a significant effect on reservoir hydraulic properties.

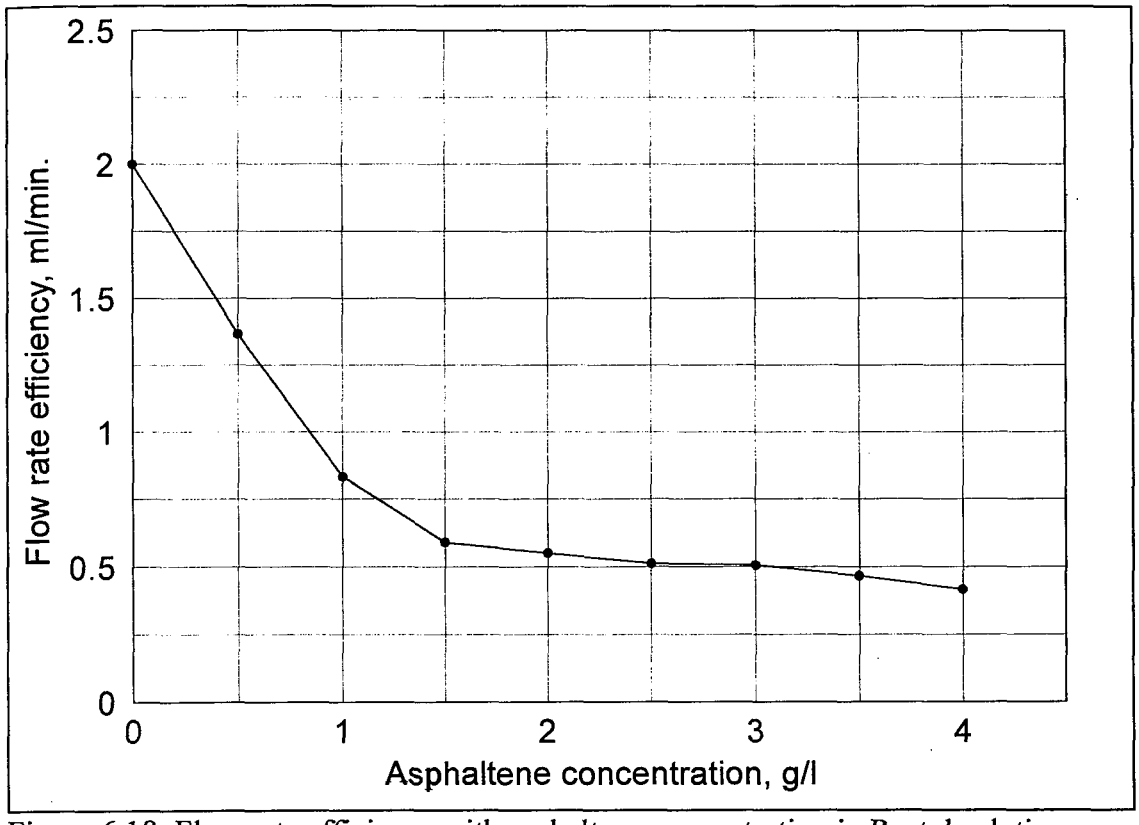

Figure 6.18. Flow rate efficiency with asphaltene concentration in Pentol solutions.

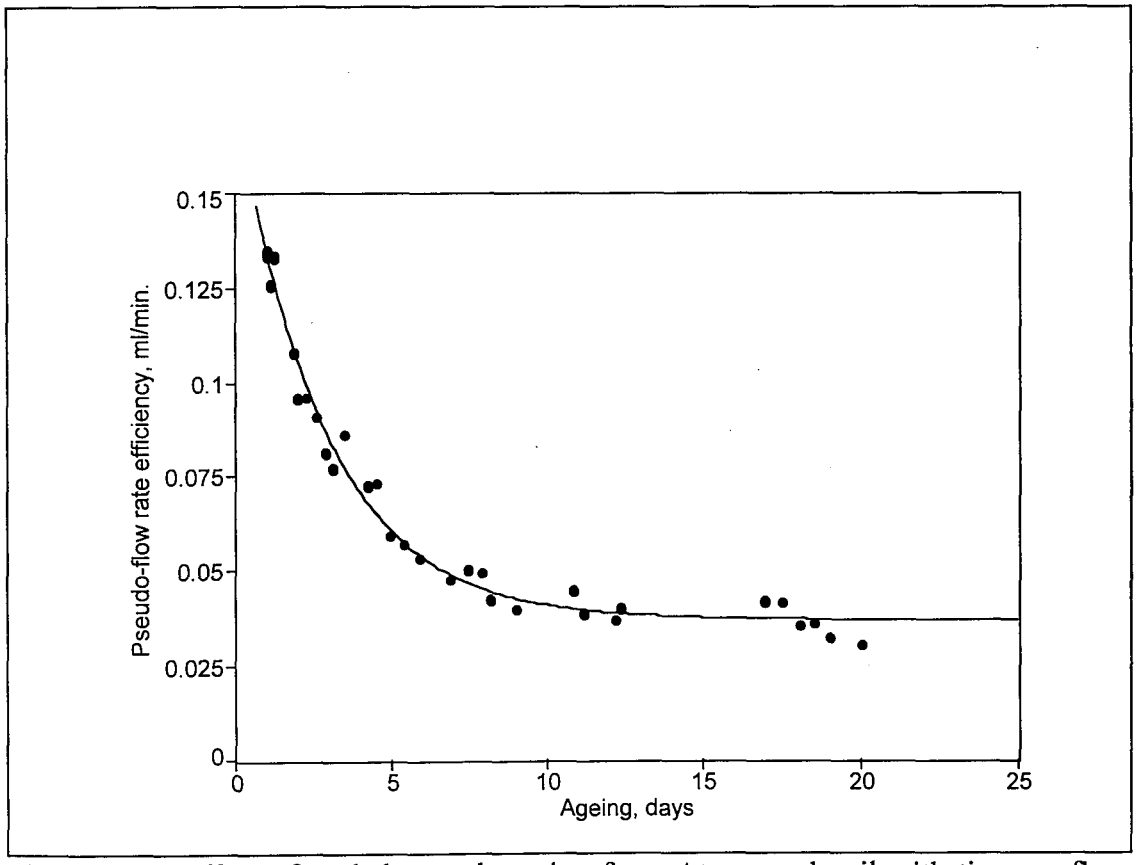

Figure 6.19. Effect of asphaltene adsorption from Atcor crude oil with time on flow rate efficiency.

6.8.4 PETROGRAPHIC ANALYSIS

Petrographic analysis of Berea sandstone core sample B-1 was performed in the Image Analysis Department at Core Laboratories Ltd. of Calgary, Alberta, Canada, the core sample being examined "before" and "after" the treatment with asphaltene in pentol solutions. Examples of the photomicrographs are shown in Figures 6.20 and 6.21 with their analytical descriptions.

Based on the porosity type observed in thin section the reservoir quality of the "before" sample can be described as good and the reservoir quality of the "after" sample as poor. The petrographic analysis shows that the porosity of these sandstones is comprised of essentially three elements; intergranular porosity between framework grain (8,16%), intragranular porosity produced by the partial dissolution of unstable framework grains (1,2%), and microporosity associated with kaolinite booklets (1%). Intergranular porosity in the "after" sample has been reduced by approximately one half (i.e., from about 16% to 8% intergranular volume) due to the presence of the asphaltene.

Total thin section porosity consists of the sum of the thin section intergranular porosity, intragranular porosity, and kaolinite microporosity. Reservoirs in which the porosity fabric is dominated by clean well interconnected intergranular pores have the best reservoir characteristics in terms of storage capacity and deliverability. The thin lining coats of asphaltene residues within the intergranular pores of the "after" sample has reduced the intergranular storge capacity from approximately 16% to 8%. The grain coating asphaltene residue also reduces pore throat diameter and in places completely bridges pore throats and has had a significant impact on reservoir permeability/deliverability as discussed in previous section.

Thin Section Analysis

Sample Number:	B-1 "Before"
Rock Name:	Sandstone
Formation:	Berea

Intergranular Porosity:	16%
Intragranular Porosity:	2%
Kaolinite Microporosity:	1%
Total Thin Section Porosity:	19%

A+B. A low magnification overview of this upper fine grained, well sorted, matrix-poor sublitharenite Berea sandstone sample. The rock framework is dominated by white coloured monocrystalline quartz frame work grains. The pore space is filled with blue dyed epoxy. Note the presence of skeletal remnants of alkali feldspar at N1 and CD8 in photo A. Pore filling calcite cement is observed at L8 in photo B and is easily recognised by its high birefringence. (63x, plane polarised light - photomicrograph A, partly crossed polarised light - photomicrograph B).

C. A high magnification view of the centre portion of photo A showing in detail the porosity fabric of this sample. Note that most of the pores are clean well interconnected primary intergranular pores. The pores in the centre of this photogragh contain scattered, floating booklets of authigenic koalinite (F6 and I6). Also note the pore filling calcite cement in the lower right corner of the photogragh (MN9). (125x, plane polarised light).

D. A high magnification view detailing the rock/porosity fabric of this sample. Again note the dominance of primary intergranular porosity and absence of detrital clay matrix. An intragranular pore produced by the partial dissolution of an alkali feldspar grain is situated at D10. The pores in the upper right corner of this photograph contain booklets of authigenic kaolinite which contributes microporosity to the pore system of this rock. (125x, plane polarised light).

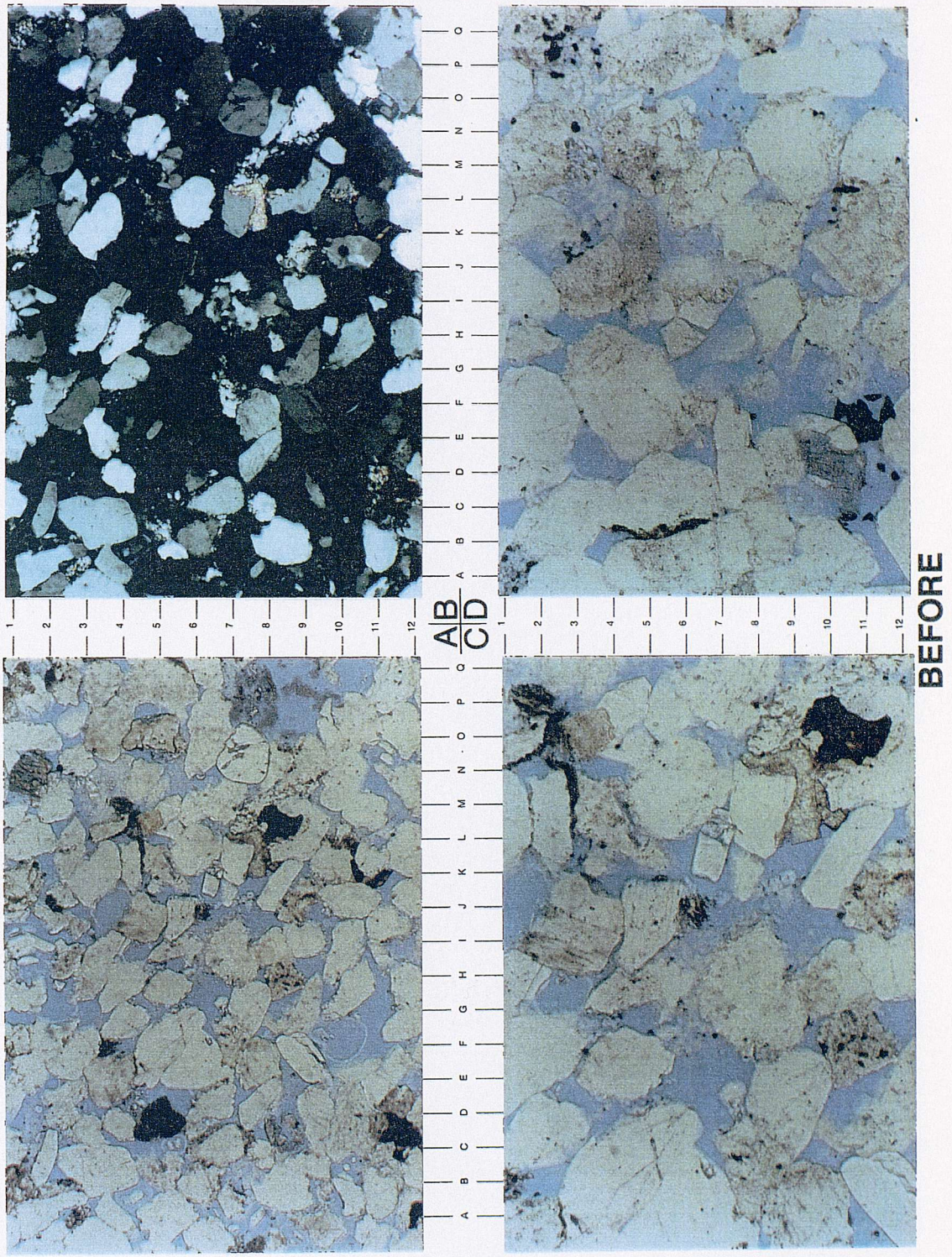

Figure 6.20 Photomicrograph of Berea sandstone (sample B-1) before asphaltene. For key see page 107.

Thin Section Analysis

Sample Number: B-1 "After"
Rock Name: Sandstone
Formation: Berea

Intergranular Porosity: 8%
Intragranular Porosity: 1%
Kaolinite Microporosity: 1%
Total Thin Section Porosity: 10%
Pore Lining Asphaltene Residue: 8%

A+B. A low magnification view (photo A) and a close up view (photo B) of an upper fine grained, well sorted sublitharenite sample similar in texture and composition to the previously described "before" sample. Most pores in photo A contain pore lining asphaltene residue. A circular shaped cluster of the pores in the left hand side of this photograph contain little to no asphaltene residue. There appears to be no mineralogical control influencing the distribution of this asphaltene residue. The close up view in photo B shows that the asphaltene occurs as grain coats of variable thickness. (63x, plane polarised light - photomicrograph A, plane polarised light - photomicrograph B).

C. A high magnification overview showing pervasive pore lining asphaltene residue and locally, pore bridging asphaltene (G7, D10). Note that the rock fragments in this sample are commonly stained brown implying that some asphaltene residue has invaded microporosity within clay rich rock fragments. (125x, plane polarised light).

D. Another high magnification view showing asphaltene lining primary intergranular pores and also residing within clay associated microporosity at OP7. This patch of brown/white coloured clay may represent a partially degraded rock fragment or may represent authigenic kaolinite booklets surrounding a partially degraded grain. Precise identification of the host mineral or minerals to the microporous clay is difficult owing to coating by asphaltene. (125x, plane polarised light).

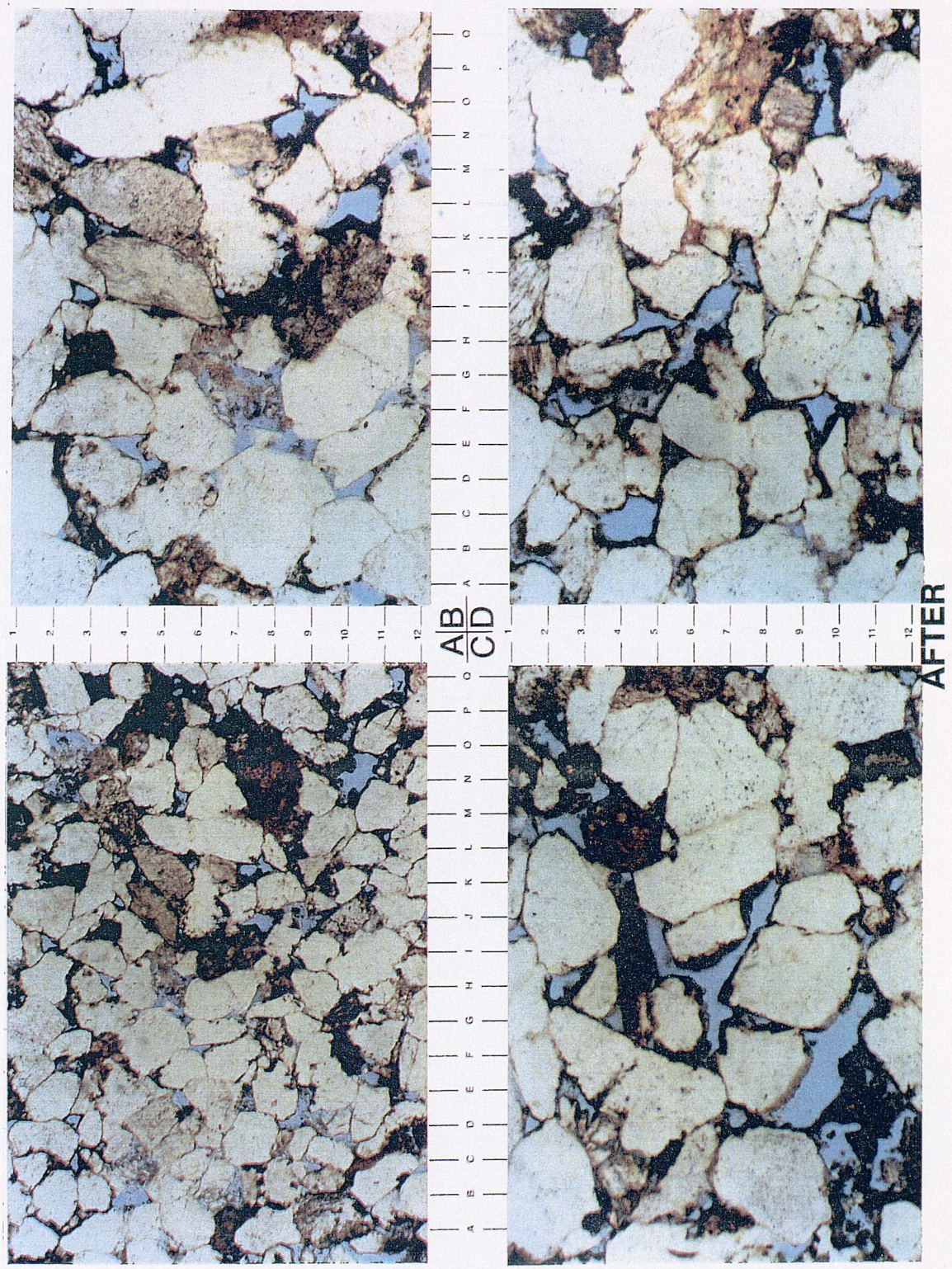

Figure 6.21 Photomicrograph of Berea sandstone (sample B-1) after asphaltene. For key see page 109.

6.8.5 X-RAY DIFFRACTION

XRD was used to provide a semi-quantitative analysis of the whole Berea sandstone (sample B-1) mineral contents "before" and "after" asphaltene treatment. This was accomplished by desegregating the sample to a less than 2 μm size fraction. To preserve the sample quality with asphaltene content no additional treatment was applied.

Based on the mineral composition types observed from XRD analysis in Berea sandstone (sample B-1), the mineral composition found to be 91-96% quartz, 0.5-4% albite, 2-3% clay and 0.3-0.5% ankerite. In this analysis only the results in terms of total quartz were used since the latter dominated the mineral present in the sample. As can been seen from XRD plots "before" and "after", Figures 6.22 and 6.23 respectively, the quartz peak at 20.8 °2θ is reduced by 1/3 in intensity terms as a result of absorption of the diffracted X-ray beam by the asphaltene. This corresponds to the reduction of the X-ray intensity counts deducted at 20.8 °2θ position from 11826 to 8226 counts before and after asphaltene respectively. In XRD analysis the 20.8 °2θ position is usually considered more representative for the actual physical quantity of quartz in the sample. The 1/3 reduction in X-ray diffraction beams represent an excellent agreement with the damage analysis determined by Poiseuille law, streaming current measurement intensities and petrographic analysis. This analysis was conducted by using a Phillips X-ray powder diffractometer at the Geology Department in the Royal School of Mines, London.

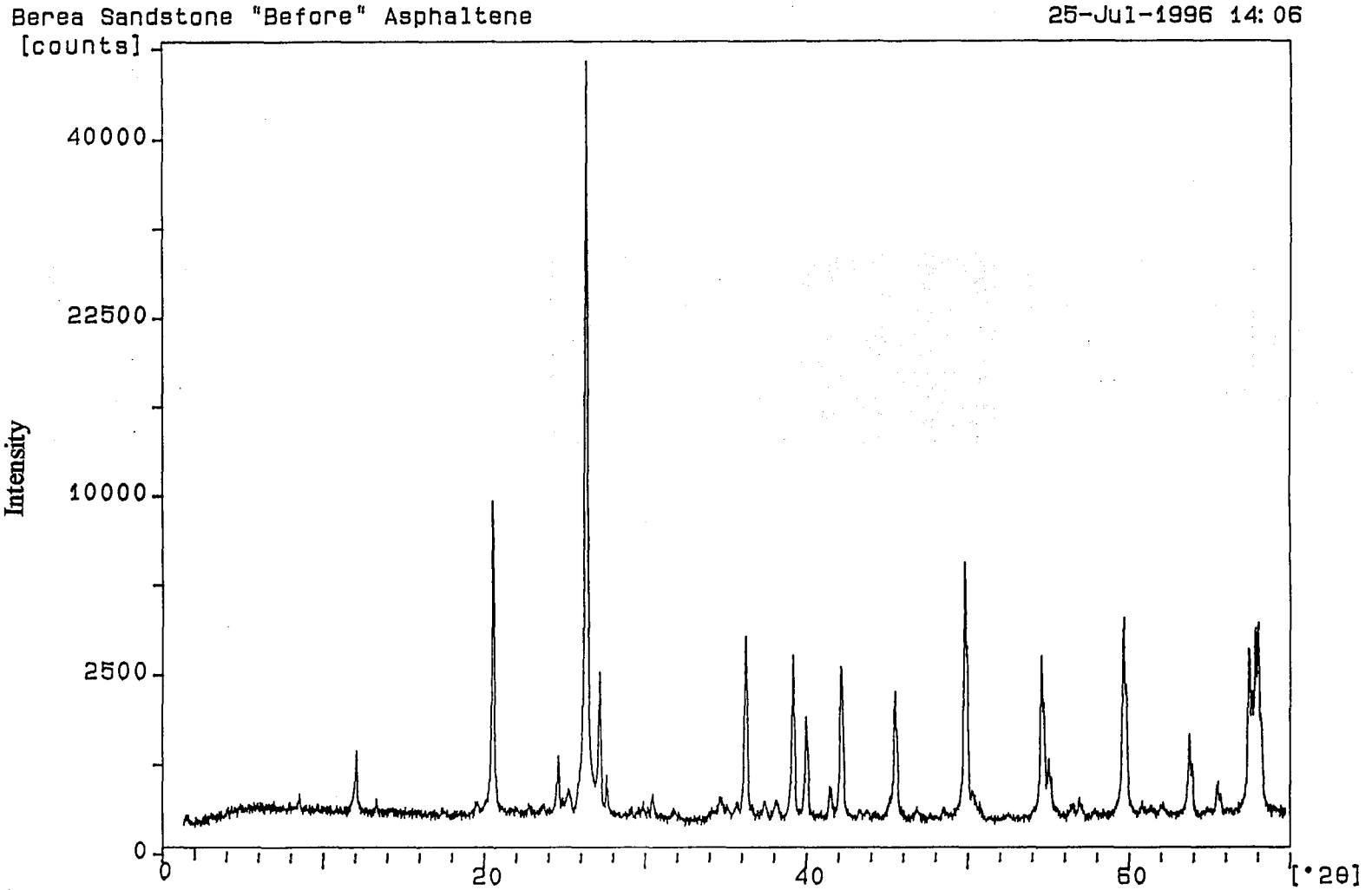

Figure 6.22. A typical whole rock XRD pattern from B-1 sample "Before" Asphaltene.

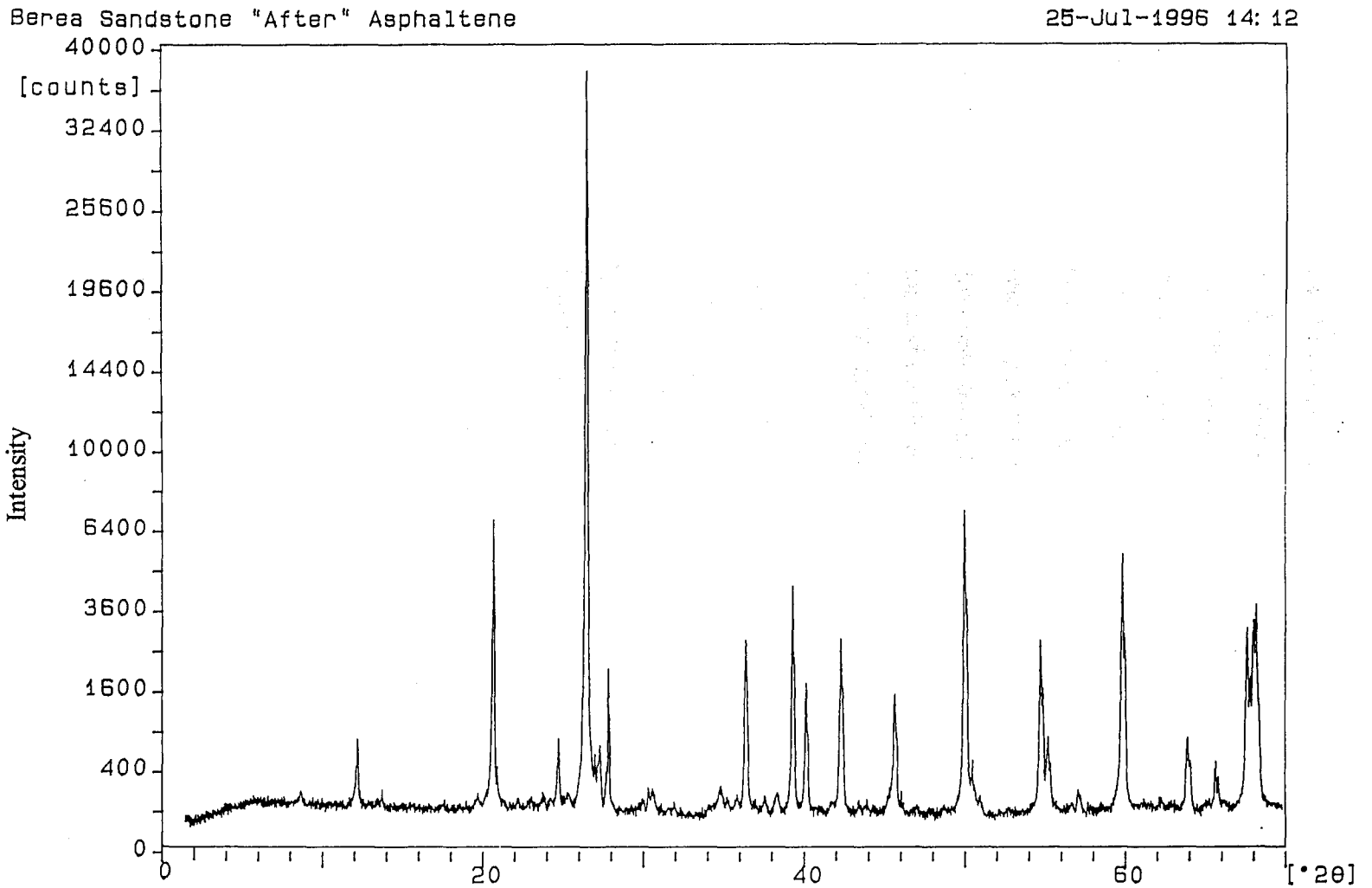

Figure 6.23. A typical whole rock XRD pattern from B-1 sample "After" Asphaltene.

6.9 ESTIMATION OF ASPHALTENE ADSORPTION ISOTHERM ON RESERVOIR ROCK CORES

The treatment so far implies that asphaltene steadily blocks the pores and gives a fractional radius of ~0.3 i.e. area blocking of ~0.5. However, an alternative view could be taken, that the asphaltene pore blocking is more the effect of closing off pore "throats" than surface restriction of the pores. After "throat" blocking and "crevice" filling the asphaltene then deposits/adsorbs on the rock pore surface as a (more or less) particle monolayer. While this view is speculative it is supported by the observation that the zeta (ζ) potential (from streaming current) reaches a plateau (seen as the asphaltene value) only toward the end of the process previously treated as a pore surface deposition and steady blocking, now seen as the completion of surface covering by a monolayer of asphaltene particles.

To make quantitative the results of asphaltene adsorption/deposition into Berea sandstones, the adsorption/deposition of asphaltene particles can be treated just like the adsorption of gas molecules into a porous solid. The interaction energy of asphaltene particles with the sandstone surfaces on this view can be obtained from the initial slope of the "adsorption isotherm". The result will be compared with a van der Waals calculation.

At any position on the adsorption/deposition isotherm assume equilibrium between asphaltene particles floating about in the liquid and those adsorbed/deposited on the surface. Thus:

$$\mu(\text{Free Asphaltene Particle}) = \mu(\text{Asphaltene Particle Adsorbed}) \qquad (6.18)$$

where μ is the chemical potential.

i.e. $\mu(A,F) = \mu(A,A)$

expanding,

$$\therefore \quad \overset{\Phi}{\mu}_{AF} + kT \ln a_{AF} = \overset{\Phi}{\mu}_{AA} + kT \ln \frac{\theta}{1-\theta} \tag{6.19}$$

where $\overset{\Phi}{\mu}$ is a standard chemical potential and the activity a of an adsorbed particle is taken by analogy with the Langmuir isotherm.

$$\therefore \quad \overset{\Phi}{\Delta G}_{(Ads)} = \overset{\Phi}{\mu}_{AA} - \overset{\Phi}{\mu}_{AF} = kT \ln \frac{x_{AF}}{\theta} \tag{6.20}$$

with $(1-\theta)$ taken as 1 at the low θ of initial conditions.

Now the intial slope, $\frac{d\theta}{dx} = \exp\left(-\frac{\Delta G}{kT}\right)$ (Langmuir adsorption isotherm) (6.21)

where,

θ = The fraction of surface covered.

$\theta = \frac{y}{0.33}$ for Berea sandstone with "Pentol solutions".

x = The volume fraction of asphaltene in Pentol.

$$= \frac{\text{volume of asphaltene particles (total)}}{\text{volume of asphaltene containing solution}}$$

Figure 6.24 shows the adsorption isotherm obtained for asphaltene particles on Berea core surfaces from pentol solutions. The initial slope of asphaltene adsorption ($d\theta/dx$) is 485. Using the above equation (6.21) to estimate the $\Delta G / kT$ value:

$$\therefore \quad -\frac{\Delta G}{kT} = \ln(485) = 6.2 \qquad \text{and} \qquad \Delta G = -6.2kT \tag{6.22}$$

The negative sign is correct, indicating an attraction of asphaltene particles to the surface. We can compare the -6.2kT value with a van der Waals calculation for the attraction energy of a single particle to the surface.

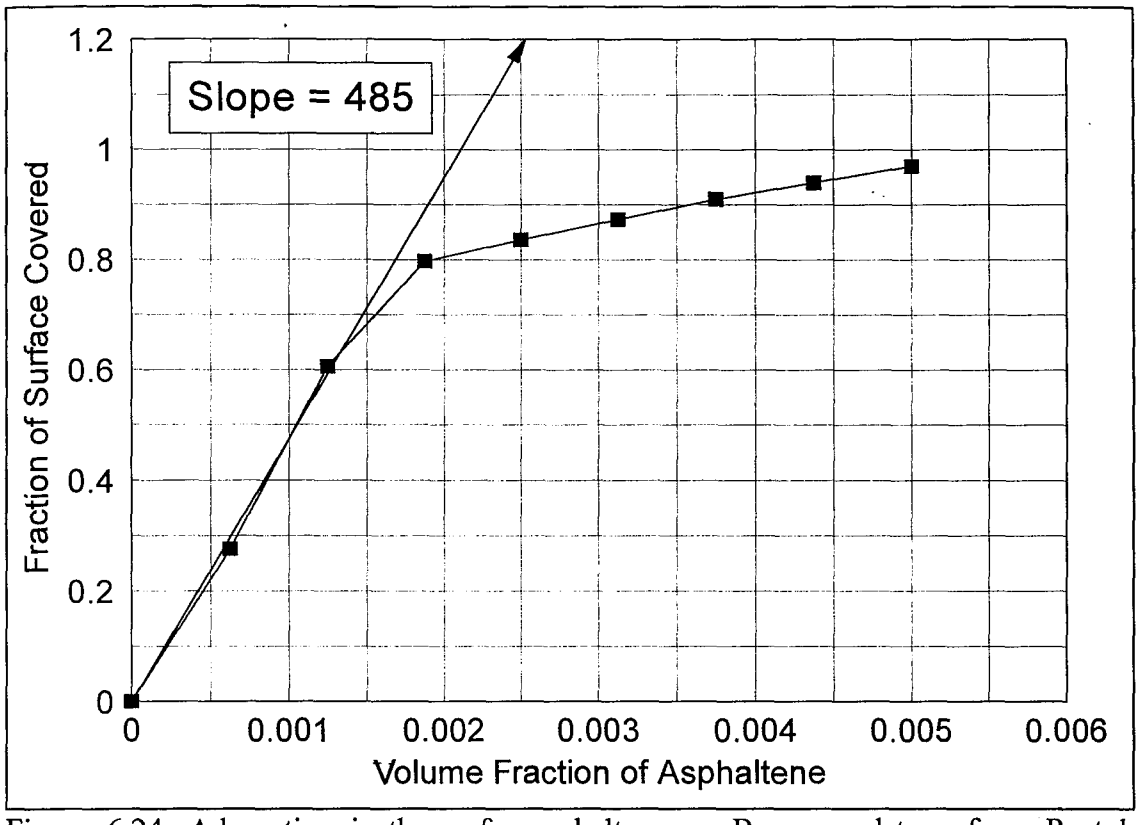

Figure 6.24. Adsorption isotherm for asphaltene on Berea sandstone from Pentol solutions.

To justify this we need the effective Hamaker constants for the oil (seen as a typical aliphatic chain), for sandstone (seen as silica) and for asphaltene, being partially aromatic, seen as polystyrene. Table 6.5 shows Hamaker constants for the three materials obtained from J. Gregory (1988).

Table 6.5. Hamaker Constants and A/kT Values. After Gregory (1988)

Material	A	A/kT
fused quartz (SiO_2)	$6.5*10^{-20}$ J	15.8
polystyrene	$6.37*10^{-20}$ J	15.5
aliphatic chain (decane)	$4.82*10^{-20}$ J	12.1

So the effective Hamaker constant A_{132}, where 1 = silica, 2 = polystyrene (≅ asphaltene), 3 = aliphatic oil.

$$A_{132} = \left(A_{11}^{1/2} - A_{33}^{1/2}\right)\left(A_{22}^{1/2} - A_{33}^{1/2}\right) \qquad (3.8)$$

$$= 0.225\ kT$$

Now the attraction potential energy (free energy ΔG) between a sphere of radius a and flat surface at close approach H is given by $-\frac{Aa}{6H}$ (Hamaker, 1937).

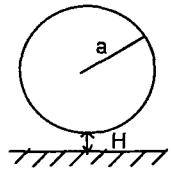

The separation H between the sphere (asphaltene particle) and the surface (silica) could not be taken as zero or the attractions would be infinite which is not realistic. We will (admittedly arbitrarily) take it as 5 Å (0.5 nm). The asphaltene particle will be of a wide range of sizes. We will take the average as 0.1 μm (1000 Å). Then $\frac{a}{H} = 200$ and the attractive energy becomes $\frac{0.225 * 200}{6} * kT = 7.5\ kT$.

While this is gratifyingly close to the experimentally required value on the model (6kT), it can hardly be taken as supporting the second model over the first since:

i. The distance 5 Å is somewhat arbitrary.
ii. The A values for the components are not very reliable (and neither would be any attempt at calculating them since the necessary data is not available).
iii. The values taken for asphaltene is a guess (though reasonable)

Overall it is difficult to decide between the two models though the author prefers the first model, describing the adsorption as a thick multilayer coating the pore surface.

6.10 ELECTRODE-DEPOSITION UNDER ELECTRIC FIELD

Figure 6.25 and 6.26 shows the results of electric field (170 volt across 2 mm) tests conducted in asphaltenic crude oil with two different time frames, one week and one month respectively. Figure 6.25 [one week] shows no clear deposition occurring on the electrodes, whereas in Figure 6.26 [one month] a large thick deposit was observed on the cathode electrode. The deposited material removed from the cathode was examined and found to be insoluble in n-pentane but soluble in toluene indicating the presence of appreciable amount of asphaltene.

From the two test observations, we can roughly calculate asphaltene zeta potential by estimating the average distance travelled by an asphaltene particle in (say) 15 days. Thus:

Average distance travelled by asphaltene particle = 1 mm

1 mm in 15 days = $7.72*10^{-10}$ m sec^{-1}.

Field (E) applied = 170 volts across 2 mm = $8.5*10^{4}$ Vm^{-1}.

Crude oil viscosity = 5 cp = 0.005 Pa.s

Crude oil dielectric constant (ε_r) = 15 , so the permittivity = (15) * $(8.854*10^{-12})$ = $1.33*10^{-10}$ $kg^{-1}m^{-3}s^{4}A^{2}$.

Since the crude oil has very low electrolyte concentration, the Henry equation (3.17) given in Chapter 3 can be applied:

$$v = \frac{2E\varepsilon\zeta}{3\eta}$$

$$\text{so} \qquad 7.72*10^{-10} = \frac{0.667*(8.5*10^{4})*(1.33*10^{-10})\zeta}{0.005}$$

$$\therefore \quad \zeta = 5.12*10^{-7} \text{ volt} = 5.12*10^{-4} \text{ mV}$$

This, of course, is a rather rough calculation e.g. taking 15 days is a little arbitrary.

These observations and calculations show that:

- Asphaltene in crude oil has very small, but just measurable (or at least assessable) zeta (ζ) potential.
- This confirms the very low positive ζ potential found by streaming current measurements.
- At very low ζ potentials where conventional quantitative electrophoresis measurements are nearly impossible, streaming current measurements can be successful.
- Electrical effects in asphaltene aggregation/deposition in/from crude oil must be utterly negligible.

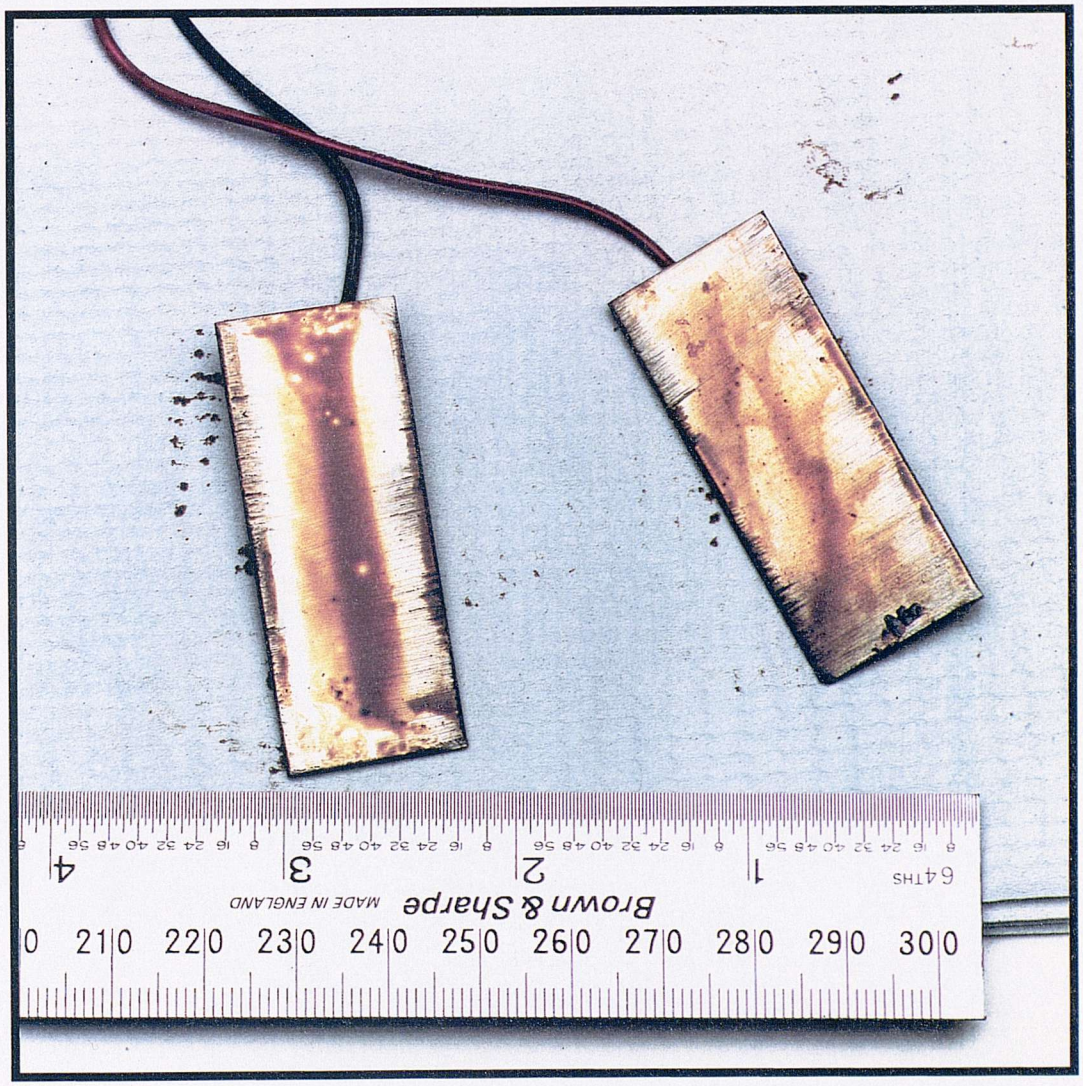

Figure 6.25 Photograph view of Electrode-Deposition sequence of asphaltene from one week experiment.

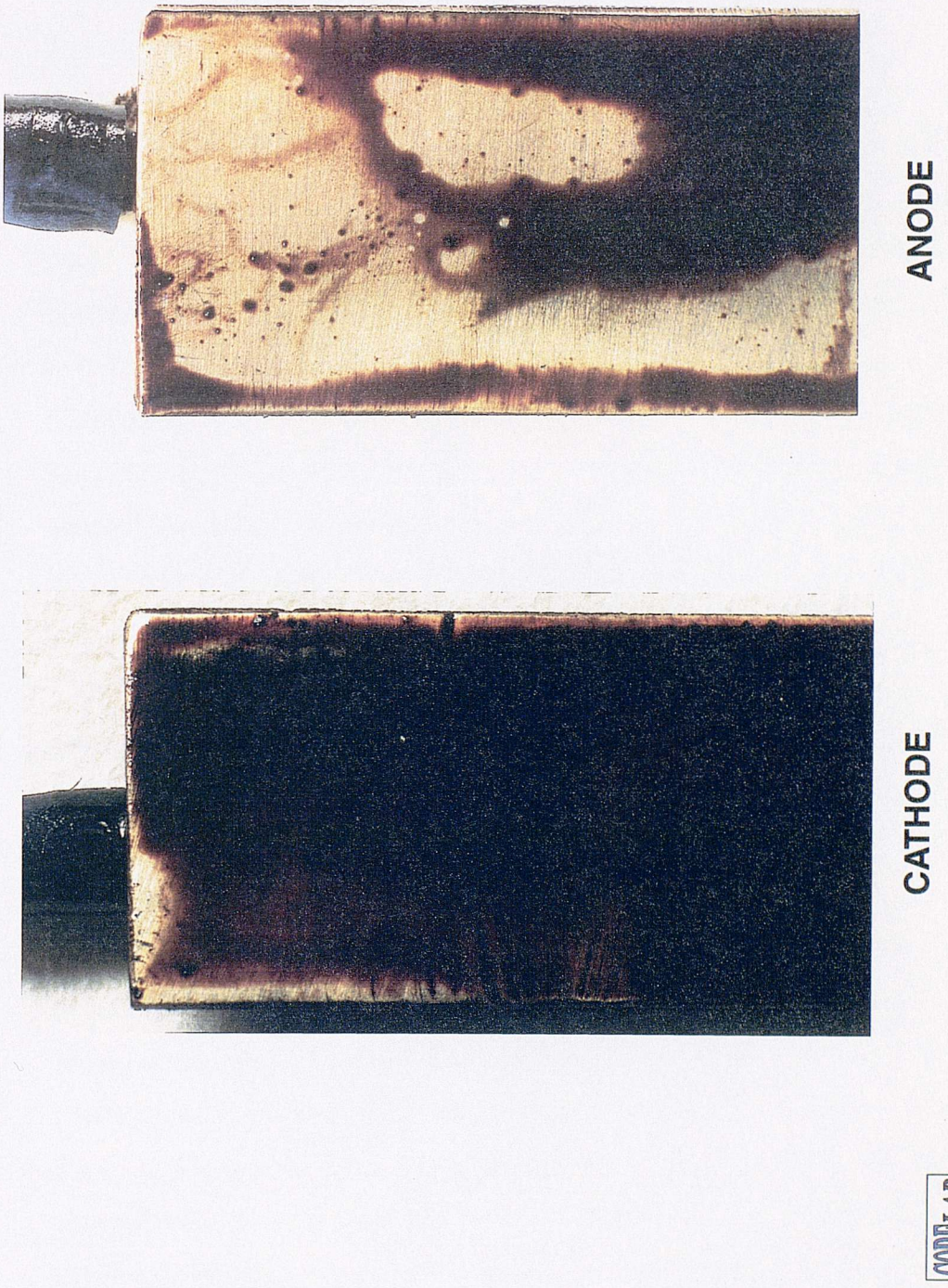

Figure 6.26 Photograph view of Electrode-Deposition sequence of asphaltene from one month experiment.

6.11 CONCLUSIONS

1. The electrical charge and consequent double layer effects of asphaltenes in crude oil and pentol systems have been examined both theoretically and experimentally and found to play an utterly negligible role in the interaction between asphaltene particles and either surface or other particles.
2. Streaming potential experiments are usualy in grave error as a result of surface conductivity, whereas streaming currents are free from this disadvantage. In order to overcome the disadvantage of having to know the pores area/ length ratio for streaming current measurements a novel method was developed to estimate this ratio by combining streaming potential and current measurements.
3. Comparison of streaming potential and current measurements using sandstone rock cores with methanol, acetone, toluene, pentol and crude oil showed that there was serious surface conductivity present in all of them. This might have been due to a water film adsorbed on the rock surfaces which was not removed by vacuum/heat treatment.
4. The sandstone rock cores were found to have negative surface potentials in water at neutral pH of some tens of millivolts (as expected for silica) and smaller but significant negative potentials in acetone and methanol, whereas in toluene, pentol and crude oil found to exhibited very small negative potentials.
5. Asphaltene particles were found to have very small positive surface potentials in crude oil, pentol, n-pentane and isopar-H. It is therefore proposed that asphaltene particle stability is caused by the steric effects of high molecular weight material (resins) adsorbed on asphaltene particles.
6. Formation damage analysis of rock cores after asphaltene containing flows showed that the open area was reduced by a fraction of 0.5 with good agreement between the values obtained from flow measurement, streaming currents, petrographic analysis and XRD.

CHAPTER SEVEN

THE EFFECT OF PORE PRESSURE, POROSITY AND DOUBLE LAYER OVERLAP ON ROCK SURFACE POTENTIAL MEASUREMENT

7.1 INTRODUCTION

This chapter presents the experimental results of streaming potential and current measurements on sandstone core samples under the effect of pore pressure, porosity and double layer overlap. The effect of these parameters on the measurements and the related surface potentials are presented and discussed. The relationship between the estimated core pores A/L ratio and rock permeability under the effect of pores pressure and pore size, and the impact of pore pressure hysteresis on the behaviour of the streaming potential and current measurements is also presented.

7.2 PORE PRESSURE

During the pore pressure test, streaming potential and current measurements were measured from one selected electrolyte solution *KCl*8 (7.456 *g/l*) with respect to the hydrostatic net confining pressure which is defined as the difference between confining pressure and pore fluid pressure. The net confining pressure applied on Berea sandstone core samples used in this study is 1500 psi [10.35 MPa], the purpose being to investigate the effect of possible rock geometry changes on the electrokinetic results. At each test the pores A/L ratios were estimated by combining the two measurements as described in previously. The rock core surface potentials were

calculated from the observed streaming current data. In the matter of understanding the relationship between the estimated rock pores A/L ratio and liquid permeability, at each test the liquid permeability was calculated from Darcy's equation.

For the study of pore pressure hysteresis, the pore pressures were varied from low to high (i.e. loading cycle) and vice versa (i.e. unloading cycle). The purpose of loading and unloading the pore pressures on core samples is to increase the understanding of the effect of this cycling on the behaviour of streaming potential and current measurements and the derived electrokinetic potentials.

7.2.1 The Effect of Pore Pressure on V_s and I_s Measurements

Figures 7.1 and 7.2 show the effect of loading pore pressure on streaming potential (V_s) and current (I_s) measurements of electrolyte solution (*KCl*8 7.456 *g/l*) in Berea sandstone core sample (B-4) at a constant net confining pressure, 1500 psi [10.35 MPa]. It can be seen from the two plots that both streaming potential and current measurements are direction dependent with respect to the application of pore pressure over a range from 150 to 700 psi [1.035 to 4.83 MPa]. It can be seen from both figures that the pore pressure effect on both the streaming potential and the streaming current are in the same direction, both revealing the saturation pressure condition at ~500 psi [3.45 MPa].

The origin of this behaviour is probably the effect on any gas bubbles and changes in the tortuosity of the current flow paths. The amount of gas (air) dissolved increases with pore pressure up to 500 psi [3.45 MPa] which can be considered as the saturation pressure point, both measurements agreeing in this respect. After the saturation pressure point, (500 psi) [3.45 MPa], the liquid flow through the core sample becomes a single phase flow with the liquid phase making a good contact (interface) with the solid (grains) surfaces. This can be seen in both figures where measurements above 500 psi [3.45 MPa] become more negative as more liquid interfaces with the B-4 sample negative surfaces. The behaviour change in streaming

potential and current measurements with pore pressure will be, of course, different for different rocks depending upon the porosity, permeability and mineral composition.

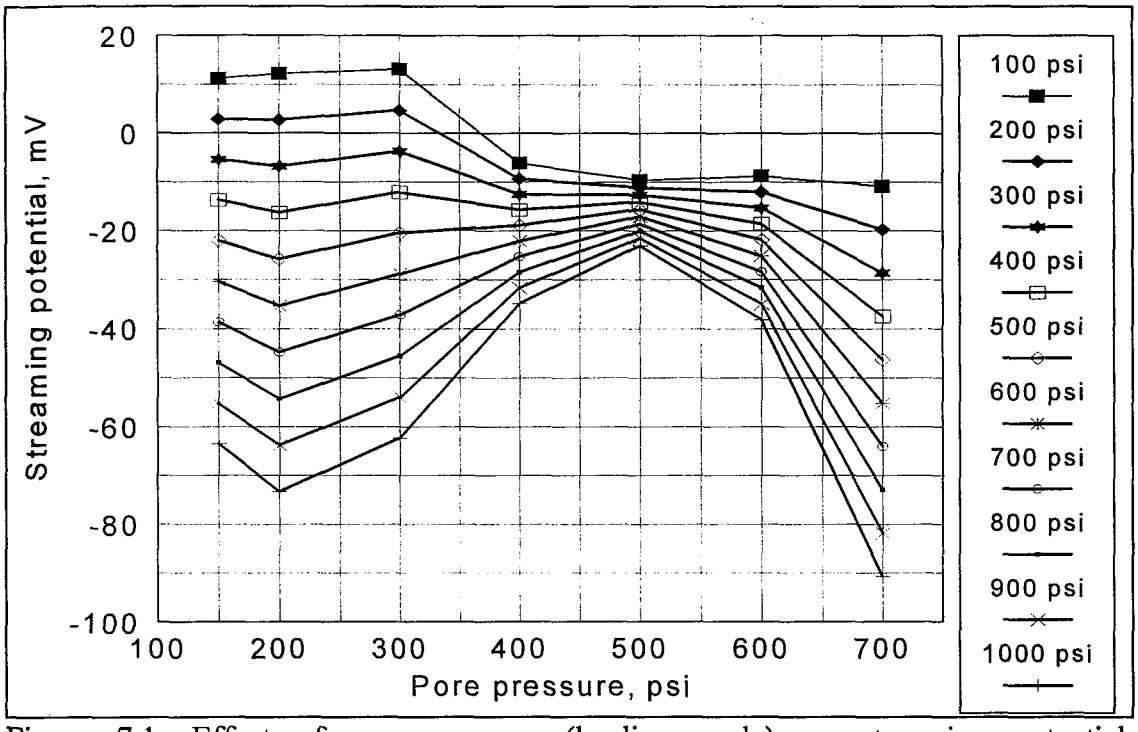

Figure 7.1. Effect of pore pressure (loading cycle) on streaming potential measurements of electrolyte solution in Berea sandstone.

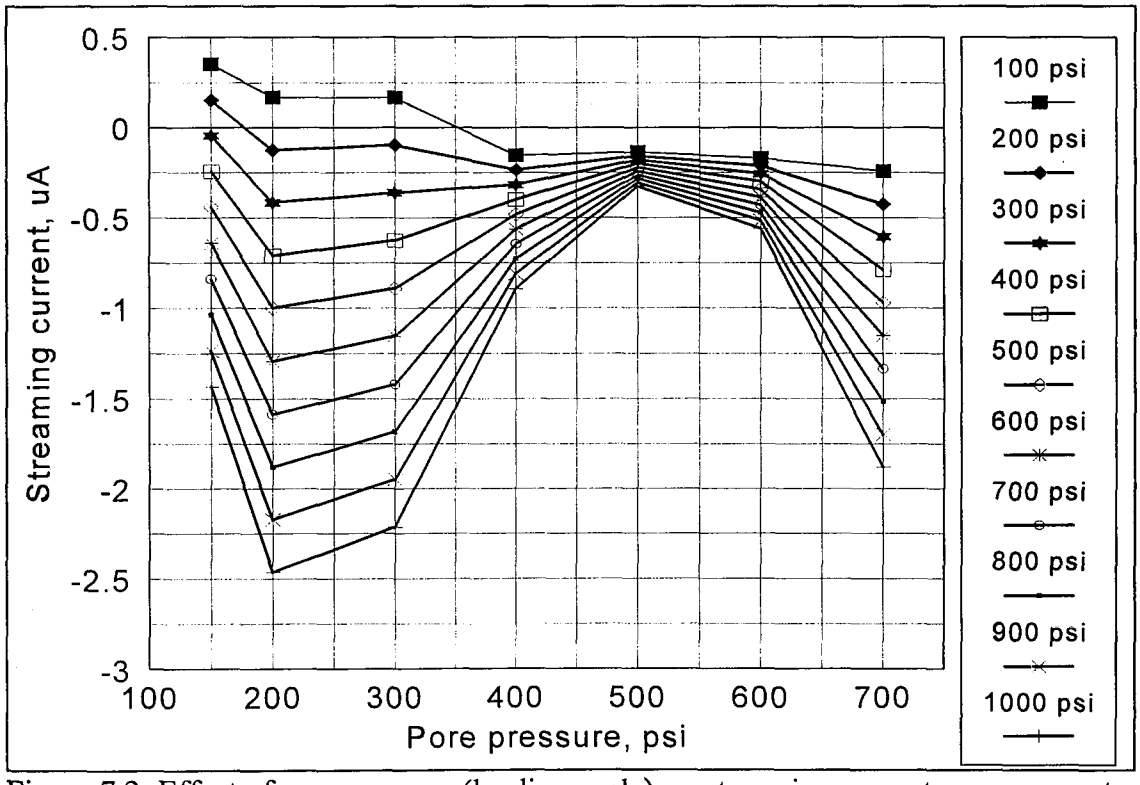

Figure 7.2. Effect of pore pressure (loading cycle) on streaming current measurements of electrolyte solution in Berea sandstone.

7.2.2 The Effect of Pore Pressure on Rock Pores A/L Ratio

As indicated in chapters three and six that the estimation of rock core pores A/L ratio involves combining streaming potential and current measurements. Figure 7.3 presents the rock core pores A/L ratio plotted against loading pore pressure. A/L increases up to 400 psi [2.76 MPa], but above 500 psi [3.45 MPa] the pores A/L ratio start to decreases where Figures 7.1 and 7.2 suggest a saturation pressure point. This is probably due to the fact that the pore geometries are pressure sensitive and deform significantly.

The effect of pores pressure on the estimation of pores A/L ratio of rock cores can be interpreted as follows:

- As the pore pressure increases, the gas (air) bubbles contained in the liquid start to dissolve giving the liquid a good contact (interface) with the solid surfaces and therefore enhanced the measurements.
- As the pore pressure increases above the saturation pressure, ~500 psi [3.45 MPa], the rock pores start to expand and therefore deformation of the grain cementation starts to occur. This will cause the liquid flow to transport fines and block some of the flow channels, thus reducing A and consequently A/L.

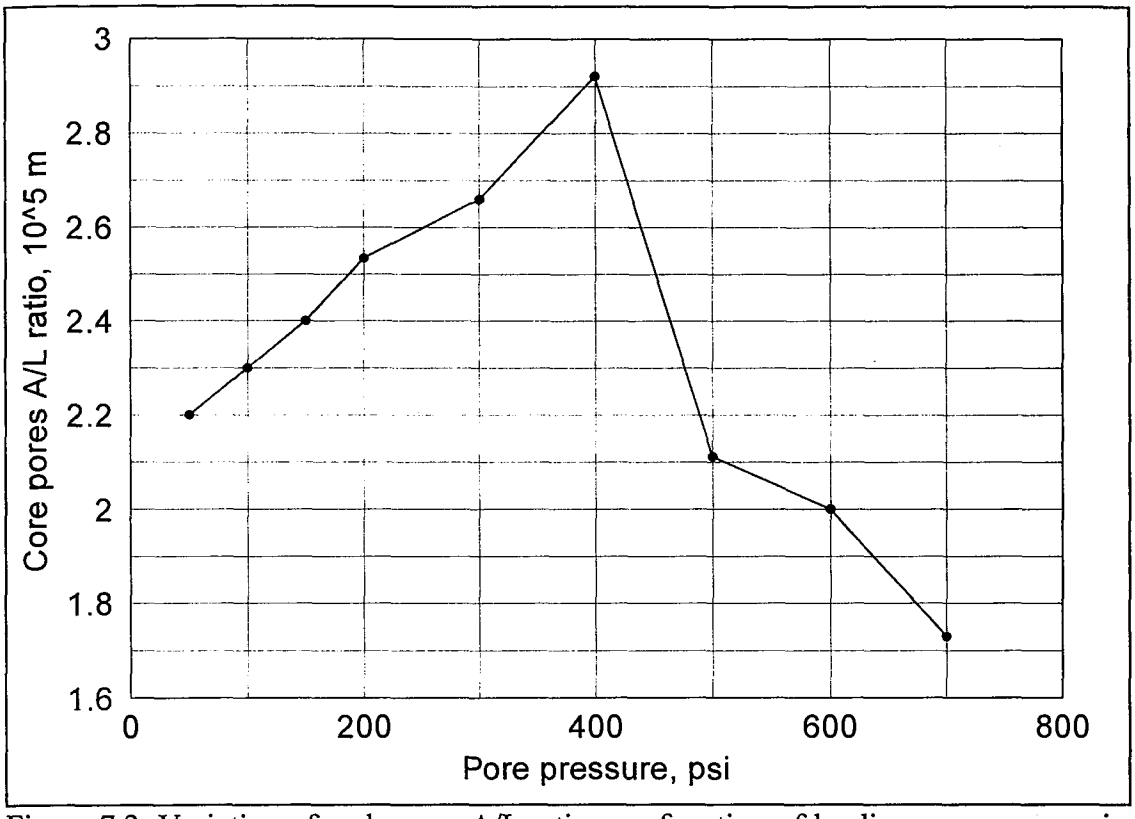

Figure 7.3. Variation of rock pores A/L ratio as a function of loading pore pressure in Berea sandstone core sample from 50 to 700 psi.

7.2.3 The Effect of Pore Pressure on Rock Surface Potential

The experimental rock surface potential, calculated from the observed streaming current at various pore pressures in the Berea sandstone sample is shown in Figure 7.4. The rock surface potential is calculated after estimating the pores A/L ratio at each elevated pore pressure condition. The Figure shows that though there is some oscillation of zeta with respect to pressure there is no systematic trend of potentials. This indicates to show that the changes in pore geometry resulting from pressure changes are not significant for zeta potential in high electrolyte concentration *KCl* solution (7.456 *g/l*). However, they may be significant in non-aqueous system as will be shown in section (7.3.1).

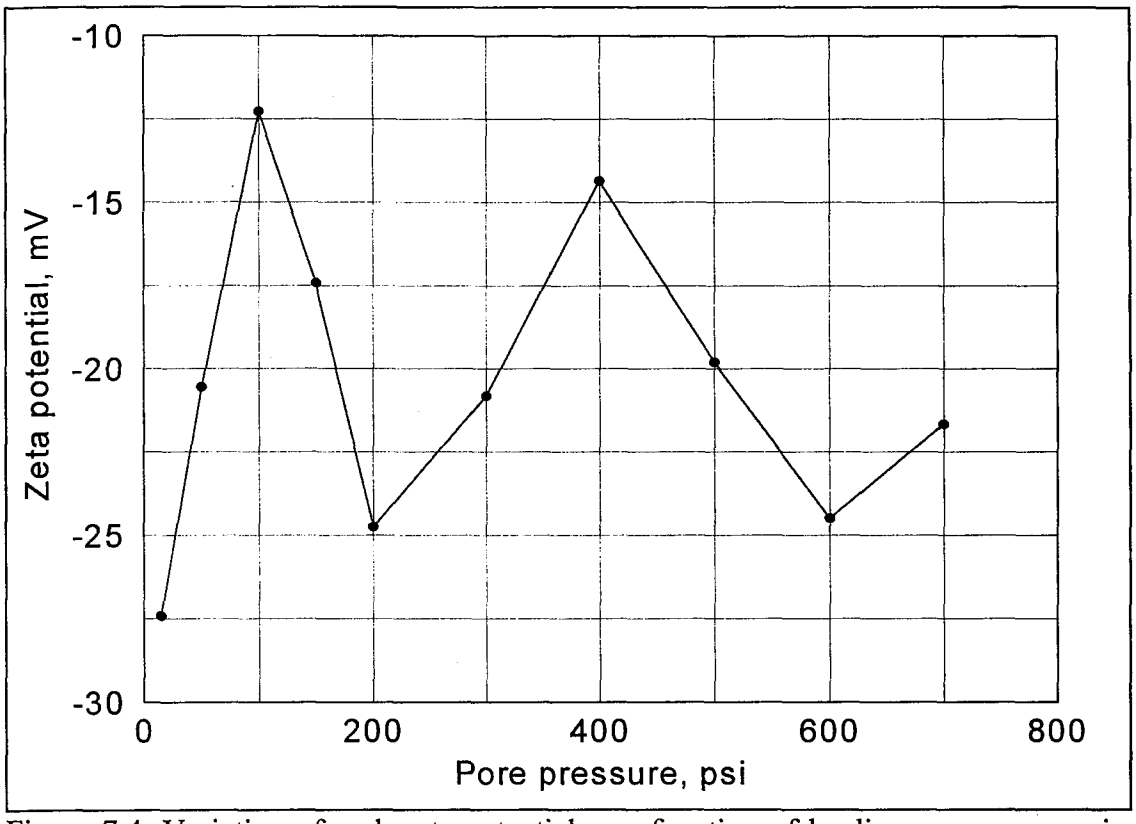

Figure 7.4. Variation of rock zeta potential as a function of loading pore pressure in Berea sandstone core sample.

7.2.4 Rock Pores A/L versus Permeability

Permeability is defined as the capacity of rocks to transmit a fluid through the interconnected pore spaces, expressed as Darcy's law after Henry Darcy who studied the liquid flowing through a horizontal sand-filter bed as a function of the pressure head above the filter and the cross-sectional area of the filter. Together with the volumetric fluid capacity of the rock, represented by the porosity, the permeability forms the most important characteristic of a reservoir rock. Darcy's law for assumed laminar flow is:

$$q = \frac{K_L A \Delta P}{\eta L} \tag{7.1}$$

in which K_L is the liquid permeability, η the viscosity, ΔP the pressure difference across a rock sample of length L and cross-sectional area of A, and finally q is the volumetric fluid flow rate. Thus:

$$K_L = \frac{q\eta L}{A\Delta P} \tag{7.2}$$

A point of interest is to see if the two quantities A/L ratio and permeability at least follow each other in direction though of course they are not the same. The permeability of sandstone samples were measured at elevated pore pressure in *KCl* solution (7.456 *g/l*) as a flow medium at a net confining pressure of 1500 psi [10.35 MPa]. Figure 7.5 show the results of liquid permeability at various pore pressures ranging from atmospheric pressure to 700 psi [4.83 MPa]. As can be seen from Figure 7.5 the liquid permeability increases with loading pore pressure which is seen as the effective (two phase) permeability region. The rate of increase slows down as the pore pressure reaches the saturation pressure and this region can be defined as the absolute permeability (liquid phase). Further increases in pore pressure decrease the permeability. This is probably due to changes in pore geometries deforming grain cementation and blocking some pore flow channels.

Comparing Figure 7.3 with Figure 7.5, it can be seen that the change in the estimated rock pores A/L ratio as a function of pore pressure follows nearly the same trend as the change in the liquid permeability.

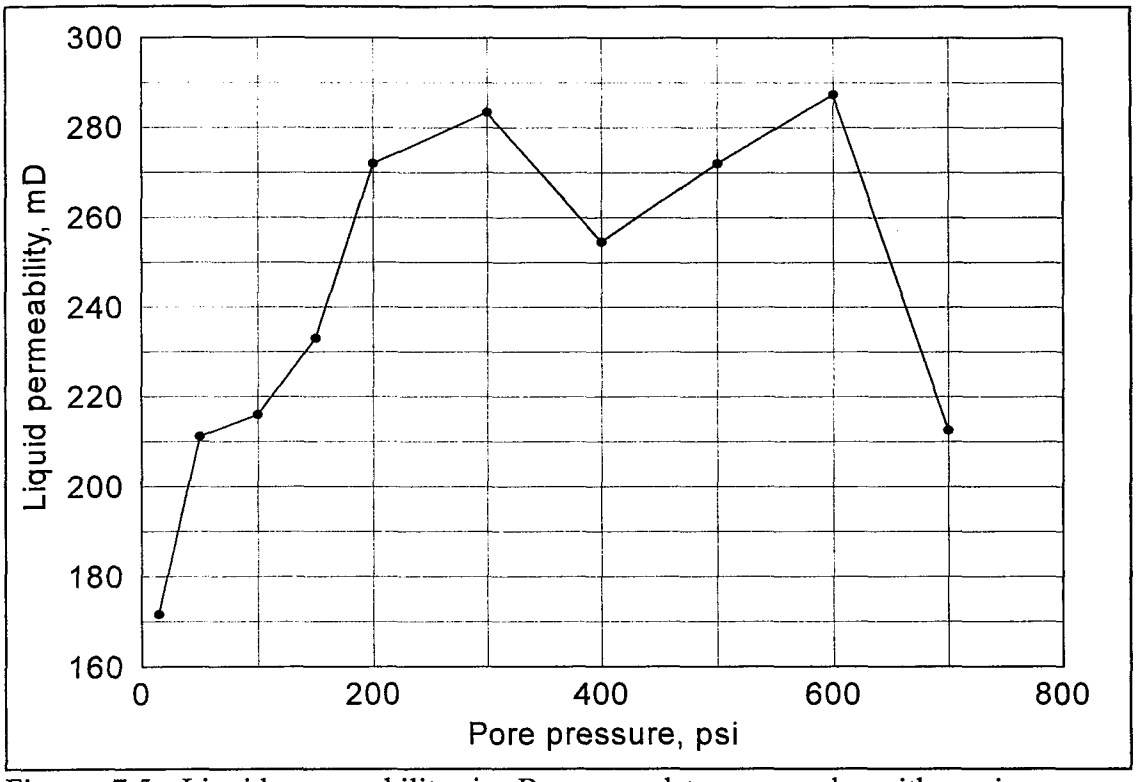

Figure 7.5. Liquid permeability in Berea sandstone sample with various pore pressures.

7.2.5 Hysteresis Effect

During the unloading cycle of pore pressure, streaming potential and current were measured. It is observed that the behaviour of streaming potential and current measurements as a function of pore pressure exhibit a marked hyteresis. This is shown for streaming potential measurements in Figure 7.1 [loading cycle] and Figure 7.6 [unloading cycle] and for streaming current measurements in Figures 7.2 [loading cycle] and 7.7 [unloading cycle]. This phenomenon of hysteresis is important because of its direct link with estimation of area and length ratio of rock pores and the related surface potential measurements.

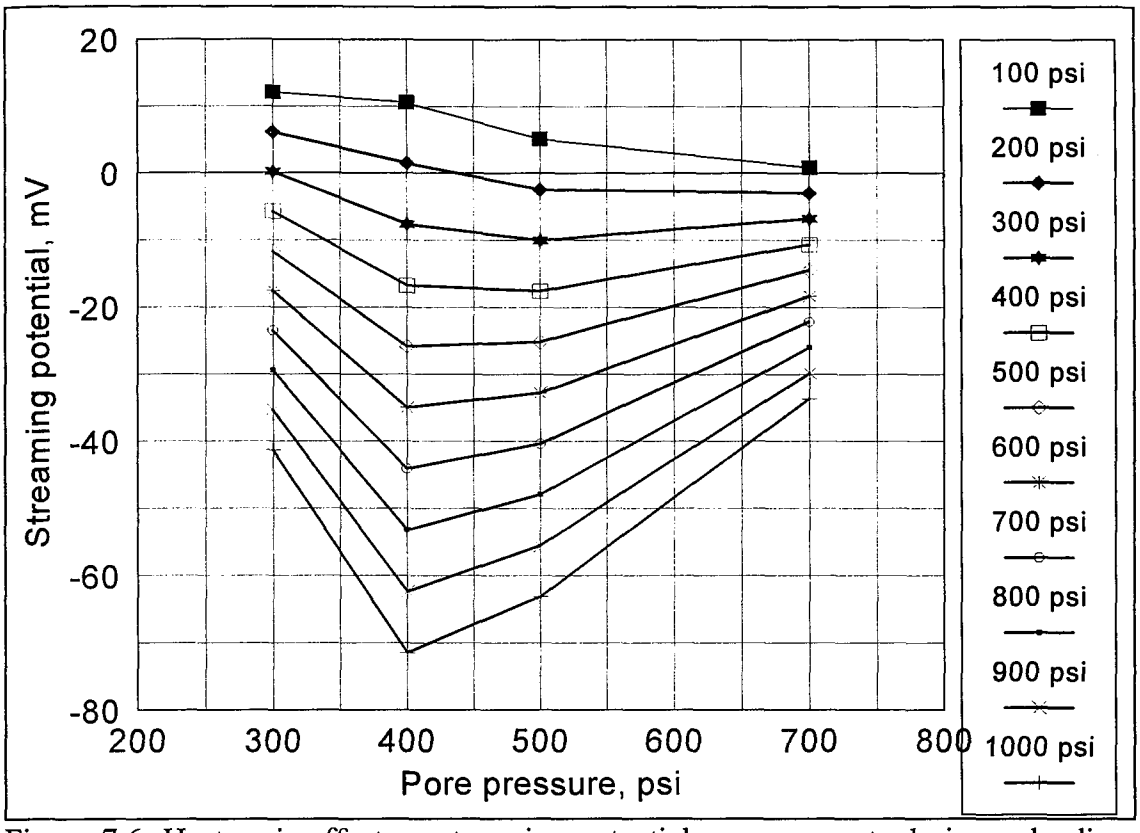

Figure 7.6. Hysteresis effect on streaming potential measurements during unloading cycle of pore pressure in Berea sandstone.

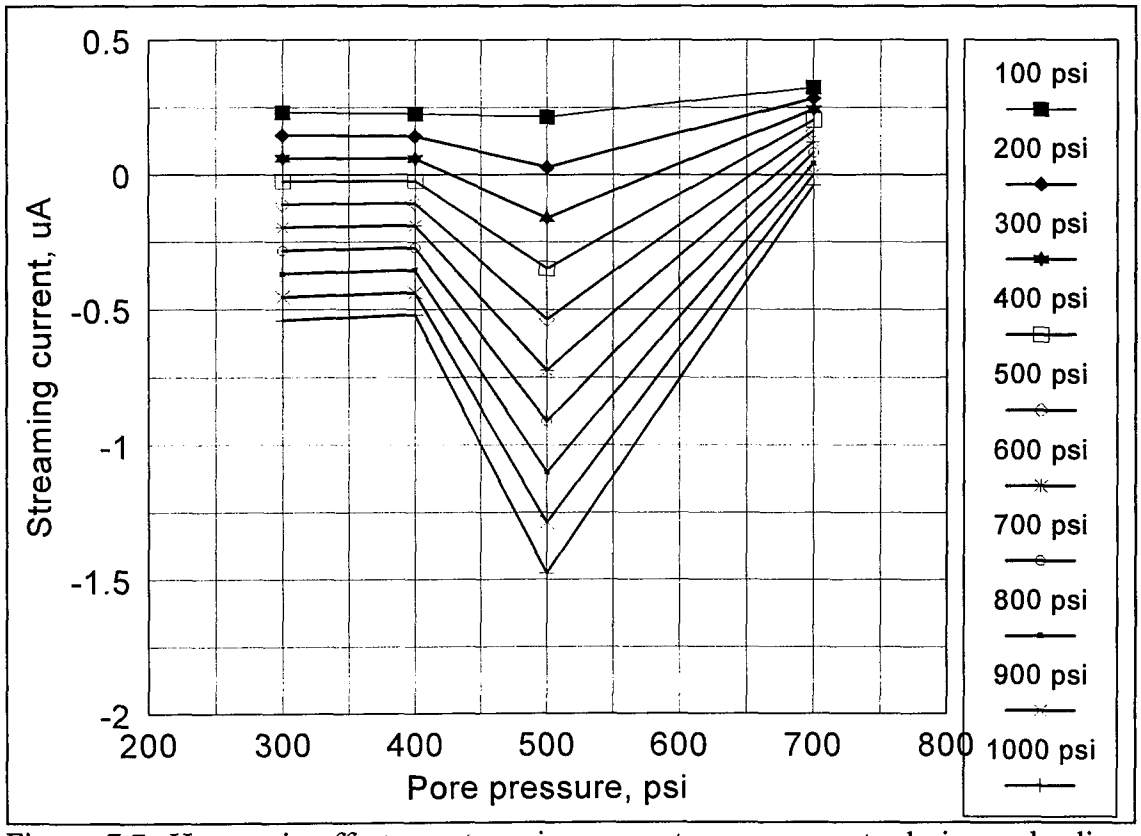

Figure 7.7. Hysteresis effect on streaming current measurements during unloading cycle of pore pressure in Berea sandstone.

7.3 POROSITY

Porosity is the pore space which contributes to fluid flow and is defined as the ratio of total pore volume to total sample volume. In this study different core samples with varying pore size distributions were used. The selected formation was Glauconitic sandstone formation in Alberta, Canada. All sample used have very similar mineral composition which were obtained by XRD analysis (Appendix A).

The flow media used were Atcor Provost brine and toluene. The purpose of choosing toluene was two-fold: firstly to represent a low permittivity non-aqueous system, secondly to represent a system in which significant double layer overlap might occur in pores. The measured values of streaming potential and current were obtained with a net confining pressure 2300 psi [15.87 MPa].

7.3.1 Rock Surface Potential versus Porosity

Figure 7.8 present Glauconitic core samples zeta potential in Atcor brine plotted against porosity. Sandstone rock surface potential is usually in the range of 20 to 30 mV in electrolyte solutions. The fluctuation in zeta potential values may be due to a slight changes in core samples mineral composition.

Figure 7.9 shows the variation of Glauconitic core samples zeta potential in toluene. It can been seen that at extremely low porosity (narrow pores) Glauconitic core samples exhibit a very small negative potential, whereas at greater (though still small) porosity the rock potential reversed its sign and becomes positive. The negative potentials at very narrow pores may be due to the effect of a water film adsorbed pushed along with the toluene, and what we are observing is the streaming current of water past silica which certainly will be negative. This has been also documented by Miller *et al.* (1992) where calcium carbonate particles exhibit a positive potential in toluene but becoming negative with the addition of water.

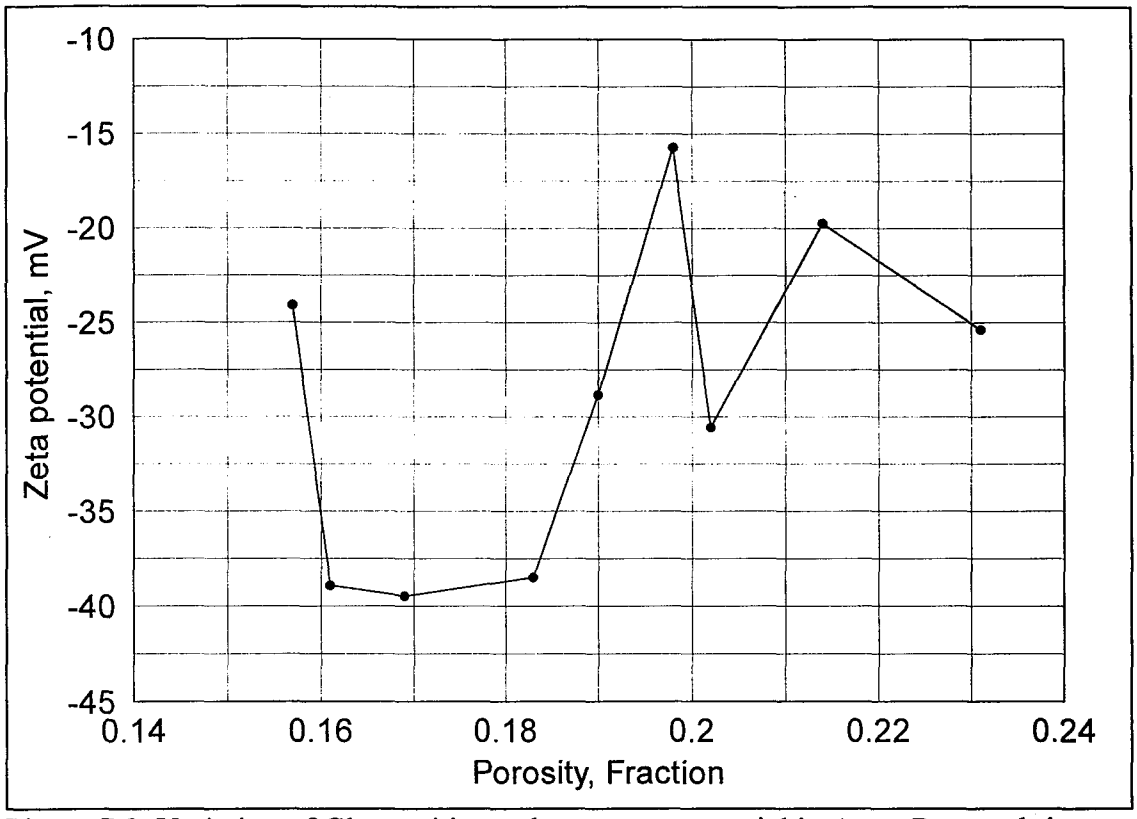

Figure 7.8. Variation of Glauconitic sandstone zeta potential in Atcor Provost brine.

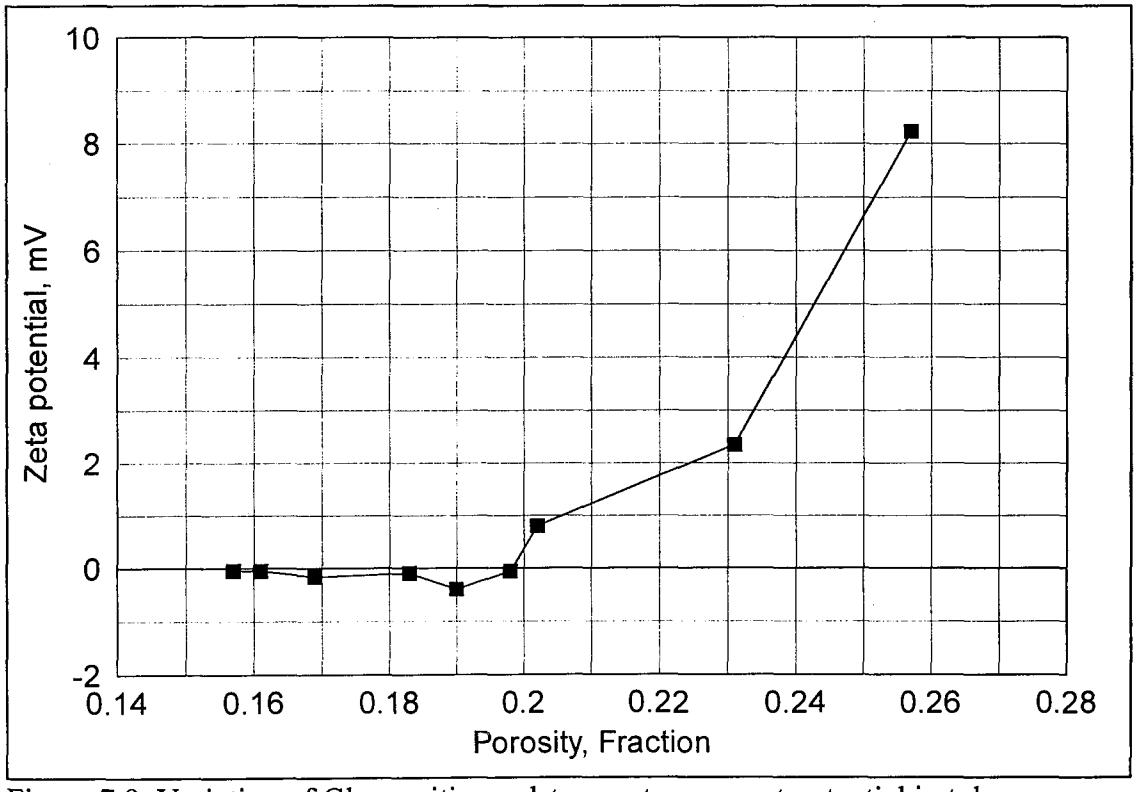

Figure 7.9. Variation of Glauconitic sandstone zeta apparent potential in toluene.

7.3.2 Rock Pores A/L versus Permeability With Porosity Distributions

Figures 7.3 and 7.5 shows that rock pores A/L and permeability follow each other in direction as a function of pore pressure. In this study both parameters were investigated at different pore size distributions. The pores A/L ratio for Glauconitic core samples were estimated by combining streaming potential and current data in Atcor Provost brine. The liquid permeability of Atcor Provost brine in Glauconitic core samples were calculated from Darcy's law. All measurements performed under ambient conditions.

Figure 7.10 shows the results of estimated core pore A/L ratio plotted against porosity. The trend of the plot indicates that the estimated pores A/L ratio increases with decreasing pore size. This arises when the rock pores get narrow (requiring high fluid pressure), the flowing fluid will occupied more spaces and then will have good contact with the solid surfaces. This will enhance the measurements which also will give the best estimation of A/L. The low values of A/L for high porosity is correct for that flow condition. This was also demonstrated in previous section with the effect of pore pressure.

Figure 7.11 shows the liquid permeability of Glauconitic core samples plotted against porosity. The plot indicate that permeability increases with increasing pore size. Comparing Figure 7.11 with Figure 7.10 of pores A/L against porosity, it is interesting to notice that the two quantities vary in opposite senses.

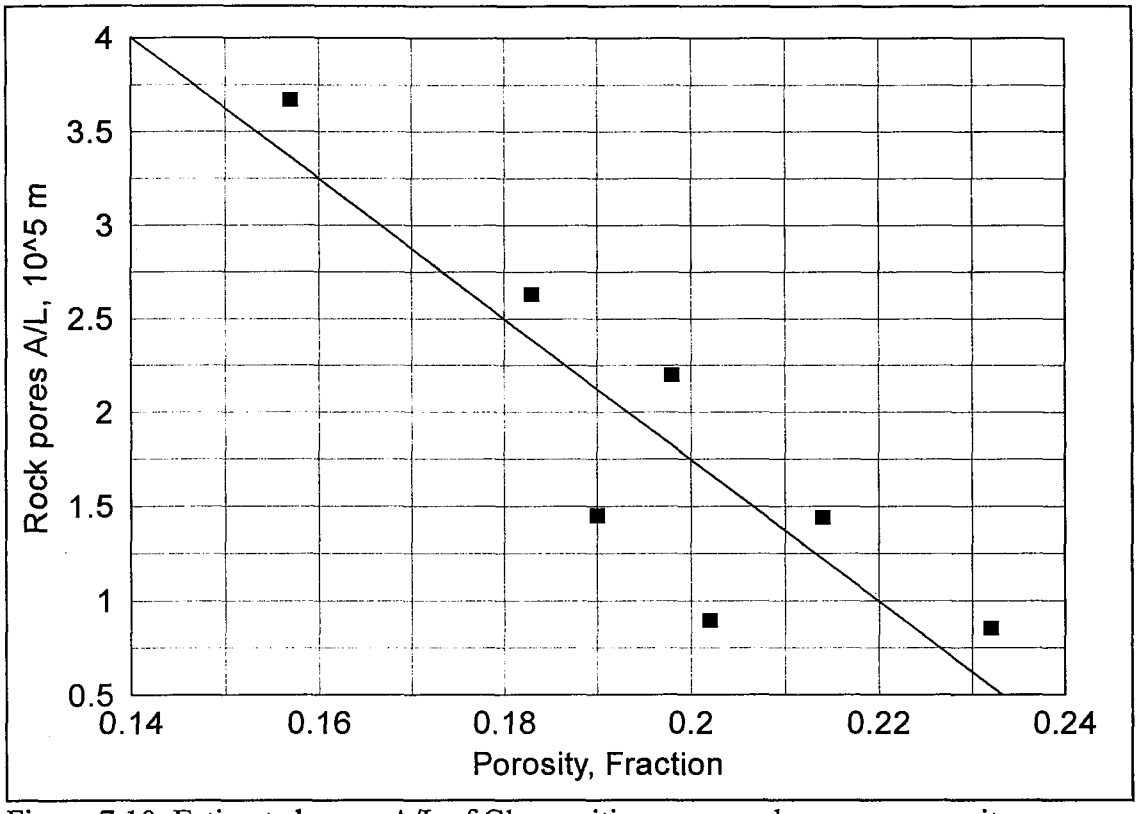

Figure 7.10. Estimated pores A/L of Glauconitic core samples versus porosity.

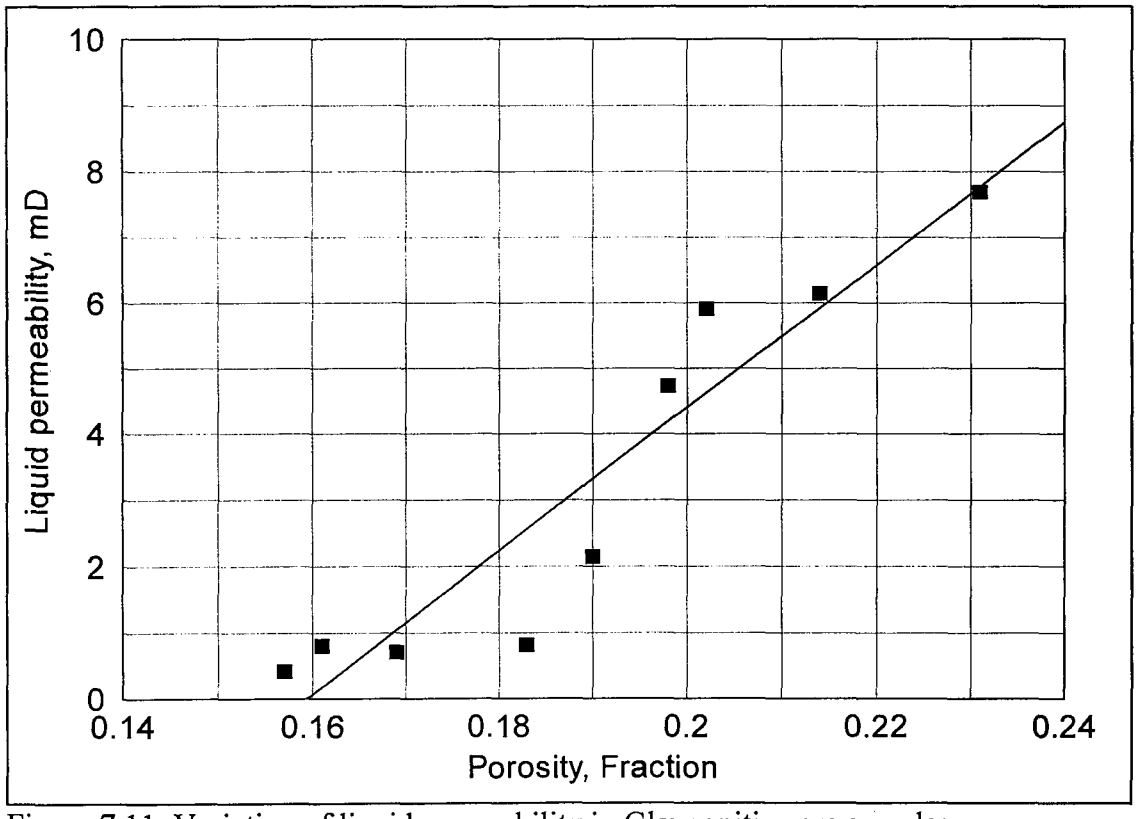

Figure 7.11. Variation of liquid permeability in Glauconitic core samples.

7.4 POTENTIAL MEASUREMENTS IN NARROW PORES

In a porous system as in an oil reservoir formation the double layers from opposite sides of the pore may overlap if the pore size is narrow. This is more likely occur in low electrolyte concentration, certainly in crude oil, and will obviously affect the streaming current (and hence the derived potential).

It is possible to evaluate the effect of overlap of the diffuse layers in narrow capillaries in crude oil flow. An approximation method will first be developed to estimate the double layer thickness in non-aqueous system and then a theory will be developed to predict the effect of double layer overlap in streaming currents and hence on the calculation of surface potentials for flat sided capillaries. The theory will be used to interpret results from sandstone formations in toluene.

7.4.1 Estimation of Double Layer Thickness in Oils

The concept of "double layer thickness" is not really precise. It arises from the low potential Debye-Hückel approximation (equation 3.4):

$$\psi = \psi_o \exp(-\kappa x)$$

where ψ_o is the wall potential and ψ is the potential at a distance x into the double layer. Thus κ the Debye-Hückel parameter has the dimensions $(\text{length})^{-1}$ and $1/\kappa$ is the distance x at which ψ has fallen to exp(-1) of its initial value ψ_o not, of course, to zero. The concept of "double layer thickness" is nevertheless widely used.

It is not easy to calculate $1/\kappa$ for a non-aqueous systems since one does not know the value of the ion concentration (n) in the medium. Also one cannot calculate $1/\kappa$ exactly from measured conductivity since the latter depends on viscosity whereas

$1/\kappa$ does not. Nevertheless an attempt will be made to get an approximation value of $1/\kappa$ from the measured conductivity of crude oil.

To do this we shall assume that the charge carriers are of valence +1 and -1, then working by analogy with *KCl* solutions in water, corrected of course for the different permittivities and viscosities. The result will be only an approximation.

The measured conductivity of Atcor crude oil (K_{obs}) is $3.74*10^{-10}$ mho/cm. The low conductivity of crude oil is mainly due to the low concentration of charge carriers but some of it is due to higher viscosity. If the viscosity of the oil is η(oil) and that of water η(water), then the effective conductivity K_{eff} of the solution on the basis of 1:1 charge carriers in water becomes:

$$K_{eff} = K_{obs} \frac{\eta(oil)}{\eta(water)} \tag{7.3}$$

In Atcor crude oil, η(oil) = 5cp, with Atcor brine η(water) = 0.9cp, then the effective conductivity K_{eff} becomes = $2.1*10^{-9}$ mho/cm. Now *KCl* (aqueous) with its charge carrier mobility and with η(water), at a concentration $1.0*10^{-3}$ mol dm^{-3} has $\kappa = 10^{6}cm^{-1}$ so $1/\kappa = 10^{-6}$cm = 100 Å =10nm. At the effective conductivity of Atcor crude oil K_{eff}, the Debye-Hückel parameter κ by analogy with *KCl* (aqueous) would be:

$$\kappa = 10^{6} * \sqrt{\frac{K_{eff}}{1.3*10^{-4}}} \tag{7.4}$$

Now taking account of permittivity ε, where ε_o for Atcor crude oil = 15 and ε_w for Atcor brine = 78.3, the corrected κ becomes:

$$\kappa = 10^{6} * \sqrt{\frac{K_{eff}}{1.3*10^{-4}}} * \sqrt{\frac{\varepsilon_w}{\varepsilon_o}} \tag{7.5}$$

Using the data in the above equation, the Debye-Hückel parameter becomes $\kappa = 9.184*10^{3}$ cm^{-1}. So the double layer thickness for Atcor crude oil (κ^{-1}) = $1.1*10^{-4}$ cm = 1.1 μm. Table 7.1 lists the estimated double layer thickness for some selected hydrocarbon system. On this basis the results must be regarded as approximate only.

Table 7.1. List of Estimated Double Layer Thickness in Hydrocarbon Systems.

Solvent	η (cp)	ε_r	K_{obs} ($ohm^{-1}cm^{-1}$)	K_{eff} ($ohm^{-1}cm^{-1}$)	κ (cm^{-1})	κ^{-1} (μm)
Atcor crude oil	5	15	$3.74*10^{-10}$	$2.1*10^{-9}$	$9.184*10^{3}$	1.1
Methanol	0.623	32.6	$5.8*10^{-6}$	$3.323*10^{-6}$	$3.323*10^{5}$	0.04
Toluene	0.59	2.4	$1*10^{-10}$	$6.555*10^{-11}$	$4.056*10^{3}$	2.465

7.4.2 Streaming Current in Flat Sided Narrow Pores

In a narrow pore the (numerical) fall of electric potential from one wall will overlap with that from opposite wall and the potential at the mid point will be (numerically) higher than would be the case in an infinitely wide pore (Figure 7.12). Since charge density is proportional to potential gradient the former will be reduced and hence the streaming current. Thus surface potentials calculated in the conventional way from the streaming current will therefore be very small whatever the actual surface potential.

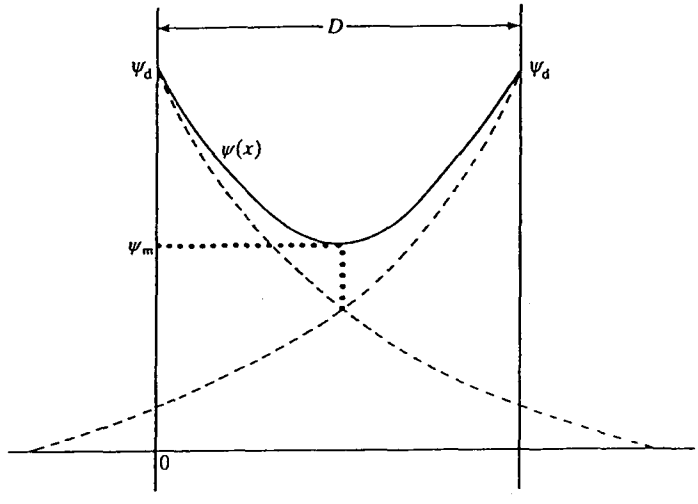

Figure 7.12. Double layer overlap curves as a function of narrow pores (Hunter,1993).

In attempting to find an expression for the streaming current to be expected in narrow pores it was assumed that the pores are slit shaped (flat sided) rather than cylindrical both for simplicity of analysis and because such pores must be at least as realistic as cylindrical ones. To correspond to the radius of cylindrical pores the half thickness of the slit pores *h* was used. The full analysis is given in Appendix C, leading to:

$$\frac{I_s}{I_{s(\infty)}} = 1 - \left(\frac{\tanh \kappa h}{\kappa h}\right) \tag{7.6}$$

where I_s is the streaming current from a pore width *2h* and $I_{s(\infty)}$ that which would result from a pore of infinite thickness at the same surface potential. κ is the Debye-Hückel reciprocal distance parameter given, for an assumed symmetrical z:z electrolyte at ion number concentration n, by:

$$\kappa^2 = \frac{2e_o^2 n z^2}{\varepsilon k T} \tag{7.7}$$

where, e_o is the proton charge, n is the ion concentration, z is valence of ions (we will take as 1), ε is permittivity, k is the Boltzmann constant and T is temperature.

Although κ can be estimated from conductivity measurements (above) such estimates cannot be relied upon. Instead κ will be derived from the streaming current data along with the surface potential.

For very fine pores (and/or very small κ) κ*h* is small and (tanh κ*h*)/κ*h* → 1, so $I_s/I_{s(\infty)} \rightarrow 0$. At large κ*h* (tanh κ*h*) →1, so that $I_s/I_{s(\infty)} \rightarrow 1$ as it must. In Figure 7.13 1-(tanh κ*h*)/κ*h* is plotted against κ*h* for the toluene/sandstone system. The point at which (tanh κ*h*)/κ*h* begins to rise can be identified (Figure 7.14) and compared with an experimental plot against *h* where *h* has been determined by a mercury injection capillary pressure technique.

since

$$\frac{I_s(h)}{I_s(\infty)} = 1 - \left(\frac{\tanh \kappa h}{\kappa h}\right)$$

and,

$$\dot{I}_s(\infty) = \frac{A}{L} * \frac{\varepsilon\psi}{\eta} \qquad (7.8)$$

where $\dot{I}_s = \frac{dI_s}{d(\Delta P)}$ (as determined experimentally)

it follows that

$$\dot{I}_s(h) = \frac{A}{L} * \frac{\varepsilon\psi}{\eta} * \left[1 - \frac{\tanh \kappa h}{\kappa h}\right] \qquad (7.9)$$

and

$$\frac{\dot{I}_s(h)}{A/L} = \frac{\varepsilon\psi(\infty)}{\eta} * \left[1 - \frac{\tanh \kappa h}{\kappa h}\right] \qquad (7.10)$$

Figure 7.15 show a plot of $\dot{I}_s(h)$ against h for toluene in Glauconitic sandstone formation (data in Table 7.2) which shows an intercept at h = 0.6 μm, whereas the κh intercept of the 1-[(tanh κh)/κh] plot was at κh = 0.25 (Figure 7.14). Since these two intercepts must correspond it follows that κ must be 0.417 μm^{-1} and $1/\kappa$ = 2.4 μm. This value compares well with the value for $1/\kappa$ of toluene from conductivity calculation (see Table 7.1) which could otherwise not have been trusted.

Plot 7.15 can also be used to estimate $\psi(\infty)$, the potential at the sandstone surface in toluene at an isolated surface in an infinite pore as follows.

Taking an arbitrary value of h, say 2.0 μm where κh = 0.834, the value of $\dot{I}/(A/L)$ is $16.5*10^{-7}$ A/psi/m, so with $\dot{I}_s$ in $(Nm^{-2})^{-1}$ rather than in $(psi)^{-1}$ $\dot{I}/(A/L)$= $2.4*10^{-10}$ $A/Nm^{-2}/m$. This can be substituted in the expression above, equation (7.10), and $\psi(\infty)$ calculated knowing toluene ε and η. Taking ε as $2.4*8.854*10^{-12}$ and η as $6*10^{-4}$ Pa.s yields $\psi(\infty)$= +37.23 mV. While this value is a little larger than expected it is quite similar to the value +34 mV found by Miller and Vincent (1992) for calcium carbonate in toluene.

This raises the question of why potentials in low ε_r solvents are most often positive whereas those in water are almost always negative, at least at neutral pH. This is sometimes for obvious reasons such as the presence of anionic surface active agents or because there are acid dissociation groups on the particle with pKa values less than 7. However the tendency is so general that one looks for general reasons (it even occurs for bubbles of nitrogen or hydrogen or oxygen in water [Kelsall and Smith, 1996]). One explanation lies in the greater hydration of cations than anions in the aqueous environment (cations being smaller in general). Thus the cation tends to be drawn into bulk water while the anion remains adsorbed on, or close to, the interface. This includes the case of H^+/OH^- and seems to be the reason for gas bubbles being negative. While not applicable to non-aqueous systems this draws attention to the importance of the supporting liquid properties rather than the more obvious particle properties.

In the case of asphaltene in oil (the latter essentially aliphatic) one therefore looks to the properties of the aliphatic liquid. It is notable that all its electrons are bonding electrons, i.e. there are few or no n-electrons (non-bonding electrons). In contact with aromatic or aromatic-containing particles such as asphaltenes there will therefore be a tendency to accept into holes/interstices in the liquid electrons from

high energy orbitals (π-electrons) in the aromatic particles. This will give the liquid a negative charge and leave the particle positively charged.

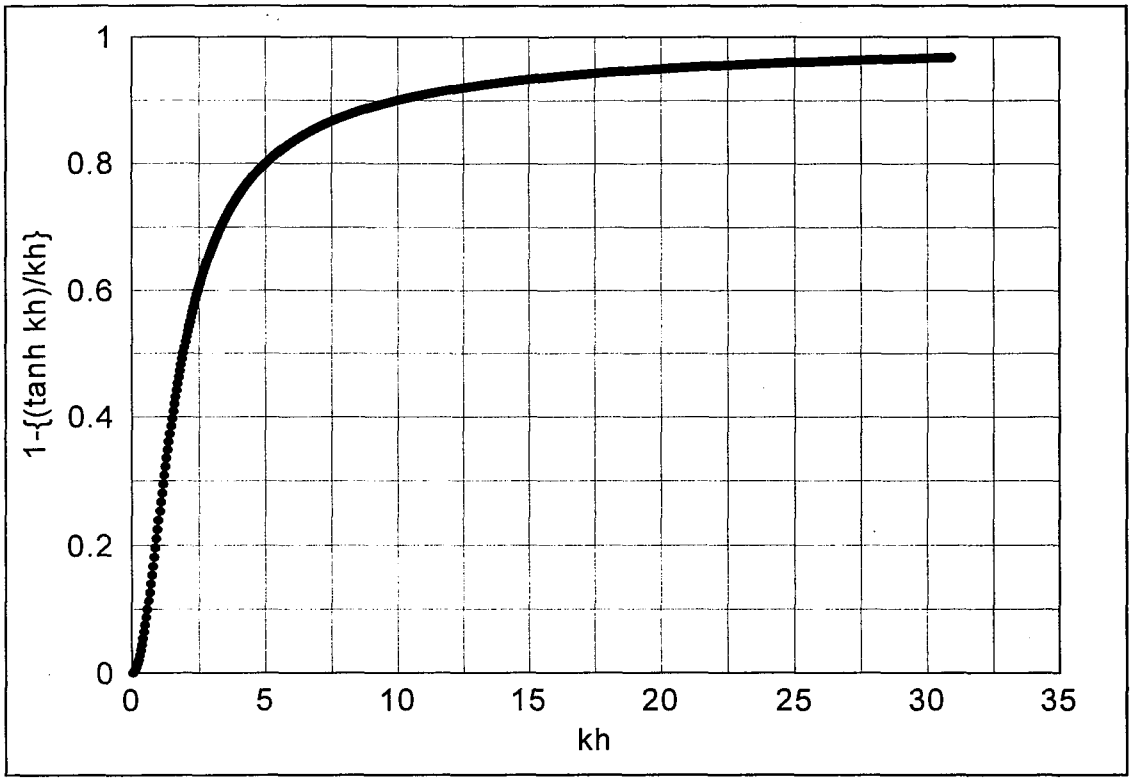

Figure 7.13. Plot of 1-(tanh κ*h*)/κ*h* against κ*h* for toluene.

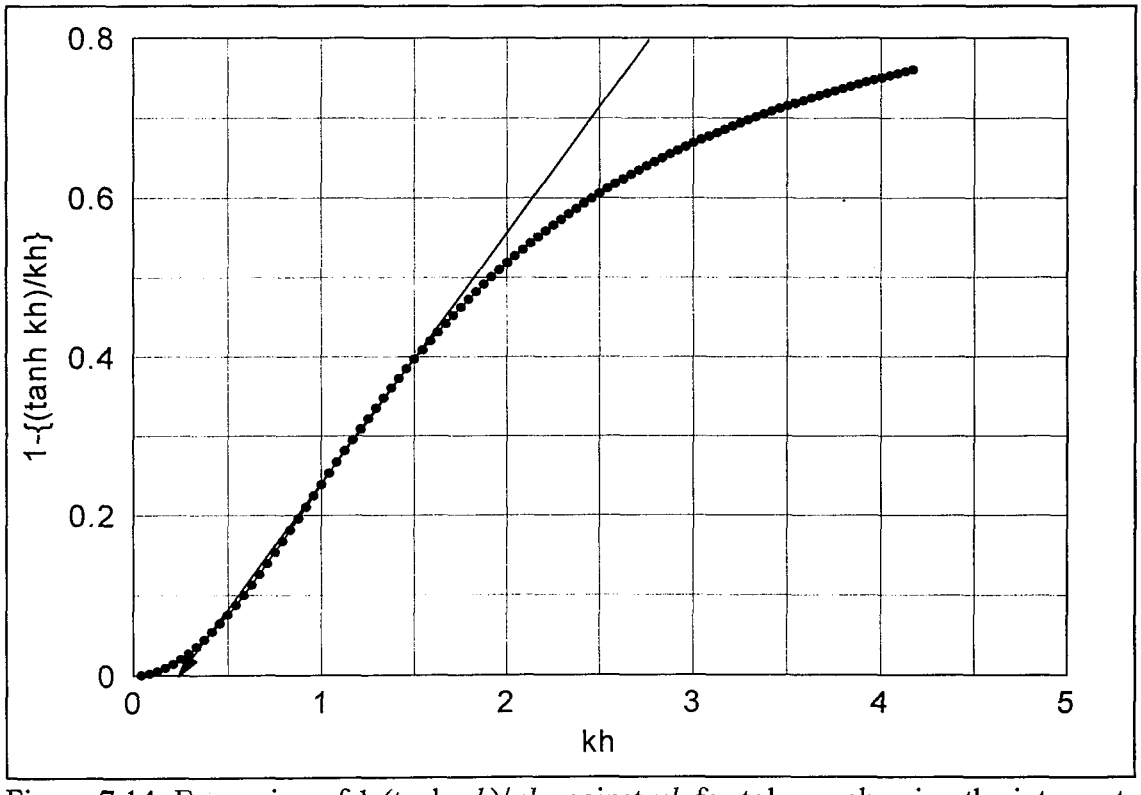

Figure 7.14. Expansion of 1-(tanh κ*h*)/κ*h* against κ*h* for toluene showing the intercept point mentioned in the text.

Table 7.2. List of Glauconitic Core Samples With Streaming Current Data.

Core No.	Porosity (Fraction)	Radius, h (μm)	$\dot{I}_s$ (A/psi)	Pores A/L (m)	$\dot{I}_s$/(A/L) (A/psi/m)
G3	0.161	0.38	-4.20E-13	3.67E-5	-1.144E-8
G6	0.19	0.369	-1.43E-12	1.45E-5	-9.862E-8
G7	0.198	0.636	-3.26E13	2.20E-5	-1.482E-8
G8	0.202	0.76	1.78E-12	8.96E-6	1.987E-7
G10	0.231	2.04	2.45E-12	4.12E-6	5.946E-7
G11	0.232	2.92	2.36E-11	8.54E-6	2.763E-6

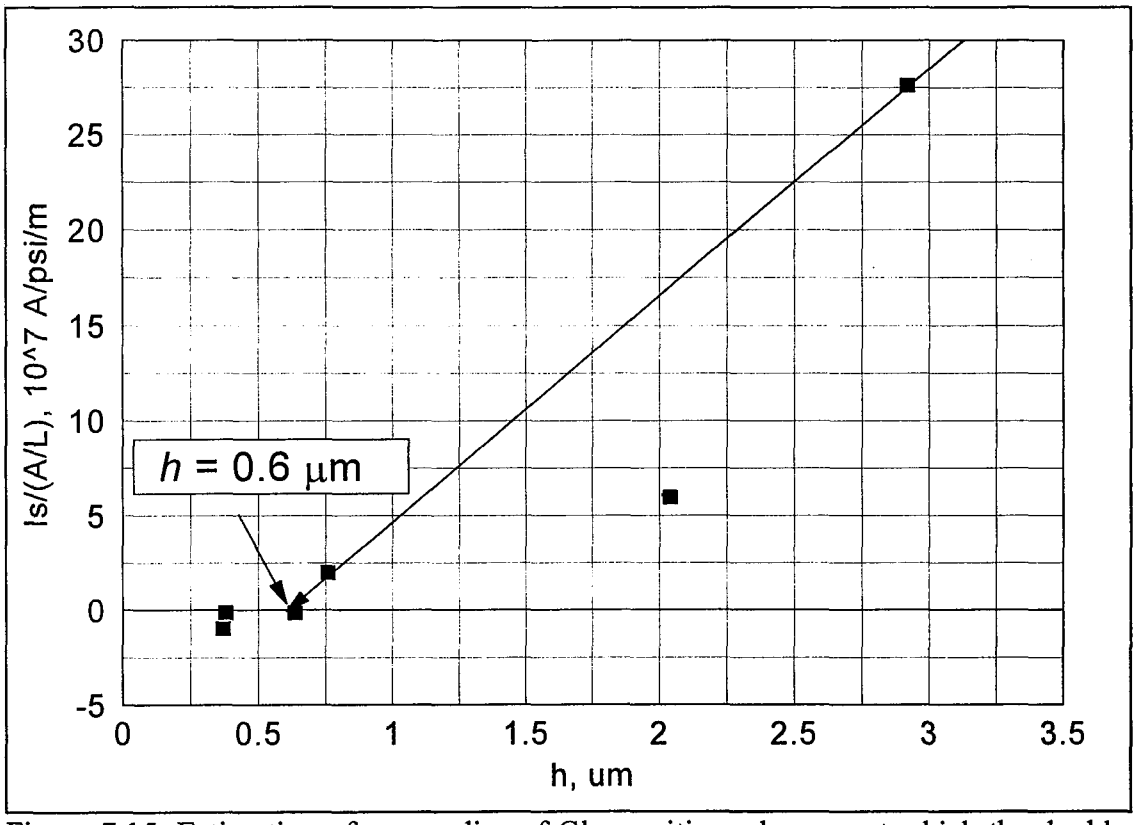

Figure 7.15. Estimation of pore radius of Glauconitic rock cores at which the double layer overlap.

Figures 7.16 through 7.19 show streaming currents and streaming potentials in very low porosity Glauconitic sandstone cores for toluene. At porosities/pore sizes below the level used for double layer thickness and large pore extrapolations it can be seen that there is a region of negative streaming current and potential.

At the very small currents being recorded in this region, of order 1 nanoamp, one might suspect instrumental artefacts. However the negative peak and its position with respect to porosity are reproducible. In looking for an origin other than artefact one notes that the sandstone surface almost certainly carries a very thin layer of irreducible water and in extremely narrow pores contained the water layers must be very close or even overlapping, and water moving across sandstone will certainly carry a negative streaming potential. This is admittedly speculative and quantitative analysis seems impossible.

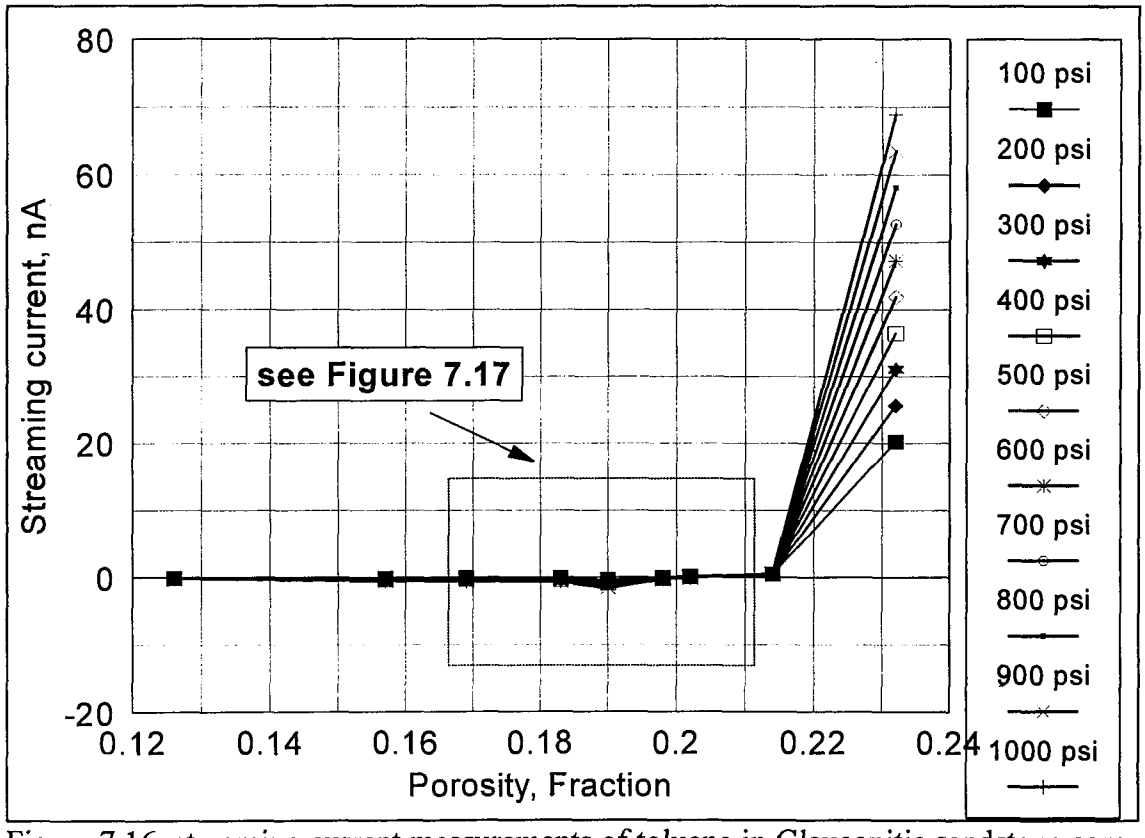

Figure 7.16. streaming current measurements of toluene in Glauconitic sandstone core samples with varying porosity.

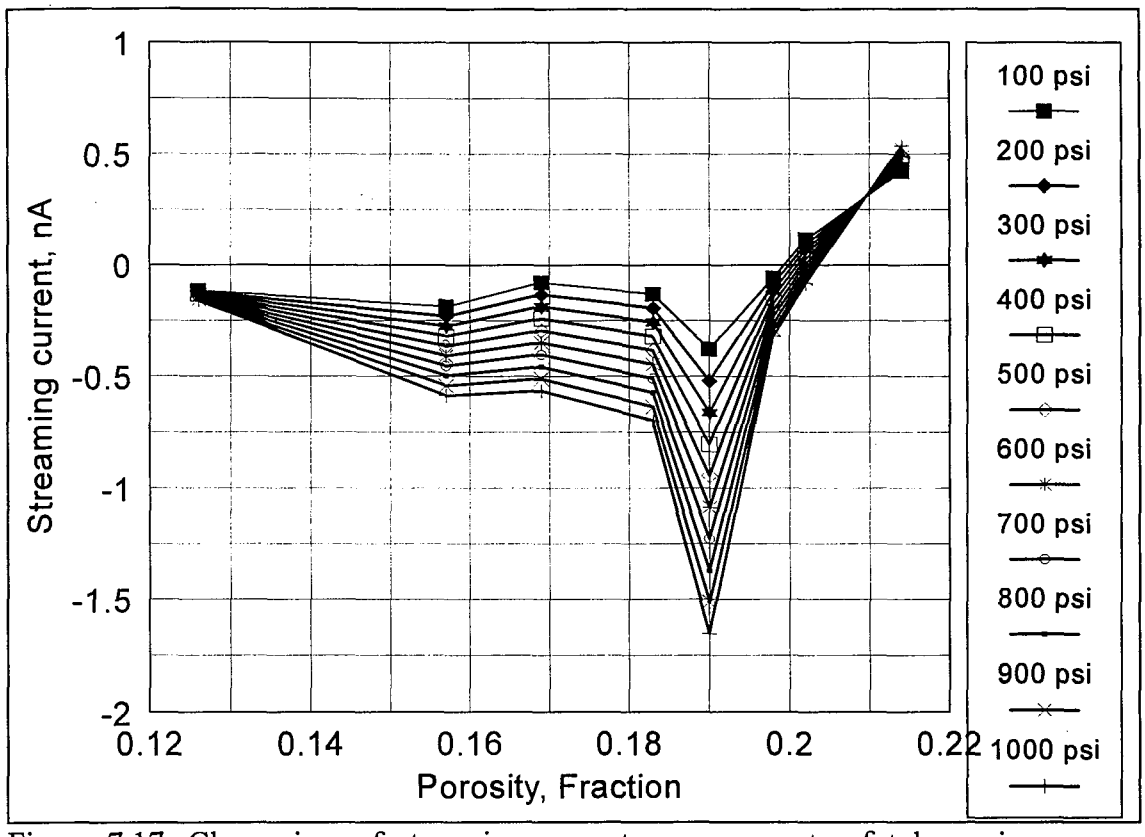

Figure 7.17. Close view of streaming current measurements of toluene in narrow porosity.

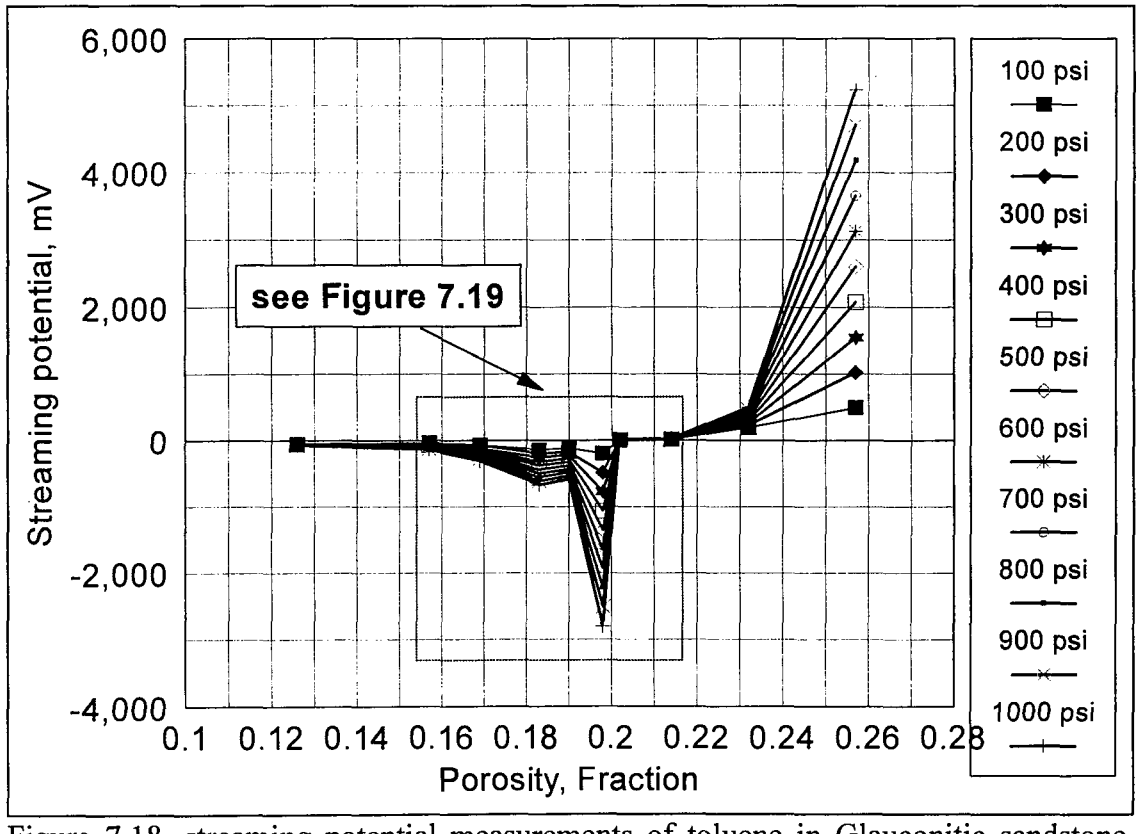

Figure 7.18. streaming potential measurements of toluene in Glauconitic sandstone core samples with varying porosity.

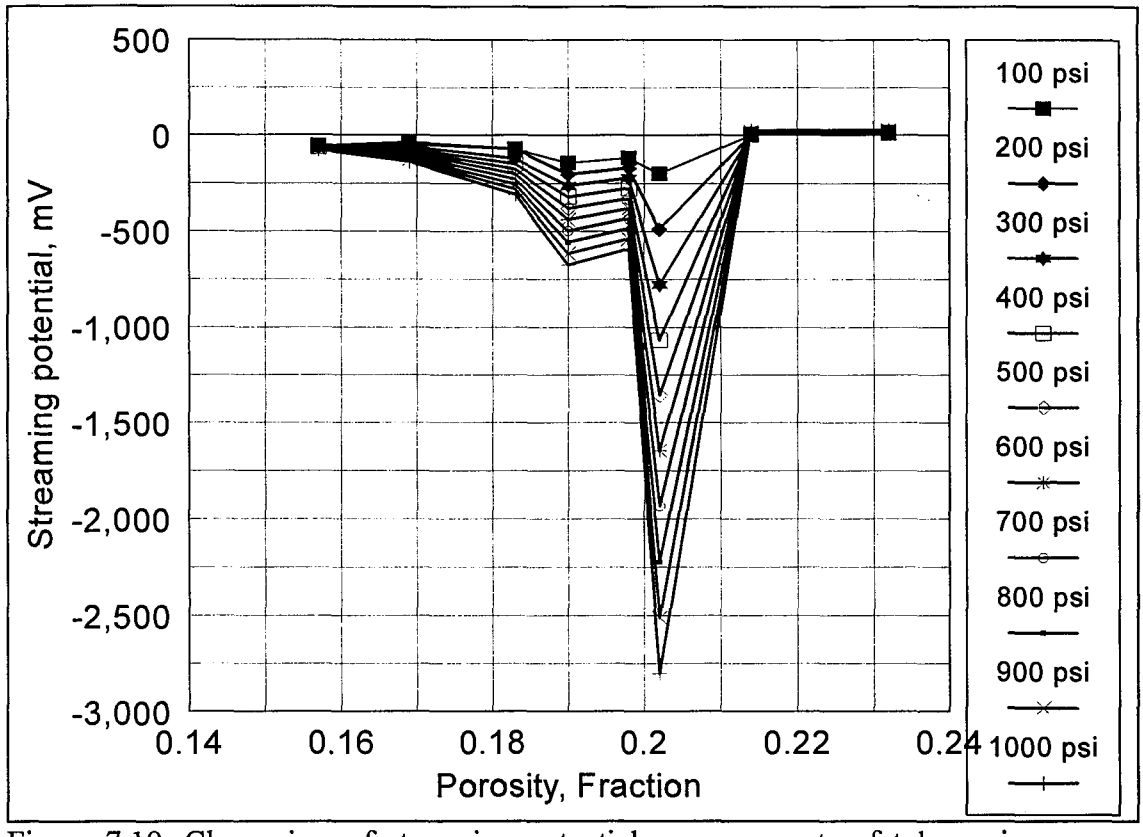

Figure 7.19. Close view of streaming potential measurements of toluene in narrow porosity.

7.5 CONCLUSIONS

1. Changes in the behaviour of streaming current and potential measurements with loading pore pressure have been observed. These have been attributed to the dissolving of gas in the liquid phase at the "saturation pressure" and to changes in pore size caused by rock matrix expansion and deformation.
2. Measured A/L ratios and permeabilities as expected follow each other as a function of loading pore pressure (fluid pressure). This does not apply to porosities which can be attributed to the effect of fluid pressure on A/L ratios.
3. Streaming current and potential measurements exhibit a strong hysteresis with respect to loading pore pressure which is probably due to rock geometry changes.
4. Double layer thickness in non-aqueous solvents estimated on the basis of 1:1 charge carriers, by analogy with aqueous systems and corrected for ε

and η differences give surprisingly good results when compared with those from $\dot{I}/A/L$ measurements.

5. A theory has been developed to handle the effect of double layer overlap in narrow pores in hydrocarbon systems.
6. An analysis of flow through narrow slit shaped pores with a surface potential has shown good correspondence with measurements on Glauconitic sandstone in toluene and allow (by extrapolation) the extraction of what the potential would have been in an infinite pore (isolated flat surface) viz 37 mV.

CHAPTER EIGHT

ASPHALTENE PARTICLE SIZE DISTRIBUTIONS IN PETROLEUM FLUIDS

8.1 INTRODUCTION

Chapter 4 introduced a method capable of measuring particle size in high particle concentrations as well as in optically dense environments, such as crude oil. This uses laser light guided to the sample cell by an optical fibre. This chapter presents the experimental results of asphaltene particle size distributions resulting from the introduction of paraffinic solvents into crude oil and asphaltene solutions. The effect of 2-hexadecyl naphthalene (HN) (Chapter 3 & Chapter 5) as a colloidal stabilising agent (i.e. a model synthetic resin) for asphaltene and for carbon dispersions in hexadecane was investigated. The interpretation of the paraffinic solvent effect on asphaltene aggregation kinetics before and after peptization by HN are presented and discussed. The adsorption of asphaltene on mineral particles is also discussed and compared with the results obtained by the surface potential method. The wax cloud-point in crude oil, has also been determined by the laser back scattering technique.

8.2 PARTICLE SIZE CALIBRATIONS

Before starting the experimental work, the laser particle analyser was tested with certified particle size standards supplied by Duke Scientific Corporation. The particles were polystyrene polymer latex. The test involved dispersing the particles in filtered water. Since reservoir crude oils contain multi-particle size distributions, a test

was carried out to verify the capabilities of the apparatus under such conditions, using a mixture of Duke standards 50 nm, 0.5 μm and 3 μm respectively. Figures 8.1 through 8.3 show the resulting particle size distributions of polystyrene polymer in water. The plots present the mean diameters in microns and show good agreement between the sizes obtained from the laser back scattering apparatus and the Duke standards.

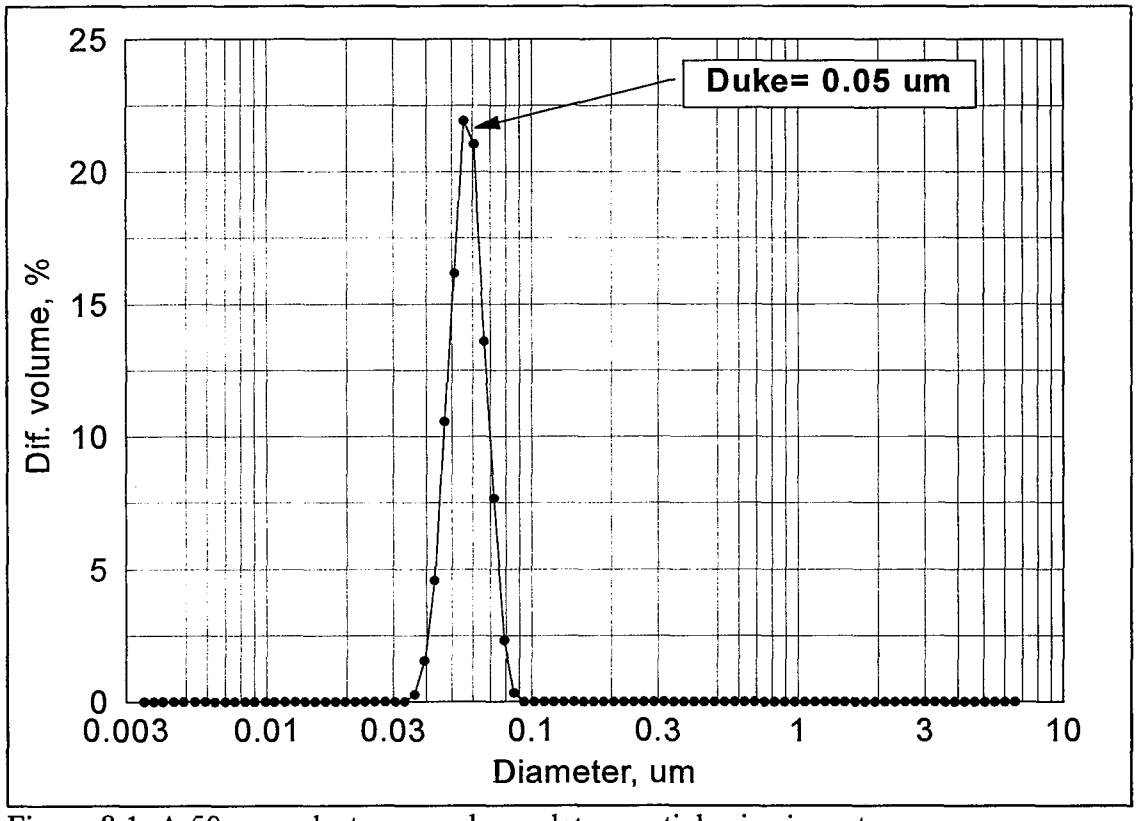

Figure 8.1. A 50 nm polystyrene polymer latex particle size in water.

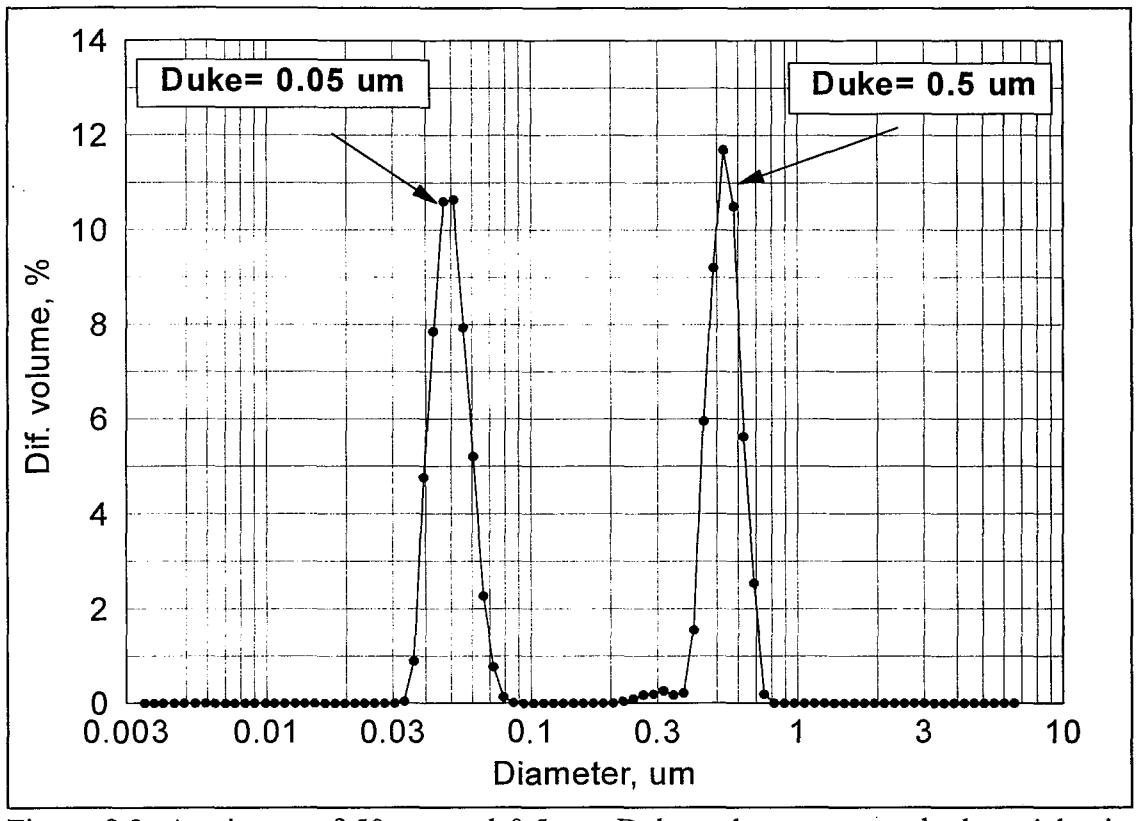

Figure 8.2. A mixture of 50 nm and 0.5 μm Duke polystyrene standard particles in water.

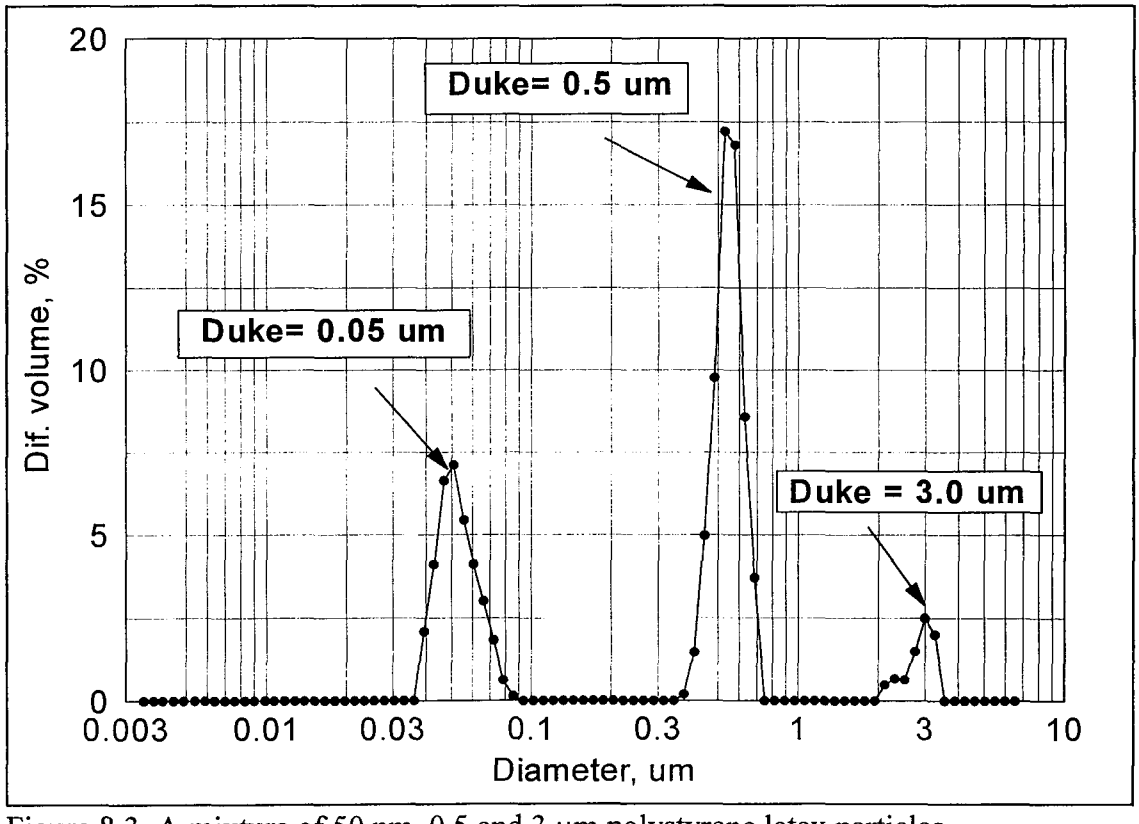

Figure 8.3. A mixture of 50 nm, 0.5 and 3 μm polystyrene latex particles.

8.3 ASPHALTENE PRECIPITATION

The experimental work consisted of determining asphaltene particle size distributions in asphaltenic crude oil and in toluene solutions after the addition of the non-solvent n-heptane. The samples of asphaltenes dissolved in toluene were isolated from Saskatchewan crude oil, the same asphaltene used in the rock surface potential experiments (Chapter 6). When the non-solvent (for asphaltene) heptane is added to a solution of asphaltene in a solvent, the asphaltene will be precipitated. Two mechanisms will then ensue:

a) Coagulation (aggregation) of the precipited particles homonucleated from the solution with other particles (including the original particles) to produce distributions containing larger particles. And/or,
b) Growth on to existing particles by precipitated material (heteronucleation) again leading to larger particles.

To distinguish between these mechanism the evolution of size distribution will be shown together with plots of average particle size versus time. The significance of the latter is that "coagulation" should lead to a linear plot of particle volume against time whereas the "growth" mechanism should lead to a linear increase of diameter versus time (see Appendix D).

8.3.1 Asphaltenic Crude Oil

Figures 8.4 through 8.9 illustrate the results of asphaltene particle size distribution determinations in Canadian asphaltenic crude oil before and after the addition of 25%, 50% and 75% (by volume) of n-heptane. Figure 8.4 shows the particle size distribution before the addition of heptane. The plot shows a combination of particle sizes, the largest size peak indicates a median diameter of about 4.5 μm, whereas the other peaks represent 1.37 μm and 0.08 μm.

Figures 8.5 to 8.7 show the aggregation of asphaltene particles after the addition of n-heptane at 25% (by volume). The results are based on 3 runs of 5 minutes each. The plots shows a clear aggregation in asphaltene particle size. The first 5 minute run was started soon after the addition of the heptane. The aggregation of asphaltene particles in such a relatively short period of time indicates a rapid accretion process. The addition of higher concentrations of heptane (50% and 75% by volume) caused an increase in the precipitation/aggregation process (Figures 8.8 and 8.9).

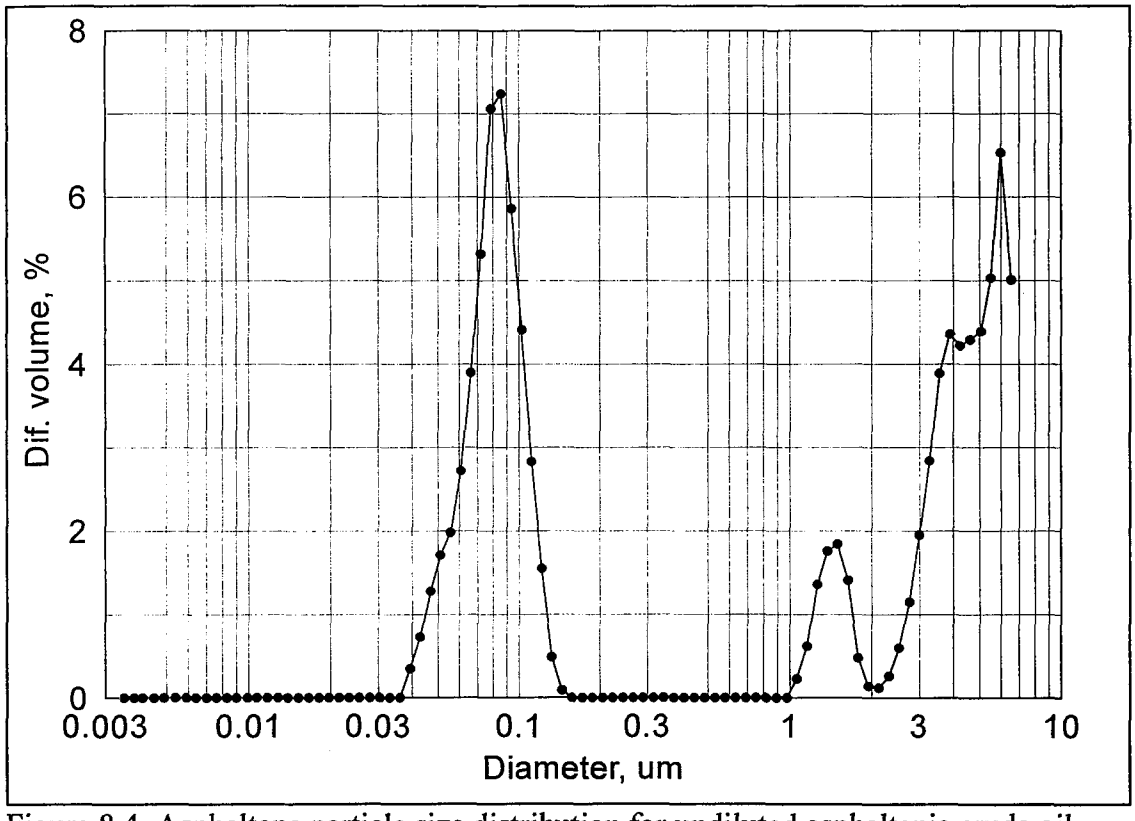

Figure 8.4. Asphaltene particle size distribution for undiluted asphaltenic crude oil.

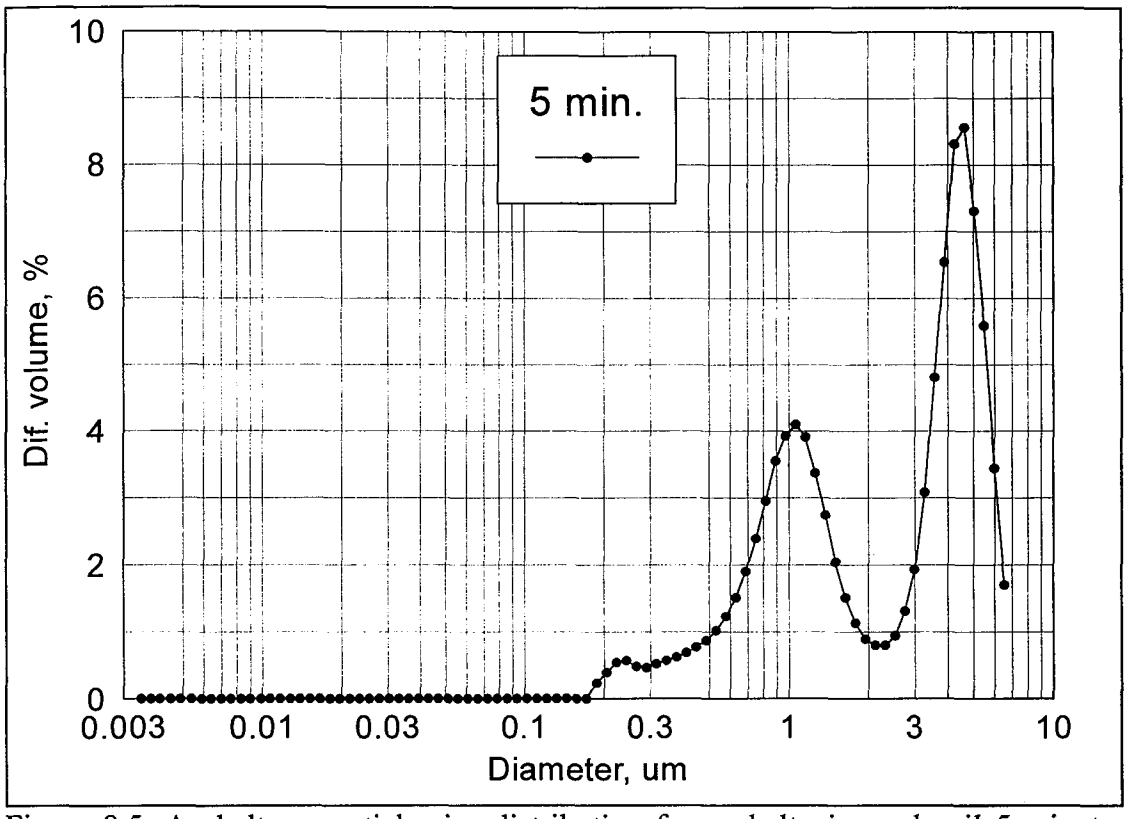

Figure 8.5. Asphaltene particle size distribution for asphaltenic crude oil 5 minutes after mixture with 25% heptane.

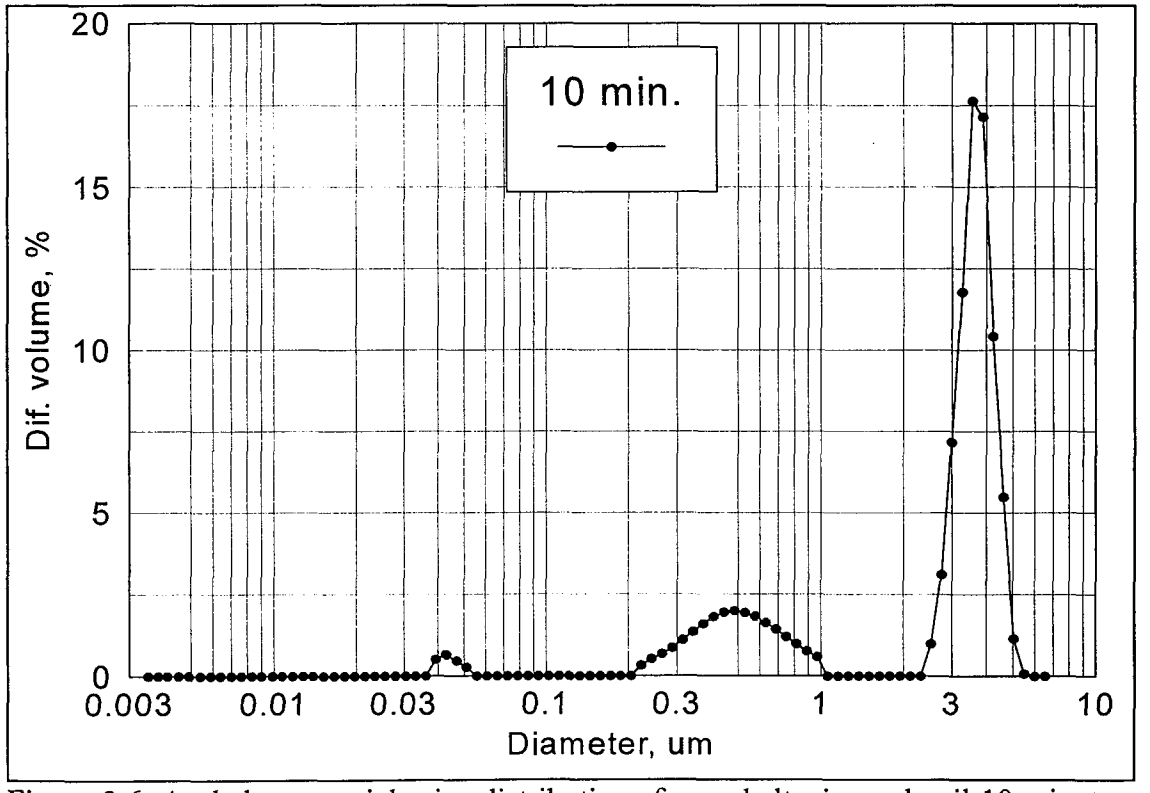

Figure 8.6. Asphaltene particle size distributions for asphaltenic crude oil 10 minutes after addition of 25% heptane.

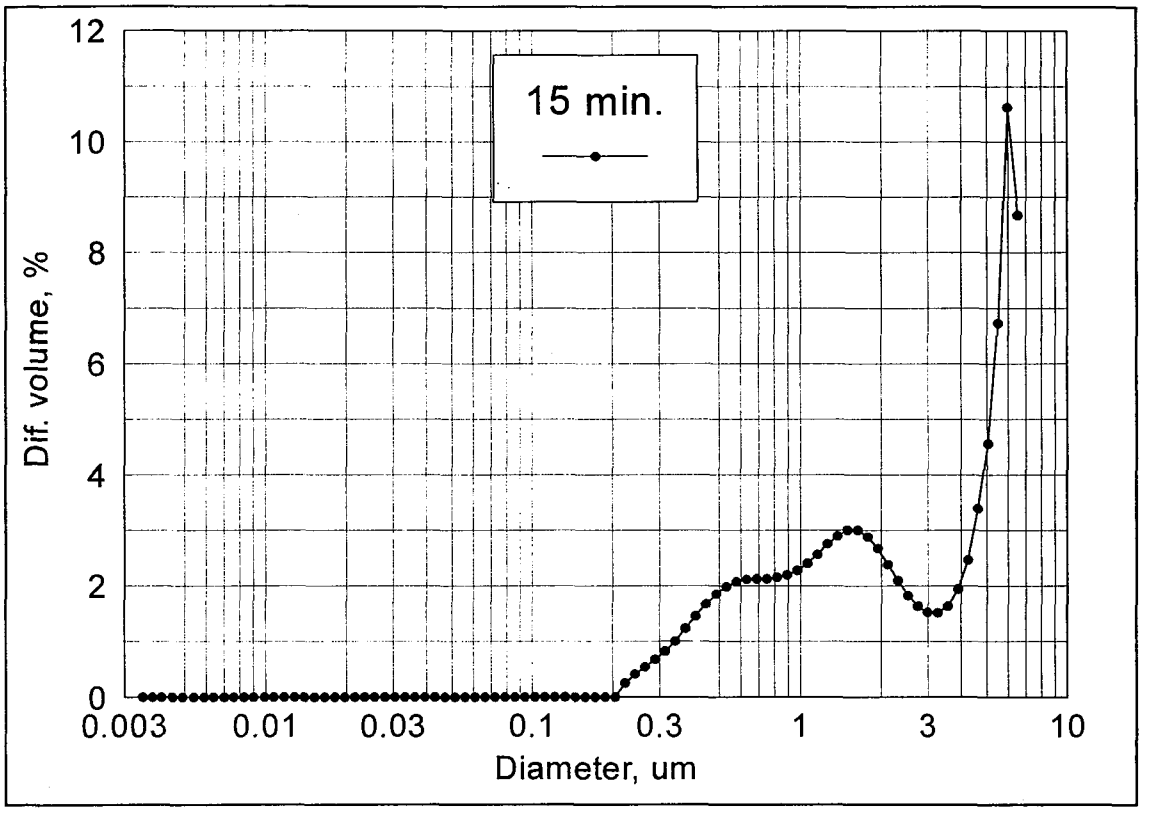

Figure 8.7. Asphaltene particle size distributions for asphaltenic crude oil 15 minutes after 25% heptane.

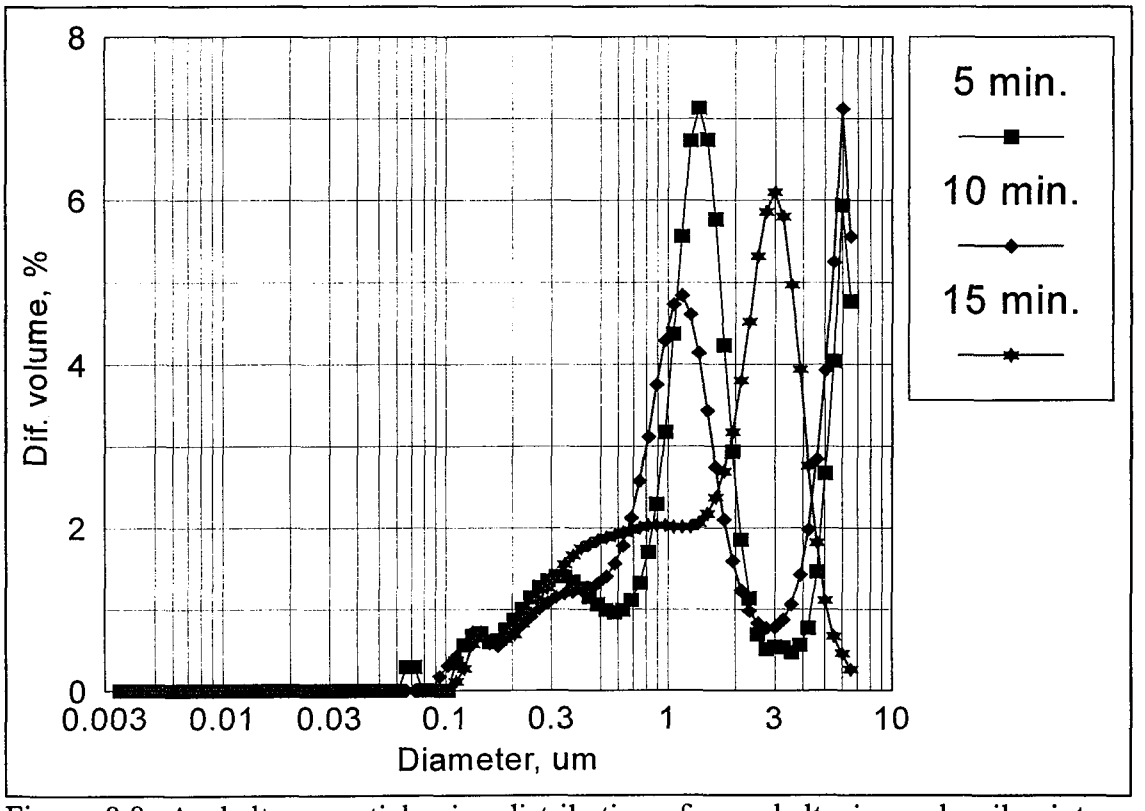

Figure 8.8. Asphaltene particle size distributions for asphaltenic crude oil mixture with 50% heptane.

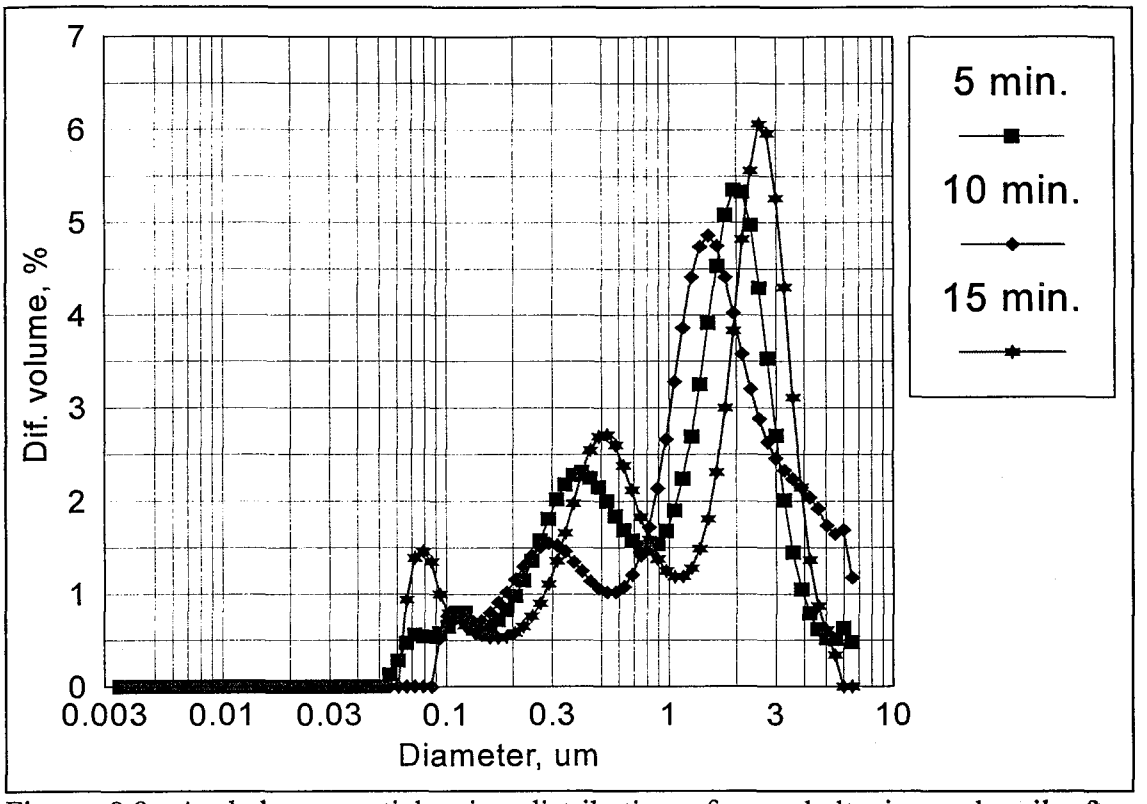

Figure 8.9. Asphaltene particle size distributions for asphaltenic crude oil after addtition of 75% heptane.

8.3.2 Asphaltenic Solutions in Toluene

This section presents the results of asphaltene precipitation from toluene solutions by the addition of n-heptane. This is distinct from the crude oil case in that the latter contains natural resin stabilising/peptising molecules which to some extent inhibit aggregation. Of course this effect depends on the concentration of resin. The asphaltenes used in this study were extracted from Saskatchewan crude oil by the addition of n-pentane. The extraction followed the ASTM procedure. The asphaltenes were dried overnight in an oven at 80 °C and dissolved in toluene at 1gram/100 ml. The solutions were equilibrated for at least 48 hours.

Asphaltene particle size distributions in toluene (1gram/100ml) were checked repeatedly and found to be reproducible, Figure 8.10. Figure 8.11 shows the size distribution of asphaltene particles after the addition of n-heptane at volume % of 7.5, 22.5, 37.5 and 50. The plot shows no significant change in asphaltene particles size

after the addition of n-heptane until the precipitant reached 50% of the asphaltene sample volume. Asphaltene is commonly defined as that portion of petroleum oil which is insoluble in heptane but soluble in toluene, i.e. in this experiments the heptane has to overcome the toluene solubility power to allow asphaltene to precipitate, and this takes at least 50% of the asphlatene/toluene sample volume.

Figures 8.12 and 8.13 show the formation process of asphaltene particles from the beginning of the addition of 50% n-heptane concentration to 1 hour at 5 minute time intervals. At short times Figure 8.12 shows that the original particle size asphaltene (0.05 μm) slowly reduced in concentration while at the same time the aggregation of other particles started to occur. An interesting point is that the aggregation of asphaltene particles occurs only to certain sizes, for example within 15 minutes from introducing 50% heptane a new peak starts to form at 1.2 μm. At the end of the first half hour a second particle size started to occur at 4.7 μm. Both peaks increased in volume concentrations with time as can be seen at the end of 1 hour measurements in Figure 8.13.

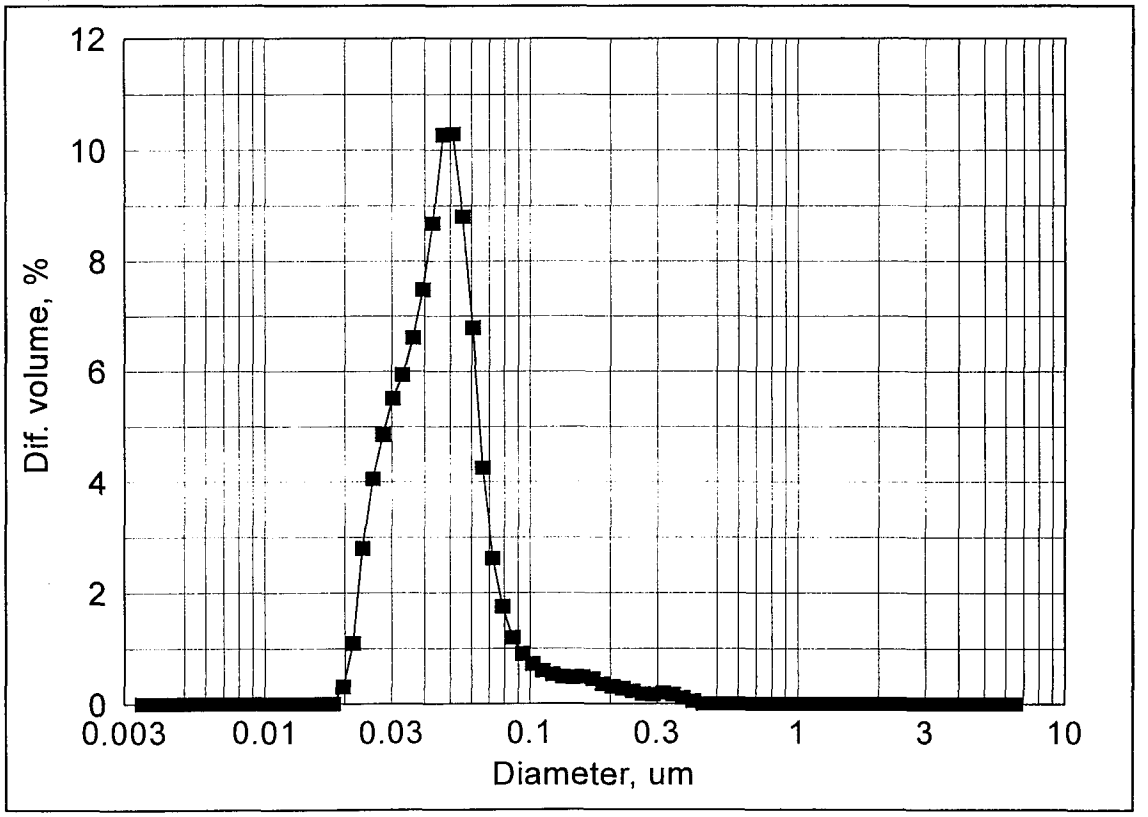

Figure 8.10. Asphaltene particle size distributions for toluene solution without any additives.

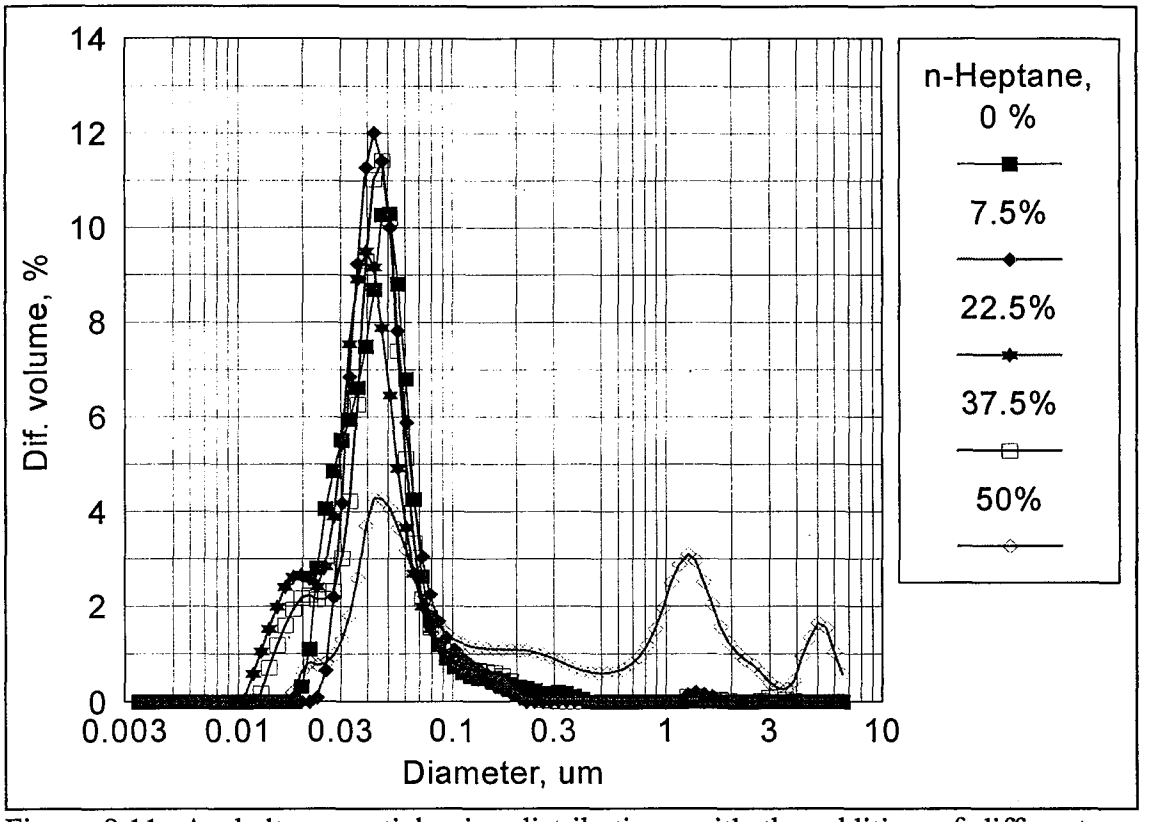

Figure 8.11. Asphaltene particle size distributions with the addition of different n-heptane concentrations.

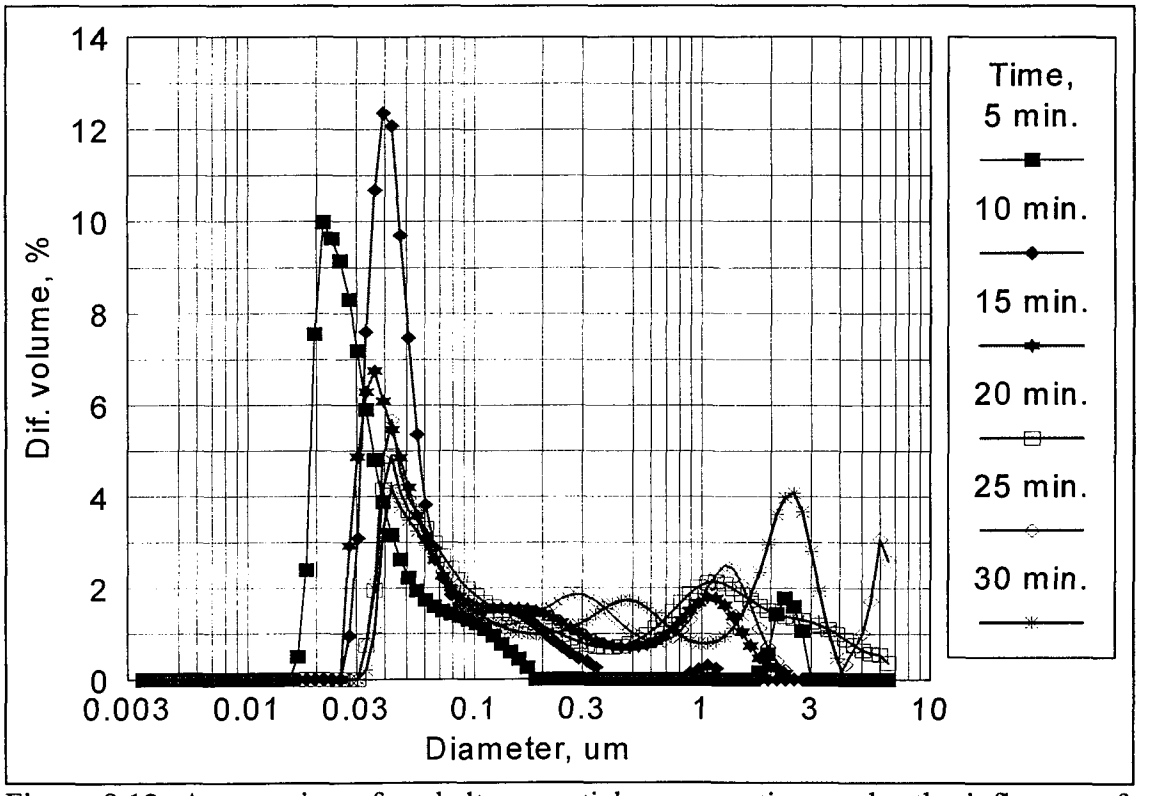

Figure 8.12. Aggregation of asphaltene particles versus time under the influence of 50% n-heptane concentration (first half hour).

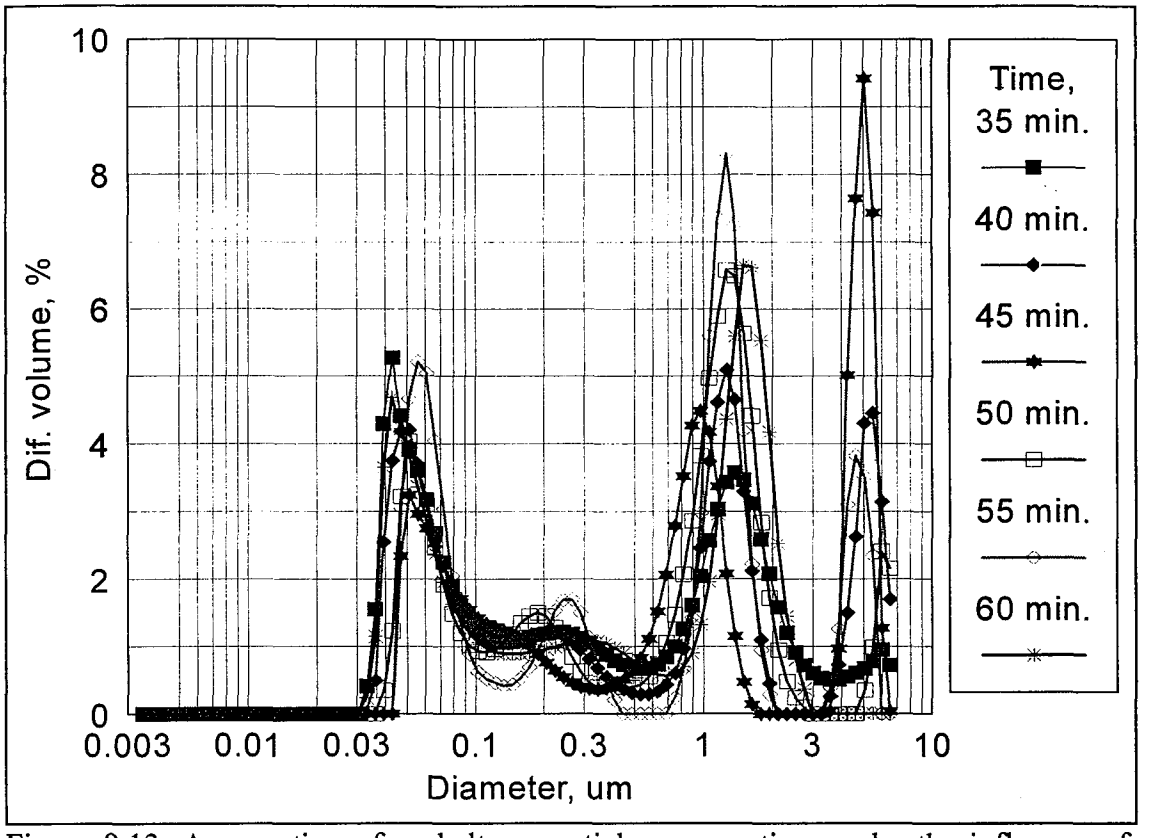

Figure 8.13. Aggregation of asphaltene particles versus time under the influence of 50% n-heptane concentration (second half hour).

8.4 ASPHALTENE PEPTIZATION BY HN

It is generally accepted that asphaltenes exist in petroleum oil as particles in a dispersed state, colloidally stabilised at least to some extent by the resins which act as peptizing agents. Resin molecules surround asphaltene particles and can form a layer giving a steric shield. If this protective shield is removed by the dissolution of the resins into the fluid phase the asphaltene particles start to aggregate into large particles (i.e.coagulate) which can result in asphaltene deposition on to available surfaces. This adsorption of resins on the surface of asphaltene particles is a function of the resin concentration in the liquid phase. Changing the resin concentration in the fluid (i.e. oil composition) will affect the resin adsorption onto asphaltene particles and hence degree of coagulation.

In this work an experimental study was carried out by using 2-hexadecyl naphthalene (HN) to stabilise asphaltene in toluene solutions, though HN was

designed (Chapter 3) for maximum effectiveness in aliphatic solvents such as crude oil. The peptization of asphaltene particles by HN occurs when HN molecules are attached to the surfaces of asphaltene particles with their naphthalene heads and stretch their aliphatic tails out into the bulk to form a steric-stabilisation layer. Though this will only happen to maximum effect in an aliphatic liquid which is a good solvent for the hexadecyl chain, it should however be partially effective in toluene.

The effectiveness of 2-hexadecyl naphthalene on asphaltene stabilisation is strongly dependent on the naphthalene head groups of HN promoting adsorption onto the asphaltene surface to form a layer which gives a steric shield. Thus it is important to make sure that the HN concentration is high enough to cover the sufficient asphaltene surface. Based on asphaltene particle size distributions in toluene an amount of 4.25% by weight of HN to cover 1% of asphaltene in toluene was used.

On the addition of HN to asphaltene/toluene solution the particle size distributions of asphaltene reduces gradually from 0.05 μm to 0.008 μm i.e. there has been some peptization of the asphaltene particles by HN.

The test of precipitation of peptized asphaltenes by HN from toluene solution involved the addition of n-heptane at various concentrations. Figure 8.14 shows the asphaltene particle size distributions at 5 minute time intervals at different n-heptane concentrations (by volume). The plot shows no significant change in asphaltene particle size during the addition of n-heptane until the precipitant reached (again) 50% concentration (by volume).

Figures 8.15 and 8.16 illustrates the evolution of asphaltene particle size in the presence of HN with the addition of 50% heptane at 5 minute time intervals for 12 runs. It can be noted from Figure 8.15 that asphaltene particles during the peptization process reduce from 0.05 μm (original size, Figure 8.10) to 0.008 μm. This suggests that the HN concentration (4.25%) completely covered (shielded) asphaltene particle surfaces and also helped in reducing asphaltene particle sizes. To permit the asphaltene particles to aggregate the precipitant solvent has first to remove the

protective shield (HN) by the dissolution of HN into the liquid phase, at least to some extent.

Figure 8.15 shows that the 50% concentration of n-heptane started to remove HN molecules from asphaltene particles surfaces. At the same time the original asphaltene particle size (0.05 μm) started to form back again. At the end of the 1 hour measurements (Figure 8.16) most of asphaltene particles formed back to the original size at 0.05 μm. Only 9% of the cumulative volume of the particles aggregated further than 0.05 μm to form a new peak at 0.36 μm, 5 times smaller than the test without HN (1.8 μm).

Figure 8.17 presents a comparison of asphaltene particle size distributions with and without HN peptization on the addition of 50% n-heptane. The Figure shows that asphaltene particle size distributions in the absence of HN aggregated from 0.05 μm and formed new particles in the range 1.8 μm, whereas in the presence of HN only from 0.05 μm to 0.36 μm. This certainly shows that HN has some effect on particle stability in toluene.

Figure 8.18 shows a comparison of asphaltene particle size distributions without and with HN at 50% and 56.25% by volume of n-heptane concentrations respectively. This suggests that to remove (dissolve) HN molecules from asphaltene particle surfaces thoroughly requires an additional 6% n-heptane.

Figure 8.19 shows a plot of average particle volume (expresed as a diameter) against time on the addition of 50% by volume of n-heptane to asphaltene solutions. The aggregation of asphaltene particles in the absence of HN is 0.037 μm/minute, whereas in the presence of HN the aggregation rate dropped to 0.0022 μm/minute. This shows that HN slows the aggregation rate by 17 times even though the HN was not designed to be specially effective in toluene. The linearity of the volume plot (even though expressed as the equivalent diameter) indicates that the major process occurring has been aggregation (coagulation) rather than growth by deposition of molecules on to existing particles.

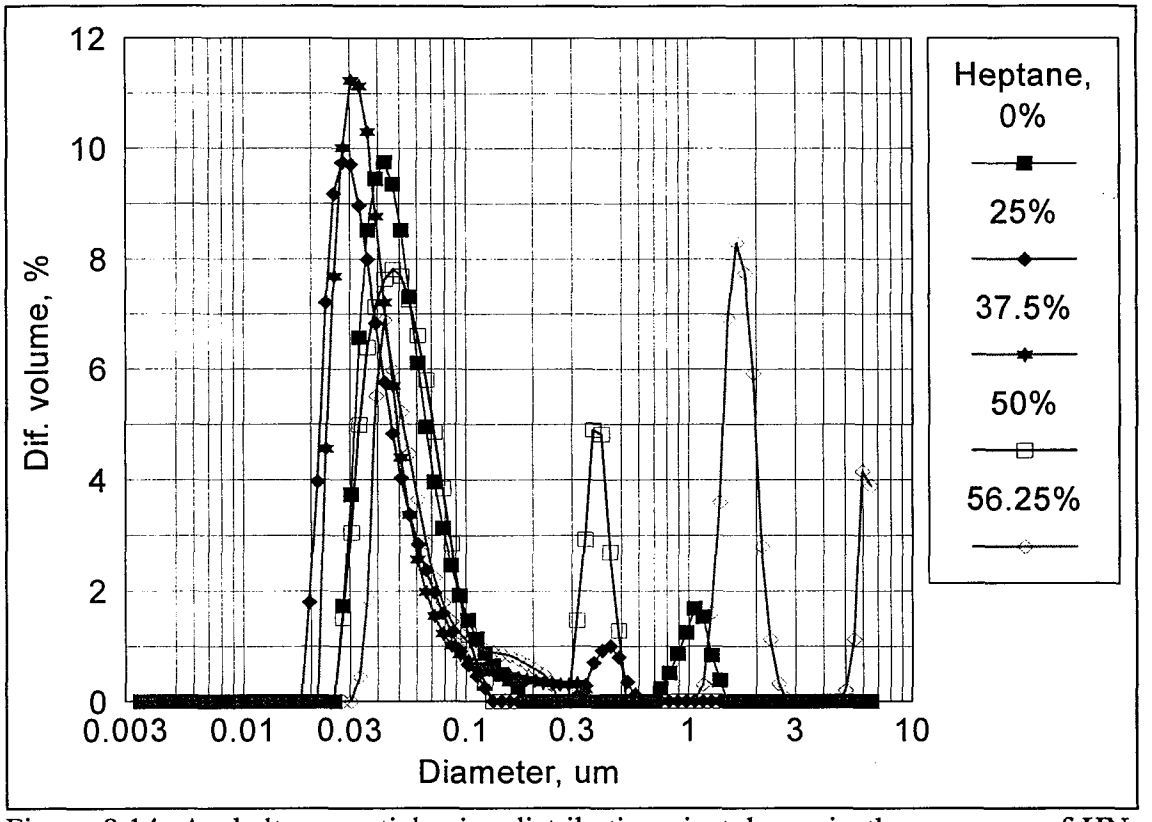

Figure 8.14. Asphaltene particle size distributions in toluene in the presence of HN with the addition of n-heptane concentrations.

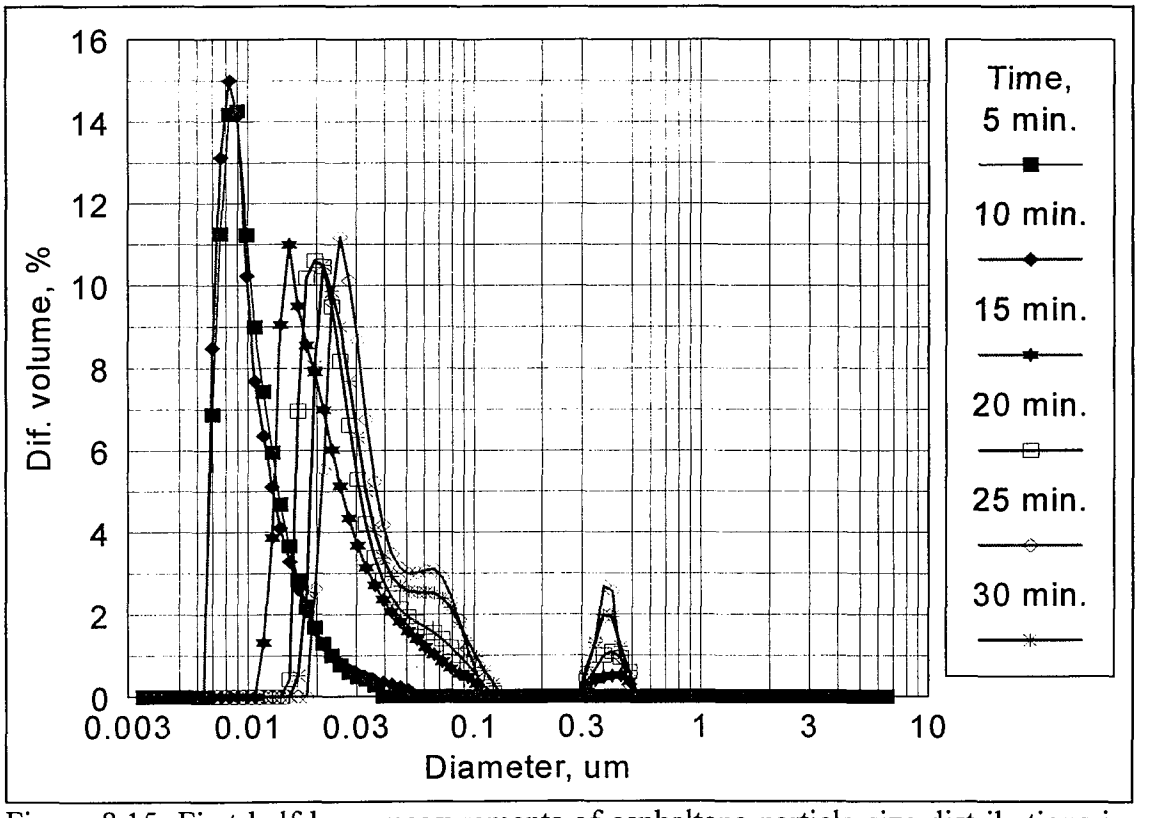

Figure 8.15. First half hour measurements of asphaltene particle size distributions in toluene in the presence of HN at 50% n-heptane concentration.

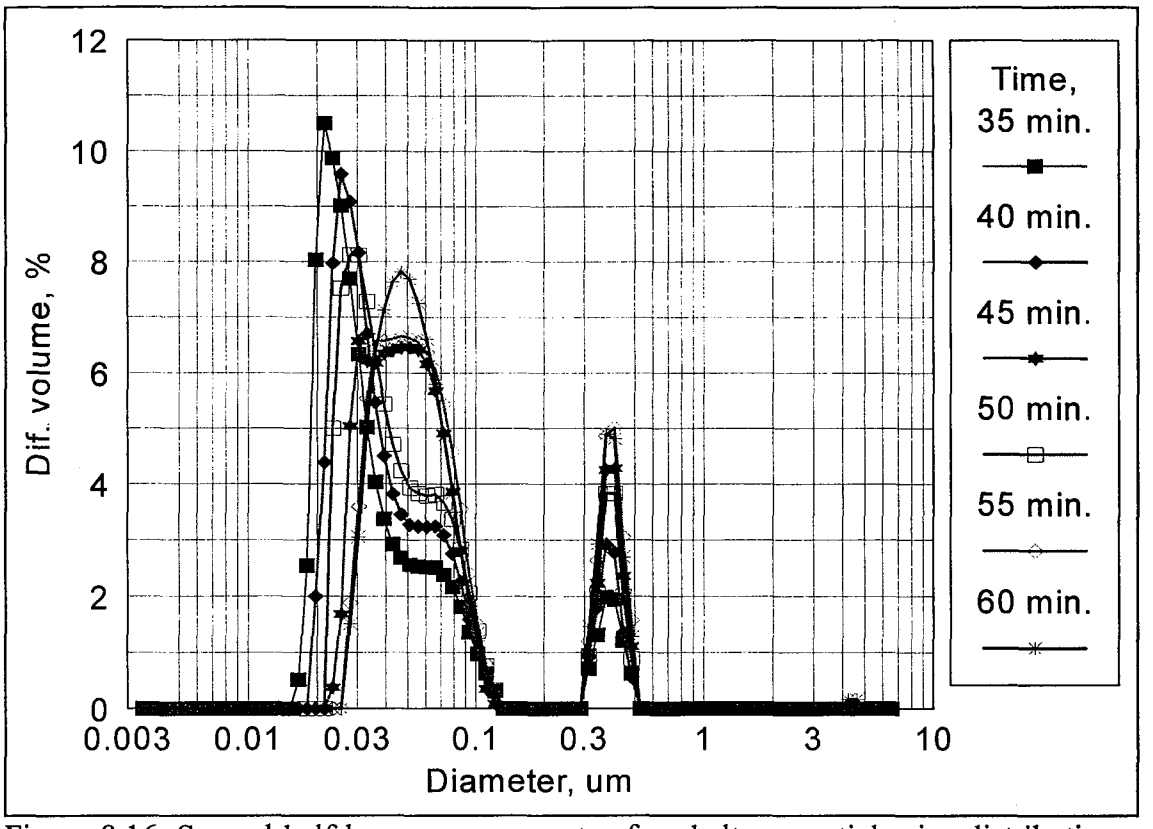

Figure 8.16. Second half hour measurements of asphaltene particle size distributions in toluene in the presence of HN at 50% n-heptane concentration.

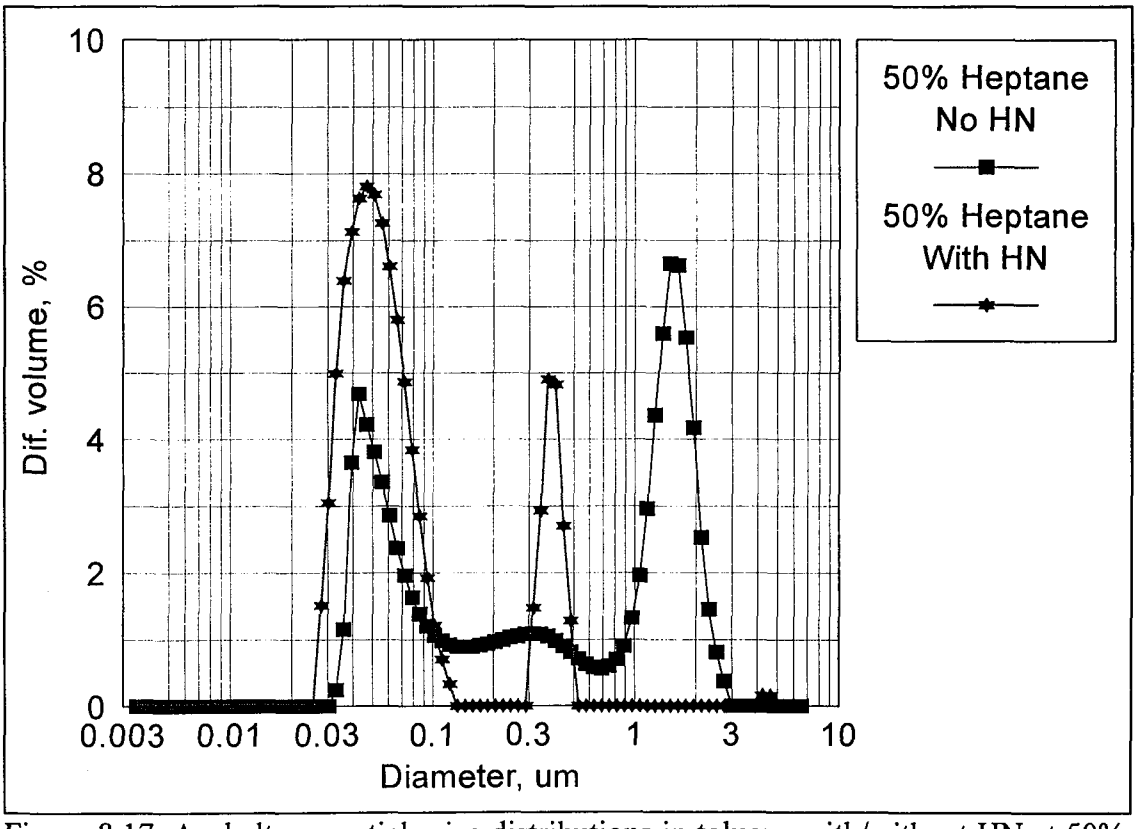

Figure 8.17. Asphaltene particle size distributions in toluene with/without HN at 50% n-heptane concentration.

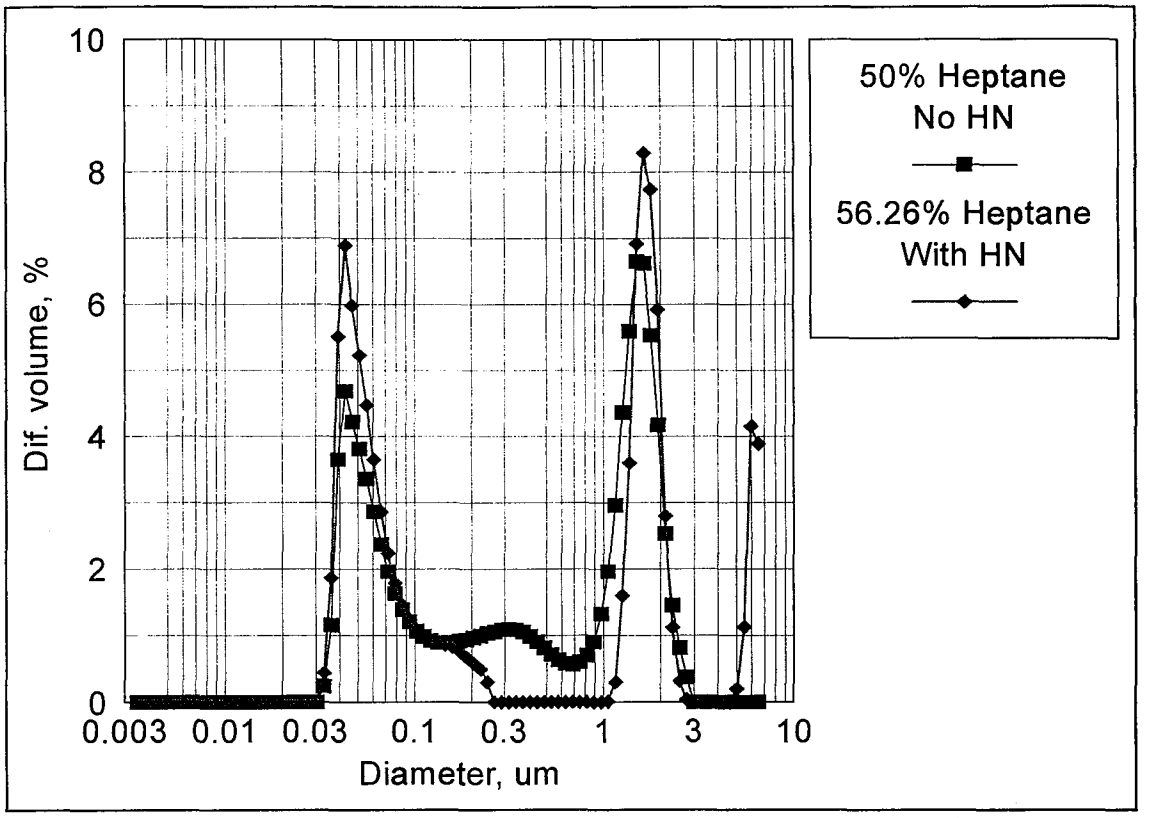

Figure 8.18. Asphaltene particle size distributions in toluene without/with HN at 50% and 56.25% n-heptane concentration.

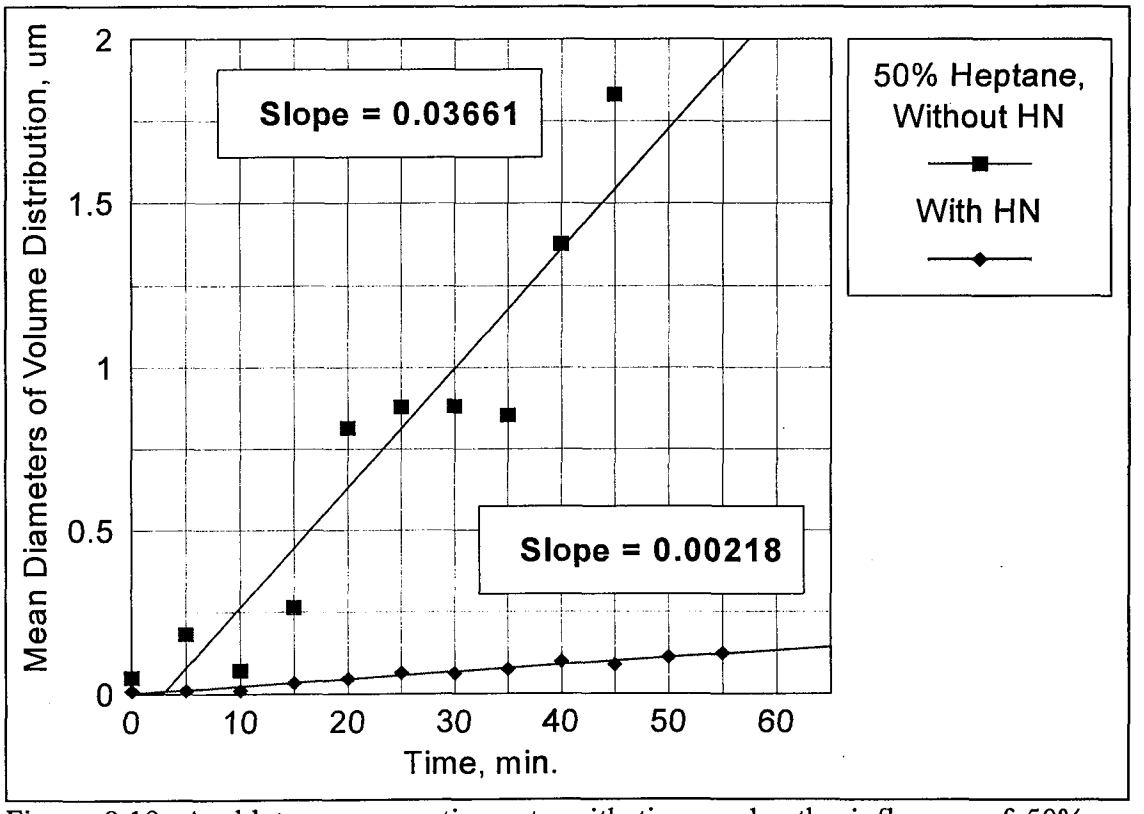

Figure 8.19. Asphlatene aggregation rate with time under the influence of 50% n-heptane.

8.5 STABILISATION OF CARBON DISPERSION IN HEXADECANE BY HN

Figure 8.20 shows the effect of HN on the stabilisation of carbon particles in hexadecane (i.e. aliphatic oil) and toluene. It clearly shows that HN is more effective in stabilising carbon particles in the aliphatic hexadecane than in toluene. This is no doubt due to the greater extension of the hexadecyl chain in hexadecane than in toluene which is not such a good solvent. The greater the extension of the hexadecyl chain the longer range the steric repulsion and the more effective the colloidal stabilisation. A (probably) much smaller effect is that toluene is a better solvent for the napthalene head group which would diminish its adsorption onto the carbon surface. However, the size, flatness and π-electrons of the aromatic rings probably mean that HN adsorbs with little difference as between hexadecane and toluene as the solvent.

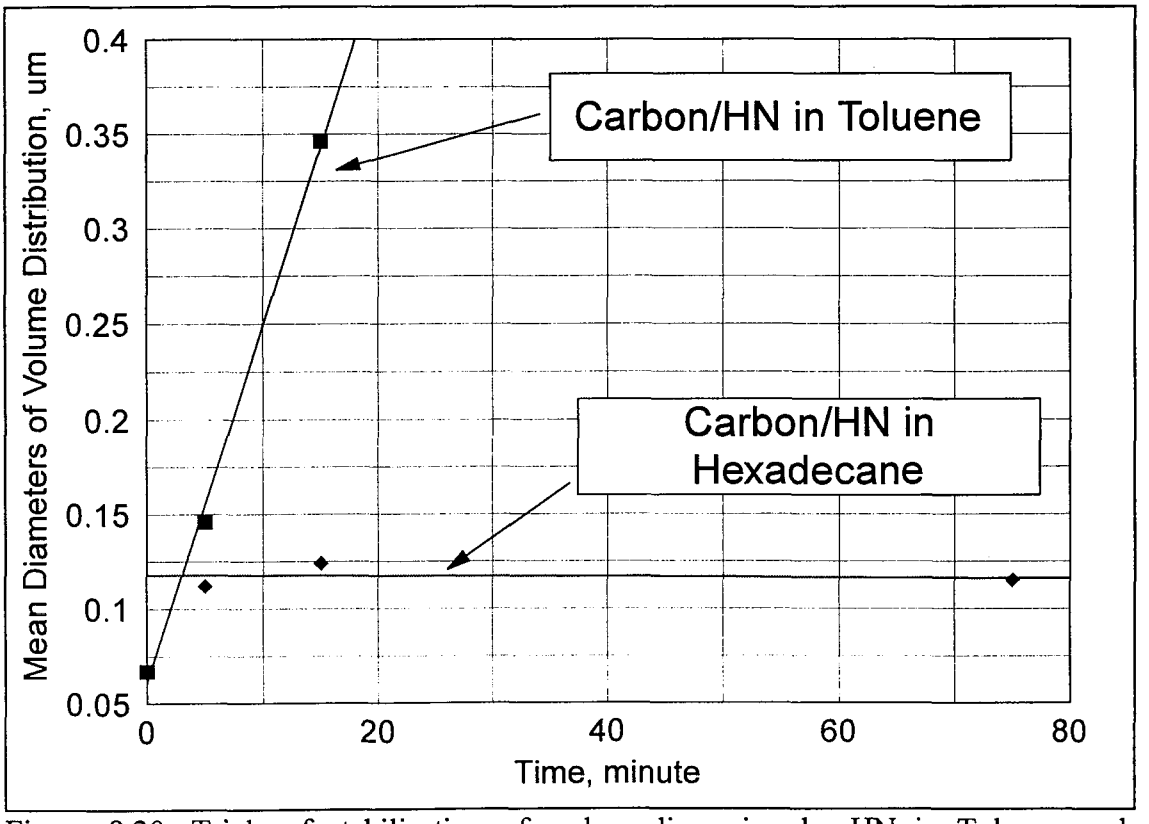

Figure 8.20. Trials of stabilisation of carbon dispersion by HN in Toluene and Hexadecane.

8.6 ASPHALTENE ADSORPTION ON PARTICLE SURFACES

The adsorption of asphaltenes on to reservoir rock core surfaces has been taken to be a thick layer reducing the rock pores radius by at least 30% amounting to a 50% damage in rock pores area (Chapter six).

Here mineral particles are used to investigate asphaltene adsorption onto their surfaces. The minerals used in this study are hydrophobic silica and carbon. The particle size of these minerals were determined by the laser back scattering technique and found to be 0.007 μm for silica and 1.2 μm for carbon. Both were ultrasonically dispersed in toluene. The test involved monitoring the mineral particle size distributions during the addition of asphaltene solutions. No measurable concentration of particles were found in the asphaltene solutions used in this study.

Figure 8.21 shows the particle size of silica before the addition of asphaltene to be 0.007 μm. Figure 8.22 shows the growth of silica particles after the addition of asphaltene at 12.5% by volume. The results were based on 3 measurements runs with 5 minute time intervals. As soon as the asphaltene was introduced to the silica sample, the particle size increased. The adsorption of asphaltene on silica particles in such a relatively short period of time represents fast adsorption rate.

In another experiment with carbon particles dispersed ultrasonically in toluene, an asphaltene solution in toluene was added to the carbon dispersion. Figure 8.23 shows carbon particle size distributions with different asphaltene concentrations. In this experiment the average diameter of carbon particles was found to be 1.2 μm in the absence of asphaltene whereas after addition of asphaltene the carbon particles size increasesd slowly to 1.8 μm., indicating that asphaltene adsorption thickness on carbon particle surfaces is ~ 0.3 μm.

In separate experiments using carbon particles with the addition of asphaltene Figure 8.24 shows asphaltene adsorption thicknesses as a function of asphaltene concentration. The plot indicates that the asphaltene adsorption thickness increases

with increasing asphaltene concentrations and reached a plateau at 0.33 μm. It must be mentioned that this contrasts with the conclusions of Dubey *et al.* (1989) and Kokal *et al.* (1994), who reported only monolayer thicknesses of asphaltene adsorbed onto various minerals from toluene solutions.

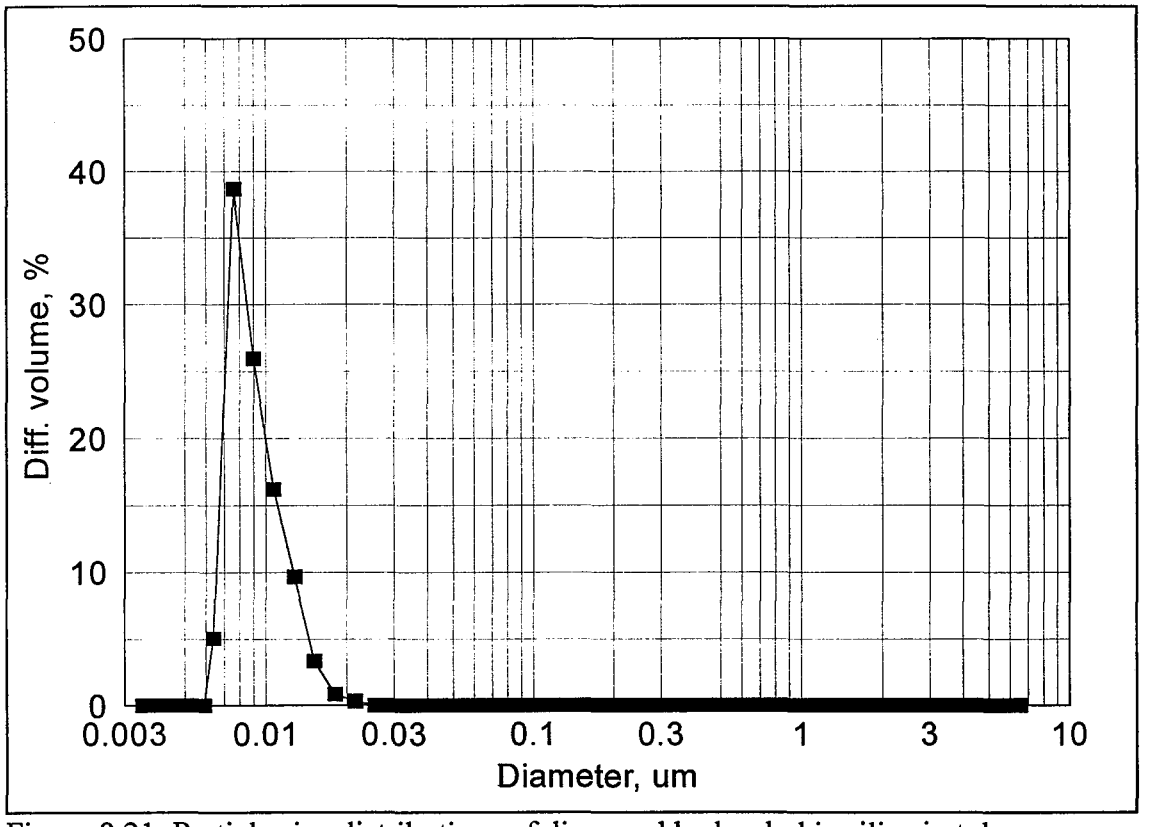

Figure 8.21. Particle size distributions of dispersed hydrophobic silica in toluene.

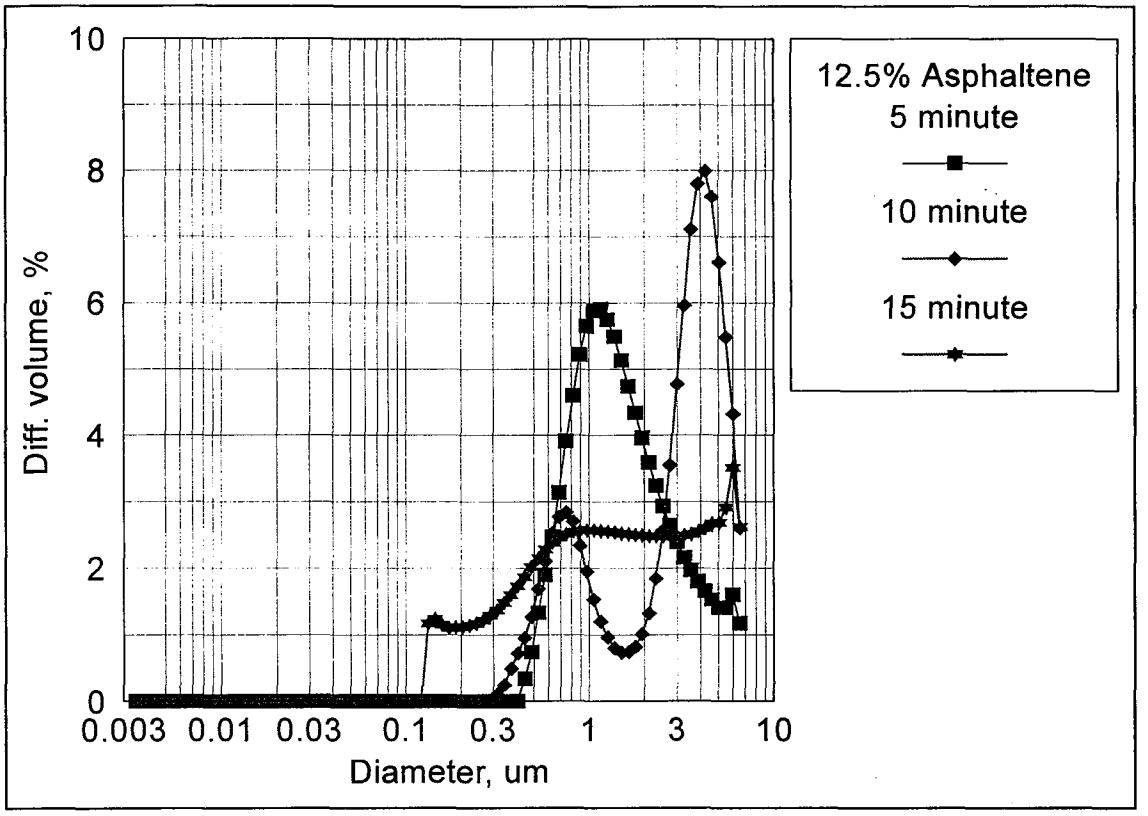

Figure 8.22. Particle size distributions of dispersed hydrophobic silica in toluene after the addition of 12.5% by volume asphaltene.

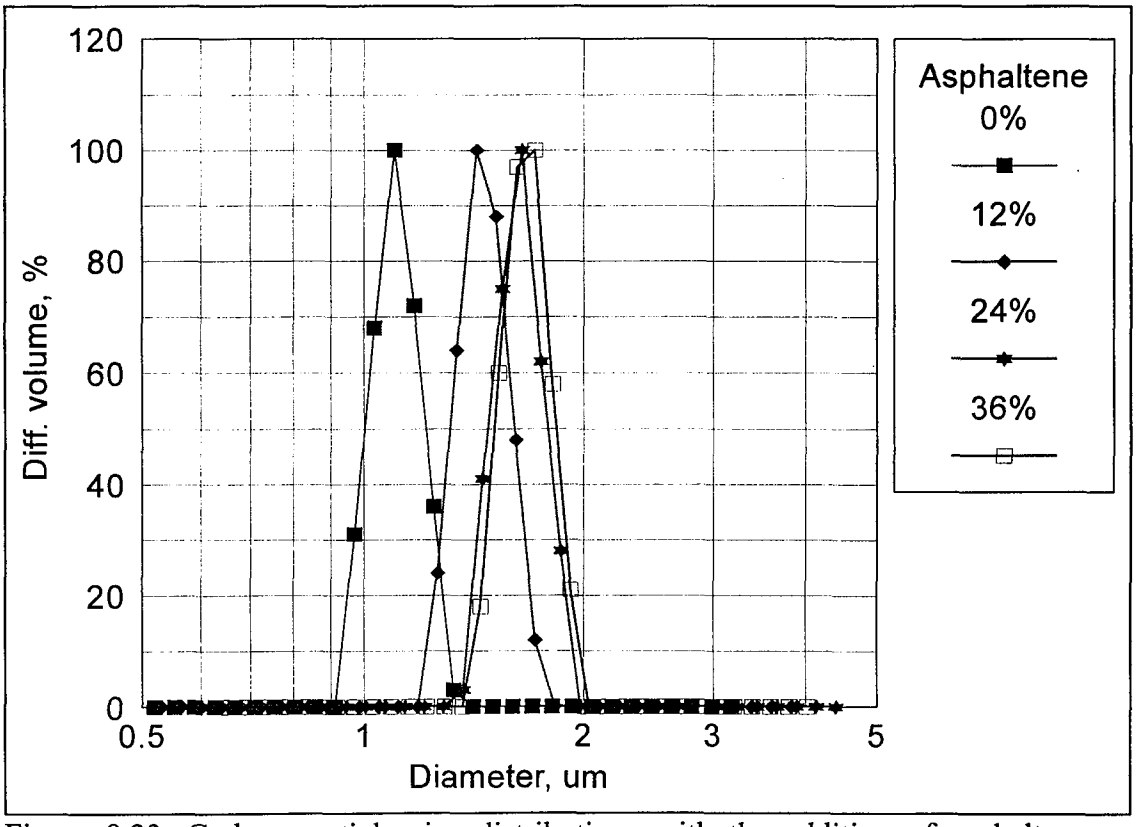

Figure 8.23. Carbon particle size distributions with the addition of asphaltene at different concentrations.

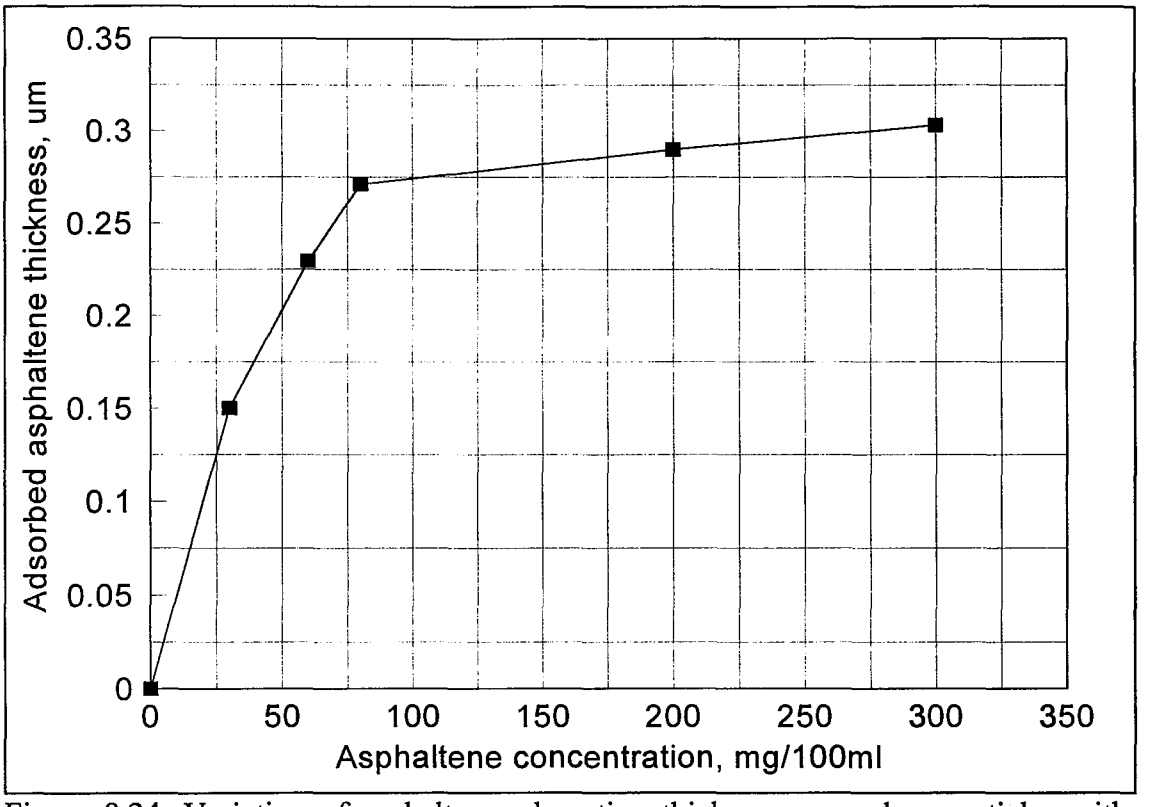

Figure 8.24. Variation of asphaltene adsorption thickness on carbon particles with different asphaltene concentrations.

8.7 WAX CLOUD-POINT

The wax cloud-point is the temperature at which wax begins to separate from a petroleum fluid. There are conventional American Society for Testing & Material (ASTM) procedures for predicting and determining wax cloud-point (Kruka *et al.*, 1995). However, the use of these procedures is limited or not applicable in the case of dark crude oils. Knowledge of wax cloud point characteristics in petroleum fluids is important to the oil industry. In this work the cloud point was detected by the laser back scattereing technique.

In the study two Canadian waxy crude oil were used to determine wax cloud-points. The two selected crude oils are free from asphaltene and their colours are very light and similar to vegetables oil. For the purposes of this work, these waxy crude oils will be called as "Crude-A" and "Crude-B". In the Crude-A case, the sample was loaded into the preheated (49 ^{o}C) particle analyser cell. Five particle size analyses

were then performed each with a 5 minute run time. The cell was then cooled at approximately 5 °C intervals and allowed to stabilise for approximately 30 minutes. Five runs were made to determine particle size, each run being 5 minute in duration as before. Figure 8.25 shows the particle size measurements at each temperature cycle. It can be seen that there was no change in particle size until the temperature fell to 20 °C. A sudden change in the particle size indicated the onset of wax separation. Cooling the cell below 20 °C caused more particles to form at 10.8 °C and 6.8 °C respectively. The onset of the 20 °C wax cloud-point in Crude-A can be seen clearly in Figure 8.26.

The method most often used in the oil industry to detect wax cloud-points is that of the oil viscosity variation test. This test is based on the effect of solid wax particles suspended in the oil leading to increase in the viscosity of the system. Howell and Jessen (1956) proposed that the wax precipitation (cloud-point) can be detected by observing a break in the viscosity/temperature curve of a waxy oil. This method can be compared with our method of predicting wax cloud-points. Figure 8.27 shows a wax cloud-point for Crude-A determined by viscosity/temperature correlation using the ASTM D341 method. The plot is of the calculated effective viscosity (z) as a function of oil temperature. The Figure shows two viscosity deviation curves during a decreasing oil temperature experiment. The wax cloud-point of Crude-A by this method was determined as the intersection of the two viscosity curves [13 °C (515 °R)]. Our method indicated that the cloud-point occurred at 22 °C, i.e. the laser back scattering technique predicted the wax cloud-point 10 °C earlier than the viscosity method.

For Crude-B, the wax cloud-point determined by the laser back scattering technique is illustrated in Figure 8.28. The plot shows that the wax separation point for Crude-B occurs when the temperature falls to 45 °C. Further growth in wax particles occurs with decreasing oil temperature. The formation of wax particles in this crude oil at higher temperature (45 °C) will cause problems in oil production facilities if the temperature falls below 45 °C. Figure 8.29 shows the average wax particle size during cooling cycles. Figure 8.30 shows wax separation reversibility

after reheating the sample to 52 °C (7 degrees above cloud-point). The plot shows that wax dissolution occurs within 15 hours.

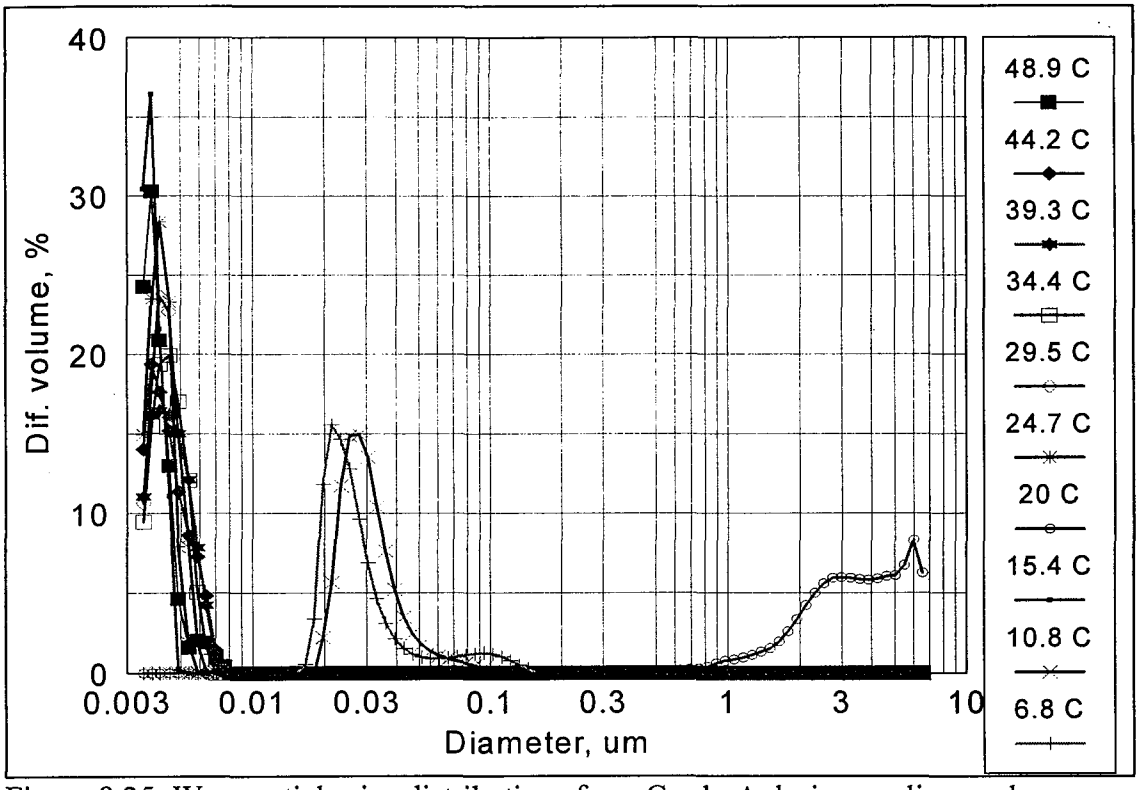

Figure 8.25. Wax particle size distributions from Crude-A during cooling cycle.

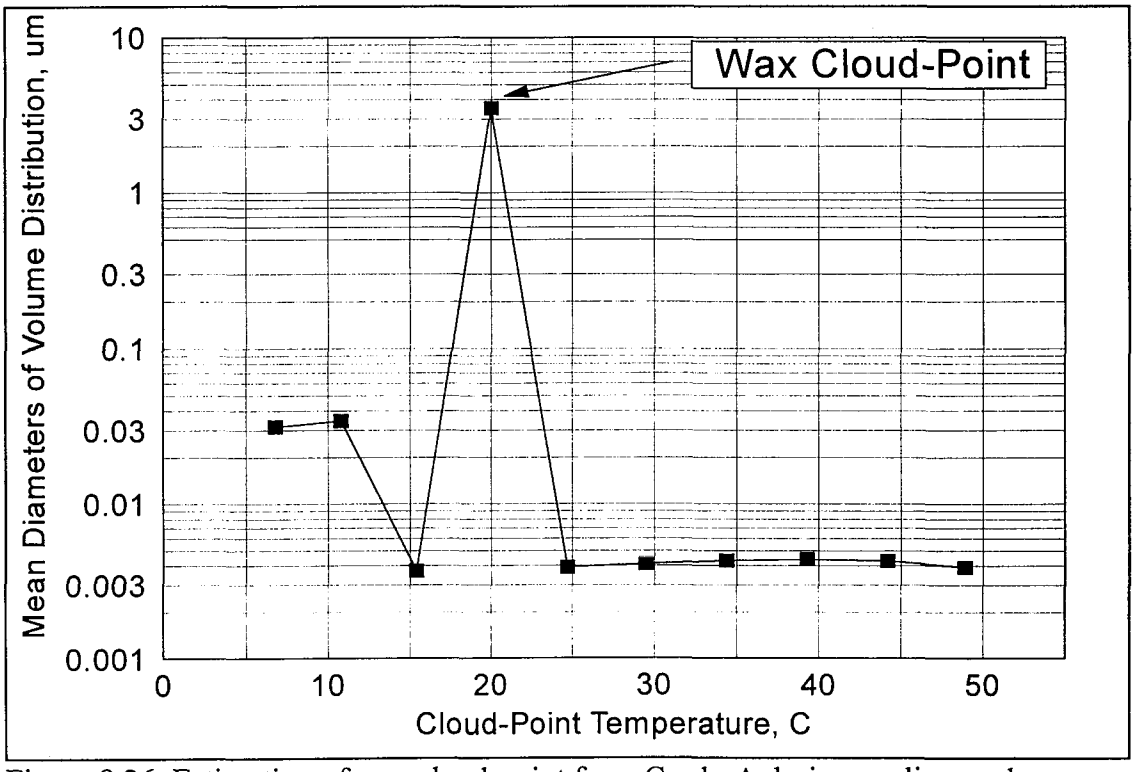

Figure 8.26. Estimation of wax cloud-point from Crude-A during cooling cycle.

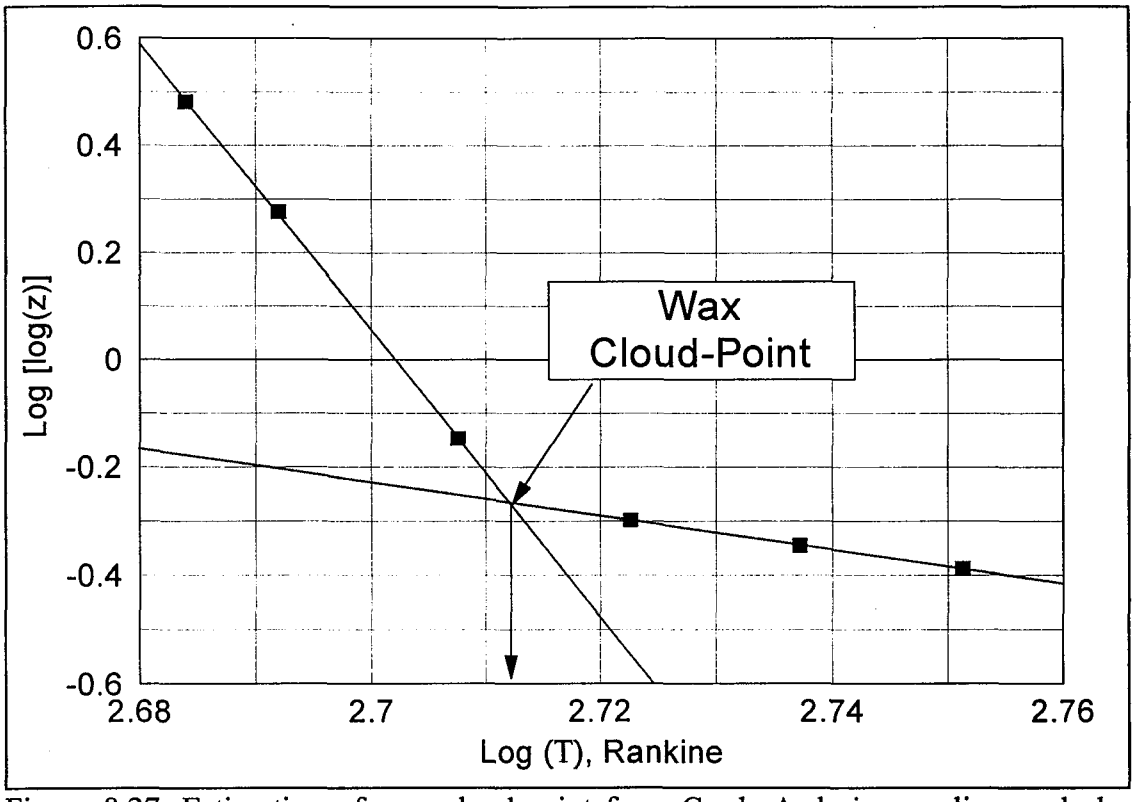

Figure 8.27. Estimation of wax cloud-point from Crude-A during cooling cycle by viscosity/temperature correlation (ASTM D-341).

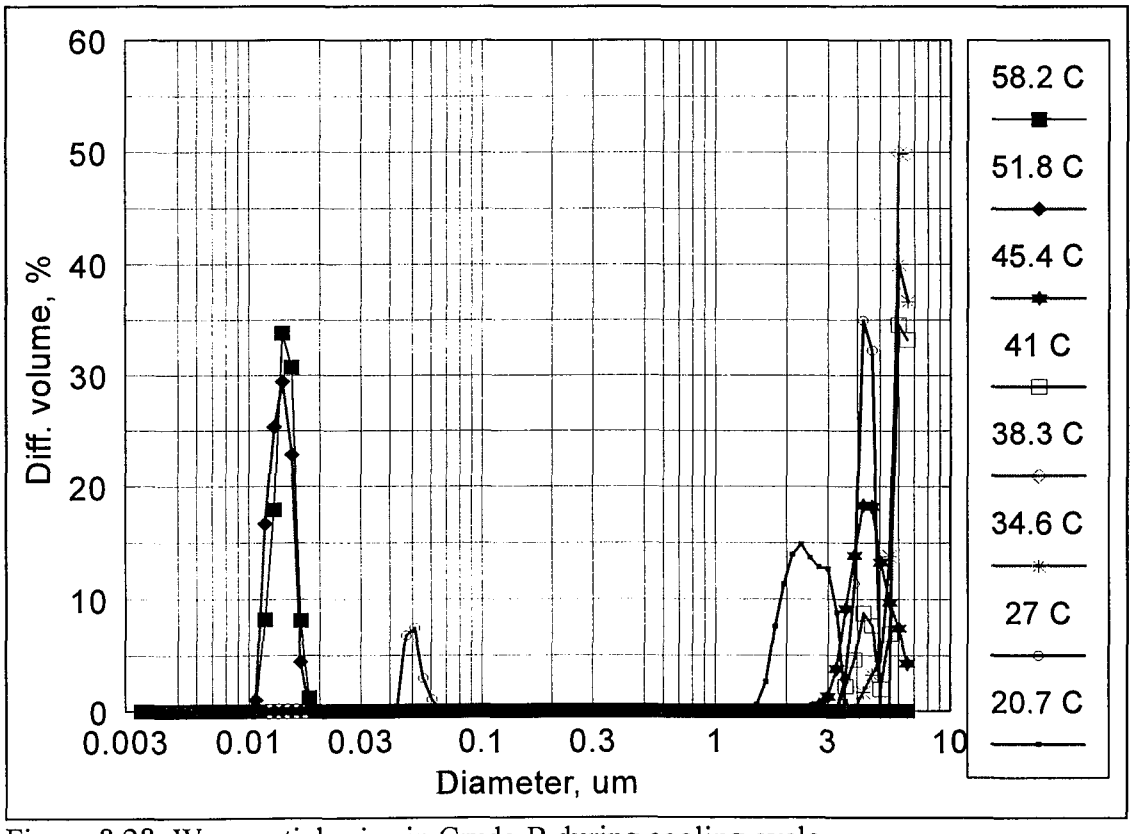

Figure 8.28. Wax particle size in Crude-B during cooling cycle.

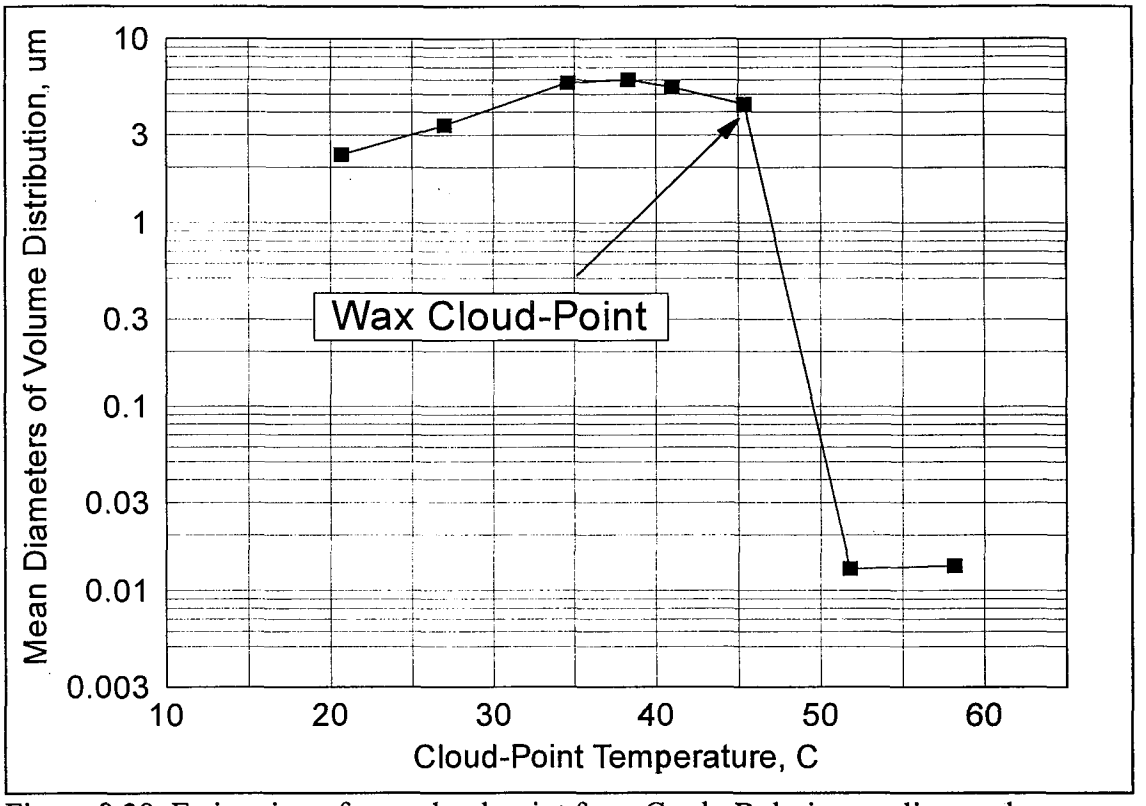

Figure 8.29. Estimation of wax cloud-point from Crude-B during cooling cycle.

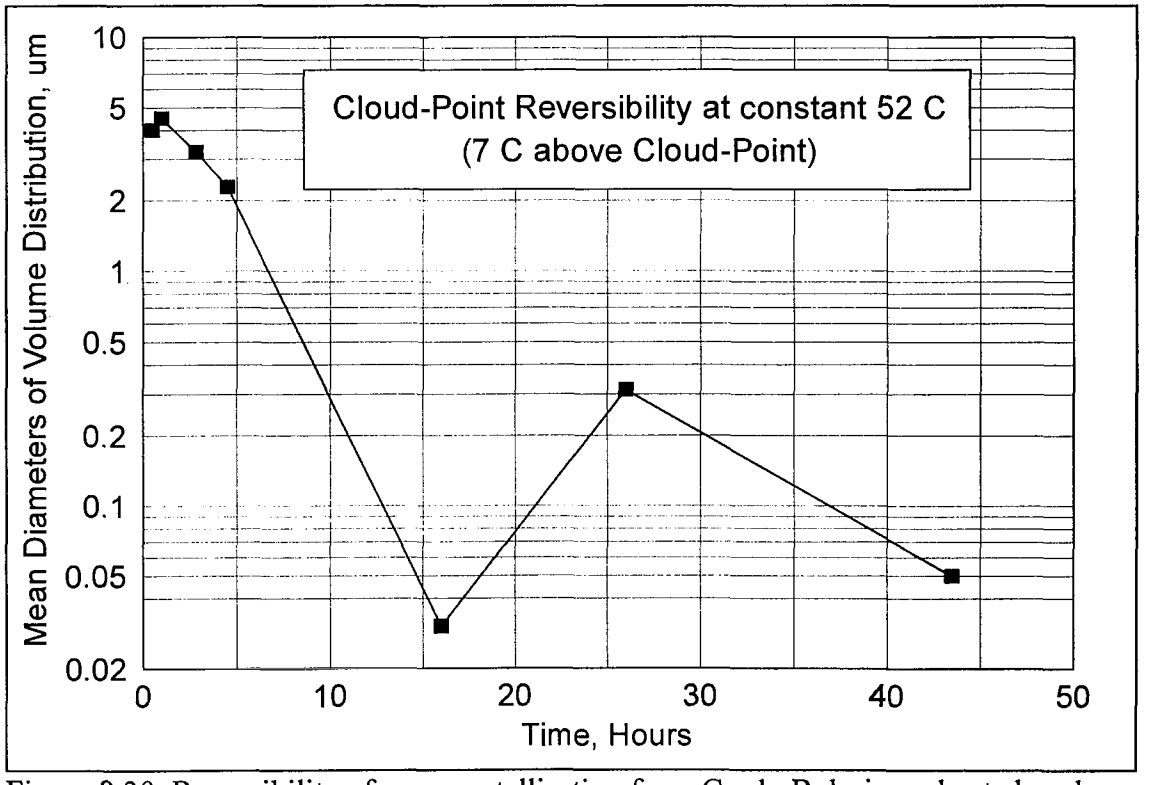

Figure 8.30. Reversibility of wax crystallisation from Crude-B during reheated cycle.

8.8 CONCLUSIONS

1. Laser back scattering using optical fibres has been used successfully to determine particle size distributions in crude oil.
2. The precipitation of asphaltene under the influence of paraffinic solvent has been determined.
3. Although not designed for this purpose 2-hexadecylnaphthalene (HN) stabilised asphaltene particles in toluene solutions to some extent and controlled their aggregation under the influence of n-heptane.
4. The onset of wax cloud-point in crude oil has been determined successfully by the laser back scattering technique.
5. HN has been shown to be most effective for colloidal stabilisations under the conditions for which it was designed i.e. in an aliphatic solvent such as hexadecane.

CHAPTER NINE

CONCLUSIONS AND RECOMMENDATIONS

This chapter summarises the key conclusions of the work described in this thesis, their relevance to the petroleum industry and provides some suggestions for further study. The main conclusions are discussed in more detail below.

9.1 Asphaltene in Crude Oil

Asphaltenes are a serious problem in some (though not all) oil fields, causing formation damage by adsorption/deposition and pore blocking and leading to pipe blockage. Mechanical cleaning of pipes and the use of unblocking solvents is widespread where the problem occurs but is extremely expensive, especially in terms of the time involved.

In this work asphaltenes have been examined with respect to mechanisms of aggregation and/or deposition and the design and synthesis of an additive to minimise both. The agents quoted in the literature appear to be based on (false) analogy with reduction of deposition in aqueous systems. This work has produced an agent hexadecyl naphthalene (HN) - which has been shown to be extremely effective at preventing aggregation in aliphatic solvents (of which crude oil is an example) and even partially effective in the aromatic solvent toluene. The dispersing mechanism has been explained as that of HN adsorption leading to repulsion between particles/surfaces, with the hexadecyl chain stretching out into the aliphatic solvent, crude oil, thus giving entropic repulsion to other coated surfaces. This should be a major contribution to avoiding deposition/blocking problems resulting from asphaltene.

9.2 Electrostatic Repulsions in Crude Oil

Several published papers have proposed using oil additives which in aqueous solutions would absorb on surfaces to give them an electrical charge and thus contribute electrostatic (double layer) particle-particle and particle-surface repulsion. This work has shown experimentally that the surface (zeta) potential of asphaltene in crude oil is extremely small and theoretically that even if it showed the same values as typical in aqueous solutions, the electrostatic double layer repulsion would be orders of magnitude less in oil than water.

In the course of such studies this work has found it possible to measure particle and surface potentials as small as $\pm$ 0.0001 mV by developing a streaming current techniques (free from the effects of surface conductivity) using a sensitive pico-ammeter. Experiments with closely spaced plates at high potential differences, left for 2 weeks in asphaltenic oil, confirmed the very low surface potential found for asphaltene.

It must be concluded that attempts to produce electric double layer effects in crude oil will be fruitless, and that steric effects as in 9.1 above are the way forward.

9.3 Sign of Asphaltene Charge in Crude Oil

Although extremely small, the sign of the charge on asphaltene in crude oil has been confirmed as positive in this work, as has been reported by others using long-term electrode deposition experiments.

This positive charge in oil, contrasting with the predominantly negative charge in aqueous solutions, has been attributed in this work to the properties of the supporting liquid (oil) as much as those of the particles - such as the π electrons from aromatic asphaltenes - can escape into the liquid, leaving the particles positively charged.

9.4 The Effect of Surface Conductivity on The Electrokinetic Phenomena

This thesis has highlighted the important of surface conductivity on the electrokinetic potential in low electrolyte system, such as petroleum fluids. As pointed out in this thesis the treatment of electrokinetic phenomena in petroleum reservoirs presents significant problems where surface conductivity becomes important e.g. at low electrolyte concentration. This led us to establish a new method to estimate the reservoir rock pores section to length (A/L) by combining streaming potential and current measurements so that the unambiguous streaming current method could be used.

9.5 Asphaltene Adsorption on Sandstone Rock Cores

In order to investigate the extent of formation damage by asphaltenes in crude oil this work has used the techniques described above to study the adsorption of asphaltenes in rock pores. Permeability, streaming current via A/L ratio, and petrographic investigations all converge to indicate a pore blocking by asphaltene equivalent to ~30% of pore diameter, corresponding to 50% of the pores cross sectional area. Alternative hypotheses involving uniform deposition or 'throat' blocking and crevice filling have been investigated and a theoretical treatment advanced describing particle deposition in the same terms as molecular adsorption and the Langmuir isotherm, with the free energy of asphaltene particle deposition on the rock surface (modelled on silica) calculated on the basis of van der Waals attraction. Acceptable agreement was obtained.

9.6 Rock Permeability Index

The permeability properties of rock formations have often been investigated by flow measurements, electrical conductivity/resistance measurements and the surface electrical potential by streaming potential measurements.

The latter two measurements have been shown in this work to be in grave error as a result of surface conductivity, itself resulting from inevitable surface double layer effects and from the ubiquitous presence of strongly bound water at the rock surface.

This work has illustrated the error and overcome it, both to derive surface potentials validly by streaming current measurements and to exploit it by obtaining the A/L ratio where A is the total cross section area of the pores and L their effective mean length.

The A/L determination is new and could be an important new index of the permeability properties of reservoir rock formations.

9.7 Pore Pressure and Hysteresis in Rock Core Measurements

During the pore pressure loading cycle for sandstone samples significant changes in the behaviour of streaming currents were observed. These were attributed to dissolved gases in the liquid phase. Streaming currents were numerically enhanced as the gas bubbles dissolved at higher pressures to give better contact between liquid and the rock surface. Indeed it was shown that the saturation pressure point can be observed by plotting the measurements against loading pore pressure, confirming this hypothesis.

Loading/unloading cycles of pore pressure showed a distinct hysteresis. For a given rock the hysteresis effect depended on the magnitude and duration of the applied pore pressure, pointing towards induced changes in rock geometry.

9.8 Fine Pores in Rock Formations

Quantities derived from resistance/conductance logging, streaming potentials and even streaming currents are subject to further errors when the pores encountered are very fine (small diameter/thickness) and the double layer at opposes surfaces overlap.

This problem has been treated theoretically in this work so as to relate measurements on fine pore rock samples to what would be obtained for macroscopic pores. For example in the case of streaming currents the following ratio was derived:

$$\frac{I_s}{I_{s(\infty)}} = 1 - \frac{\tanh \kappa h}{\kappa h}$$

Where I_s is measured for pores of thickness $2h$, $I_{s(\infty)}$ is what would have been obtained for macroscopic pores (or flat surfaces) and κ is the Debye reciprocal distance parameter.

The formula above has been verified for rock cores of varying porosities and used to extrapolate the results to a value for a plane surface in good agreement with literature values for a mineral surface in oil.

This type of correction should be applied to all measurements on rock samples with fine pores, especially where the liquid is oil or other low permitivity liquid.

9.9 Light Scattering Measurements in Coloured/Turbid Oils

Ordinary transmission light scattering measurements of particle size become impossible in the situation of the turbid, light-absorbing, properties of most crude oils. However, such measurements have been achieved in this work by using a laser back scatter technique. An instrument supplied by Brookhaven Instruments of New York,

USA, with a probe carrying two red laser transmitting fibre-optics, has been modified and used with success in such systems. Simple cells have been designed (and then manufactured for the project by Rank Brothers of Cambridge, UK) constructed of carbon-filled (black) PTFE with quartz windows of a thickness calculated to give no undue reflected light intensity (local oscillator strength) and yet allowing laser light penetration into the oil of only 1 mm or less. The black, light absorbing walls of the cell effectively reduced stray reflections.

The system has been used in all the studies of the effect of additives on dispersions of asphaltenes, waxes, carbons and silica in oils. This type of size measurements of particles in crude oils has hitherto been impossible.

9.10 Waxes in Crude Oils

High molecular weight aliphatics (waxes) as well as high molecular weight aromatics (asphaltenes) are potential sources of formation damage and well tubings. The waxes are miscible with oil at high temperatures but separate as temperature is lowered. Such wax separation temperatures have commonly been assessed by visual or transmission turbidity with all the difficulties associated with strongly light absorbing oils and are reported to vary with previous temperature cycling. This work has shown that the wax separation point can be detected much more sensitively in such conditions by the laser back scatter technique.

9.11 Suggestions For Future Work

1. The A/L technique should be further validated by its use in model systems of known pore geometry.
2. Asphaltene deposition in porous systems should be studied as a function of pore diameters to elucidate the factors controlling the extent of pore blocking.

3. The laser back scatter technique should be extended to give measurements of electrophoretic mobility simultaneously with those of size.
4. Hexadecyl napthalene and analogous molecules should be tested under oil field conditions as anti-fouling agents.
5. Determine the saturation and cementation exponents of reservoir rocks from streaming current data.
6. The effect of pressure, temperature and surface potential on rock surfaces wettability due to asphaltene adsorption.
7. The effect of clay content on the rock surface potential should be studied both in cores and in the presence of asphaltene.
8. Investigation of the stability of colloidal asphaltene particles in petroleum fluids under varying temperature and pressure by using laser back scattering technique.
9. The laser back scatter technique should be used to detect the wax separation temperature of crude oils to see whether the separation temperature is really independent of temperature cycling.

REFERENCES

Akbar, S.H. and Saleh, A.A.: "A Comprehensive Approach to Solve Asphaltene Deposition Problem in Some Deep Wells", SPE paper 17965, presented at the Middle East Oil Technical Conference and Exhibition in Manama, Bahrain, 11-14 March (1989).

Ali, L.H., AL-Ghannam, K.A. and AL-Rawi, J.M.: "Chemical Structure of Asphaltenes in Heavy crude Oils investigated by n.m.r.", Fuel, Vol. 69 (1990), pp. 519-521.

Alkafeef, S.F., Gochin, R.J. and Smith, A.L.: "Surface Potential and Permeability of Rock Cores Under Asphaltenic Oil Flow Conditions", SPE paper 30539, presented at the SPE Annual Technical Conference & Exhibition held in Dallas, TX, 22-25 Oct. (1995).

Anderson, D.J., Smith, J.C. and Rallings, R.J.: "The Synthesis and Physical Properties of alkyl naphthalenes", J. Am. Chem. Soc., (1953), pp. 449.

Ball, J.S., Wenger, W.J., Hyden, H.J., Horr, C.A. and Myers, A.T.: "Metal Content of Twenty-Four Petroleums", J. of Chem. and Eng. Data, Vol. 5 (Oct. 1960), 4, pp. 553-557.

Berne, B.J. and Pecora R.: "*Dynamic Light Scattering*", Wiley-Interscience Publication, (1976).

Booth, F.: "The Cataphoresis of Spherical, Solid Nonconducting Particles in a Symmetrical Electrolyte", Proc. Roy. Soc. London, A203 (1950a), pp. 514-533.

Briggs, D.R.: "The Determination of The Zeta Potential on Cellulose-a Method", J. Phys. Chem., Vol. 32 (1928), pp. 641-675.

Brown, C.E. and Neustadter, E.L.: "The Wettability of Oil/Water/Silica Systems With Refernce to Oil Recovery", J. of Canadian Petroleum, July-September (1980), Montreal, pp. 100-110.

Buckley, J.S., Takamura, K. and Morrow, N.R.: "Influence of Electrical Surface Charge on the Wetting Properties of Crude Oils", SPE paper 16964, presented at 62nd Annual Technical Conference and Exhibition of SPE held in Dallas, TX, 27-30 September (1987).

Buu-Hoi, M.M. and Cangnint, P.: "Des alkoyl-β naphtyl-cétones", Bull. Soc. Chim., Vol. 12 (1945), pp. 307.

Casimir, H.B.G. and Polder, D.: "Influence of Retardation on London-van der Waals Forces", Phys. Rev., Vol.73 (1948), pp.360-372.

Chapman, D.L., as discussed in **Hunter, R.J.:** *Zeta Potential in Colloid Science*, Academic Press, (1988), p. 22.

Craig, F.F.: *The Reservoir Engineering Aspects of Waterflooding*, Monograph Series, SPE, Richardson, TX. (1971), 3.

Crocker, M.E., and Marchin, L.M.: "Wettability and Adsorption Characteristics of Crude Oil Asphaltene and Polar Fraction", SPE/DOE 14885, EOR Symposium of SPE and DOE, Tulsa, OK, 20-23 April (1986).

Debye, P. and Hückel, E., as discussed in **Hunter, R.J.:** *Zeta Potential in Colloid Science*, Academic Press,(1988), p. 24.

Derjaguin, B.V. and Landau, L.D., as discussed in **Dukhin, S.S. and Deryaguin, B.V.:** "Surface and Colloid Science" (E. Matijevic *editor*), Vol. 7 (1974) "Electrokinetic Phenomena", John Wiley Interscience, N.Y. and London, p. 110.

Dickie, J.P. and Yen, T.F.: "Macrostructures of Asphaltic Fractions by Various Instrumental Methods", Anal. Chemistry, Vol. 39 (1967), No. 14, pp.1847-1852.

Dickie, J.P., Haller, M.N. and Yen, T.F.: "Electron Microscopic Investigations on the Nature of Petroleum Asphaltics", J. of Colloid and Interface, Vol. 29 (March 1969), No. 3, pp. 475-484.

Dubey, S.T., and Waxman, M.H. "Asphaltene Adsorption and Desorption from Mineral Surfaces", SPE paper 18462, presented at SPE Inter. Symposium on Oilfield Chemistry, Houston, TX, 8-10 Feb. (1989).

Dunning, H.N., Moore, J.W., Bieber, H. and Williams, R.B.: "Porphyrin, Nickel, Vanadium and Nitrogen in Petroleum", J. of Chem. and Eng. Data, Vol. 5 (Oct. 1960), No. 4, pp. 546-549.

Eldib, I.A., Dunning, H.N. and Bolen, R.J.: "Nature of Colloidal Materials in Petroleum", J. of Chem. and Eng. Data, Vol. 5, (Oct. 1960), No. 4, pp. 550-553.

Eldib, I.A.: "The solvation, Ionic and Electrophoretic Properties of Asphaltenes in Petroleum", Presented Before The Division of Petroleum Chemistry, American Chemical Society, Washington, D.C., 20-29 March (1962), pp. 31-42.

Escobedo, J. and Mansoori, G.A.: "Heavy Organic Deposition and Plugging of Wells (Analysis of Mexico's Experience)" SPE paper 23696, SPE 2nd LAPEC held in Caracas, Venezuela, 8-11 March (1992).

Fussel, L.T.: "A Technique for Calculating Multiphase Equilibria", SPE J. Aug. (1979), pp.203-208.

Gonzalez, G. and Moreira, B.C.: "The Wettability of Mineral Surfaces Containing Adsorbed Asphaltenes", Colloid and Surfaces, Vol. 58 (1991), pp. 293-302.

Gonzalez, G.: "Asphaltene Adsorption by Quartz and Feldspar", J. Dispersion Science and Technology, Vol. 8 (1987), No. 5&6, pp 525-548.

Gouy, G., as discussed in **Hunter, R.J.:** *Zeta Potential in Colloid Science*, Academic Press, (1988), p. 22.

Gregory J.: "Colloid Interactions", Material Science Forums, Vols. 25-26 (1988), pp. 125-144.

Hamaker, H.C., as discussed in **Shaw, D.J.:** "*Introduction to Colloid and Surface Chemistry*" 4th Edition, Butterworth-Heinemann Ltd, (1992), pp. 215-219.

Hasan, M.U., Bukhari, A. and Ali, F.M.: "Structural Characterization of Saudi Arabian Medium Crude Oil by n.m.r. Spectroscopy", Fuel, Vol. 64 (1985), pp. 839-841.

Henry, D.C., as discussed in **Shaw, D.J.:** "*Introduction to Colloid and Surface Chemistry*" 4th Edition, Butterworth-Heinemann Ltd, (1992), p. 202.

Hill, H.J. and Anderson, A.E.: "Streaming Potential Phenomena in SP log Interpretation", Trans. AIME, Vol. 216 (1959), pp. 203-208.

Hirschberg, A., deJong, L.N.J., Schipper, B.A. and Meijer, J.G.: "Influence of Temperature and Pressure on Asphaltene Flocculation", J.Pet. Tech., (June 1984), pp. 283.

Howell, J.N. and Jessen, F.W.: "Determination of the Viscosity-Temperature Relationship for Crude Oils With the Ultra-Viscoson", J. of Petroleum Technology, September (1956), pp. 95.

Hückel, E., as discussed in **Hunter, R.J.:** *Zeta Potential in Colloid Science*, Academic Press, (1988), p. 70.

Ignasiak, T.M., Kemp-Jones, A.V. and Strausz, O.P.: "The Molecular Structure of Asphaltene. Cleavage of the Carbon-Sulfur Bonds by Radical Ion Electron Transfer Reactions", J. Org. Chem., Vol. 42 (1977), pp. 312-320.

Jan, D.E. and Raghavan, S.: "Adsorption of Metanil Yellow on a Positively Charge Modified Nylon 66 Membrane", Colloid and Surfaces A-Physicochememical & Engineering Aspects, Vol. 92 (1994), No. 1-2, pp. 1-7.

Katz, D.J. and Beu, K.E.: "Nature of Asphaltic Substances", Ind. & Eng. Chem., Vol. 37 (1945), pp. 195-200.

Kawanaka, S., Park, S.J. and Mansoori, G.A.: "The Role of Asphaltene Deposition in EOR Gas Flooding: A Predictive Technique", SPE paper No. 17376, Proc. EOR Symposium of SPE, Tulsa, OK, 17-20 April (1988).

Kelsall, G.H., Tang, S., Yurdakul, S. and Smith, A.L., "Electrophoretic Behaviour of Bubbles in Aqueous Electrolytes", J. Chem. Soc., Faraday Trans., Vol. 92 (1996), No. 20, pp. 3887-3893.

Kim, S.T., Boudh-Hir, M-E, and Mansoori, G.A.: "The Role of Asphaltene in Wettability Reversal" SPE paper 20700, SPE Annual Tech. Conf. and Exhibition, New Orleans, LA, 23-26 Sept. (1990).

Kokal, S., Tang, Th., Schramm, L., and Sayegh, S.: "Electrokinetic and Adsorption Properties of Asphaltenes", Colloid and Surfaces A: Physicochemical and Engineering Aspects, Vol. 94 (1995), pp. 253-265.

Koots, J. A. and Speight, J. G.: "Relation of Petroleum Resins to Asphaltenes", Fuel, Vol. 54 (1975) pp. 179-184.

Kruka, V.R., Candena, E.R. and Long, T.E.: "Cloud-Point Determination for Crude Oils", J. of Petroleum Technology, August (1995), pp. 681-687.

Labib, M.E. and Williams, R.: "Effect of Moisture on the Donor-Acceptor Properties of Solid Surfaces", Proc. 5th Int. Conf. Surf. Coll. Sci., Potsdam, June (1985).

Labib, M.E. and Williams, R.: "The Use of Zeta Potential Measurements in Organic Solvents to Determine the Donor-Acceptor Properties of Solid Surfaces", J. of Colloid and Interface Science, Vol. 97 (1984), No. 2, pp. 356-365.

Leontaritis, K.J. and Mansoori, G.A.: "Asphaltene Deposition: A Survey of Field Experiences and Research Approaches", J. of Petroleum Science and Engineering, 1 (1988), pp. 229-239.

Leontaritis, K.J. and Mansoori, G.A.: "Asphaltene Flocculation During Oil Production and Processing: A Thermodynamic-Colloidal Model", SPE paper 16258, presented at SPE Inter. Symp. on Oilfield Chem., San Antonio, Texas, (Jan.1987), pp.149-158.

Leontaritis, K.J.: "Asphaltene Deposition: A Comprehensive Description of Problem Manifestations and Modeling Approaches", SPE paper 18892, presented at SPE Production Operation Symposium held in Oklahoma City, OK. 13-14 March (1989).

Leontaritis,K.J.: "Asphaltene Deposition: A Thermodynamic-Colloidal Model", Dissertation for the degree of Doctor of Philosophy in Chemical Engineering, March (1988), University of Illinois, Chicago, Illinois.

Lichaa, P.M.: "Asphaltene Deposition Problem in Venezuela Crudes - Usage of Asphaltenes in Emulsion Stability", Oil Sands, June (1977), pp. 609-624.

Lichaa, P.M.: "Electrical and Other Effects Related to The Formation and Prevention of Asphaltene Deposition Problem in Venezuelan Crudes" SPE of AIME, SPE 5304, (1975), pp. 107-125.

London, F.: "Theory and Systematics of Molecular Forces", Z. Physik, Vol. 63 (1930), pp. 245-279.

Lyklema, J.: "Principles of the Stability of Lyophopic Colloidal Dispersions in Non-Aqueous Media", Advances in Colloid and Interface Science, Vol. 2 (1968), pp. 65-114.

Mack, C.: "Colloid Chemistry of Asphaltene", J. Phys. Chem., Vol. 36 (1932), pp. 2901-2914.

Menon, V.B. and Wasan, D.T.: "Particle-Fluid Interactions With Application to Solid-Stabilized Emulsions, Part I. The Effect of Asphaltene Adsorption" Colloid and Surfaces, Vol. 19 (1986), pp. 89-105.

Menon, V.B. and Wasan, D.T.: "Particle-Fluid Interactions With Application to Solid-Stabilized Emulsions, Part II. The Effect of Adsorbed Water" Colloid and Surfaces, Vol. 19 (1986), pp. 107-122..

Miller, J.F., Clifton, B.J., Benneyworth, P.R., Vincent, B., MacDonald, I.P. and Marsh, J.F.: "Electrophoretic Studies of Calcium Carbonate Particles Dispersed in Various Hydrocarbon Liquids", Colloids and Surfaces, Vol. 66 (1992), pp. 197-202.

Misbah-ul-Hasan, M., Siddiqui, N. and Arab, M.: "Chromatographic Separation and Characterization of Asphaltene Subfractions from Saudi Arabian Crudes", Fuel, Vol. 67 (September 1988), pp. 1307-1309.

Mitchell, D.L., and Speight, J.G.: "The Solubility of Asphaltenes in Hydrocarbon Solvents", Fuel, Vol. 52 (1973), pp. 149-152.

Moschopedis, S.E., and Speight, J.G.: "Investigation of Hydrogen Bonding by Oxygen Functions in Athabasca Bitumen", Fuel, Vol. 55 (1976), pp. 187-192.

Moschopedis, S.E., Fryer, J.F. and Speight, J.G.: "Investigation of Asphaltene Molecular Weights", Fuel, Vol. 55 (1976), pp. 227-232.

Nellensteyn, F.J.: "Theortical Aspect of the Relation of Bitumen to Solid Matter", In Proc. World petroleum Congress, Vol. 2 (1933), pp. 616-618.

Nellensteyn, F.J.: "The Constitution of Asphalt", Chem. Weekbland, Vol. 21 (1924), pp. 42-51.

Newberry, M.E., and Barker, K.M.: "Formation Damage Prevention Through the Control of Paraffin and Asphaltene Deposition" SPE paper 13796, SPE Production Operations Symposium, Oklahoma City, OK, 10-12 March (1985).

O'Brien, R.W. and White, L.R.: "Electrophoretic Mobility of a Spherical Colloidal Particle", J. Chem. Soc., Faraday Trans. *II,* Vol. 74 (1978), No. 9, pp. 1607-1626.

Osman, M.E.: "An Approach to Predict Tarmat Breakdown in Minagish Reservoir in Kuwait" JPT, Nov. 1985, SPE paper 11492, presented at the Middle East Oil Technical of SPE. Bahrain (1983).

Overbeek, J.Th.G.: "Quantitaive Interpretation of the Electrophoretic Velocity of Colloids", Advance in Colloid Science, Vol. 3 (1950), pp.79-135.

Pfeiffer, J.P. and Saal, R.N.J.: "Asphaltic Bitumen as a Colloid System", J. Phys. Chem. Vol. 44 (1940), pp.139.

Poindexter, E. H.: "Dynamic Nuclear Polarization and Molecular Aggregation in Asphaltene Suspensions" J. of Colloid and Interface Scie., Vol. 38 (1972), No.2, pp. 412-423.

Preckshot, G.W.,Delisle, N.G., Cottrell, C.E. and Katz, D.L.: "Asphaltic Substances in Crude Oils", Transactions, American Institute of Mining, Metallurgical, and Petroleum Engineers, Vol. 151 (1943), pp.188-194.

Ramsden, W., as discussed in **Menon, V.B. and Wasan, D.T.:** "Particle-Fluid Interactions With Application to Solid-Stabilized Emulsions, Part I. The Effect of Asphaltene Adsorption" Colloid and Surfaces, Vol. 19 (1986) p. 89.

Sanchanen, A.N. and Wassiliew, L., as discussed in **Koots, J. A. and Speight, J. G.:** "Relation of Petroleum Resins to Asphaltenes", Fuel, Vol. 54 (1975), p. 179.

Schenkel, J.H. and Kitchener, J.A.: "A Test of the Derjaguin-Verwey-Overbeek Theory with a Colloidal Suspension", Trans. Faraday Soc., Vol. 56 (1960), pp. 161-173.

Schramm, L.L., Mannhardt, K. and Novosad, J.J.: "Electrokinetic Prpperties of Reservoir rock Particles", Colloids and Surfaces, Vol. 55 (1991), pp. 309-331.

Smith, A.L.: "Dispersions of Powders in Liquids", (G. Parfitt ed.), (1969), Applied Science Publishers, Barking, England.

Smoluchowski, M.: in Graetz, *Handbuch der Elektrizität und des Mgnetismus*, Vol. 2 (1921), Barth, Leipzig, p. 366.

Strausz, O.P., Mojelsky, T.W. and Lown, E.M.: "The molecular structure of asphaltene: an unfolding Story", Fuel, Vol. 71 (1992), pp. 1355-1363.

van der Minne, J.L. and Hermanie, P.H.J.,: "Electrophoresis Measurements in Benzene Correlation With Stability. I. Development of Method", J. of Colloid Science, Vol. 7 (1952), pp. 600-615.

Verwey, E.J.W. and Overbeek, J.Th.G.: "Theory of Stability of Lyophobic Colloids", Elsevier, Amsterdam, (1948).

Washburn, E.W., (editor-in-chief): "International Critical Tables for Numerical Data, Physics, Chemistry and Technology", Prepared under the Auspices of the

International Research Council and the National Academy of Sciences by the National Research Council of USA,Vol. 6 (1929).

Winniford, R.S.: "The Influence of Asphalt Composition on Its Rheology", Am. Soc. Testing Materials Special Tech. Pub. No. 294 (1960).

Witherspoon, P.A. and Munir, Z.A.: "Size and Shape of Asphaltic Particles in Petroleum". Producer Monthly, Vol. 24 (1960), pp. 20-31.

Witherspoon, P.A., Ray, B.R. and Grim, R.E.: "A study of the Colloidal Characteristics of Petroleum Using the Ultracentrifuge", J. Phys. Chem., Vol. 61 (1957), pp. 1296-1302.

Wright, J.R. and Minesinger, R.R.: "The Electrophoretic Mobility of Asphaltenes In Nitromethane" J. of Colloid Science, Vol. 18 (1963), pp. 223-236.

Wyllie, M.R.J.: "An Investigation of the Electrokinetic Component of the Self Potential Curve", Trans. AIME, Vol. 192 (1951), pp. 1-18.

BIBLIOGRAPHY

Alkafeef, S.F., Daltaban, T.S., Gochin, R.J.: "Electrokinetic Aspects of Asphaltene Deposition in Petroleum Reservoirs", ADSPE paper 26, Presented at the 6th Abu Dhabi International Petroleum Exhibition & Conference in Abu Dhabi City, UAE, 16-19 Oct. (1994).

Boduszynski, M.M.: "Asphaltenes in Petroleum Asphalts", The Advances in Chemistry Series, No.195 (1981), p.119.

Crow, D.R.: *Principles and Applications of Electrochemistry*, Chapman and Hall Chemistry Series, Second Eddition, (1979).

Dukhin, S.S. and Deryaguin, B.V.: "Surface and Colloid Science" (E. Matijevic *editor*), Vol. 7 (1974) "Electrokinetic Phenomena", John Wiley Interscience, N.Y. and London.

Everett, D.H.: *Basic principles of Colloid Science*, Royal Society of Chemistry Paperbacks, (1988).

Galtsev, V.E., Ametov, I.M., Kuznetsov, A.M., Kovalev, A.G. and Salnikov, D.I.: "Asphaltene Molecules Association Effect on Crude Oil Flow Through Porous Medium", Paper No. 9632 presented at the International Symposium of the Society of Core Analysts, Montpellier, France, 8-10 September (1996).

Gonzalez, G. and Louvisse, A.M.T.: "The Adsorption of Asphaltene and its Effect on Oil Production", SPE Paper No. 21039, presented at the SPE International Symposium on Oilfield Chemistry held in Anaheim, California, 20-22 Feb. (1991).

Gregory J.: "The Calculation of Hamaker Constants", Advances in Colloid and Interface Science, Vol. 2 (1969), pp. 396-417.

Hirasaki, G.J.: "Wettability: Fundamentals and Surface Forces", SPE/DOE Paper No. 17367, presented at the SPE/DOE Enhanced Oil Recovery Symposium held in Tulsa,OK, 17-20 April (1988).

Hunter, R.J.: *Zeta Potential in Colloid Science*, Academic Press, (1988).

Long, R.B.: "The Concept of Asphaltene", The Advances in Chemistry Series, No.195 (1981), p.17.

Marlow, B.J., Sresty, G.C., Hughes, R.D. and Mahajan, O.P.: "Colloidal Stabilization of Clays by Asphaltenes in Hydrocarbon Media", Colloid and Surfaces, Vol. 24 (1987), pp. 283-297.

Pfeiffer,J., editor: *The Properties of Asphaltic Bitumen*, Elsevier Publishing Company, (1950).

Shaw, D.J.: "*Introduction to Colloid and Surface Chemistry*" 4th Edition, Butterworth-Heinemann Ltd, (1992).

APPENDIX A

X-RAY DIFFRACTION ANALYSIS

COMPANY: ASPHALTENE RESEARCH PROJECT
FORMATION: GLAUCONITIC SANDSTONE, ALBERTA, CANADA
SAMPLE: G3
DEPTH/INTERVAL: 1108.6 meters

	< 2 MICRON MATERIAL	> 2 MICRON MATERIAL	CALCULATED BULK COMPOSITION
QUARTZ	0	68	66
PLAGIOCLASE	0	16	15
K FELDSPAR	0	12	12
CALCITE	0	0	0
DOLOMITE	0	0	0
SIDERITE	0	0	0
PYRITE	0	0	0
KAOLINITE	82	4	7
ILLITE	11	0	trace
CHLORITE	7	0	trace
SMECTITE	0	0	0
MIXED LAYER CLAY	0	0	0
ANHYDRITE	0	0	0
HEMATITE	0	0	0

PERCENT MATERIAL <2 MICRONS: 3.9
PERCENT MATERIAL >2 MICRONS: 96.1

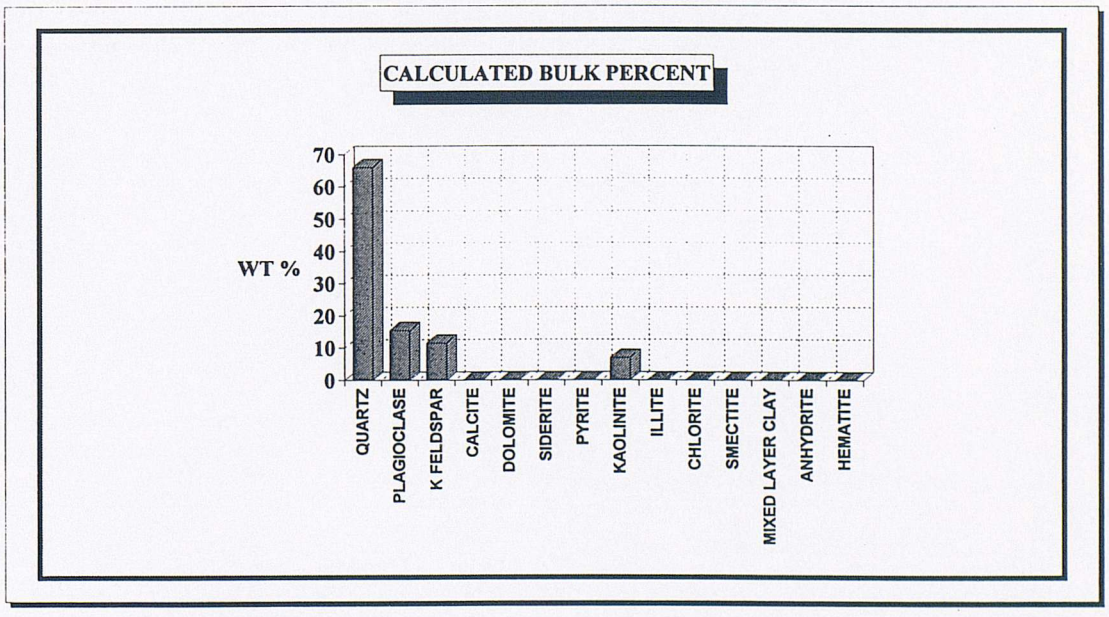

X-RAY DIFFRACTION ANALYSIS

COMPANY: ASPHALTENE RESEARCH PROJECT
FORMATION: GLAUCONITIC SANDSTONE, ALBERTA, CANADA
SAMPLE: G6
DEPTH/INTERVAL: 1038.77 meters

	< 2 MICRON MATERIAL	> 2 MICRON MATERIAL	CALCULATED BULK COMPOSITIOI
QUARTZ	3	75	70
PLAGIOCLASE	0	12	11
K FELDSPAR	0	10	9
CALCITE	0	0	0
DOLOMITE	0	0	0
SIDERITE	0	0	0
PYRITE	0	0	0
KAOLINITE	92	3	9
ILLITE	5	0	trace
CHLORITE	0	0	0
SMECTITE	0	0	0
MIXED LAYER CLAY	0	0	0
ANHYDRITE	0	0	0
HEMATITE	0	0	0

PERCENT MATERIAL <2 MICRONS: 6.9
PERCENT MATERIAL >2 MICRONS: 93.1

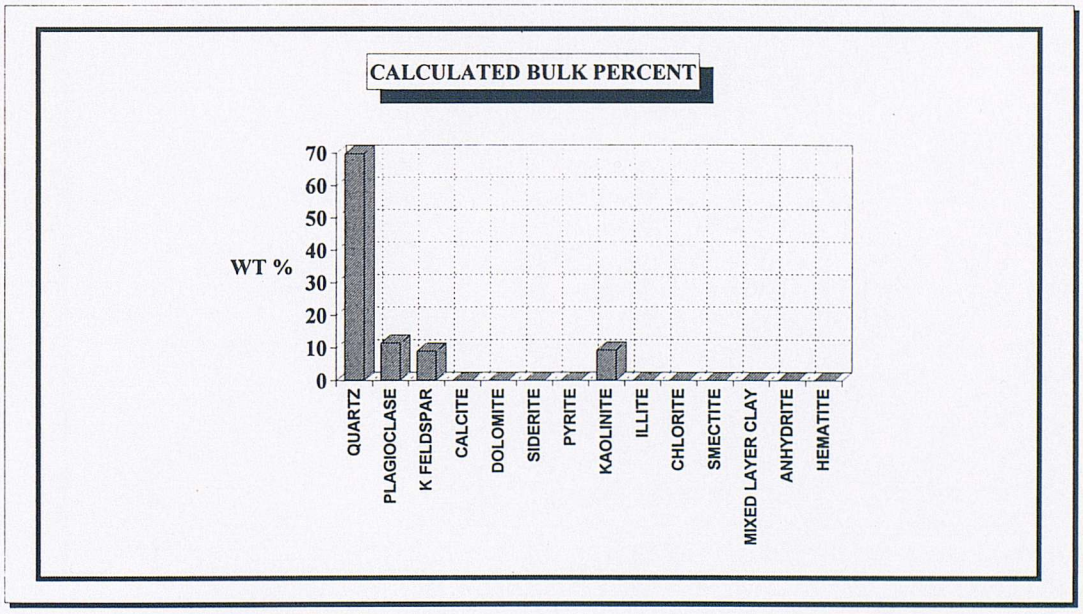

X-RAY DIFFRACTION ANALYSIS

COMPANY: ASPHALTENE RESEARCH PROJECT
FORMATION: GLAUCONITIC SANDSTONE, ALBERTA, CANADA
SAMPLE: G7
DEPTH/INTERVAL: 1114.05 meters

	< 2 MICRON MATERIAL	> 2 MICRON MATERIAL	CALCULATED BULK COMPOSITION
QUARTZ	6	67	64
PLAGIOCLASE	4	20	18
K FELDSPAR	3	9	9
CALCITE	0	0	0
DOLOMITE	0	0	0
SIDERITE	0	0	0
PYRITE	1	2	2
KAOLINITE	71	2	6
ILLITE	15	0	1
CHLORITE	0	0	0
SMECTITE	0	0	0
MIXED LAYER CLAY	0	0	0
ANHYDRITE	0	0	0
HEMATITE	0	0	0

PERCENT MATERIAL <2 MICRONS: 4.6
PERCENT MATERIAL >2 MICRONS: 95.4

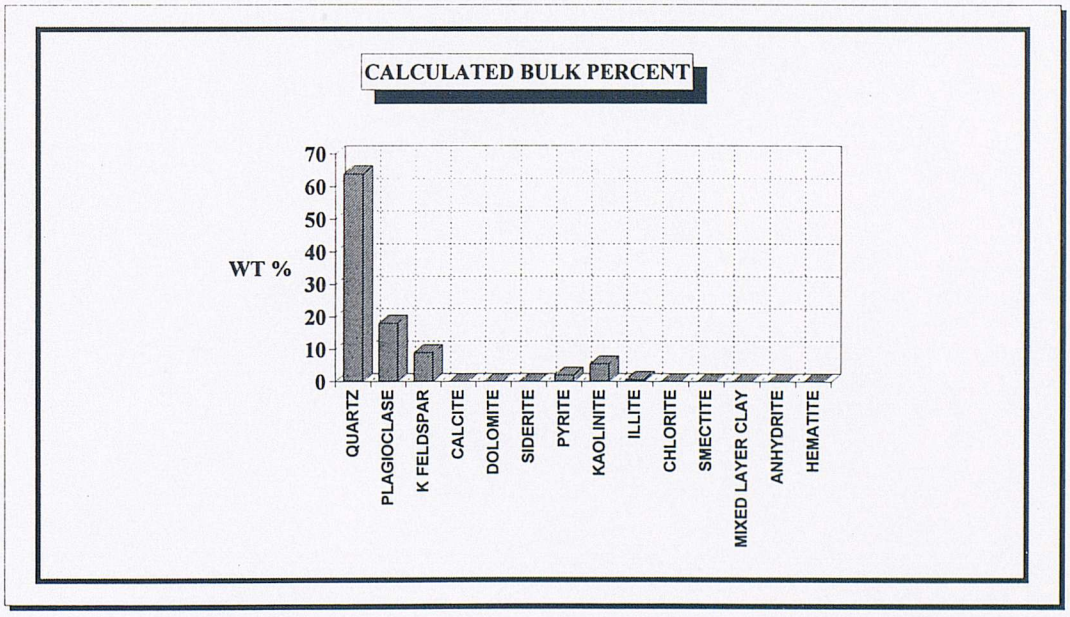

X-RAY DIFFRACTION ANALYSIS

COMPANY: ASPHALTENE RESEARCH PROJECT
FORMATION: GLAUCONITIC SANDSTONE, ALBERTA, CANADA
SAMPLE: G8
DEPTH/INTERVAL: 1113.34 meters

	< 2 MICRON MATERIAL	> 2 MICRON MATERIAL	CALCULATED BULK COMPOSITION
QUARTZ	0	70	66
PLAGIOCLASE	0	19	18
K FELDSPAR	0	9	9
CALCITE	0	0	0
DOLOMITE	0	0	0
SIDERITE	0	0	0
PYRITE	0	0	0
KAOLINITE	86	2	6
ILLITE	14	0	1
CHLORITE	0	0	0
SMECTITE	0	0	0
MIXED LAYER CLAY	0	0	0
ANHYDRITE	0	0	0
HEMATITE	0	0	0

PERCENT MATERIAL <2 MICRONS: 4.6
PERCENT MATERIAL >2 MICRONS: 95.4

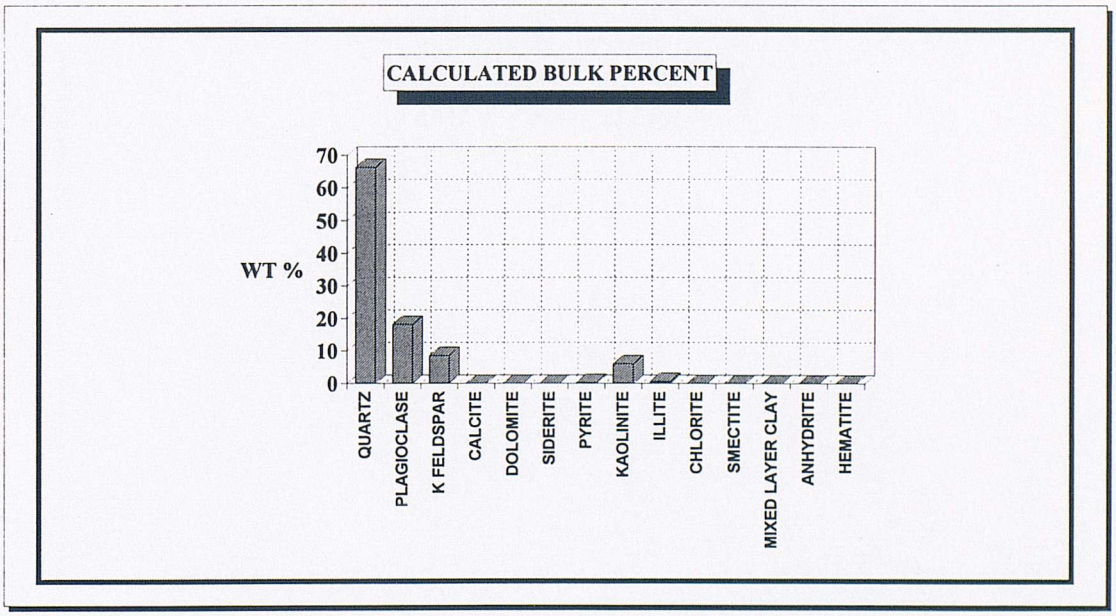

X-RAY DIFFRACTION ANALYSIS

COMPANY: ASPHALTENE RESEARCH PROJECT
FORMATION: GLAUCONITIC SANDSTONE, ALBERTA, CANADA
SAMPLE: G10
DEPTH/INTERVAL: 1112.44 meters

	< 2 MICRON MATERIAL	> 2 MICRON MATERIAL	CALCULATED BULK COMPOSITION
QUARTZ	6	74	72
PLAGIOCLASE	3	17	16
K FELDSPAR	3	8	8
CALCITE	0	0	0
DOLOMITE	0	0	0
SIDERITE	0	0	0
PYRITE	0	0	0
KAOLINITE	78	1	4
ILLITE	10	0	trace
CHLORITE	0	0	0
SMECTITE	0	0	0
MIXED LAYER CLAY	0	0	0
ANHYDRITE	0	0	0
HEMATITE	0	0	0

PERCENT MATERIAL <2 MICRONS: 3.5
PERCENT MATERIAL >2 MICRONS: 96.5

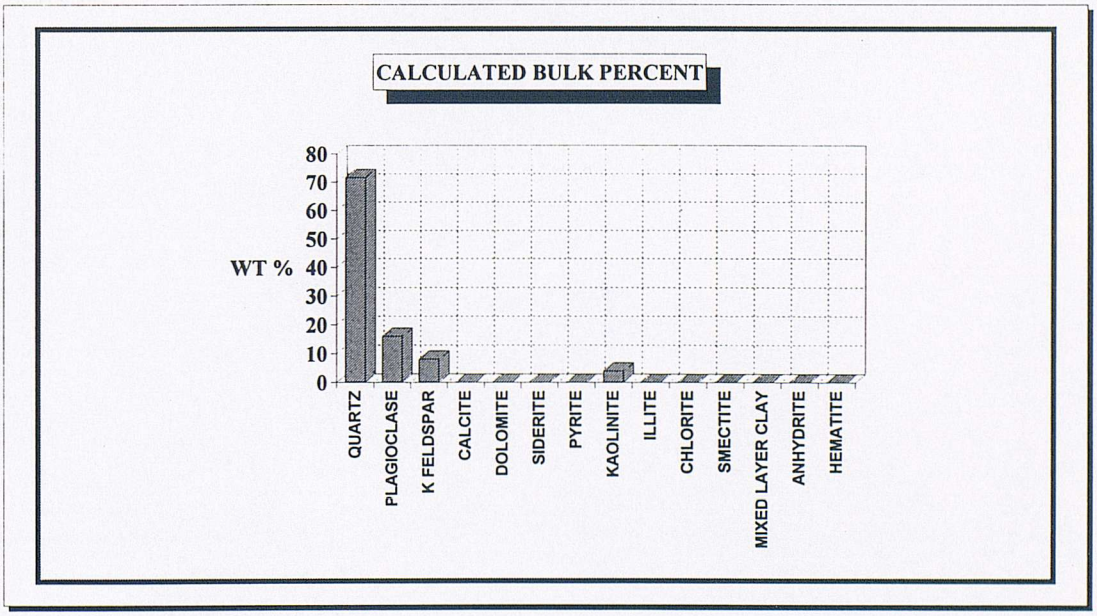

X-RAY DIFFRACTION ANALYSIS

COMPANY: ASPHALTENE RESEARCH PROJECT
FORMATION: GLAUCONITIC SANDSTONE, ALBERTA, CANADA
SAMPLE: G11
DEPTH/INTERVAL: 1112.18 meters

	< 2 MICRON MATERIAL	> 2 MICRON MATERIAL	CALCULATED BULK COMPOSIT
QUARTZ	5	77	75
PLAGIOCLASE	0	16	16
K FELDSPAR	0	5	5
CALCITE	0	0	0
DOLOMITE	0	0	0
SIDERITE	0	0	0
PYRITE	0	0	0
KAOLINITE	83	2	4
ILLITE	12	0	trace
CHLORITE	0	0	0
SMECTITE	0	0	0
MIXED LAYER CLAY	0	0	0
ANHYDRITE	0	0	0
HEMATITE	0	0	0

PERCENT MATERIAL <2 MICRONS: 2.5
PERCENT MATERIAL >2 MICRONS: 97.5

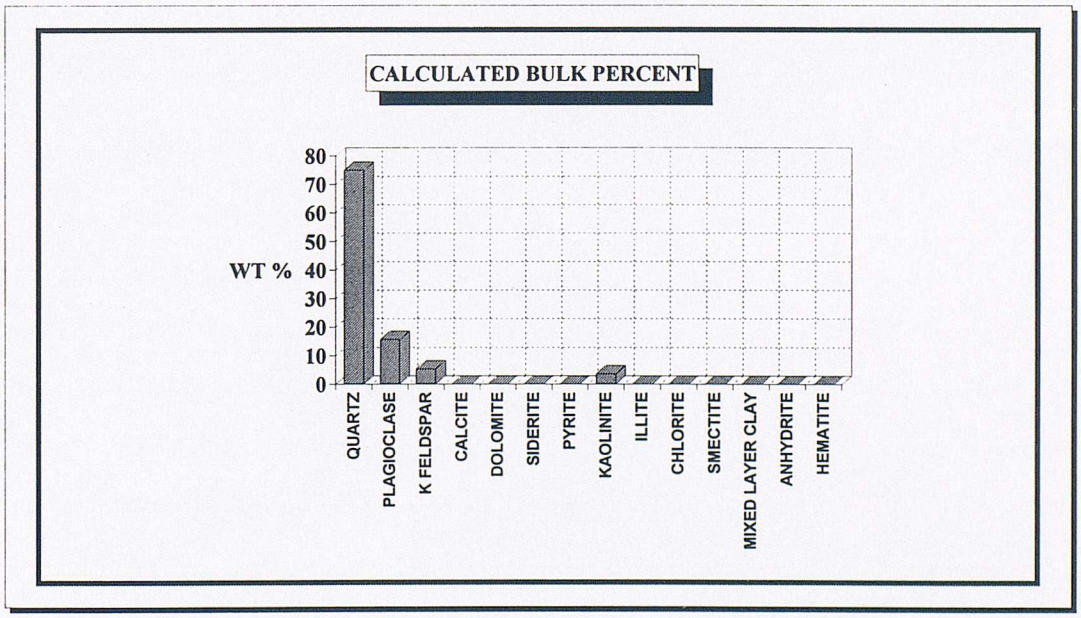

APPENDIX B

CALCULATION OF ZETA POTENTIAL FROM STREAMING CURRENT AND POTENTIAL MEASUREMENTS

This Appendix shows an example of how streaming current and potential measurements was treated in this thesis to calculate the reservoir rock cores zeta potential.

If we take for example streaming current and potential measurements of aqueous *KCl8* (7.456 g/*l*) in Berea sandstone from Table 6.1:

Data:

* Streaming current $\left(\dot{I}_s\right)$ slope $\frac{dI_s}{d\Delta P}$ =-4.10*10^{-9} A/psi =-5.946*10^{-13} Amps/Nm^{-2}.
* Streaming potential $\left(\dot{V}_s\right)$ slope $\frac{dV_s}{d\Delta P}$ =-5.04*10^{-5} V/psi =-7.314*10^{-9}Volt/Nm^{-2}.
* Estimated pores A/L ratio of Berea sandstone (sample B-1) from aqueous *KCl* solutions is ~7*10^{-5} m.
* *KCl8* conductivity = 1.162 $ohm^{-1}m^{-1}$.
* *KCl8* viscosity = 1 cp = 0.001 Pa.sec
* The permittivity of aqueous *KCl8* (ε) = ε_r * ε_o
* Dielectric constant of *KCl8* (ε_r) = 78.3
* Permittivity of free space (ε_o) = 8.854*10^{-12}

Calculations of Berea Sandstone Zeta Potential

(A) By Streaming Current Method:

Using equation (3.22) for streaming current;

$$I_S = f\left(\frac{\Delta P \varepsilon \zeta}{\eta}\right)$$

Where f = A/L estimated from combining streaming current and potential measurements ($7*10^{-5}$ m)

$$\zeta = \left(\frac{dI_S(A)}{d\Delta P(Nm^{-2})}\right) * \left(\frac{\eta}{\varepsilon}\right) * \left(\frac{1}{f}\right)$$

$$\zeta = \left(-5.946*10^{-13}\,\frac{A}{Nm^{-2}}\right) * \left(\frac{0.001}{78.3*8.854*10^{-12}}\right) * \left(\frac{1}{7*10^{-5}}\right) = -0.01225 \text{ Volt}$$

$\therefore\ \zeta =$ -12.25 mV

(B) By Streaming Potential Method:

Using Equation (3.21) for streaming potential;

$$V_S = \left(\frac{\Delta P \varepsilon \zeta}{K'\eta}\right)$$

$$\zeta = \left(\frac{dV_S(V)}{d\Delta P(Nm^{-2})}\right) * \left(\frac{\eta}{\varepsilon}\right) * K$$

$$\zeta = \left(-7.314*10^{-9}\,\frac{V}{Nm^{-2}}\right) * \left(\frac{0.001}{78.3*8.854*10^{-12}}\right) * (1.162) = -0.01225 \text{ Volt}$$

$\therefore\ \zeta =$ -12.25 mV

Note: Here both methods yield the same ζ value. This due to the fact that surface conductivity is negligible in high electrolyte *KCl8* solution.

APPENDIX C

THEORY OF STREAMING CURRENT IN FLAT SIDED NARROW PORES

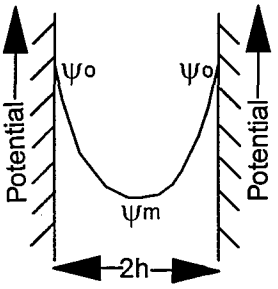

Using the older unrationalised system:

Poisson equation:

$$\frac{d}{dx}\left(\varepsilon\frac{d\psi}{dx}\right) = -4\pi\rho \tag{C1}$$

Assume ε independent of κ or ψ

$$\frac{d^2\psi}{dx^2} = -\frac{4\pi}{\varepsilon}\rho \tag{C2}$$

Where, $\rho = \sum n_i z_i e_o$ (C3)

$$\frac{d^2\psi}{dx^2} = -\frac{4\pi}{\varepsilon}\sum n_i z_i e_o \tag{C4}$$

Now, $n_i = n_i^o \exp\left(\frac{z_i e_o \psi}{kT}\right)$ (C5)

$$\frac{d^2\psi}{dx^2} = -\frac{4\pi}{\varepsilon}\sum z_i e_o n_i^o \exp\left(-\frac{z_i e_o \psi}{kT}\right) \tag{C6}$$

for symmetrical z:z electrolyte, with $z = |z|$ i.e. always positive

$$\frac{d^2\psi}{dx^2} = -\frac{4\pi}{\varepsilon} e_o \left\{ zn_i^o \left[\exp\left(-\frac{ze_o\psi}{kT} \right) - \exp\left(+\frac{ze_o\psi}{kT} \right) \right] \right\} \tag{C7}$$

$$= +\frac{4\pi}{\varepsilon} e_o zn_i^o 2\sinh\left(\frac{ze_o\psi}{kT} \right) \tag{C8}$$

Multiply both sides by $\frac{d\psi}{dx}$

$$\frac{d\psi}{dx} * \frac{d^2\psi}{dx^2} = \frac{8\pi e_o zn_i^o}{\varepsilon} \sinh\left(\frac{ze_o\psi}{kT} \right) * \frac{d\psi}{dx} \tag{C9}$$

$$\frac{1}{2} d\left(\frac{d\psi}{dx} \right)^2 = \frac{8\pi e_o zn_i^o}{\varepsilon} \sinh\left(\frac{ze_o\psi}{kT} \right) * \frac{d\psi}{dx} \tag{C10}$$

$$d\left(\frac{d\psi}{dx} \right)^2 = \frac{16\pi e_o zn_i^o}{\varepsilon} \sinh\left(\frac{ze_o\psi}{kT} \right) d\psi \tag{C11}$$

Integrate both sides;

$$\left(\frac{d\psi}{dx} \right)^2 = \frac{16\pi e_o zn_i^o}{\varepsilon} \frac{kT}{ze_o} \cosh\left(\frac{ze_o\psi}{kT} \right) + \text{Constant} \tag{C12}$$

Now at x=*h* (and $\psi=\psi_m$) $\frac{d\psi}{dx} = 0$

$$\therefore \left(\frac{d\psi}{dx} \right)^2 = \frac{16\pi n_i^o kT}{\varepsilon} \left[\cosh\frac{ze_o\psi}{kT} - \cosh\frac{ze_o\psi_m}{kT} \right] \tag{C13}$$

now let $\frac{e_o\psi}{kT} = y$, $\frac{e_0 y_m}{kT} = y_m$

$$\left(\frac{d\psi}{dx} \right)^2 = \frac{16\pi n_i^o kT}{\varepsilon} \left[\cosh(zy) - \cosh(zy_m) \right] \tag{C14}$$

now let y be small (the low potential Debye-Hückel approximation)

$$\left(\frac{dy}{dx} \right)^2 \cong \frac{8\pi n_i^o kT}{\varepsilon} \left[(zy)^2 - (zy_m)^2 \right] \tag{C15}$$

$$\text{so } \frac{d\psi}{dx} \cong \sqrt{\frac{8\pi n_i^o kT}{\varepsilon} \left[(zy)^2 - (zy_m)^2 \right]} \tag{C16}$$

$$\text{or} \quad \frac{kT}{e_o}\frac{dy}{dx} \cong \sqrt{\frac{8\pi n_i^o kT}{\varepsilon}\left[(zy)^2 - (zy_m)^2\right]} \tag{C17}$$

take $z = 1$

$$\frac{dy}{dx} = \sqrt{\frac{8\pi n_i^o e_o^2 z^2}{\varepsilon kT}\left(y^2 - y_m{}^2\right)} \tag{C18}$$

$$\text{i.e.} \quad \frac{dy}{dx} = \pm\kappa\sqrt{y^2 - y_m^2} \tag{C19}$$

- sign if origin ($x = 0$) is at the edge (plate), + sign if origin ($x = 0$) is at the middle.

Origin at the middle,

$$\frac{dy}{dx} = +\kappa\sqrt{y^2 - y_m^2} \tag{C20}$$

Substitute $y = y_m \cosh z$ (C21)

$$\text{i.e.} \quad dy = y_m \sinh z dz \tag{C22}$$

$$\frac{dy}{\sqrt{y^2 - y_m^2}} = \kappa dx \tag{C23}$$

$$\frac{y_m \sinh z dz}{\sqrt{y_m^2 \cosh^2 z - y_m^2}} = \kappa dx \tag{C24}$$

$$\frac{y_m \sinh z dz}{y_m\sqrt{\cosh^2 z - 1}} = \kappa dx \tag{C25}$$

$$\frac{\sinh z dz}{\sqrt{\cosh^2 z - 1}} = \kappa dx \tag{C26}$$

$$dz = \kappa dx \tag{C27}$$

$$\text{so} \quad z = \kappa x + \text{Constant} \tag{C28}$$

$$\text{Now when } x = 0, \ \frac{y}{y_m} = 1 \ \text{ so } \ z = 0 \quad \therefore \ \text{Constant} = 0 \tag{C29}$$

$$z = \kappa x \tag{C30}$$

$$\therefore \ \cosh z = \cosh \kappa x \tag{C31}$$

$$\frac{y}{y_m} = \cosh \kappa x \tag{C32}$$

when x = d (edge) y = y_o (identify with ζ)

$$\therefore \quad \frac{y}{y_m} = \cosh \kappa d \tag{C33}$$

divide equation C32/C33, $$\frac{y(x)}{y_o} = \frac{\cosh \kappa x}{\cosh \kappa d} \tag{C34}$$

or if we insist on having origin at the edge (plane, plate) x become h-x

and $$\frac{y(x)}{y_o} = \frac{\cosh \kappa (h - x)}{\cosh \kappa h} \tag{C35}$$

for example,

when x = 0 (edge), $y(x) = y_o$ and when x = h, $$\frac{y(x)}{y_o} = \frac{1}{\cosh \kappa h} \tag{C36}$$

or ,of course, $$\frac{\psi(x)}{\psi_o} = \frac{\cosh \kappa (h - x)}{\cosh \kappa h} \tag{C37}$$

Flat capillaries;

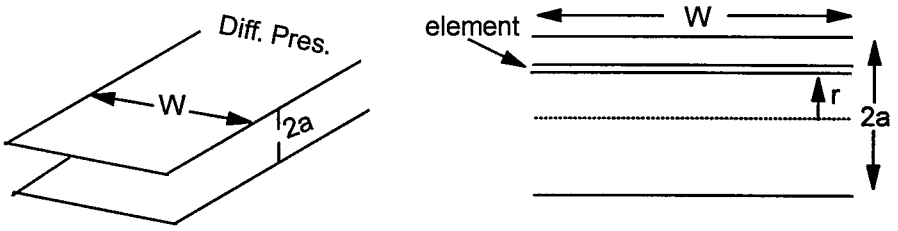

Flat Capillaries

$$\text{drag} = \eta \frac{dv}{dr} \text{ per unit area} \tag{C38}$$

$$= \eta \frac{dv}{dr} lw \tag{C39}$$

$$\therefore \quad \Delta P w dr = -\eta l w \, d\left(\frac{dv}{dr}\right) \tag{C40}$$

$$d\left(\frac{dv}{dr}\right) = -\frac{\Delta P}{\eta l} dr \tag{C41}$$

$$\text{Integrating} \qquad \frac{dv}{dr} = -\frac{\Delta P}{\eta l} r + \text{constant} \tag{C42}$$

$$\text{but } \frac{dv}{dr} = 0 \text{ at } r = 0 \text{ (the middle)} \quad \therefore \text{ constant } = 0 \tag{C43}$$

$$\frac{dv}{dr} = -\frac{\Delta P}{\eta l} r \tag{C44}$$

$$dv = -\frac{\Delta P}{\eta l} r dr \tag{C45}$$

$$\text{integrate} \qquad v(r) = -\frac{\Delta P}{\eta l}\frac{r^2}{2} + \text{constant} \tag{C46}$$

but v = 0 when r = a (and when r = -a)

$$0 = -\frac{\Delta P}{\eta l}\frac{a^2}{2} + \text{constant} \tag{C47}$$

$$\text{constant} = +\frac{\Delta P}{\eta l}\frac{a^2}{2} \tag{C48}$$

$$\therefore \quad v(r) = \frac{\Delta P}{\eta l}\frac{1}{2}\left(a^2 - r^2\right) \tag{C49}$$

Now we work with distance from wall x rather than centre

$$r = a - x \tag{C50}$$

$$r^2 = a^2 + x^2 - 2ax \tag{C51}$$

$$v(x) = \frac{\Delta P}{2\eta l}\left(a^2 - a^2 - x^2 + 2ax\right) \tag{C52}$$

$$v(x) = \frac{\Delta P}{2\eta l}\left(2ax - x^2\right) \tag{C53}$$

volume per second flowing through element = v(x)wdx (C54)

charge carried per second (current) = $\rho(x)v(x)wdx$ (C55)

$$I_{total} = \int_{x=0}^{x=h} \rho(x)v(x)wdx \quad \text{(C56)}$$

$$= \frac{w\Delta P}{2\eta l}\int_{x=0}^{x=h}\left(2ax - x^2\right)\rho(x)dx \quad \text{(C57)}$$

$$= \frac{A}{2a}\frac{\Delta P}{2\eta l}\int_{x=0}^{x=h}\left(2ax - x^2\right)\rho(x)dx \quad \text{(C58)}$$

Now, $\rho(x) = -\varepsilon\frac{d}{dx}\left(\frac{d\psi}{dx}\right)$ (C59)

$$\therefore\ I_{total} = \left(-\frac{A}{2a}\frac{\Delta P}{2\eta l}\right)\int_{x=0}^{x=h}\left(2ax - x^2\right)\varepsilon\frac{d}{dx}\frac{d\psi}{dx}dx \quad \text{(C60)}$$

$$= \left(-\frac{A}{2a}\frac{\Delta P}{2\eta l}\right)\varepsilon\int_{x=0}^{x=h}\left(2ax - x^2\right)d\left(\frac{d\psi}{dx}\right) \quad \text{(C61)}$$

$$= \left(-\frac{A}{2a}\frac{\varepsilon\Delta P}{2\eta l}\right)\int_{x=0}^{x=h}\left(2ax - x^2\right)d\left(\frac{d\psi}{dx}\right) \quad \text{(C62)}$$

$$\int_{x=0}^{x=h}\left(2ax - x^2\right)d\left(\frac{d\psi}{dx}\right) = \int_{x=0}^{x=h}(2ax)d\left(\frac{d\psi}{dx}\right) - \int_{x=0}^{x=h}x^2 d\left(\frac{d\psi}{dx}\right) \quad \text{(C63)}$$

if we integrate the terms separately, then the first integral becomes

$$\int_{x=0}^{x=h}(2ax)d\left(\frac{d\psi}{dx}\right) \quad \text{(C64)}$$

$$= 2a\int_{x=0}^{x=h}xd\left(\frac{d\psi}{dx}\right) \quad \text{(C65)}$$

$$= 2a\left[x\frac{d\psi}{dx} - \int\frac{d\psi}{dx}dx\right]_o^h \quad \text{(C66)}$$

$$= 2a\left[x\frac{d\psi}{dx} - \psi\right]_o^h \quad \text{(C67)}$$

$$= 2a\left[\left(hxo - ox\left(\frac{d\psi}{dx}\right)_o - (\psi_m - \psi_o)\right)\right] \tag{C68}$$

$$= 2a\left[-(\psi_m - \psi_o)\right] \tag{C69}$$

$$= 2a(\psi_o - \psi_m) \tag{C70}$$

since a = h,

$$= 2h(\psi_o - \psi_m) \tag{C71}$$

now for the second integral

$$\int_{x=0}^{x=h} x^2 d\left(\frac{d\psi}{dx}\right) \tag{C72}$$

$$= x^2 \frac{d\psi}{dx}\Big]_o^h - \int_o^h \frac{d\psi}{dx} d(x^2) \tag{C73}$$

$$= x^2 \frac{d\psi}{dx}\Big]_o^h - \int_o^h \frac{d\psi}{dx} 2x dx \tag{C74}$$

$$= x^2 \frac{d\psi}{dx}\Big]_o^h - 2\int_o^h x d\psi \tag{C75}$$

$$= x^2 \frac{d\psi}{dx}\Big]_o^h - 2\left[x\psi\Big]_o^h - \int_o^h \psi dx\right] \tag{C76}$$

$$= x^2 \frac{d\psi}{dx}\Big]_o^h - 2x\psi\Big]_o^h + 2\int_o^h \psi dx \tag{C77}$$

$$= \left(h^2 xo - 0^2\left(\frac{d\psi}{dx}\right)_o\right) - 2(h\psi_m - 0\psi_o) + 2\int_o^h \psi dx \tag{C78}$$

$$= 0 - 2h\psi_m + 2\int_o^h \psi dx \tag{C79}$$

so for each half,

$$I_{total} = \left[-\frac{A}{a}\frac{\varepsilon \Delta P}{2\eta l}\right]\left[2h(\psi_o - \psi_m) + 2h\psi_m - 2\int_o^h \psi dx\right] \tag{C80}$$

$$= \left[-\frac{A}{a}\frac{\varepsilon \Delta P}{2\eta l} \right] \left[h(\psi_o - \psi_m) + h\psi_m - \int_o^h \psi dx \right] \tag{C81}$$

For both halves i.e. the real total current,

$$I_{total} = \left[-\frac{A}{a}\frac{\varepsilon \Delta P}{2\eta l} \right] \left[h(\psi_o - \psi_m) + h\psi_m - \int_o^h \psi dx \right] \tag{C82}$$

$$= \left[-\frac{A}{a}\frac{\varepsilon \Delta P}{2\eta l} \right] \left[h\psi_o - \int_o^h \psi dx \right] \tag{C83}$$

so now we just have to evaluate $\int_o^h \psi dx$ and we have ψ as function of x in equation (C37), to do this.

so $$\int_o^h \psi dx = \int_o^h \psi_o \frac{\cosh \kappa(h-x)}{\cosh \kappa h} dx \tag{C84}$$

$$= \frac{\psi_o}{\cosh \kappa h} \int_o^h \cosh \kappa(h-x) dx \tag{C85}$$

$$= \frac{\psi_o}{\cosh \kappa h} \frac{1}{\kappa} \sinh \kappa h \tag{C86}$$

$$= \frac{\psi_o}{\kappa} \tanh \kappa h \tag{C87}$$

Putting this into the expression (C83), then total (both halves) current becomes,

$$I_{total} = \left[-\frac{A}{h}\frac{\varepsilon \Delta P}{2\eta l} \right] \left[h\psi_o - \frac{\psi_o}{\kappa} \tanh \kappa h \right] \tag{C88}$$

$$= \left[-\frac{A}{l}\frac{\varepsilon \Delta P}{\eta} \right] \left[\psi_o - \frac{\psi_o}{\kappa} \tanh \kappa h \right] \tag{C89}$$

We need to remember that a = h and $\psi_o = \zeta$.

Now for high electrolyte/wide pores:

$$I_{total} = -\frac{A}{l}\frac{\varepsilon \Delta P \psi_o}{\eta} \tag{C90}$$

$$\therefore \quad \frac{I_{total}\ \text{narrow pores}}{I_{total}\ \text{wide pores}} = 1 - \frac{1}{\kappa h} \tanh\ \kappa h \qquad \text{(C91)}$$

Numerical example:

Suppose slit of diameter 2 μm, h = 1 μm and electrolyte 10^{-7} M, then κh = 1.

$$\frac{I\ (\text{narrow})}{I\ (\infty)} = 1 - \frac{1}{1} \tanh\ 1 = 1 - 0.76 = 0.24$$

APPENDIX D

If we have a growth process in which asphaltene molecules nucleate on a surface site on an existing particle then:

$$\frac{dV}{dt} = kAC \qquad (D1)$$

where V and A are the volume and surface area of a particle respectively. C, the concentration of asphaltene molecules in solution can be taken constant over the period of an experiment; k is rate constant.

now $$V = \frac{\pi D^3}{6} \qquad (D2)$$

and $$A = \pi D^2 \qquad (D3)$$

so $$\frac{d}{dt}\left(\frac{\pi D^3}{6}\right) = k'\pi D^2$$

where k' is a new constant

thus $$\frac{dD}{dt} = 2k' \qquad (D4)$$

And the diameter D increases linearly with time. On the other hand if the process is treated as an aggregation/coagulation then during such a process

$$\text{average particle volume} = \frac{n_{1,o} V_1}{n} \qquad (D5)$$

where,

$n_{1,o}$ = Number concentration of single particles at time zero.

V_1 = Volume of a single (original) particle.

n = Number concentration of particles (of any type) at any time.

Now $$\frac{dn}{dt} = -k_2 n^2 \qquad (D6)$$

where k_2 is a second order rate constant.

so $$\frac{dn}{n^2} = -k_2 dt \qquad (D7)$$

integrating $$-\frac{1}{n} = -k_2 t + \text{constnat} \tag{D8}$$

Now at $t = 0$, $n = n_{1,o}$

so $$\text{constant} = \frac{1}{n_{1,o}}, \tag{D9}$$

and $$\frac{n_{1,o}}{n} = 1 + n_{1,o} k_2 t \tag{D10}$$

so average particle volume at any time t, $\left(\frac{n_{1,o} V_1}{n}\right)$

is $$V_1\left(1 + n_{1,o} k_2 t\right) \tag{D11}$$

i.e. $$V(t) = V_1\left(1 + n_{1,o} k_2 t\right) \tag{D12}$$

Thus V(t), rather than the diameters, goes up linearly with time in distinction to previous case, In practice (chapter 8) the volume increases linearly of with time confirming a predominantly coagulation mechanism (N.B. the apparent linearity of diameter with time arises only because the diameter plotted is derived from the volume).

APPENDIX E

SPE PAPER 30539

SPE 30539

Surface Potential and Permeability of Rock Cores Under Asphaltenic Oil Flow Conditions

S. F. Alkafeef, SPE, R. J. Gochin, and A. L. Smith, Imperial College of Science, Technology and Medicine, London, U.K.

Copyright 1995, Society of Petroleum Engineers, Inc.

This paper was prepared for presentation at the SPE Annual Technical Conference & Exhibition held in Dallas, U.S.A., 22-25 October, 1995.

This paper was selected for presentation by an SPE Program Committee following review of information contained in an abstract submitted by the author(s). Contents of the paper, as presented, have not been reviewed by the Society of Petroleum Engineers and are subjected to correction by the author(s). The material, as presented, does not necessarily reflect any position of the Society of Petroleum Engineers, its officers, or members. Papers presented at SPE meetings are subject to publication review by Editorial Committees of the Society of Petroleum Engineers. Permission to copy is restricted to an abstract of not more than 300 words. Illustrations may not be copied. The abstract should contain conspicuous acknowledgement of where and by whom the paper was presented. Write Librarian, SPE, P.O. Box 833836, Richardson, TX 75083-3836, U.S.A., fax 01-214-952-9435.

Abstract

The surface properties, wetting behaviour and permeability of rock samples are central to understanding recovery behaviour in oil reservoirs. This paper will present a method new to petroleum engineering to show how area/length ratios for porous systems can be obtained by combining streaming potential and streaming current measurements on rock cores. This has allows streaming current measurements (independent of surface conductivity errors) to be made on rock samples using hydrocarbon solvents with increasing concentrations of asphaltene. Negative surface potentials for the rock became steadily more positive as asphaltene coated the pore surfaces, with permeability reduction agreeing well with petrographic analysis.

Introduction

The surface potential of oil reservoir rocks plays a significant role in oil recovery[1]. The adsorption of components in crude oil affect rock wettability[2-6] , this in turn influences reservoir fluid relative permeabilities and therefore recovery efficiency. The total factors concerned in reservoir wettability are not well understood

Adsorption is clearly one of the factors that affect rock wettability, permeability and electrical properties. In this work, an investigation of asphaltene adsorption on sandstone rock surfaces was conducted whose objective was determination of the influence of this mechanism on rock properties .

The contact between crude oil and rock is strongly dependent on the stability of an irreducible water film adsorbed on the rock surface not removed by vacuum/heat treatment[7-8]. The existence of a stable water film, with the reservoir water-wet before the migration of oil, will reduce the adhesion of the oil heavy end to the rock surfaces. This is mediated by electrical double layer effects arising from the surface charges at the solid/water and water/oil interfaces.

The interactions involved include van der Waals forces, steric effects and, in principle, electric double layer effects arising from charge at the interfaces. The combination of van der Waals and electric double layer forces was treated by Derjaguin, Landau, Vervey and Overbeek (the DLVO theory) originally applied to colloid particle stability.

In the case of crude oil, surface active polar and semi-polar compounds of O, N and S contained in resins and asphaltenes are believed to play an important role in rock wettability[9].

The activation of crude oil surfactants by the aqueous phase at the oil/water/silica interface was studied by Brown and Neustadter[10]. They showed that wettability, as indicated by contact angle, is strongly dependent on pH, interpreted as due to the activation of crude oil surfactant by the aqueous phase. The silica surface electric potential as shown by the electrokinetic zeta potential will clearly be a function of both pH and salinity, as will that of oil/water emulsions[11].

An investigation of the crude oil heavy end adsorption behaviour is therefore required in order to develop an understanding of the behaviour in reservoir rock porous systems.

The primary purpose of this paper is to introduce a novel method to show how the pore area/length ratios of a porous system can be obtained by combining streaming current and potential measurements. Such area/length ratios then allow streaming current measurements to be used to get surface (zeta) potentials free from the effects of surface conduction which can dominate and completely invalidate streaming potential measurements. The technique can then be extended to the case where rock pores are partially blocked by adsorption/deposition of asphaltenes.

Electrokinetic Techniques

The most frequently used electrokinetic technique for aqueous solution measurements is that of electrophoresis. In very low electrical conductivity liquids, such as oil, difficulties arise such as that of maintaining a suitably uniform potential gradient. In the streaming current technique the liquid is caused to flow through (past) the solid surface, carrying with it the electrical charge compensating that on the solid surface. If electrodes at each end of the cell are joined by a wire then the charge returns along this wire and can be measured as such over a known time or measured as a current using a sufficiently low impedance ammeter.

If no low resistance return path is present then the charge (current) returns through the liquid itself, generating a potential difference between the end electrodes which is then termed the streaming potential. If the streaming current is I_s and the liquid path resistance is R then the streaming potential V_s will of course be I_sR. However, R cannot be directly related to the conductivity of the liquid since a low resistance path at the solid surface (surface conductivity) will often exist which is difficult or impossible to estimate. This will be particularly so for oil flowing through rock pores which may have adsorbed water at the walls. Such errors may be of many orders of magnitude. For a sufficiently high conductivity liquid the error will be negligible but, apart from this case, the method of streaming charge (current) is much to be preferred as being both more fundamental and free from surface conductivity errors.

For a capillary path of cross section A and length l the streaming current I_s is related to the zeta potential (ζ) by

$$I_s = \frac{A}{l}\frac{\Delta P \epsilon \zeta}{\eta}$$

or, for an array of capillaries of length l

$$I_s = \frac{\sum A}{l}\frac{\Delta P \epsilon \zeta}{\eta} \quad \text{.....} \quad (1)$$

where, ΔP is the pressure difference between the ends, η is the viscosity of the liquid and ϵ its (rationalised) permittivity. Clearly A/l needs to be known or determined. For a single uniform capillary this is straightforward, but for the practical situation of a rock core a special technique is required.

Determination of Area/Length Ratios

For a collection of capillaries all of length l and total cross section A the streaming current I_s given by equation (1) above can be written as:

$$I_s = f\frac{\Delta P \epsilon \zeta}{\eta}$$

Where $f = \frac{\sum A}{l}$

Since $R = l/\kappa' \sum A$,

the streaming potential will therefore be given by

$$V_s = \frac{1}{\kappa'}\frac{\Delta P \epsilon \zeta}{\eta} \quad \text{.....} \quad (2)$$

where κ' is the effective conductivity of the current return path which includes a (possibly large) contribution from surface conductivity.

Thus, for the same values of all the parameters,

$$\frac{I_s}{V_s} = f\kappa'$$

If κ is the actual conductivity of the liquid (if necessary determined by a separate measurement), independent of surface conductivity, then

$$\frac{1}{\kappa}\frac{I_s}{V_s} = f\frac{\kappa'}{\kappa} \quad \text{.....} \quad (3)$$

Figure 1 shows a plot of $I_s/\kappa V_s$ against KCl (aqueous) concentrations for a core of Berea sandstone. This is seen to level out at higher KCl concentrations where κ' becomes equal to κ so that $\kappa'/\kappa = 1$ and f is given by the value of $I_s/\kappa V_s$ at the levelled off value ($7*10^{-5}$ m in Figure 1).

Both the expression for streaming current (1) and streaming potential (2) make the assumption that the capillary (pore) diameter is a good deal larger than the double layer thickness. This is certainly valid for the KCl solution measurements used to obtain f but must in general be questioned for non-aqueous measurements. However, this assumption will be made for sandstone samples used in this work, for which we have microscopic evidence that the pores are of order 80 μm diameter which should sufficiently validate the expressions given.

Of course as the pores become blocked the value of A/l will fall. The amount can be estimated by assuming Poiseuille laminar flow conditions in the pores so that for a liquid of viscosity η under a pressure difference ΔP between the capillary ends, assuming that the capillary lengths remain at l, the flow rate Q will be given by:

$$Q \alpha \Delta P r^4/\eta l$$

i.e. $$Q \alpha A^2$$

and $$(A/l)_1/(A/l)_0 = (Q_1/Q_0)^{1/2}$$

If the pore radius is reduced from r_0 to $r_0 - \gamma$ by the deposition of asphaltene for instance, then;

$$(A/l)_1/(A/l)_0 = (1-\gamma/r_0)^2 \quad \text{.....} \quad (4)$$

i.e. $$Q_1/Q_0 = (1-\gamma/r_0)^4 \quad \text{.....} \quad (5$$

Experimental

Materials

In this study Berea sandstone cores (Cleveland Quarries, Amherst,Ohio) with an average porosity of 22% were used as the porous medium. The core samples used had an average 80-90% of monocrystalline and polycrystalline quartz, 3-5% feldspar and 1-3% chert. The core samples were cleaned using a flow through method, which involves a succession of solvents through the samples. The samples were then placed in a vacuum oven at 100°C.

The aqueous solutions used for estimating the pore A/l ratios were made up in de-ionized water at KCl concentrations from 0 to 7.456 g/l (0.1 molar). The electrical conductivity and pH of the solution were measured. The non aqueous solutions were a 1:1 by volume mixture of n-pentane and toluene. For the purposes of this work, this liquid will be called "Pentol". Asphaltene used in this study was extracted from Saskatchewan, Canada crude oil. The extraction procedure involved the precipitation of the asphaltenes from the oil by an excess of n-pentane. The separation procedure followed the method described in ASTM D-3279.

Methods

A Berea core sample was placed in a core holder between two platinum faced stainless steel electrodes. The two electrodes were connected to a Keithley 617 electrometer to measure the current and the resulting potential produced by liquid flow through the core sample. An Isco 500D model pump was used to displace the fluid through the core sample at different pressures and rates. An overburden pressure (1000 psi) was applied to the core sample to prevent the liquid flow from overriding the porous media. The differential pressure of liquid flow in the core sample was controlled by a digital high pressure transducer. The work began by estimating the initial core pore $(A/l)_0$ ratio. This was accomplished by streaming potential and current measurements for each KCl solution flowing through the core over a range of differential pressures. The core pore A/l ratios were determined by plot based on equation 3 and shown in Figure 1. The surface electrical potential of Berea core in KCl solutions was then calculated from the streaming current. The core sample was then cleaned from KCl solutions by the previous indicated cleaning method.

The extracted asphaltene was dissolved first in a known volume of toluene and stirred for two hours, n-pentane of the same volume as the toluene was added to the solution and again stirred for anther two hours. The Pentol solutions at different asphaltene concentrations were flooded into the core. Streaming currents and flow rates were measured for each asphaltene concentration. All measurements were conducted at ambient conditions.

Results and Discussion

Surface conductivity errors caused by water film adsorptio on silica surface was revealed by a comparison of streamin potential and current measurements obtained in both aqueous and non-aqueous systems.

The streaming current and potential measurements indicated that asphaltene adsorption affects Berea sandstone electrical properties. The influence of asphaltene adsorption on Berea sandstone zeta potential is depicted in Figure 2. The zeta potential of Berea sandstone in the non-aqueous (Pentol) phase was derived from measurements of streaming current and calculated using equation 1 after the A/l ratios were obtained as indicated above. The (negative) zeta potential of Berea sandstone in Pentol appears to decrease (numerically) with increasing amounts of adsorbed asphaltene, Figure 2. Berea sandstone in the absence of any adsorbed asphaltene has a zeta potential of only -0.05 mV in Pentol solution. This value is very low compared to that found in brine. At around 1.5 g/l asphaltene concentration the zeta potential changes sign, indicating that asphaltene carries a small positive charge in Pentol. The change in the surface potential (zeta potential) values indicated that adsorption of oil heavy end (asphaltene) was taking placed on the mineral surfaces.

The adsorption thickness of asphaltene on Berea sandstone surfaces was estimated using equation 5. Figure 3, shows that the adsorption thickness increased rapidly at equilibrium concentrations of 0.5 to 1.5 g/l and then increased at a lower rate for higher concentrations to reach a value of 0.3 for γ/r. Asphaltene adsorption on Berea sandstone surfaces thus results in major permeability reductions. Figure 4 shows the reduction in A/l calculated using equations 4 and 5. A/l decreased rapidly but appeared to level off at about 50% of its initial value. Figure 5 shows the effective permeability calculated for the same conditions from flow rate data using the Darcy equation and a reduction of 70% from 30 md to about 9 md is evident. The plateau in asphaltene adsorption indicated by Figures 4 and 5 corresponded to the conditions at which zeta potential became positive (Figure 2). The adsorption of asphaltene on reservoir porous media is thus shown to reduce permeability and change the interfacial zeta potential, both of which may influence reservoir recovery efficiency.

Petrographic analyses of the Berea sandstone core samples used was performed in the Image Analysis Department at Core Laboratories Canada Ltd in Calgary, Canada. The core sample being examined "before" and "after" the treatment with asphaltene in Pentol, examples of photomicrographs are shown in Figure 6. Based on the porosity types observed in thin section the reservoir quality of the "after" sample is described as poor. Petrographic analysis showed that the intergranular porosities between the framework grains of the Berea sandstone were 20% and 10% respectively. The intergranular porosity in the "after" sample was reduced by approximately one half due to the

presence of asphaltene, in agreement with the reduction in permeability.

Conclusions

1. A novel method has been developed to estimate the ratio of pore cores section to length (A/l) by combining streaming potential and streaming current measurements.
2. The surface electrical potential of porous system can be determined by the streaming current method which is independent of surface conductivity errors.
3. Pentol, free from asphaltene, was found to gave a negative potential (~0.05 mV) at the sandstone surface which steadily went to small positive (~0.0005 mV) when asphaltene was introduced.
4. Although electric charge and consequent interparticle repulsion have frequently been suggested in the literature[12,13] as an important factor in asphaltene colloid stability in hydrocarbon solvents and crude oil, this work indicates that this can play only a minor role due to the very small potentials involved.
5. It is therefore proposed that asphaltene particle stability is caused by the steric effects of high molecular weight material (resins) adsorbed on asphaltene particles.
6. The flow rates indicated a plateau of asphaltene adsorption at around a pore blocking thickness of $\gamma/r = 0.3$ which was also the point at which the streaming current reached a plateau.
7. A microscope study of thin sections of rock after the experiments showed the open area reduced by a fraction of ~0.5 in excellent agreement with the value obtained from flow measurement shown in Figure 4.
8. Streaming current measurements and their interpretation are possible in resistive non-aqueous liquids such as crude oils, though requiring the measurement of currents of order only picoamps.

Nomenclature

A	=	Pores area of porous system.
f	=	Pores area/length of porous system.
η	=	Liquid viscosity.
I_s	=	Streaming current.
κ	=	Solution specific conductivity.
κ'	=	Solution specific conductivity including surface conductivity.
l	=	Length of the capillaries.
P	=	Pressure.
Q	=	Liquid flow rate.
R	=	Solution electrical resistance.
r	=	Radius of the capillaries.
V_s	=	Streaming potential.
ζ	=	Zeta potential.
ϵ	=	Permittivity.
γ	=	Thickness of adsorbed asphaltene layer.

Acknowledgements

The authors wish to express their thanks to the Public Authority for Applied Education and Training of Kuwait for financial support and to Core Laboratory Canada Ltd., Calgary, Alberta, Canada for their co-operation in this research project.

References

1. Alkafeef, S.F., Daltaban, T.S., Gochin, R.J.:"Electrokinetic Aspects of Asphaltene Deposition in Petroleum Reservoirs," paper ADNOC/SPE 26 presented at the 6th Abu Dhabi Petroleum Exhibition & Conference in Abu Dhabi City, UAE, Oct. 16-19, 1994.
2. Clementz, D.M.:"Alternation of Rock Properties by Adsorption of Petroleum Heavy Ends: Implications for Enhanced Oil Recovery," paper SPE 10683 presented at Third SPE/DOE Joint Symposium on Enhanced Oil Recovery, Tulsa, OK., April, 1982.
3. Cuiec, L.:"Rock/Crude-Oil Interaction and Wettability: An Attempt to Understand Their Interaction," paper SPE 13211 presented at the 1984 Annual Technical Conference and Exhibition, Houston, TX., Sept. 16-19.
4. Collins, S.H., Melrose, J.C.: "Adsorption of Asphaltenes and Water on Reservoir Rock Minerals,"paper SPE 11800 presented at the Symposium on Oilfield and Geothermal Chemistry, Denver, CO, June 1-3, 1983.
5. Crocker, M.E., Marchin, L.M."Wettability and Adsorption Characterstics of Crude Oil Asphaltene and Polar Fractions,"paper SPE/DOE 14885 presented at the SPE/DOE Fifth Symposium on Enhanced Oil Recovery, Tulsa, OK, April 20-23, 1988.
6. Gonzalez, G., Moreira, M.B.C.: "The Wettability of Mineral Surfaces Containing Adsorbed Asphaltenes," *Colloids and Surfaces*, 58 (1991) 293-302.
7. Hirasaki, G.J.:"Wettability: Fundamentals and Surface Forces,"paper SPE/DOE 17367 presented at the SPE/DOE Enhanced Oil Recovery Symposium, Tulsa, OK, April 17-20, 1988.
8. Morrow, N.R.:"Wettability and Its Effect on Oil Recovery", *JPT* (Dec 1990) 1476-1484.
9. Anderson, W.G.:"Wettability Literature Survey - Part 1: Rock/Oil/Brine Interactions and the Effects of Core Handling on Wettability," *JPT* (Oct. 1986) 1125-1144.
10. Brown, C.E., Neustadter, E.L.:"The Wettability of Oil/Water/Silica Systems With Reference to Oil Recovery," *J Canadian PT* (July-September, 1980) 123.
11. Buckley, J.S., Morrow, N.R., and Takamura, K.:"Influence of Electrical Surface Charges on the Wetting Properties of Crude Oil" paper SPE 16964 presented at the 1987 Annual Technical Conference, Dallas, TX, September 27-30.
12. Preckshot, G.W., Delisle, N.G., Cottrell, C.E., and Katz, D.L.:"Asphaltic Substances in Crude Oils," *Trans AIME*, **151** (1943) 188-194.
13. Leontaritis,K.J."Asphaltene Deposition: A Comprehensive Description of Problem Manifestations and Modelling Approaches," paper SPE 18892

presented at the SPE Prod. Operations Symposium
held in Oklahoma City, OK, March 13-14, 1989.

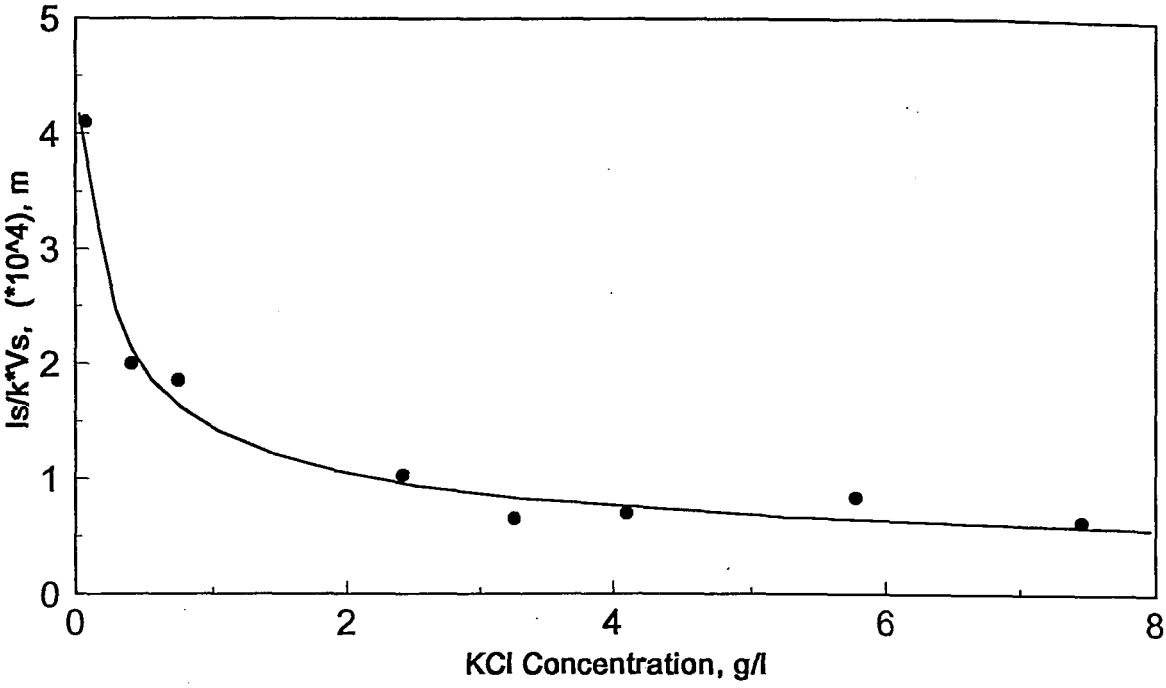

Figure 1-Estimating Berea sandstone pore A/l ratios in aqueous solutions.

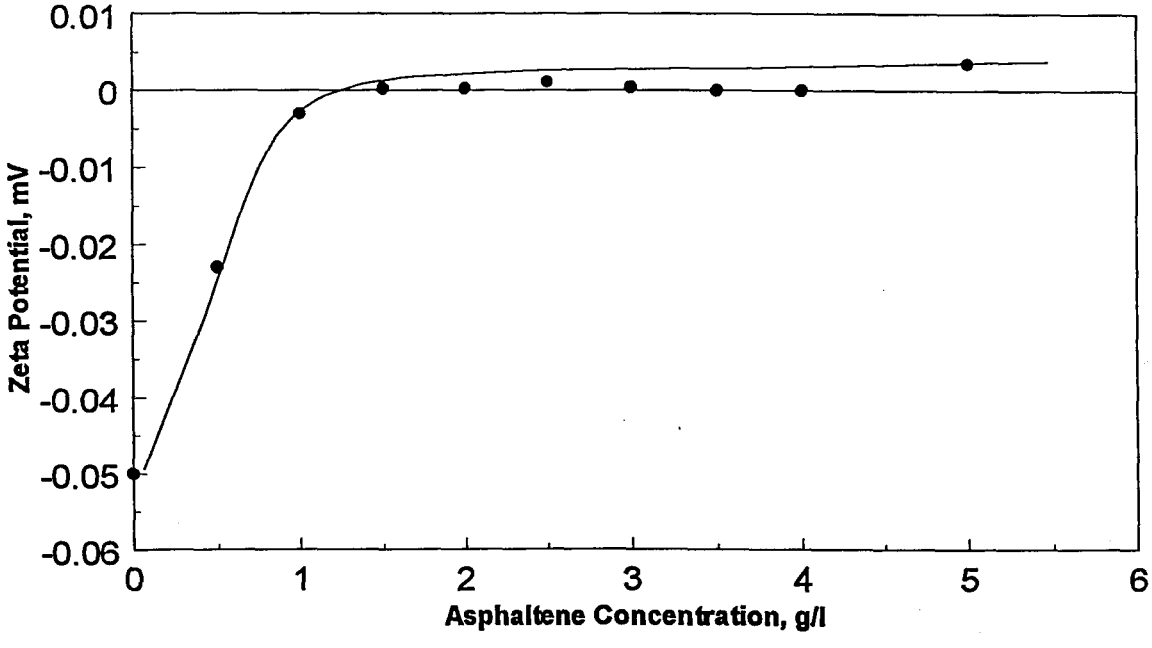

Figure 2-Variation of Berea sandstone zeta potential with asphaltene concentration in Pentol solutions.

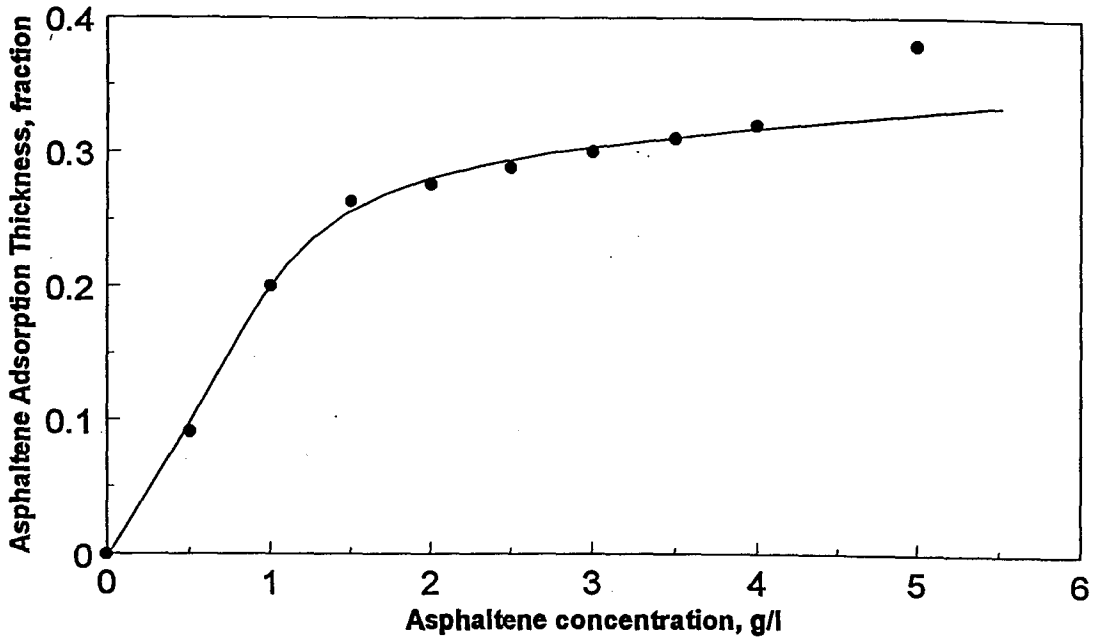

Figure 3-Variation of adsorption thickness with asphaltene concentration in Pentol solutions.

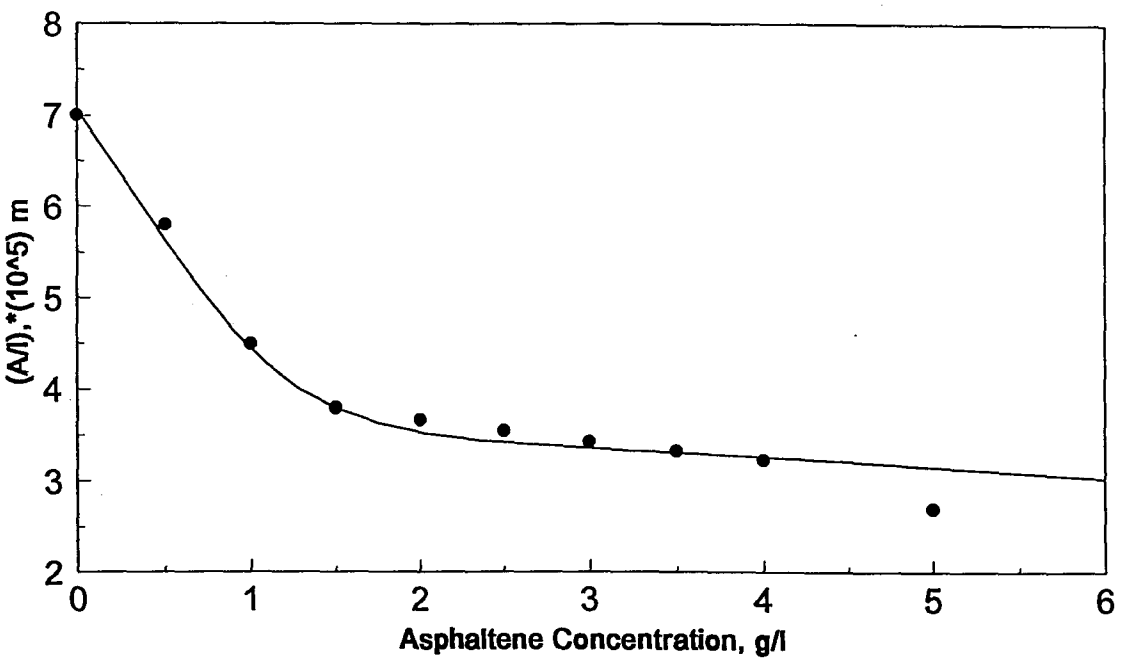

Figure 4-Reduction of Berea sandstone A/l with asphaltene concentration in Pentol solutions.

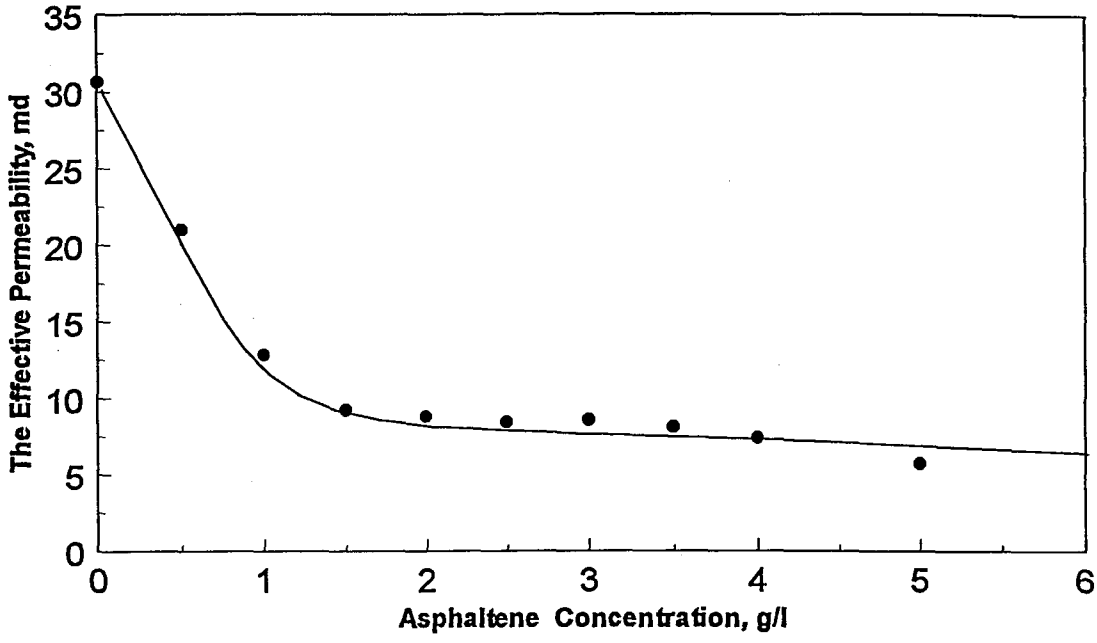

Figure 5-Effect of asphaltene adsorption on permeability of a sample of Berea sandtone.

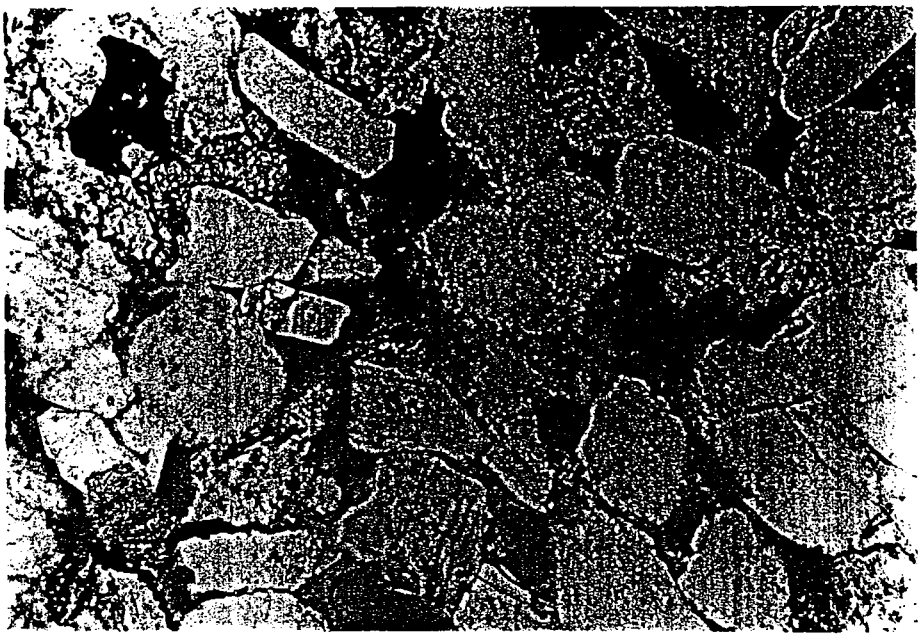

Before

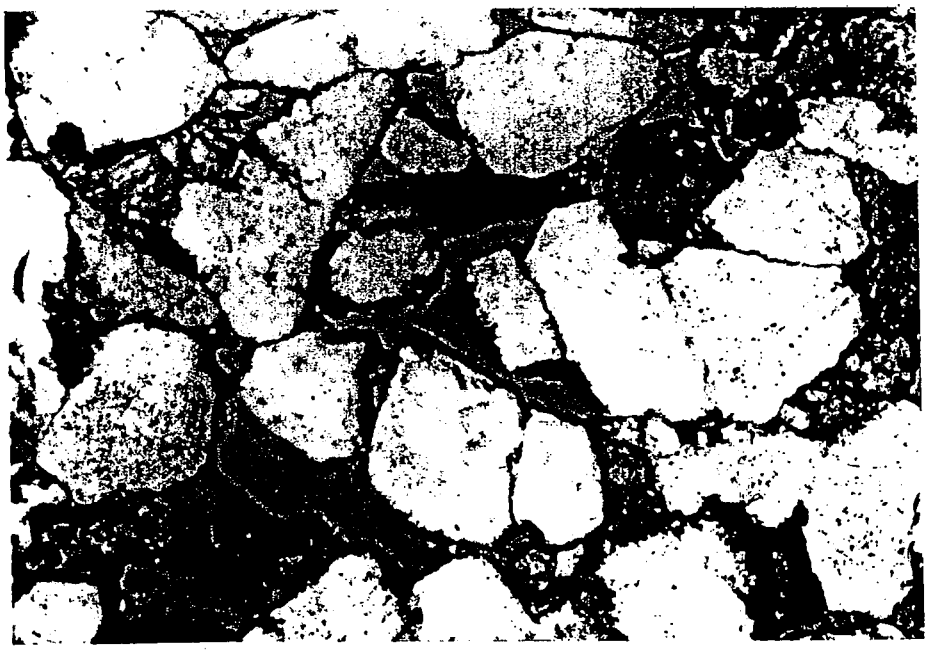

After

Figure 6-Thin sections of Berea sandstone core before and after asphaltene adsorption.